Universidade de Aveiro Departamento de Química
Ano 2012

MARIA BEATRIZ DA ROCHA VELEIRINHO

ELECTROSPUN FIBROUS MATS FOR SKIN AND ABDOMINAL WALL REPAIR

MATRIZES FIBROSAS PRODUZIDAS POR ELETROFIAÇÃO PARA REGENERAÇÃO DE PELE E REPARO DE PAREDE ABDOMINAL

Tese apresentada à Universidade de Aveiro para cumprimento dos requisitos necessários à obtenção do grau de Doutor em Química, realizada sob a orientação científica do Doutor José António Teixeira Lopes da Silva, Professor Auxiliar do Departamento de Química da Universidade de Aveiro e da Doutora Rosa Maria Ribeiro-do-Valle Nicolau, Professora Voluntária do Departamento de Farmacologia da Universidade Federal de Santa Catariana.

Apoio financeiro do POPH- QREN âmbito do III Quadro Comunitário de Apoio.

Apoio financeiro da FCT e do FSE no âmbito do III Quadro Comunitário de Apoio.

To my parents for their never ending love…

o júri

presidente

Doutor Vitor José Babau Torres
Professor catedrático da Universidade de Aveiro

Doutora Maria Helena Mendes Gil
Professora catedrática da Universidade de Coimbra

Doutora Maria Helena Figueira Vaz Fernandes
Professora associada da Universidade de Aveiro

Doutor Lino da Silva Ferreira
Investigador auxiliar do Centro de Neurociências e Biologia Celular da Universidade de Coimbra

Doutor José António Teixeira Lopes da Silva
Professor auxiliar da Universidade de Aveiro

Doutora Rosa Maria Ribeiro do Valle Nicolau
Professora voluntária da Universidade Federal de Santa Catarina

agradecimentos

It is with great pleasure that I acknowledge so many people who helped me during this journey…

First, I would like to express my sincere gratitude to my supervisor Dr. José António Lopes da Silva, for his support and guidance, but most of all for giving me freedom to explore this amazing research world. It is always pleasant and simple to talk with him about science…

I am also profoundly grateful to my co-supervisor Dr. Rosa Maria Ribeiro do Valle… She received me in her lab with great affection and had always supported and encouraged me in all stages of my life.

I would like to express my deepest gratitude to Dr. Paulo Dias, who more than a great collaborator of this work, is a great friend… always waiting for our meetings with a chocolate or a cereal bar… Paulinho, the world lacks people like you.

Very special thanks to Dr. José António Sousa, to Dr. Eduardo Cargnin-Ferreira, and to Ana Peixoto for the support in abdominal hernia experiments.

I also appreciate the help of Dr. Ricardo Tramonte, Dr. Armando D'Acampora, MSc. Geraldo Bernardes, BSc. Sandro Sgrott in the wound healing experiments with PET mat.

I am in debt with many technicians from UA and UFSC who helped me in analytical procedures: Marta Ferro, Luciano Oliveira, Chirle Ferreira, Demétrio Gomes, Eliana Oliveira, Renata Ozório, Dulce Helena Teixeira, Denis Agnolo, and Luisa Peixoto.

I am also very grateful to Luis (CCA/UFSC), Leila, and Murilo (CCB/ UFSC) who were always glad to provide some assistance in the lab.

I take this opportunity to sincerely acknowledge "Naturama, Ltda" (SC/Brazil) for Aloe vera samples donation, "Matel Erva Mate Verdinha, Ltda" (SC/Brazil) for providing the "erva-mate" sample, "Tyson, S.A." (SC/Brazil) for the donation of the chicken fertilized eggs, and "Flexitex" (Portugal) for the PET sample donation.

I am thankful to *Fundação para a Ciência e Tecnologia* (Portugal) for the Ph.D. Grant (SFRH / BD / 38881 / 2007 -POPH – QREN) and also to FAPESC/CNPq for the financial support through PRONEX (n.17420/2011/3).

I also thank to Marcela Prudêncio who introduced me in the aseptic world of cell culture with lots of laughing!

A great partner during this Ph.D. journey was Daniela Coelho who helped me in all animal experiments… I am very privileged to have had you working with me…

A special thanks to Fernanda Berti… the world has conspired against our partnership :) but we were always somewhere together (sometimes secretly!!) working with our biomaterials stuff …

To Rúbia Pinto… for helping with animals experiment… and for the friendship that was born during protein quantification!

To my adorable and fellow dogs Kika, Tag, Fly (in memory), and Brisa who snugly laid down on my feet during writing issues… and to my special *cachorreira* friend Tais Bressan Ruas. I know you won't bother to be included in this topic of acknowledgement section; actually I think you'll be proud! I have spent nice evenings with you and our *girls*.

To all my lab friends in Portugal and Brazil … I am very fortunate to work with so many nice people around me.

I'd like to thank all the support and friendship from my family and friends.

To my daughter Mariana, she is in this exact moment at my side laughing deeply at a little joke … what just makes me realize how wonderful is my world with her … being a mom in the meantime of my PhD has also made me realize how simple are all these chemistry, biology, and materials stuff comparing to taking care of this little one.

Marcelo, I have no words to express my gratitude for your love and support … It is a blessing to have someone like you in my life… you see, as you say "Don't worry, at the end everything is gonna be alright!"

I am deeply and forever grateful to my mom and to my dad (in memory)… Now I can understand their love… now I can see that their biggest dream was making our dreams come true and their biggest effort was to teach us to believe and to pursuit them… to them I dedicate this thesis. Special thanks to the best baby-sitting service that I could ever have… without it I would not have finished this thesis!

Most of all I acknowledge God… who makes everything possible…for every single opportunity… and every single person that He put in my live.

palavras-chave

Eletrofiação, suportes celulares, engenharia de tecidos, hérnia abdominal, poli(3-hidroxibutirato-*co*-3-hidroxivalerato), quitosana, poli(tereftalato de etileno).

resumo

Esta tese centra-se no desenvolvimento de materiais biodegradáveis e não-degradáveis produzidos por eletrofiação com aplicação na área biomédica. O poli(3-hidroxibutirato-*co*-3-hidroxivalerato) (PHBV), um poliéster biodegradável, foi selecionado como base dos materiais biodegradáveis, enquanto o poli(tereftalato de etileno) (PET), um polímero sintético, estável e biocompatível, foi selecionado para a produção das matrizes não degradáveis. Adicionou-se quitosana aos sistemas com o objetivo de melhorar o processo de eletrofiação e as propriedades morfológicas, físico-químicas e biológicas dos materiais resultantes.

A composição química, bem como as características morfológicas e físico-químicas dos materiais em estudo, foram manipuladas de modo a otimizar a sua performance como suportes celulares para engenharia de tecidos. Foram realizados estudos *in vitro* com cultura de fibroblastos L929 para avaliar o comportamento das células, *i.e.* viabilidade, adesão, proliferação e morte, quando cultivadas nas matrizes produzidas por eletrofiação. Adicionalmente foram realizados ensaios *in vivo* para investigar o potencial dos materiais em estudo na regeneração cutânea e como tela abdominal.

Os principais resultados encontrados incluem: o desenvolvimento de novas matrizes híbridas (PHBV/quitosana) adequadas ao crescimento de fibroblastos e ao tratamento de lesões de pele; o desenvolvimento de um sistema de eletrofiação com duas seringas para a incorporação de compostos bioativos; diversas estratégias para manipulação das características morfológicas dos materiais de PHBV/quitosana e PET/quitosana produzidos por eletrofiação; uma melhoria do conhecimento das interações fibroblastos-suporte polimérico; a verificação de uma resposta inflamatória desencadeada pelos materiais não-degradáveis quando utilizados no tratamento de defeitos da parede abdominal, o que sugere a necessidade de novos estudos para avaliar a segurança do uso de biomateriais produzidos por eletrofiação.

keywords

Electrospinning, scaffold, tissue engeniering, abdominal hernia, poly(3-hydroxybutyrate-*co*-3-hydroxyvalerate), chitosan, polyethylene terephthalate.

abstract

This thesis focuses on the development of biodegradable and non-degradable electrospun materials with application in the biomedical field. Poly(3-hydroxybutyrate-co-3-hydroxyvalerate) (PHBV), a natural biodegradable polyester, was selected as the basis of the biodegradable materials while polyethylene terephthalate (PET), a biocompatible stable synthetic polyester, was selected for the production of the non-degradable ones. Chitosan was added to both systems in order to enhance electrospinnability as well as morphological, physico-chemical, and biological features of the biomaterials. The chemical composition, morphological and some physico-chemical characteristics of these materials were manipulated toward an optimized biological performance as scaffolds for tissue engineering. *In vitro* cell culture studies were performed with L929 fibroblasts in order to study the cell behavior, *i.e*. viability, adhesion, proliferation and death, when cultured on the electrospun materials. Furthermore, *in vivo* assays were conducted in order to investigate the potential of the materials under study for skin and abdominal wall repair.

The main achievements of this thesis include: the development of new PHBV/chitosan hybrid mats suitable for fibroblasts growth and with a good performance when used as a scaffold for skin repair; the development of a dual syringe electrospinning system for incorporation of bioactive compounds; several strategies to manipulate the morphological characteristics of electrospun materials of both PHBV/chitosan and PET/chitosan blends; an improvement of the knowledge of cell-scaffolds interactions; the detection of an important inflammatory response elicited by the non-degradable electrospun materials when used as prosthetic meshes for abdominal defect repair, suggesting the need of further studies on the safety of nanosized electrospun biomaterials.

Table of Contents

Table of Contents ..... **I**
List of Figures ..... **V**
List of Tables ..... **XIII**
Abbreviations ..... **XV**
Preface **1**
1. Bibliographic Review **3**
1.1. Biomaterials **5**
1.2. Electrospinning **5**
1.2.1. Governing parameters of the electrospinning process 7
1.3. Tissue Engineering **8**
1.3.1. Application of polymers in tissue engineering 9
1.3.1.1. PET 9
1.3.1.2. PHBV 9
1.3.1.3. Chitosan 10
1.3.2. Scaffolds: a provisory environment for cells 10
1.3.2.1. Focal adhesion 11
1.3.2.2. Adhesion in artificial substrata 12
1.3.3. Skin engineering 13
1.3.3.1. Wound healing 14
1.3.3.2. Impairment of wound healing 15
1.3.3.3. Electrospun mats as scaffolds for skin engineering 16
1.4. Concluding remarks **17**
2. Electrospun PHBV/chitosan blends as scaffolds for skin engineering **19**
2.1. Introduction **21**
2.2. Experimental **22**
2.2.1. Materials 22
2.2.2. Oxidative depolymerisation of chitosan 22
2.2.3. Preparation of electrospinning solutions 23
2.2.4. Optimization of the electrospinning process 23
2.2.5. Characterization of electrospun mats 24
2.2.5.1. Morphology 24
2.2.5.2. *In vitro* degradation 24
2.2.5.3. Attenuated total reflection-Fourier transform infrared spectroscopy (ATR-FTIR) 25
2.2.5.4. Biological *in vitro* studies 25

2.2.5.4.1. Indirect cytotoxicity assay 25
2.2.5.4.2. Cell viability 26
2.2.5.4.3. Cell adhesion, spreading, and proliferation 26
2.2.5.4.4. Annexin V and propidium iodide (PI) staining 27
2.2.5.5. Wound healing assay 27
2.2.6. Statistics 28
2.3. Results and discussion 29
2.3.1. Characteristics of the chitosan samples 29
2.3.2. Electrospinning process optimization 29
2.3.3. Solvent effects 30
2.3.4. Effects of PHBV/C ratio and chitosan MW on fiber formation and morphology 31
2.3.4.1. Formation of nanofibers 32
2.3.4.2. Morphological characterization of the mats 33
2.3.5. FTIR analysis 38
2.3.6. *In* vitro degradation of the scaffolds 41
2.3.7. Biological studies 42
2.3.7.1. Cell culture studies 43
2.3.7.2. Wound healing assay 51
2.4. Conclusion 55
3. Dual-fiber mats as new support matrices and vehicles for bioactive compounds 57
3.1. Introduction 59
3.1.1. Nanofiber mats as vehicles for bioactive compounds 59
3.1.2. *Aloe barbadensis* Miller 60
3.1.3. *Ilex paraguariensis* 61
3.1.4. Electrospinning solvents and the incorporation of biocompounds 62
3.1.5. Electrospinning in aqueous solution 63
3.2. Experimental 63
3.2.1. Materials 63
3.2.2. Preparation of aloe gel 64
3.2.3. *Ilex paraguariensis* 64
3.2.3.1. Preparation of aqueous extract 64
3.2.3.2. Effect of aqueous extract on vasculogenesis and angiogenesis 64
3.2.4. Scaffolds fabrication by electrospinning 66
3.2.5. Scaffolds characterization 68
3.2.6. Biological studies 68
3.2.7. Statistics 69

3.3. Results and discussion 69
3.3.1. Morphological analysis of PVA/chitosan nanofibers 69
3.3.2. Distribution of PHBV/chitosan and PVA/chitosan fibers in the dual-fiber mat 70
3.3.3. Distribution of bioactive extracts in the dual-fiber mats 72
3.3.4. Biological studies 77
3.3.4.1. Pro-vasculogenic and pro-angiogenic effects of the aqueous extract of *I. paraguariensis* 78
3.3.4.2. Cell viability and growth 80
3.3.5. Wound healing assay 87
3.4. Conclusions and further studies 89
4. Electrospun PET mat as a non-absorbable wound dressing 91
4.1. Introduction 93
4.2. Experimental 95
4.2.1. Materials 95
4.2.2. Fabrication of PET mat by electrospinning 95
4.2.3. Morphological analysis 95
4.2.4. Wound healing assay 96
4.2.4.1. Histopathological analysis 96
4.2.5. Statistics 97
4.3. Results and discussion 97
4.3.1. Morphological analysis 97
4.3.2. Macroscopic observations of the wound healing process 99
4.3.3. Histopathological analysis 100
4.3.3.1. Effect of PET wound dressing on the inflammatory phase of the wound healing process 103
4.3.3.2. Proliferative phase 104
4.3.3.3. Re-epithelialization 105
4.4. Conclusions 107
5. PET/chitosan non-degradable scaffolds for tissue engineering 109
5.1. Introduction 111
5.2. Experimental 112
5.2.1. Materials 112
5.2.2. Scaffolds fabrication by electrospinning 113
5.2.3. Morphological analysis 113
5.2.4. FTIR 113
5.2.5. Water contact angle (WCA) measurements 113
5.2.6. Cell culture 114
5.2.7. Statistics 114

5.3. Results and discussion 114
5.3.1. Effect of chitosan concentration and MW on fiber diameter 115
5.3.2. Pore area characterization 118
5.3.3. Post-electrospinning cross-linking 119
5.3.4. Surface properties 121
5.3.5. Cell studies 123
5.4. Conclusions 132
6. PET and PET/chitosan electrospun hybrid mats as abdominal meshes for hernia repair 133
6.1. Introduction 135
6.1.1. Incisional hernias: occurrence and treatment 135
6.1.2. Complications of prosthetic mesh use 135
6.1.2.1. Intestinal adhesions 136
6.1.2.2. Foreign body reaction 137
6.1.3. Electrospun materials as meshes for abdominal hernia repair 137
6.2. Experimental 139
6.2.1. Material 139
6.2.2. Meshes fabrication 139
6.2.3. Animal model 140
6.2.4. Statistics 143
6.3. Results and discussion 144
6.3.1. Characterization of meshes 144
6.3.2. Surgical procedure and postoperative period 145
6.3.3. Histopathological analysis 147
6.4. Concluding remarks and future work 155
7. Concluding remarks and recommendations for future work 157
References 163

List of Figures

Figure 2.1. *Illustrative representation of the electrospinning system.* *24*

Figure 2.2. *Schematic illustration of wound healing assay in rats.* *28*

Figure 2.3. *SEM images showing the morphology of fibers electrospun from PHBV/C 48 kDa solutions in TFA/HFIP 3:7 (v/v), at different polymer ratios: (a) 4:1 (b) 3:2 (c) 2:3 (d) 1:4 (w/w).* *33*

Figure 2.4. *SEM images showing the morphology of fibers electrospun from PHBV/C 48 kDa solutions in TFA/HFIP 1:1 (v/v), at different polymer ratios: (a) 4:1 (b) 3:2 (c) 2:3 (d) 1:4 (w/w).* *34*

Figure 2.5. *Relative frequency of secondary fibers in electrospun PHBV/C mats: (a) TFA/HFIP 3:7 (v/v) (b) TFA/HFIP 1:1 (v/v).* *35*

Figure 2.6. *Average main fiber diameters of PHBV/C mats: (a) TFA/HFIP 3:7 (v/v) (b) TFA/HFIP 1:1 (v/v).* *36*

Figure 2.7. *Average secondary fiber diameters of PHBV/C mats: (a) TFA/HFIP 3:7 (v/v) (b) TFA/HFIP 1:1 (v/v).* *37*

Figure 2.8. *SEM micrographs showing broken fibers: (a) PHBV/C 5:0 (w/w) in TFA/HFIP 1:1 (b) PHBV/$C_{1500\ kDa}$ 2:3 (w/w) in TFA/HFIP 1:1 (v/v).* *38*

Figure 2.9. *FTIR spectra obtained for electrospun fibers of PHBV/C 5:0 (w/w), PHBV/C $_{48\ kDa}$ 4:1 (w/w), PHBV/C $_{48\ kDa}$ 2:3 (w/w), and for as-received chitosan.* *40*

Figure 2.10. *In vitro degradation of mats containing different PHBV/C ratios and chitosan MW.* *41*

Figure 2.11. *SEM images of electrospun fibers degraded in PBS (pH 7.4) at 37 ºC for (a-c) 0, (d-f) 1 hour, and (g, h, and i) 28 days. Left column for a PHBV/C 5:0 (w/w), middle column PHBV/$C_{48\ kDa}$ 4:1 (w/w), and right column for PHBV/$C_{48\ kDa}$ 2:3 (w/w).* *42*

Figure 2.12. *SEM images showing the morphology of fibers electrospun from PHBV/C 48 kDa solutions in TFA/HFIP 1:1 (v/v), at two different polymer ratios: (a) 4:1 and (b) 2:3 (w/w). Also shown are the fiber average diameters, pore area, and degradation rates (as % mass loss) obtained after 14 days in a phosphate buffer solution (pH 7.4) at 37 °C.* *43*

Figure 2.13. *Absorbance 540 nm (% of control) obtained in the indirect cytotoxicity assay of L929 cells cultured on PHBV/C 2:3 (w/w) and PHBV/C 4:1 (w/w) scaffolds. No significant differences were detected.* 44

Figure 2.14. *Viability of L929 cells cultured on PHBV/C 2:3 and 4:1 (w/w) scaffolds for 2, 7, and 14 days measured via MTS assay. No significant differences were detected.* 45

Figure 2.15. *SEM images of L929 cells cultured on PHBV/C 2:3 (w/w) (a and b) and 4:1 (w/w) (c and d) scaffolds for 12 hours (a and c) and 2 days (b and d). Bar = 5 µm.* 46

Figure 2.16. *CLSM images of L929 fibroblasts cultured on PHBV/C 2:3 (w/w) (a-c) and PHBV/C 4:1 (w/w) (d-f), for 12 hours (a and d), 2 days (b and e), and 7 days (c and f). F-actin (red) and nucleus (blue) stained with Alexafluor 546 conjugated to phalloidin and DAPI, respectively. Scale bar = 10 µm (a, b, d, and e) and = 50 µm (c and f).* 46

Figure 2.17. *Immunolabeling of extracellular fibronectin (green) deposited on the surface of PHBV/C 2:3 (w/w) (a) and PHBV/C 4:1 (w/w) (b) scaffold after 48 days of incubation with L929 cells. Bar = 50 µm.* 47

Figure 2.18. *Cytoskeleton area of L929 cells cultured on PHBV/C scaffolds as a function of culture time. Different letters indicate significant differences ($p < 0.05$).* 48

Figure 2.19. *CLSM images of L929 fibroblasts cultured on (a) PHBV/C 2:3 (w/w) and (b) and (c) PHBV/C 4:1 (w/w), for 2 days (a and b) and 7 days (c). Vinculin (green) and nucleus (blue) stained with anti-vinculin monoclonal antibody followed by Alexafluor 488 goat anti-mouse and DAPI, respectively. Scale bar =10 µm.* 49

Figure 2.20. *Percentage of proliferating cells measured by the EdU assay. Different letters indicate significant differences ($p < 0.05$).* 50

Figure 2.21. *Annexin V-FITC/PI flow cytometry analysis of cell death after 48 hours of incubation on (a) control, (b) PHBV/C 2:3 (w/w), and (c) PHBV/C 4:1 (w/w). Viable cells (Annexin V-FITC negative/PI negative) are in the lower left quadrants; apoptotic cells (Annexin V-FITC positive/PI negative) are in the lower right quadrants; late apoptotic cells (Annexin V-FITC positive/PI positive) are in the upper right quadrants; and necrotic cells (Annexin V-FITC negative/PI positive) are in the upper left quadrants. The cytograms are representative of three independent experiments. Mean ± standard deviation of cell stages (d).* 51

Figure 2.22. *Wound area for PHBV/C 2:3 (w/w), PHBV/C 4:1 (w/w), and control groups during the wound-healing assay. Different letters indicate significant differences ($P<0.05$).* 52

Figure 2.23. *Histological classification of wound tissues 3, 7, 14, and 21 days after injury for control and PHBV/C scaffolds: IF (inflammatory infiltrate), GT (granulation tissue), IM (immature regenerated tissue), and RT (remodeled tissue).* 53

Figure 2.24. *PMN and MN leukocyte densities during the wound healing process in rats.* *54*

Figure 2.25. *Histological sections showing the HE staining 21 days after surgical injury. Control (a), PHBV/C 2:3 (w/w) (b), and PHBV/C 4:1 (w/w) (c). Bar = 50 μm.* *55*

Figure 3.1. *Illustrative representation of the blood vessel analysis in the yolk-sac membrane assay.* *66*

Figure 3.2. *Schematic representation of the dual syringe electrospinning system.* *68*

Figure 3.3. *Representative SEM images of fibers obtained from electrospinning solutions of (a) PVA/chitosan 9:1 (w/w) (10 wt.%) in acetic acid 0.2 M (spun S_2), (b) S_2 + 1 wt.% of A. barbadensis, (c) S_2 + 0.01 wt.% of I. paraguariensis aqueous extract, and (d) S_2 + 1wt.% of A. barbadensis + 0.01 wt.% of I. paraguariensis aqueous extract. Bar = 5μm.* *70*

Figure 3.4. *SEM images of (a) PHBV/C mat, (b) PVA/C mat, and (c) dual-fiber mat. Blue arrows evidence details from the PHBV/C fibers and red arrows from the PVA/C ones. Bar = 1μm.* *71*

Figure 3.5. *FTIR spectra obtained for electrospun fibers of PHBV/C 4:1 (w/w) and dual-fiber mat.* *72*

Figure 3.6. *SEM pictures of (a and c) dual-fiber mat and (b and d) bioactive dual-fiber mat at 6000x (a and b) and 10000x magnification (c and d). Bar = 5μm (a and b) and bar = 3μm (c and d).* *73*

Figure 3.7. *FTIR spectra obtained for electrospun fibers of dual-fiber, aloe_dual-fiber, and lyophilized aloe vera gel. Whole spectra (top) and fingerprint region (bottom).* *75*

Figure 3.8. *FTIR spectra obtained for electrospun fibers of dual-fiber, ilex_dual-fiber, and lyophilized I. paraguariensis aqueous extract. Whole spectra (top) and fingerprint region (bottom).* *76*

Figure 3.9. *FTIR spectra obtained for electrospun fibers of dual-fiber and bioactive dual-fiber mats. Whole spectra (top) and fingerprint region (bottom).* *77*

Figure 3.10. *Effects of I. paraguariensis aqueous extract on the formation of blood vessels by (a) vasculogenesis and (b) angiogenesis. Different letters indicate significant differences at $P<0.05$.* *79*

Figure 3.11. *Representative examples illustrating the effects of I. paraguariensis aqueous extract on vasculogenesis and angiogenesis.* *80*

Figure 3.12. *Absorbance (% of control, i.e. TCP) of L929 cells cultivated on the PHBV/C 4:1 (w/w), dual-fiber, and bioactive dual-fiber scaffolds extraction media. No significant differences were observed (P>0.05).* *81*

Figure 3.13. *MTS assay for cells cultured on the PHBV/C 4:1 (w/w), dual-fiber, and bioactive dual-fiber scaffolds for 2, 7, and 14 days. No significant differences were observed (P>0.05).* *82*

Figure 3.14. *Live/dead assay of cells cultured on the PHBV/C 4:1 (w/w), dual-fiber, and bioactive dual-fiber scaffolds for 2, 7, and 14 days. Live cells appear in green and dead cells in red. Bar=100 μm.* *83*

Figure 3.15. *SEM analysis of cells cultured on PHBV/C 4:1 (w/w), dual-fiber, and bioactive dual-fiber scaffolds for 12 hours, 2 days, and 7 days after seeding. Bar= 10μm.* *84*

Figure 3.16. *SEM analysis (high magnification) of cells cultured on PHBV/C 4:1 (w/w), dual-fiber, and bioactive dual-fiber scaffolds for 12 hours, 2 days and 7 days after seeding. Bar = 5 μm.* *85*

Figure 3.17. *CLSM images (a) low magnification and (b) high magnification of L929 fibroblasts cultured on bioactive dual-fiber scaffolds for 12 hours. F-actin (red) and nucleus (blue) stained with Alexafluor 546 conjugated to phalloidin and DAPI, respectively. Bar = 50 μm.* *86*

Figure 3.18. *CLSM images of L929 fibroblasts cultured on (a) PHBV/C 4:1 (w/w), (b) dual-fiber, and (c) bioactive dual-fiber scaffolds for 7 days. F-actin (red) and nucleus (blue) stained with Alexafluor 546 conjugated to phalloidin and, respectively. Scale bar = 10 μm.* *86*

Figure 3.19. *CLSM images of L929 fibroblasts cultured on (a) PHBV/C 4:1 (w/w) and (b) bioactive dual-fiber scaffolds for 2 days. Vinculin (green) and nucleus (blue) stained with anti-vinculin monoclonal antibody followed by Alexafluor 488 goat anti-mouse and DAPI, respectively. Scale bar =10 μm.* *87*

Figure 3.20. *Wound area (% of initial wound area) as a function of time for different treatments tested. Different letters indicate significant difference (P<0.05).* *88*

Figure 3.21. *PMN and MN cell densities during the wound healing process.* *89*

Figure 4.1. *SEM image of PET mat.* *97*

Figure 4.2. *Pore area distribution of PET mat.* *98*

Figure 4.3. *Macroscopic observation of the wound bed on control (a-c) and PET group (d-f) on the 3rd (a and d), 7th (b and e), and 14th (c and f) postoperative day.* *100*

Figure 4.4. *HE staining of histological sections (magnification = 40x) representative of control (a-c) and PET (d-f) wounds on the 3rd (a and d), 7th (b and e), and 14th (c and f) postoperative day. (II) Inflammatory infiltrate, (GT) granulation tissue, (AT) adipose tissue, (RT) regenerated tissue. Bar = 500 μm* *101*

Figure 4.5. *HE staining of histological sections (magnification = 400x) of control (a, c, and e) and PET treated (b, d, and f) wounds on the 3rd (a and b), 7th (c and d), and 14th (e and f) postoperative day. Red arrow points to a fibroblast and black arrow points to a fibrocyte typical morphology. Bar = 50 μm.* *102*

Figure 4.6. *(a) PMN and (a) MN leucocyte densities for control and PET treated groups at 3, 7, and 14 days after injury. (*) Indicates significant differences between control and PET groups (P<0.05).* *104*

Figure 4.7. *(a) Fibroblast and (b) fibrocyte densities for control and PET groups 3, 7, and 14 days after injury. (*) Indicates significant differences between control and PET groups (P<0.05).* *105*

Figure 4.8. *Average wound area of control and PET groups on the 3rd, 7th, and 14th day after injury. (*) Indicates significant differences between control and PET groups (P<0.05).* *106*

Figure 4.9. *HE staining of a histological section of PET group at the 7th day after injury illustrating the incorporation of PET mat in the subcutaneous region of the newly formed tissue. The arrow points to PET wound dressing lying beyond the dermal tissue. Bar=500 μm.* *107*

Figure 5.1. *Fiber diameter histograms of PET and PET/C scaffolds, obtained by changing chitosan concentration (0, 2, 4, and 6 wt.%) and MW (15, 22, and 48 kDa).* *117*

Figure 5.2. *Pore area distributions of as-electrospun (AS) and CL scaffolds a) PET, b) $PC_{48}15:1$, c) $PC_{48}5:1$, d) $PC_{15}15:1$ and e) $PC_{15}5:1$. Inserts show the average values. x-Axis represents pore areas (μm^2) and y-axis the relative frequency (%).* *118*

Figure 5.3. *SEM micrographs of scaffolds a) PET, b) PETCL, c) PETCL high magnification, d) $PC_{48}5:1$, e) $PC_{48}5:1CL$, f) $PC_{48}5:1CL$ high magnification, g) $PC_{15}5:1$, h) $PC_{15}5:1CL$ and i) $PC_{15}5:1CL$ high magnification. Bar = 10 μm (a, b, d, e, g, and h) or = 1 μm (c, f, and i).* *120*

Figure 5.4. *FTIR spectra (1700 – 1500 cm^{-1} region) of $PC_{15}5:1$ and $PC_{15}5:1CL$ scaffolds.* *121*

Figure 5.5. *Indirect cytotoxicity evaluation of nanofibrous scaffolds based on the viability of fibroblasts (L929) cultured in the extraction media. The viability of cells cultured in fresh media was used as control. No significant differences were found.* 123

Figure 5.6. *Viability of L929 cells cultured on PET, PC_{48}5:1, and PC_{48}5:1CL scaffolds for 2, 7, and 14 days measured via MTS assay. No significant differences were found.* 124

Figure 5.7. *SEM images (a-c) and CLSM images (d-f) of L929 fibroblasts cultured on PET scaffold for 12 hours (a and d), 48 hours (b and e), and 7 days (c and f). F-actin (red) and nucleus (blue) stained with Alexafluor 546 conjugated to phalloidin and DAPI, respectively. Scale bar = 10 µm.* 125

Figure 5.8. *SEM micrographs of L929 fibroblasts cultured on a) PET, b) PC_{15}5:1, and c) PC_{15}5:1 CL scaffolds after 48 hours incubation. Scale bar = 5 µm.* 125

Figure 5.9. *CLSM images of L929 fibroblasts after 7 days of incubation on PET (a-c) and PC_{15}5:1 (d-f) scaffolds. F-actin (red), vinculin (green) and nucleus (blue) stained with phalloidin Alexafluor 546 conjugated, anti-vinculin monoclonal antibody followed by Alexafluor 488 goat anti-mouse, and DAPI, respectively. Scale bar = 100 µm (a and d) or =10 µm (b, c, e, and f).* 126

Figure 5.10. *Cell density (a) and cytoskeleton area (b) of L929 cells as a function of culture time, obtained for PET, PC_{15}5:1, and PC_{15}5:1CL scaffolds. Different letters indicate significant differences ($p < 0.05$).* 127

Figure 5.11. *Immunolabeling of extracellular fibronectin (green) deposited on the surface of PET scaffold after 7 days of incubation with L929 cells. Bar= 50 µm.* 128

Figure 5.12. *Annexin V-FITC/PI flow cytometry analysis of cell death after 48 hours of incubation in a) PET, b) PC_{15}5:1, and c) PC_{15}5:1 CL. Viable cells (Annexin V-FITC negative/PI negative) are in the lower left quadrants; Apoptotic cells (Annexin V-FITC positive/PI negative) are in the lower right quadrants; late apoptotic cells (Annexin V-FITC positive/PI positive) are in the upper right quadrants; necrotic cells (Annexin V-FITC negative/PI positive) are in the upper left quadrants. The cytograms are representative of three independent experiments.* 129

Figure 5.13. *EdU incorporation assay of L929 cultured on PET, PC_{15}5:1, and PC_{15}5:1 CL. (a) Fluorescence micrographs of proliferative cells (green) stained with EdU Alexafuor 488 and nuclei (blue) counterstained with DAPI (100x magnification). (b) Quantitation of proliferative cells mean ± S.D measured from 10 fields from 3 independent experiments. Results are expressed as % of control, i.e. TCP. Different letters indicate significant differences ($P < 0.05$).* 130

Figure 5.14. *SEM image evidencing the relative size of L929 fibroblasts (12 hours after seeding) and PC_{15}5:1 scaffold pore size. Bar= 10 µm.* 131

Figure 5.15. *CLSM 3D projection of L929 cells cultivated on PC_{15}5:1 scaffold for 48h. Fibers (green), F-actin (red) and nucleus (blue) stained with FITC, Alexafluor 546 conjugated to phalloidin and DAPI, respectively. Scale bar = 50 μm.* *132*

Figure 6.1. *Graphic illustration of the incisional hernia model.* *142*

Figure 6.2. *Illustrative representation of (a) excision of abdominal mesh and surrounding tissues and (b) preparation of histological sections.* *143*

Figure 6.3. *SEM image of a transversal section of DL mesh.* *145*

Figure 6.4. *Examples of (a) skin dehiscence and (b) omentum adhesion to a PET mesh.* *147*

Figure 6.5. *Histological sections evidencing the foreign body granuloma (Giemsa staining) of (a) Marlex30, (b) PET30, (c) PET/C, and (d) DL groups. (D) dermis, (SC) subcutaneous tissue, and (FBG) foreign body granuloma. Bar=220 μm.* *148*

Figure 6.6. *(a) Granuloma thickness and (b) number of FBGC surrounding the abdominal meshes. Different letters indicate significant differences (P<0.05).* *149*

Figure 6.7. *Representative examples of the foreign body reaction (HE staining) of (a- c) Marlex30, (d- f) PET30, (g- i) PET/C, and (j-l) DL groups. Bar = 100 μm (a, d, g, and j) = 25 μm (b, e, h, and k), and = 10 μm (c, f, i, and l).* *151*

Figure 6.8. *Representative examples of the foreign body reaction (HE staining) of (a) Marlex90 and (b) PET90. Bar = 50 μm.* *152*

Figure 6.9. *Representative examples at different magnification of the foreign body reaction observed on wovenPET group (HE staining). (D) dermis, (SC) subcutaneous tissue, and (FBG) foreign body granuloma. Bar = 200 μm (a), 100 μm (b), and 25 μm (c).* *153*

List of Tables

Table 2.1. *Solvent properties.* *31*

Table 2.2. *Electrospinnability of PHBV/C (10 wt.%) in TFA/HFIP (22 kV of applied voltage, flow rate of 8 μL/min).* *32*

Table 3.1. *Solution and electrospun mat composition.* *67*

Table 5.1. *Fiber diameters (mean ± standard deviation) obtained for scaffolds prepared from PET and PET/C solutions, at different chitosan concentrations (2, 4, and 6 wt.%, corresponding to PET/C ratios of 15:1, 7.5:1, and 5:1, respectively) and MW, and for selected cross-linked fibers (CL). Abbreviated designations for each scaffold are also shown and will be used throughout the text. Different superscript letters within a column indicate significant differences (P < 0.05).* *116*

Table 5.2. *WCA (mean ± standard deviation) and drop life time for PET and PET/C scaffolds. Different superscript letters within a column indicate significant differences (P < 0.05).* *122*

Table 6.1. *Experimental groups of incisional hernia repair.* *140*

Table 6.2. *Occurrence rate (%) of complications during postoperative period (PO) and euthanize day (E).* *146*

Abbreviations

3D	Three-dimensional
ANOVA	Analysis of variance
AS	As-electrospun
CL	Cross-linked fibers
CLSM	Confocal laser scanning microscopy
DAPI	4',6-diamidino-2-phenylindole
DL	Double layer
ECM	Extracellular matrix
EdU	5-ethynyl-2'-deoxyuridine
EGF	Epidermal growth factor
FBGC	Foreign body giant cells
FGF	Fibroblast growth factor
FITC	Fluorescein isothiocyanate
FTIR	Fourier transform infrared spectroscopy
HE	Hematoxylin and eosin
HFIP	1,1,1,3,3,3-hexafluoro-2-isopropanol
MN	Mononuclear
MTS	3-(4,5-dimethylthiazol-2-yl)-5-(3-carboxymethoxyphenyl)-2-(4-sulfophenyl)-2H-tetrazolium
MTT	3-(4,5-dimethylthiazol-2-yl)-2,5-diphenyl-tetrazolium bromide
MW	Molecular weight
PBS	Phosphate buffer solution
PLA	Polylactic acid
PCL	Policaprolactone
PDGF	Platelet derived growth factor
PEO	Poly(ethylene oxide)
PET	Polyethylene terephthalate

PHB	Poly(3-hydroxybutyrate)
PHBV	Poly(3-hydroxybutyrate-*co*-3-hydroxyvalerate)
PI	Propidium iodide
PMN	Polymorphonuclear
PVA	Polyvinyl alcohol
PVP	Polyvinyl pyrrolidone
RGD	Arginine-glycine-aspartic acid
SEM	Scanning electron microscopy
TCP	Tissue culture plate
TFA	Trifluoracetic acid
TGF-β	Transforming growth factor beta
VEGF	Vascular endothelial growth factor
WCA	Water contact angle

Preface

One of the biggest challenges of biomaterials development is to integrate knowledge from different scientific fields such as chemistry, pharmacology, materials science, biology, and medicine. From the raw material to the final design, there is a long journey to be travelled before obtaining a biomaterial with characteristics that matches specific requirements for a certain application. This development process includes several steps since the first experiments on the lab bench until the last clinical trials. This PhD research comprises the first exploratory phases of the development of electrospun materials with application in the tissue engineering field. We have focused on two main nanofibrous systems: a biodegradable one based on a bacterial polyester, poly(3-hydroxybutyrate-*co*-3-hydroxyvalerate) (PHBV), and a non-degradable based on a synthetic polyester, polyethylene terephthalate (PET). In both systems chitosan was added as a tool to manipulate morphological, physico-chemical, and biological features of the biomaterials. The electrospinning fabrication process and the properties of the nanofibrous materials such as morphology, biodegradability, and surface properties were studied. Fibroblasts were selected to analyze the behavior of cells when cultured on the scaffolds, since they are the most abundant cells of connective tissue and they play a determinant role not only in the wound healing of skin, but in several other body processes. Viability, adhesion, spreading, proliferation, ECM secretion, and dead of cells cultured on the scaffolds were studied *in vitro*, and *in vivo* models were applied as preliminary tests to evaluate the performance of those materials in specific applications.

The main objectives of this thesis are:

I. To develop PHBV/chitosan (PHBV/C) electrospun hybrid mats suitable for skin engineering applications;

II. To incorporate bioactive extracts from *Aloe barbadensis* and *Ilex paraguariensis* in the PHBV/C blends and to study their effects on cell behavior and wound healing process;

III. To manipulate the chemical composition and architecture of non-biodegradable PET/chitosan (PET/C) scaffolds and to study their effects on L929 cell behavior;

IV. To study the performance of an electrospun mat of PET as a non-absorbable wound dressing membrane;

V. To evaluate the potential of PET and PET/C non-degradable electrospun mats as abdominal meshes for incisional hernia repair.

This thesis is organized in seven chapters. The **first Chapter** presents a bibliographic review of the main issues treated in this thesis including the electrospinning process and some key topics in the biomaterials and tissue engineering fields. In the subsequent 2 chapters, the development of biodegradable materials with application in skin engineering is reported. Indeed, in **Chapter 2** we describe the development of a new hybrid nanofibrous material of PHBV and chitosan with potential of application in the wound healing process. Several issues were studied, including the optimization of the electrospinning process, the characterization of hybrid mats, and the evaluation of their potential as scaffolds for skin engineering using both *in vitro* and *in vivo* methodologies. The PHBV/C blend that exhibited the best performance for skin engineering purposes was selected as the basis of the dual-fiber mats developed in **Chapter 3**. In this chapter, our main purpose was to develop a dual syringe electrospinning system with one aqueous polymer solution that allows the incorporation of herbal extracts. Phytochemical extracts from *Aloe barbadensis* and from *Ilex paraguariensis* with biological activities in the wound healing process were chosen.

In Chapter 4 the application of an electrospun mat of PET as a removable wound dressing material is discussed and **Chapter 5** is dedicated to the development of non-degradable fibrous scaffolds made of PET and chitosan. In a similar approach to that of Chapter 2, we studied the nanofibers production by electrospinning, the characteristics of the electrospun mats, and we evaluated the potential of these materials in tissue engineering with *in vitro* cell culture studies. **Chapter 6** reports the application of PET and PET/C hybrid mats as meshes for abdominal defects repair.

Finally, **Chapter 7** is devoted to the main conclusions as well as some suggestions for future work.

1. Bibliographic Review

1.1. Biomaterials

A biomaterial is defined as any substance (other than a drug) or combination of substances, synthetic or natural in origin, which can be used for an extended period of time, as a whole or as a part of a system which treats, augments, or replaces any tissue, organ, or function of the body (Boretos and Eden 1984).

Polymers are the most widely used materials in the biomedical field. Because of their easy manufacturability and good processability, as well as the wide range of mechanical, chemical, and physical properties available, polymers are often the material of choice in medical applications. Numerous polymeric biomaterials are currently available in the market, including orthopedic prosthesis, abdominal meshes, vascular grafts, scaffolds for tissue engineering, breast implants, contact lens, sutures, and wound dressings.

Synthetic polymers are by far the most used in biomaterials due to their mechanical properties, thermo stability and easy processability. Nevertheless, there has been an increasing interest in natural polymers, mainly because of their biocompatibility and biofunctionality. Blending synthetic and natural polymers has been an alternative approach to obtain materials with increased mechanical and biological performances, compared with those of single components.

Many techniques have been used to fabricate a broad variety of polymeric biomaterials. Among them, electrospinning has become an outstanding technology for the fabrication of micro and nanofibrous materials. The following subsection provides a brief review of the electrospinning process and the production of nanofibrous biomaterials with application in medicine.

1.2. Electrospinning

Electrospinning technique uses an electric field to produce micro and nanofibers from a polymeric solution. Although it was first patented in 1934 by Formhals (Formhals 1934), electrospinning has only become popular in the 90s. In fact, the growing interest in nanotechnology and the search for new materials have reintroduced this technique. Since then, most of the research effort has focused on exploring what polymers can be

electrospun and on optimizing the nanofiber production towards specific applications. Numerous polymers have been successfully electrospun into nanofibers including synthetic polymers such as polyvinyl alcohol (PVA), poly(ethylene oxide) (PEO) and polylactic acid (PLA), and biopolymers, *e.g.* collagen, silk, and chitosan (Koski *et al.* 2004; Jin *et al.* 2002; Kenawy *et al.* 2002; Chen *et al.* 2008).

The standard configuration of the electrospinning system consists of a high voltage power supply, a syringe pump with a syringe and a metallic needle, and a grounded collector. During the electrospinning process, a high voltage current is applied to create electrically charged jets of a polymeric solution. As these jets travel from the needle tip to the collector, the polymer molecules are stretched and the solvent evaporates generating fibers. Usually, these fibers are collected as nonwoven fibrous mats on a static or rotating collector. The electrospun mats are characterized by a high porosity, small pore sizes with an interconnected structure, and a large surface area per unit volume. These characteristics have made the electrospun mats attractive in a variety of applications, including filtration (Shin *et al.* 2005; Gopal *et al.* 2006), protective clothing (Schreuder-Gibson *et al.* 2002), and biomedical applications (*e.g.,* tissue engineering scaffolds, vascular grafts, and drug delivery systems) (Barnes *et al.* 2007; Khil *et al.* 2005; Chen *et al.* 2006; Ma *et al.* 2005; Powell and Boyce 2008; Sikareepaisan *et al.* 2008).

Versatility is one of the most important advantages of electrospinning technique. Different morphologies can be achieved by varying configuration and parameters of the electrospinning process. Creative electrospinning setups have been developed in order to obtain mats with distinctive characteristics such as aligned (Li *et al.* 2003), porous (Hsu and Shivkumar 2004), hollow (Li and Xia 2004), and core-shell nanofibers (Sun *et al.* 2003). Furthermore, many systematic studies have brought advances in the knowledge of the governing parameters of the electrospinning process. In spite of it, optimizing the electrospinning system is still a laborious task due to the high number of parameters that affect the process and the interdependence among them. Even more, the electrospinning setup and the parameters optimization are tightly related to the polymer and solvent system. Nevertheless, some general principles about the parameters that affect the electrospinning process will be discussed in the following section.

1.2.1. Governing parameters of the electrospinning process

The chemical composition of the electrospinning solution is the key component of the physico-chemical, mechanical, and biological properties of the electrospun mat. The intrinsic proprieties of the selected polymers reflect on the final characteristics of the electrospun mat, while the nanofibrous arrangement brings unique features to the material. Varying concentration and molecular weight (MW) of the polymer are the most effective way to control the morphology of the electrospun mats, especially the diameter of the fibers. Rising concentration and MW increases the fiber diameter as a result of the increase in solution viscosity. The diameter of PET nanofibers, for example, augmented from 201 nm to 729 nm by changing the solution concentration from 10 wt.% to 30 wt.% (Veleirinho *et al.* 2008). Koski *et al.* (2004) have reported augmented PVA fiber diameters from 250 nm to 2 μm, by increasing the polymer concentration and MW .

In case of polymer blends, changing the polymer ratio can be a strategy to modify not only the morphology but also mechanic and physicochemical characteristics of the electrospun mats. For example, by increasing the chitosan concentration in hybrid systems of PVA and chitosan, the electrospinnability and uniformity of fibers have been improved (Lin *et al.* 2006). Modifications on mechanical properties have also been achieved by changing polymer ratio in blends of pullulan and PVA (Karim and Islam 2011). In PVA and quaternized chitosan blends, the increase of chitosan derivative ratio resulted in smaller fiber diameters and higher antibacterial effect (Alipour *et al.* 2009). Another example is the improved hydrophilicity, cell viability, and proliferation of vascular smooth muscle cells in poly (l-lactide)/polyvinyl pyrrolidone (PVP) systems with the increasing ratio of PVP (Xu *et al.* 2009).

The effect of solvent is complex since several properties affect the electrospinning process. In general, solvents with low surface tension, high volatility, and high dielectric constant improve the electrospinnability and decrease the diameter of the electrospun fibers (Veleirinho *et al.* 2008; Chuangchote *et al.* 2009).

Lastly, the operational parameters and the collection conditions also influence the final traits of the electrospun mats. The applied voltage is the most critical parameter as there is a minimum voltage required for the fiber formation according to the polymer/solvent system. Above such value, the increase of applied voltage results, generally, in smaller fiber diameters, as a result of the increased stretching. There are several reports showing a

strong dependence of the fiber collection conditions such as collector distance, humidity, and temperature on the final characteristics of the mats. Amiraliyan *et al.* (2009) have shown that the shape of silk-based nanofibers changed from a circular morphology with smooth surface to flattened with ribbon-like shape with the increase of temperature from 25ºC to 75 ºC. Additionally, Casper *et al.* (2004) have demonstrated the formation of pores on the surface of polystyrene fibers for environmental humidity above 30%.

1.3. Tissue Engineering

Over the past decades tissue engineering has emerged as a field of growing importance with promising solutions for tissue and organ regeneration, and as one of the most important areas for application of electrospun micro- and nanofibrous mats. A general overview of the aims of tissue engineering and the use of electrospun scaffolds in this field is presented subsequently.

Tissue engineering is an interdisciplinary field that combines the knowledge of multiple disciplines, *i.e.* biology, chemistry, materials engineering, and clinical research, towards the development of substitutes that restore or improve the function of a biological tissue. One outstanding strategy has been the use of artificial scaffolds to provide a propitious environment for the regeneration of a certain tissue or organ.

Several attempts have been made to create either biodegradable or non-degradable materials that mimic the complex structure of the natural (cell-derived) extracellular matrix (ECM). Biodegradable scaffolds are thought to support cells for a temporary period, until they produce native ECM components. Numerous biodegradable scaffolds have been developed for different uses *e.g.* skin (Blackwood *et al.* 2008; Lee *et al.* 2007; Huss *et al.* 2010), bone (Kim *et al.* 2006; Yoshimoto *et al.* 2003), and cartilage (Lubiatowski *et al.* 2006) repair. However, in some situations, where a complete regeneration cannot be achieved or when tissue withstands high tensile loads, a long-term non-degradable scaffold is required. Vascular grafts (Ma *et al.* 2005; Blanchemain *et al.* 2005), abdominal wall repair meshes (Klosterhalfen *et al.* 1998), ligament and tendon grafts (Seitz *et al.* 1998; Iannace *et al.* 1995), and bone tissue engineering (Jansen *et al.* 2005) are some examples where non-degradable biomaterials are applied.

Among the several polymers that have been used to produce electrospun mats, PET, PHBV, and chitosan possess several attributes that make them particularly interesting in tissue engineering. These were the polymers used in this thesis and, therefore, further details covering this subject will be reviewed following in this chapter.

1.3.1. Application of polymers in tissue engineering

1.3.1.1. PET

PET is a linear aromatic polyester with remarkable biological features, including biocompatibility and biostability (Moukwa 1997) . PET has long been used in vascular grafts, orthopedic prosthesis, and abdominal meshes, for example. More recently, PET materials have been developed for tissue engineering of bone, cartilage, tendon, and blood vessels (Moreno *et al.* 2011; Neves *et al.* 2005; Lu *et al.* 2005). PET has been successfully electrospun into nanofibers with potential application as scaffolds for blood vessel or bone engineering (Ma *et al.* 2005; Veleirinho *et al.* 2008; Lu *et al.* 2005). Despites the potential of PET nanofibrous mats, few studies are available regarding their application in the biomedical field. Particularly less frequent are the reports describing the biomedical potential of usage of these non-degradable nanofibrous mats based on *in vivo* models. Such an approach is essential taking into consideration the protocols for developing products for human health.

1.3.1.2. PHBV

Polyhydroxyalkanoates are an emerging class of biodegradable polyesters that have been widely studied as an alternative to petroleum based plastics, due to their similarities in mechanical, physical and thermoplastics properties (Avella *et al.* 2000). Moreover, these polymers have shown to be biocompatible and non-toxic turning them also attractive for biomedical applications (Sombatmankhong *et al.* 2007). Among the polyhydroxyalkanoates, poly(3-hydroxybutyrate) (PHB) and its copolymer PHBV have been the most explored in both scientific and industrial fields. Compared to PHB, PHBV is less crystalline, more flexible, and more biodegradable (Avella *et al.* 2000; Chen *et al.* 2002; Chan *et al.* 2004). These characteristics make PHBV especially attractive in the

biomedical field. There are several reports about electrospinning of PHBV, pure or blended with other polymers, including gelatin, collagen, and keratin (Meng *et al.* 2008; Meng *et al.* 2007; Yuan *et al.* 2009; Suwantong *et al.* 2007b). Interestingly, the electrospun nanofibers of PHBV have demonstrate ability to support *in vitro* growth of fibroblast (Suwantong *et al.* 2007b). More recently, *in vivo* animal models have revealed promising results regarding the application of PHBV mats in skin engineering (Han *et al.* 2007; Kuppan *et al.* 2011). However, the cellular responses involved in the skin regeneration process are not enough explored, hampering a more rational strategy for developing skin repair products with technological and economical appeal.

1.3.1.3. Chitosan

Chitosan is a cationic polysaccharide essentially composed by a linear chain of N-acetyl-glucosamine and glucosamine residues linked by β-(1-4) bonds, with a predominance of the non-acetylated residues. Chitosan has been one of the most studied biopolymers in the biomedical field due to its notable proprieties *i.e.* biocompatibility, wound healing effect, anti-inflammatory, and antimicrobial activity (Ueno *et al.* 2001; VandeVord *et al.* 2002; Zheng and Zhu 2003; Ueno *et al.* 1999). Chitosan fibers were successfully produced by electrospinning using concentrated acetic acid (Geng *et al.* 2005) and trifluoracetic acid (TFA) (Ohkawa *et al.* 2004). However, the poor mechanical properties of these fibers have restricted biomedical applications and therefore a number of blends with other polymers have been proposed, *e.g.* chitosan blends with PET (Lopes-da-Silva *et al.* 2009), polylactide (Peesan *et al.* 2006), PVA (Li and Hsieh 2006; Lin *et al.* 2006), and PEO (Duan *et al.* 2004; Spasova *et al.* 2004; Subramanian *et al.* 2005).

When used in polymer blends, chitosan not only improves biological properties of hybrid electrospun mats, but also their morphology, hydrophilicity, and biodegradability (Lin *et al.* 2006; Lopes-da-Silva *et al.* 2009; Peesan *et al.* 2006).

1.3.2. Scaffolds: a provisory environment for cells

The comprehension of the basic phenomena of cell-substratum interaction is claimed as essential for the development of tissue engineering scaffolds. In the subsequent

subsections, a brief review of key aspects of cell adhesion in natural and artificial environments will be presented.

1.3.2.1. Focal adhesion

In their natural environment, anchorage dependent cells adhere to the ECM. The ECM is a network of macromolecules, including proteins and polysaccharides. There are several forms of ECM found in connective tissues such as bone, tendon, and skin. In the skin, for example, EMC is a thin, tough, flexible sheet of macromolecules usually denominated basal lamina. The basal lamina supports the epidermis and is essential for the barrier and mechanical attributes of the skin.

The ECM not only provides support for cells but also participates in numerous cellular events, including attachment, proliferation, communication, differentiation, and morphogenesis (Lukashev and Werb 1998; Brown 2000; Bowers *et al.* 2010; Boudreau and Bissell 1998). Cell adhesion proteins from the plasma membrane, *i.e.* integrins, attach the cell to the external environment and function as a communication gate with a powerful influence on cell behavior. Integrins are heterodimeric glycoproteins composed of two subunits (α and β). The extracellular domain of integrin binds to specific amino acid sequences from ECM proteins. The most important one is the arginine-glycine-aspartic acid (RGD) peptide. The intracellular domain is linked to the β-actin from the cytoskeleton via a complex of proteins that includes talin, vinculin, α-actin, and paxillin. When integrin binds to a ligand, several intracellular events occur initiating different signaling pathways. This is an outside-in regulation, as outside signals modulate intracellular events. Additionally, cells also regulate its interaction with ECM by activating integrin receptors or by changing the conformation of the cytoskeleton (inside-out signaling). In this context, the substratum is an active participant of the cell adhesion process, commanding several cellular events. In anchorage dependent cells, adhesion to a substratum is even more important for cell survival. It is well established that focal adhesion has an anti-apoptotic effect on anchorage dependent cells. In a remarkable study, Chen *et al.* (1997) have shown that cells underwent programmed cell death when spreading was limited to islands of 20 μm of diameter. However, if the spaces among multiple islands were lower than 10 μm, cells were able to spread across the spaces and establish focal adhesion points on the neighbor adhesion islands, switching off apoptosis.

1.3.2.2. Adhesion in artificial substrata

As in natural environment, adhesion of cells to artificial scaffolds is also crucial for the viability and subsequent activities of cells. Scaffolds must provide conditions for cell adhesion and spreading. In the absence of RGD motifs, adhesion initially occurs through proteins adsorbed on the surface of the biomaterial from blood, plasma or serum.

Several strategies have been adopted to improve the adhesion of cells to biomaterials. Coating artificial substrata with ECM components, *e.g.* fibronectin and collagen, has been a common approach (Vo *et al.* 2001; Min *et al.* 2004). Although *in vitro* this procedure is usually successful, the use of proteins bears some disadvantages. Firstly, proteins have to be extracted and purified from organisms and the use of proteins has been many times associated with inflammatory or immune responses. Moreover, interactions with the biomaterial surface can alter the protein conformation, obstructing the cell binding motifs, and hampering the adhesion process. To overcome these limitations, immobilization of RGD motifs on the surface of biomaterials has been another adopted strategy, with several studies reporting an improvement in cell adhesion by immobilization of RGD sequences on electrospun mats (Gentsch *et al.* 2011; Wang *et al.* 2012; Kim and Park 2006). However, mimicking the natural pattern of RGD distribution at the molecular level is a challenging task. Moreover, the RGD motif is not an isolated binding site. The surrounding amino acids, the conformation of the protein, and the distance among RGD residues also influence the adhesion and spreading of the cell. Even more, the distribution and arrangement of ECM on natural proteins depends on the cell type. Providing an attachment that allows and stimulates ECM synthesis and deposition in the scaffold may be a preferable strategy. An improved biocompatibility and adhesion could be achieved since cells would produce ECM according to their own needs. Additionally, ECM deposition, as well as cell proliferation, could occur in parallel to the biodegradation of the scaffold, replacing the provisory substratum with the regenerated tissue.

Architecture ultimately determines the cell-scaffold interactions and the functionality of the regenerated tissue. Porosity, distribution and pore size of biomaterials affect cell behavior, *i.e.* morphology, attachment, differentiation, and function (Ng *et al.* 2009; Kasten *et al.* 2008; Papenburg *et al.* 2009). Fiber diameters and orientation are also thought to have an important effect on the potential of fibrous scaffolds as substratum for cells (Yang *et al.* 2005; Moroni *et al.* 2006). For instance, for poly(D, L-lactic-*co*-glycolic acid)

electrospun scaffolds, Bashur *et al.* (2006) showed that the fibroblast area increased with the augment of fiber diameter from 0,14 μm to 3.6 μm, but proliferation was not sensible to fiber diameter. On the other hand, Badami *et al.* (2006) revealed an increase of osteoblastic cells density on PLA fibrous scaffolds, with the enlargement of fiber diameter from 0.14 μm to 2.1 μm. In a recent paper, Lowery *et al.* (2010) showed a faster rate of proliferation of human dermal fibroblasts in policaprolactone (PCL)/PEO nanofibers for pore diameters greater than 6 μm. Also, when the pore diameter changed from 12 μm to 23 μm cells tended to adhere to single fibers instead of multiple ones. Thus, as a general remark, the ideal design of a scaffold is always dependent on its composition and application and the manipulation of its architecture constitutes an important tool to control scaffold-cell interactions and, ultimately, to obtain the best design for a certain application.
The regeneration of skin has been an important target for tissue engineering. In this context the morphology of the electrospun nanofibrous scaffolds is particularly relevant for skin repair. In the following sections the application of electrospun mats for the treatment of skin will be discussed.

1.3.3. Skin engineering

The skin is the largest organ of the human body and constitutes the major physical barrier to external pathogens, as well as mechanical, chemical, thermal or radiation insults. The skin also controls the body temperature and prevents the loss of body fluid. Several metabolic pathways such as the vitamin D synthesis take part in the skin. It is also the main sensory organ, richly supplied by nerve terminals and receptors for touch, temperature, and other stimuli.
The skin is composed of two main layers, the epidermis and the dermis. The epidermis comprises several layers of keratinocytes fusing together and establishing an effective barrier against the outside environment. Three less abundant cells, *i.e.* melanocytes, Langerhans cells, and Merkel cells, are also found in the epidermis. The dermis consists of vascularized connective tissue with abundant ECM, especially collagen. It is normally subdivided in two sub layers, the papillary and the reticular layers. The first one is more cellular and has thin and less organized collagen arrangement. The reticular dermis is

mostly composed by bundles of tick collagen fibers aggregated. The dermis contains several appendages including hair follicles, sweat, and sebaceous glands.

1.3.3.1. Wound healing

In case of injury, when the skin barrier is destroyed, the body immediately initiates a complex wound healing process. The duration of this process depends on the extension of the damage; nevertheless, wound healing is typically divided in four phases: hemostasis, inflammation, proliferation, and maturation. These phases are not strictly separated events; on the contrary, they overlap each other.

The wound healing process begins with hemostasis. The main purpose of hemostasis is to control bleeding. This is achieved by a rapid vasoconstriction, followed by platelets aggregation in order to provide a provisionary plug. The coagulation cascade is then initiated to form the fibrin clot. The coagulation cascade is a series of enzymatic reactions in which prothrombin is activated into thrombin and thrombin converts fibrinogen to fibrin. Fibrin is then cross-linked, resulting in a polymeric mesh with platelets embedded that constitutes the fibrin clot.

The fibrin clot protects the wound against external contaminants and serves as a provisional matrix during the repair process. The fibrin clot has also an important function in signaling further events of the healing process since it provides numerous cytokines and growth factors. The most important ones are platelet derived growth factor (PDGF) and transforming growth factor beta (TGF-β). PDGF attracts neutrophils, macrophages, fibroblasts, and smooth muscle cells to the wound site and also stimulates the proliferation of fibroblasts and smooth muscle cells. In its turn, TGF-β has an important function in attracting and activating macrophages.

The degranulation of platelets triggers the recruitment of inflammatory cells to clean the wound. This is the beginning of the inflammatory phase, which can be macroscopically identified by redness, heat swelling, and pain. Vasodilation and increased permeability of blood vessels occur to facilitate plasma proteins and leucocytes penetration in the wound area. Polymorphonuclear (PMN) cells, mainly neutrophils, are the first cells to arrive at the wound site, usually four hours after injury. The main role of these cells is to eliminate bacteria, debris, and foreign bodies. Despite the rapid action of neutrophils, the activity of these cells is strictly associated to damages in the surrounding tissues. Mononuclear (MN)

cells, especially monocytes, arrive in the wound site approximately 48 hours after injury. Monocytes are activated into macrophages, a key cell on the wound repair process. Macrophages continue to clean the wound by phagocytosis and by secreting cytokines and growth factors, including PDGF, fibroblast growth factor (FGF), tumor necrosis alpha, and interleukin I.

During the proliferative phase, fibroblasts are activated, proliferate and start to produce and secrete collagen, which replaces the provisional ECM. The granulation tissue is characterized by a high density of new blood vessels as a result of the intense angiogenesis. Angiogenesis is essential for the nutrition of the developing tissue and is stimulated by several growth factors including vascular endothelial growth factor (VEGF), FGF and TGF-β that are secreted by fibroblasts, macrophages, epidermal, and endothelial cells. Simultaneously, re-epithelialization is stimulated by epidermal growth factor (EGF) and transforming growth factor alpha that are produced by macrophages, platelets, and keratinocytes. Re-epithelialization occurs as a result of keratinocytes proliferation and migration from the wound edges and skin appendages towards the center of the wound.

Wound contraction is another important phenomenon in the wound closure process. During contraction the surrounding skin is pulled toward the wound in order to decrease the wound site without the need of new tissue formation. Although contraction is important for a rapidly closure, a decrease in function of the tissue is usually a consequence of this phenomenon.

Remodeling of tissue initiates during the proliferative phase and persists for weeks, months or years. During remodeling the cellularity of the granulation tissue gradually decreases as a result of cell apoptosis. Additionally, a series of rearrangements of ECM take place, *i.e.* changes in the ratio of various collagen types, fibril arrangement, and cross-linking of collagen in order to maximize the tissue strength.

The consequence of wound repair is a scar, which is brittle, less elastic than normal skin, and does not contain skin appendages.

1.3.3.2. Impairment of wound healing

Several conditions can lead to prolonged healing times or even to a failure of wound healing process. Upon such conditions, wounds are classified as chronic wounds. The factors that contribute to the non-healing condition of these wounds include foreign bodies,

infection, pressure, advanced age, diabetes, or other chronic diseases. The most common chronic wounds are venous ulcers, pressure ulcers, and diabetic foot ulcers.

The major goal of skin engineering is to develop strategies to help the body to complete the regeneration when a given clinical condition hampers the normal healing process. A common approach has been the use of biodegradable scaffolds to sustain and guide cellular growth through the regeneration process. The scaffold role is to provide an artificial environment for cell adhesion, migration, and spread thus allowing the cell proliferation and ECM synthesis.

1.3.3.3. Electrospun mats as scaffolds for skin engineering

Several characteristics of the electrospun mats are attractive for skin engineering. These includes:

- Architecture and dimensional similarity with the ECM structure;
- Ability to promote attachment, migration, and proliferation of cells, such as fibroblasts and keratinocytes;
- The microporous structure that confers protection against bacteria and other contaminants and allows gas exchanges while maintaining a moist environment;
- The high surface area to volume ratio, which enhances the ability to absorb exudate;
- The possibility to make fibers of functional polymers or add bioactive compounds in the polymeric mesh. Even more, a system with controlled release of bioactive compounds can be developed.

Several electrospun mats have been proposed as wound dressing materials including polyurethane (Khil *et al.* 2003), collagen/chitosan (Chen *et al.* 2008; Ma *et al.* 2003), chitosan/ polyethylene glycol (Tchemtchoua *et al.* 2011), PVA/silver (Hong 2007), and water-soluble carboxyethyl chitosan/PVA (Zhou *et al.* 2008) mats. Additionally, electrospun mats for controlled release of drugs (Katti *et al.* 2004) or even herbal extract (Sikareepaisan *et al.* 2008) have also been developed. Incorporation of growth factors such as FGF (Yang *et al.* 2012) and EGF (Choi *et al.* 2008) or angiogenesis factors (Kuppan *et al.* 2011) has successfully improved the wound healing process, even in diabetic animals. More refined approaches, such as co-culture of hair follicular epithelial and dermal cells on

PHBV based mats have also demonstrated great potential in the wound healing treatment (Han *et al.* 2007).

Despite the enormous research progress over the past decades, the development of electrospun scaffolds for skin engineering is still in the laboratory phase. The current scenario of increasing age-related problems and chronic diseases urge for new cost-effective solutions to treat extensive or chronic wounds.

1.4. Concluding remarks

Electrospinning has attracted the interest of researchers from different fields as a simple and versatile technique to produce nanofibers with a wide range of application in medicine. Many studies have improved the knowledge of the electrospinning process and different approaches have confirmed the potential of the electrospun materials in the biomedical field. Despites all the promising results, much remains to be studied, particularly the design of strategies to manipulate the morphological characteristics of the electrospun mats. Also, the development of hybrid systems of natural or synthetic polymers with superior features is still a wide-open subject. Other interesting but poorly explored approach is the combination of polymers with plant extracts through electrospinning. The key challenge in this issue is to point out solutions for replacing the organic solvents usually required, thus allowing the incorporation of bioactive compounds without losing activity. Moreover, *in vitro* studies regarding the development of non-degradable scaffolds are particularly scares. Besides, a deeper characterization of the inflammatory tissue response to these new nanodimensional materials is also recognized as fundamental for future technological applications. The use of electrospun mats as prosthetic abdominal wall substitutes, for example, is a promising alternative that has never been reported. Lastly, studies regarding cell nanofibers interactions, *i.e.* cell adhesion, spreading, and proliferation, as well as apoptotic or necrotic death of cells when cultivated on these scaffolds are indispensable for achieving a successful design.

2. Electrospun PHBV/chitosan blends as scaffolds for skin engineering

2.1. Introduction

Among all the applications of the electrospinning technique, the fabrication of scaffolds for tissue engineering is probably the one that attracts the most attention. The morphological and structural similarities between the electrospun structures and the natural ECM make these materials potential substrata for cell growth. Several electrospun scaffolds have been proposed for skin regeneration based on different polymers and their blends (Rho *et al.* 2006; Chong *et al.* 2007; Kumbar *et al.* 2008). In this chapter our main purpose was to develop new hybrid nonwoven scaffolds of PHBV and chitosan to act as cytocompatible temporary templates for cell growth.

As previously mentioned (§1.3.1), PHBV and chitosan are biopolymers with remarkable properties in the biomedical field, including biocompatibility and biodegradability (Avella *et al.* 2000; Chen and Wu 2005). PHBV is a bacterial polyester with good mechanical properties and nonwoven electrospun PHBV fibrous mats have already been produced and revealed (*in vitro*) a better performance for chondrocytes and fibroblasts attachment, growth, and proliferation when compared to their 2D film counterparts (Suwantong *et al.* 2007b; Lee *et al.* 2004). Despite these advantages for biomedical purposes, PHBV applications as scaffold materials for cell colonization are restricted due to its intrinsic hydrophobicity.

A well-known strategy to improve the mechanical and surface properties of the PHBV, and its cellular response, is the blending with other polymers (Sombatmankhong *et al.* 2007; Li *et al.* 2009). Here we followed a similar approach by blending the polyester with chitosan, a hydrophilic and biocompatible biopolymer. As already mentioned, chitosan has been extensively explored for biomedical applications due to its notable properties *i.e.* biocompatibility, wound healing effect, anti-inflammatory, and antimicrobial activities (Liu *et al.* 2011). Recently, chitosan electrospun nanofibers have been demonstrated as advantageous wound-healing biomaterials, improving cell adhesion and proliferation *in vitro* and inducing a fast regeneration of both the epidermis and dermis tissues *in vivo* (Tchemtchoua *et al.* 2011).

PHBV grafted with chitosan and oligochitosans has shown improved protein adsorption and fibroblast attachment *in vitro* (Hu *et al.* 2003a, 2003b). Here, our objective was to

develop hybrid nanofibrous mats that combine PHBV and chitosan and to control the scaffolds architecture and degradation rate through the manipulation of polymer ratio, solvent composition, and chitosan MW.

In addition to epithelial (keratinocytes) and endothelial cells in the skin injury region, other essential cell types are involved in the wound healing process. Amongst them, fibroblasts are a critical cellular element in the proliferative phase (Pitzer and Patel 2011), being involved in the production of ECM constituents as well as growth factors, which are crucial in the subsequent phases of wound healing. Due to the relevance of the fibroblasts for skin healing processes, we have performed *in vitro* studies using L929 fibroblastic cell line to study cell-scaffold interaction, based on adhesion, viability, proliferatiobn, and death. Afterwards, the PHBV/chitosan (PHBV/C) electrospun scaffolds were tested *in vivo* using a rat skin full-thickness wound model.

2.2. Experimental

2.2.1. Materials

PHBV (12 wt.% poly (3-hydroxyvalerate) content) and chitosan (medium MW, 85% deacetylated) were purchased from Sigma-Aldrich Chemical Company. All chemicals were of analytical grade and obtained from Sigma-Aldrich Chemical Company. All biological supplies were purchased from Invitrogen (Invitrogen Grand Island, NY, USA) unless otherwise noted.

2.2.2. Oxidative depolymerisation of chitosan

Chitosan samples with varying MW were obtained by oxidative depolymerisation (Tommeraas 2001). Briefly, a solution of 7.5×10^{-3} M $NaNO_2$ was added to a 1% chitosan solution in 0.1 M acetic acid and allowed to react under N_2 gas at room temperature. After moderate stirring for 45 minutes and 180 minutes, 0.1 M NaOH was added to the reaction mixture up to pH=8. After centrifugation, the precipitate was washed with water/ethanol mixtures of increasing ethanol concentration until neutrality, followed by acetone. Samples

were dried in an oven at 35°C for 12 hours. The two different reaction times were selected to originate chitosan samples with different and desired MW, based on previous reported results (Lopes-da-Silva *et al.* 2009).

The MW was calculated using the MarkHouwink–Sakurada equation proposed by Kasaai *et al.* (2000). The relative viscosities in 0.25 M acetic acid/0.25 M sodium acetate were measured using a Cannon-Fenske capillary viscometer at 25.0 ± 0.1 °C. The intrinsic viscosity was determined by extrapolating to infinite dilution, using the combined Huggin's and Kraemer's equations (Santos *et al.* 2006).

2.2.3. Preparation of electrospinning solutions

In order to prepare the electrospun mats, 20 mL of polymer solutions (total polymer content = 10% w/v) of several PHBV/C ratios (5:0, 4:1, 3:2, 2:3, 1:4, and 0:5 w/w) in blends of TFA/ 1,1,1,3,3,3-hexafluoro-2-isopropanol (HFIP) (3:7 and 1:1 v/v) were prepared. For that, chitosan was dissolved in the selected solvent mixture for 24 hours, followed by PHBV addition and dissolution for another 24 hours. Three chitosan samples with distinct MW (§ 2.2.2.) were tested.

2.2.4. Optimization of the electrospinning process

Electrospinning was performed using a typical experimental set up, that consisted on a syringe with a metallic needle, a syringe pump (Harvard apparatus PHD 2000), a high-voltage power supply (Spellman CZE 1000R), and a grounded rotating collecting drum (**Figure 2.1**). The operational parameters of the electrospinning process (applied voltage, solution flow rate, needle to collector distance, and collector rotation speed) were optimized in order to obtain nanofibrous mats free of beads or clusters. Fibers were collected as nonwoven mats, on the rotating drum in air and at room conditions (20 ± 2ºC, 45–50% relative humidity).

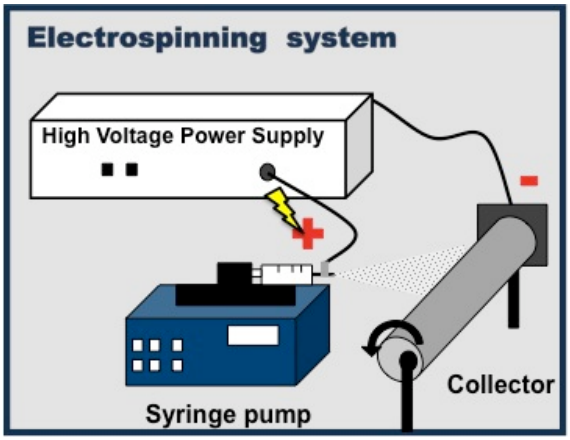

Figure 2.1. Illustrative representation of the electrospinning system.

2.2.5. Characterization of electrospun mats

2.2.5.1. Morphology

Morphology and diameter of the nanofibers were analyzed by scanning electron microscopy (SEM, Hitachi S4100) at an accelerating voltage of 25 kV. The average fiber diameters were calculated from 100 measurements, using the SEM images and appropriate software (Image J 1.37c, Wayne Rasband, National Institute of Health, USA).

2.2.5.2. *In vitro* degradation

For *in vitro* degradation tests, mats were cut into squares (1x1 cm^2) and dried at 45 °C for 24 hours and then in a desiccator in vacuum at room temperature for 1 hour. Each specimen was accurately weighed and introduced in 100 mL phosphate buffer solution (PBS, pH 7.4) and incubated for a requisite time at 37ºC, under moderate stirring. Samples were removed from the solution at different intervals (1, 3, 12, 24, 48, 168, 336, 504, and 672h), washed with distilled water, dried and weighed. The % mass lost was calculated based on initial and final mass of the specimen. Morphological changes were examined by SEM.

2.2.5.3. Attenuated total reflection-Fourier transform infrared spectroscopy (ATR-FTIR)

The nanofibrous mats were characterized by ATR-FTIR, using a Golden-gate single reflection ATR in a Bruker IFS-spectrometer at a resolution of 8 cm^{-1} and 256 co-added scans.

2.2.5.4. Biological *in vitro* studies

Mouse fibroblast cells (L929) were cultured in Dulbecco's Modified Eagle's Medium supplemented with 10% fetal bovine serum, 10 mM HEPES, 2mM L-glutamine, 100 units/mL penicillin, and 100 g/mL streptomycin. The medium was replaced every 48 hours and all the cultures were maintained at 37 °C in a wet atmosphere containing 5% CO_2. When the cells reached 70% confluence, they were treated with 0.25% trypsin containing 1mM EDTA and counted by a hemacytometer prior to use. Scaffold pieces with an average thickness of 0.5 ± 0.2 mm were selected to perform the *in vitro* cell culture studies. Previously to biological assays, all scaffolds were sterilized under UV light for 1 hour (both faces) and immersed in ethanol 70% (v/v) for 30 minutes. All the experiments were performed in triplicate, unless otherwise stated.

2.2.5.4.1. Indirect cytotoxicity assay

The indirect cytotoxicity evaluation of scaffolds was adapted from ISO 10995-5. Scaffold pieces (4 mm diameter) were placed in a 96-well tissue culture plate (TCP, Techno Plastic Products) and incubated at 37 °C in fresh culture medium for 24 hours to prepare the extraction media (100 µL/well). L929 cells were seeded in empty wells (2 x 10^3 cells/well). After an attachment period of 24 hours, the culture medium was removed, replaced with the extraction medium of each specimen, and the cells were further incubated. Fresh medium was used as control. After 24 hours, the extraction medium was removed and the viability of cells was determined by the 3-(4,5-dimethylthiazol-2-yl)-2,5-diphenyl-tetrazolium bromide (MTT) assay. 100 µL of MTT solution (0.5 mg/mL) in fresh medium was added to each well and incubated for 2.5 hours at 37 ºC. After discarding the culture medium, 200 µL of dimethyl sulfoxide was added to dissolve the intracellular crystalline formazan product. The absorbance at 540 nm was read by spectrophotometry using a

microplate reader (TP-Reader, Thermoplate). The results were expressed as a percentage of the absorbance of control (n=24).

2.2.5.4.2. Cell viability

Cell viability was evaluated by the 3-(4,5-dimethylthiazol-2-yl)-5-(3-carboxymethoxyphenyl)-2-(4-sulfophenyl)-2H-tetrazolium (MTS) assay. L929 cells were seeded on sterile scaffold pieces (24-well plates, 1 x 10^5 cells/well) and incubated at 37 °C in a wet atmosphere containing 5% CO_2 for 2, 7, and 14 days. MTS solution (Promega) was added and cells were incubated for 2 hours in the dark, at 37ºC. Absorbance at 490 nm was measured using a plate reader (TP-Reader, Thermoplate).

2.2.5.4.3. Cell adhesion, spreading, and proliferation

SEM and confocal laser scanning microscopy (CLSM) were used to study cell adhesion, morphology, spreading, and proliferation on the scaffolds. For that, L929 cells were seeded on sterile scaffold pieces (24-well plates, 1 x 10^5 cells/well) and incubated at 37 °C in a wet atmosphere containing 5% CO_2 for 12 hours, 2 days and 7 days. For SEM analysis cells were fixed with 2.5% glutaraldehyde solution in PBS, dehydrated in increasing concentrations of ethanol (80, 90, and 100% (v/v)) and dried in air for 12 hours. Samples were mounted in aluminum stubs and sputter-coated with gold prior to observation in a scanning electron microscope (JEOL JSM-6390LV) with an accelerating voltage of 10 kV. For CLSM analysis, cells were fixed with 3.7% paraformaldehyde in PBS. Actin filaments were stained with Alexafluor 546 conjugated to phalloidin (A22283, Invitrogen). Vinculin was labeled with mouse monoclonal antibody (90227, Millipore) followed by Alexafluor 488 goat anti-mouse IgG conjugated as secondary antibody (A11029, Invitrogen). Extracellular fibronectin was immunolabeled with mouse monoclonal antibody anti-fibronectin (SC-271098, Santa Cruz Biotech) followed by Alexafluor 488 goat anti-mouse IgG conjugated (A11029, Invitrogen). DNA was stained with 1 mg/mL of 4',6-diamidino-2-phenylindole (DAPI). Scaffolds were mounted on slides in ProLong Gold antifade reagent and covered with a coverslip. The cells were analyzed using a confocal laser-scanning inverted microscope (Leica DMI6000 B Microscope). L929 cell outlines were traced from CLSM pictures and the cytoskeleton areas were measured using the ImageJ software (n>50).

Cell proliferation was also evaluated with 5-ethynyl-2'-deoxyuridine (EdU) incorporation assay. L929 cells were seeded (1 x 10^5 cells/well) on sterile scaffold pieces (24-well plates; treated group) or in TCP (control group), and incubated at 37 °C in a wet atmosphere containing 5% CO_2 for an attachment period of 12 hours. EdU was added to the culture medium (10 μM) and incubated for 4 hours. Further, fixation, permeabilization, and EdU staining, were carried out according to the kit's protocol (Click-iT EdU Alexa Fluor 488 Imaging Kit, C10337, Invitrogen,). Cell nuclei were stained with DAPI. Cells were analyzed by fluorescence microscopy (Olympus BX41 Fluorescence Microscope) and the percentage of proliferative cells was calculated from 10 random captured fields (total magnification 100x) from three independent experiments.

2.2.5.4.4. Annexin V and propidium iodide (PI) staining

L929 cells were seeded on sterile scaffold pieces (24-well plates, 1 x 10^5 cells/well) or control, *i.e.* TCP, and incubated for 48 hours. The culture supernatant (which contained some floating cells) was collected and the adherent cells harvested by a brief trypsinization. The two fractions were combined, centrifuged, and resuspended in fresh medium. Cells were labeled with annexin V- fluorescein isothiocyanate (FITC) (Immunostep SL) and PI and analyzed in a flow cytometer FACSCanto II (Becton Dickinson). 10000 events were collected for each sample. Data were processed using FlowJo 7.6.5 software (Tree Star, Ashland, OR, US) and the percentages of cells gated were calculated from at least three separate experiments.

2.2.5.5. Wound healing assay

The wound healing experiment was approved by Animal Ethics Committee of Federal University of Santa Catarina (UFSC, PP0531). Male Wistar rats 2 months age and weighting 250-300 g were obtained from the Central Biotery of UFSC.

Animals were anesthetized with an intramuscular injection of ketamine (90 mg/kg) and xylazine (15 mg/kg). After shaving, 4 incisional full-thickness wounds were made in the dorsum of each animal using a sterile surgical scalpel blade (**Figure 2.2**). Sterile PHBV/C scaffold pieces (1.0 x 1.0 cm) were implanted on the top of the wound. Tegaderm® (3M, St. Paul, MN, US) was used as control. Treatments were alternately distributed on each quadrant. After anesthesia recovery, animals were placed in individual

cages and observed during the total period of experiment.

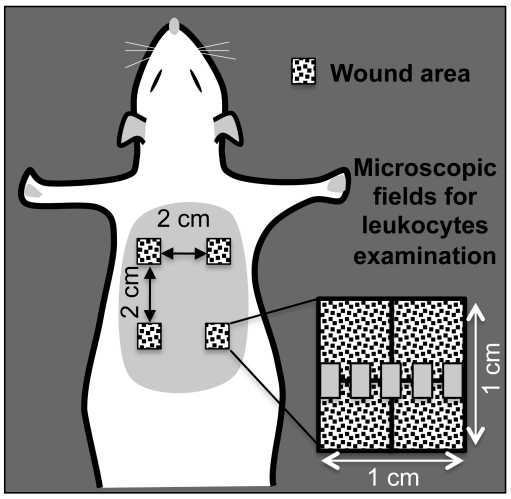

Figure 2.2. Schematic illustration of wound healing assay in rats.

On days 3, 7, 14, and 21 post-surgery, animals were sacrificed in a carbon dioxide chamber, the wounds were measured with a caliper, and the wound tissues were collected for histological examination. Tissues were fixed in buffered formaldehyde solution (10%, pH 7.2), embedded in paraffin, sectioned at 4 μm thickness, and stained with hematoxylin and eosin (HE). Samples were analyzed under an optical microscope. For leukocyte count and tissue classification, 5 microscopical fields were captured at 400x magnification (Figure 2.2). PMN and MN leukocyte densities were calculated and the tissues were classified as inflammatory infiltrate (mostly composed by inflammatory cells and fibrin clot elements), granulation tissue (high density of fibroblasts and new blood vessels), immature regenerated tissue (with newly synthetized unarranged collagen fibers) or remodeled tissue (presence of skin appendages, mature blood vessels, and arrangement of collagen fibers resembling normal skin tissue).

2.2.6. Statistics

Statistical analysis was carried out using Instat 3.0 (GraphPad Software, San Diego, CA, US). Results were expressed as the mean ± standard deviation and compared through one-

way analysis of variance (ANOVA) and Tukey-Kramer multiple comparisons test. $P < 0.05$ was considered statistically significant.

2.3. Results and discussion

In this chapter we report the preparation of new electrospun hybrid nanofibers of PHBV and chitosan with potential application in the biomedical field. The effects of polymer ratio, chitosan MW, and solvent composition on the morphology of the nanofibers were investigated. Cell culture studies with L929 fibroblasts and an *in vivo* wound healing assay with Wistar rats were performed in order to evaluate the performance of the electrospun mats as scaffolds for skin engineering.

2.3.1. Characteristics of the chitosan samples

In order to obtain chitosan samples with distinct MW, oxidative depolymerization of a commercial sample (1500 kDa, 85% deacetylated) was performed. The MW of chitosan was reduced to 48 kDa after 90 minutes and to 15 kDa after 180 minutes. Those samples with distinct MW (1500, 48, and 15 kDa) were used to prepare the PHBV/C blends for the hybrid mats fabrication.

2.3.2. Electrospinning process optimization

The success of electrospinning, *i.e.* fiber formation from a polymeric solution, depends on the optimization of several electrospinning parameters, including solution and operational ones. This optimization is often a laborious task, due to the high number of variables and their inter-dependence. In this study, the effect of operational parameters, including the applied voltage, the solution flow rate, the needle to collector distance, and the collector rotation on the final fiber characteristics was studied in order to improve the fiber production. The selected values for each operational parameter are presented below:

(1) Applied voltage: The applied voltage was fixed at 22 kV. Above this voltage, the electrospinning system became instable due to the occurrence of sparks on the needle and electric current cuts.

(2) Solution flow rate: The flow rate depends on the maximum amount of polymer that the system is able to stretch. When the feeding rate increases, more solution will be ejected from the needle tip at the same time. When the electric field force is not able to stretch the jet, the superfluous solution is deposited as beads or droplets (Zuo *et al.* 2005). The maximum flow rate reached for this system without beads or droplets formation was 8 μl/min.

(3) Syringe-collector distance: During travelling of the jet from the needle to the collector, solvent has to evaporate, so that fibers could be formed. The minimum distance for adequate solvent evaporation was 14 cm, as bellow this value the solvent reached the collector creating fusion and beads in fibers.

(4) Rotation of the cylinder: Regarding to the collector rotation, a nonwoven fibrous mat, with an essentially random fiber arrangement was produced at 900 RPM.

2.3.3. Solvent effects

As previously mentioned, solvent evaporates during the travelling of the electrospinning jet to the collector. Although it is not present in the final mat, solvent plays a determinant role on the formation and characteristics of electrospun nanofibers.

TFA/HFIP blends were selected as solvent for co-dissolving PHBV and chitosan. Co-solubilization was achieved from TFA/HFIP 3:7 to 1:1 (v/v). The effects of TFA/HFIP ratio on the fiber morphology were analyzed.

The most considerable effect of solvent composition was in the main fiber diameter. In general, main fibers with higher diameters were obtained for TFA/HFIP 3:7 (v/v). For PHBV/C 5:0 (w/w), for example, the average diameter was 115 ± 35 nm for TFA/HFIP 1:1 (v/v) and 227 ± 72 nm for TFA/HFIP 3/7 (v/v). The same effect was observed for the other PHBV/C ratios (as will be discussed in more detail § 2.3.4.2). The increase in the main fiber diameter observed with the increase of HFIP content is explained by the lower dielectric constant and the higher surface tension of this solvent. Solutions obtained from solvents with lower dielectric constants are expected to have a lower conductivity, resulting in a lower jet stretching during its flight to the collector. A higher surface tension also acts against the charged jet stretching, resulting in larger fibers (Tan *et al.* 2005; Uyar

and Besenbacher 2008). Some properties of TFA and HFIP are summarized in **Table 2.1.**

Table 2.1. Solvent properties.

Solvent properties	TFA	HFIP
Molar mass (g/mol)	114.02	168.05
Boiling point (ºC)	72.4	58.2
Density 25ºC (g/mL)	1.48	1.6047
Dielectric constant (20ºC)	42.1	16.7
Surface tension 25ºC (N/m)	0.0134	0.0161
Viscosity 25º C ($X10^{-3}$ Pa s)	0.81	1.64

As it will be described below, solvent composition also affected the relative frequency and the mean diameter of secondary fibers. The mean diameter of secondary fibers increased as the HFIP content decreased. HFIP is a better solvent for PHBV than TFA. So, as HFIP decreases and the PHBV solubility decreases, more PHBV molecules branch off into secondary fibers and, consequently, the diameter of these fibers is increased. More details on this subject will be discussed below.

2.3.4. Effects of PHBV/C ratio and chitosan MW on fiber formation and morphology

The morphology of an electrospun mat is ruled, in the first instance, by solution composition. Defining polymer and solvent is the most effective way to control mat characteristics. In hybrid mats, the polymer ratio has an important effect on the final characteristics of the mats. Here, PHBV/C ratio was varied from pure PHBV until pure chitosan, using as solvents TFA/HFIP 1:1 or 7:3 (v/v), and the effects on fiber characteristics were examined.

2.3.4.1. Formation of nanofibers

Well-defined continuous fibrous structures could be obtained by changing the PHBV/chitosan ratio from 5:0 to 2:3 (w/w), for chitosan 1500 kDa and 15 kDa, while for chitosan 48 kDa, fibers were also formed for a PHBV/C ratio of 1:4 (w/w) (**Table 2.2**).

Table 2.2. Electrospinnability of PHBV/C (10 wt.%) in TFA/HFIP (22 kV of applied voltage, flow rate of 8 μL/min).

TFA/HFIP (v/v)	Chitosan Mw (kDa)	PHBV/C ratio (w/w)					
		5:0	4:1	3:2	2:3	1:4	0:5
3:7	1500		✓	✓	✓	☒	☒
	48	✓	✓	✓	✓	✓	×
	15		✓	✓	✓	×	×
1:1	1500		✓	✓	✓	☒	☒
	48	✓	✓	✓	✓	✓	×
	15		✓	✓	✓	×	×

✓ Complete dissolution; formation of fibers;

× Complete dissolution; fibers were not formed;

☒Polymers were not soluble.

Regarding to the highest MW chitosan, the maximum solubility was 6 wt.% for both solvents tested. The low solubility of this sample limited the production of fibers with higher chitosan contents. For lower MW chitosan samples (15 and 48 kDa), solutions were prepared until a chitosan content of 10 wt.%. Nevertheless, the maximum chitosan content that resulted in formation of fiber was 8 wt.% (PHBV/C $_{48\ kDa}$ 1:4 w/w). Above this concentration, electrospray took place, as chain entanglements were insufficient to form continuous structures, *i.e.* nanofibers, resulting in the spraying of droplets that were deposited on the collector. According to Tan *et al.* (2005), polymer MW plays an important role in determining the minimum polymer concentration to produce fibers via

electrospinning. As the MW decreases, polymer concentration needs to be improved in order to raise polymer entanglements.

2.3.4.2. Morphological characterization of the mats

In general, all mats showed a typical nonwoven nanofibrous structure, with a layer-by-layer deposition of nanofibers, and a high porosity. Nanofibers were predominantly cylindrical, uniform, and free of beads. **Figure 2.3 and 2.4** illustrate the morphology of hybrid fibers as a function of PHBV/C ratio, for two different solvents.

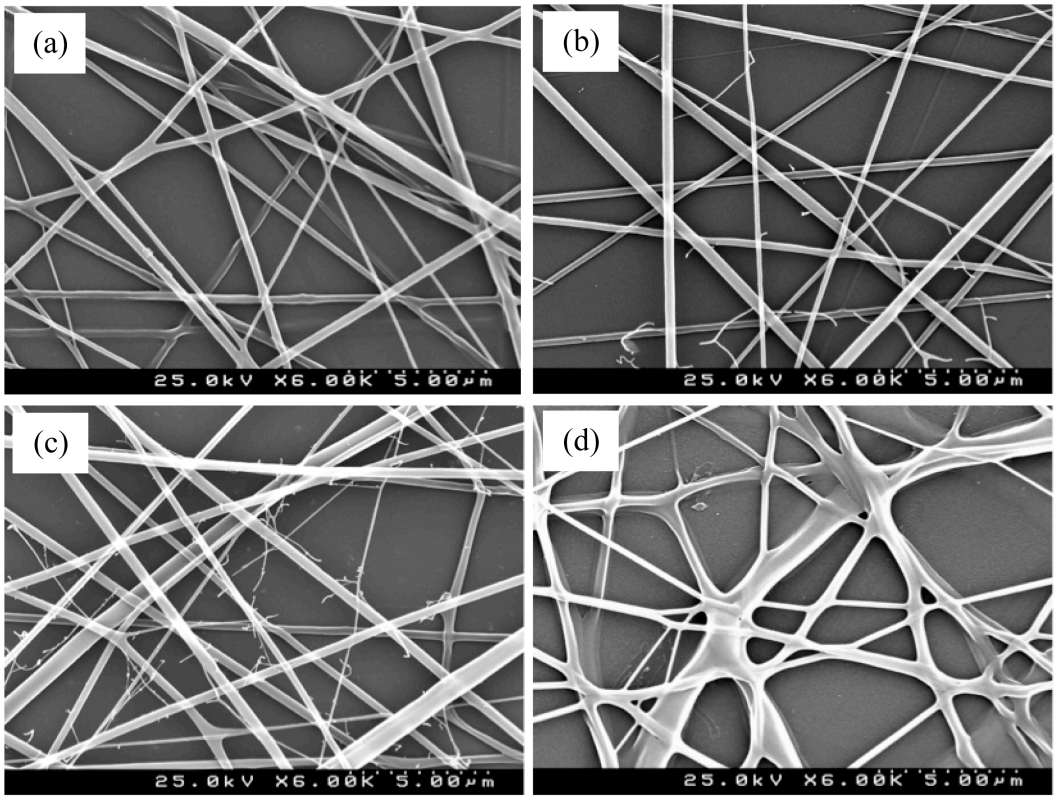

Figure 2.3. SEM images showing the morphology of fibers electrospun from PHBV/C 48 kDa solutions in TFA/HFIP 3:7 (v/v), at different polymer ratios: (a) 4:1 (b) 3:2 (c) 2:3 (d) 1:4 (w/w).

For certain electrospun mats, SEM images revealed the occurrence of ramifications of the backbone fiber, giving rise to secondary fibers, predominantly interrupted, with smaller diameters (Figure 2.3b and 2.3c). The frequency of occurrence of the secondary fibers varied with the PHBV/C ratio and chitosan MW and, as previously mentioned, with the

solvent characteristics. To better understand the fiber branching process, the relative frequency of secondary fibers was calculated for each mat (**Figure 2.5**).

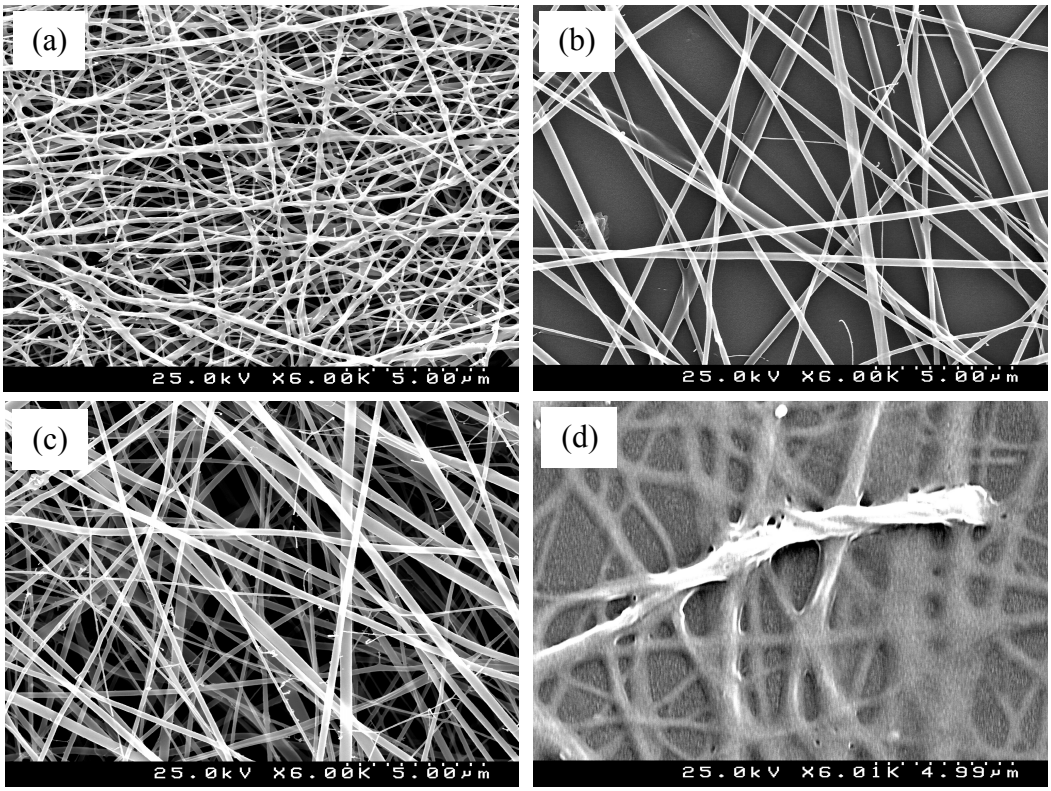

Figure 2.4. SEM images showing the morphology of fibers electrospun from PHBV/C 48 kDa solutions in TFA/HFIP 1:1 (v/v), at different polymer ratios: (a) 4:1 (b) 3:2 (c) 2:3 (d) 1:4 (w/w).

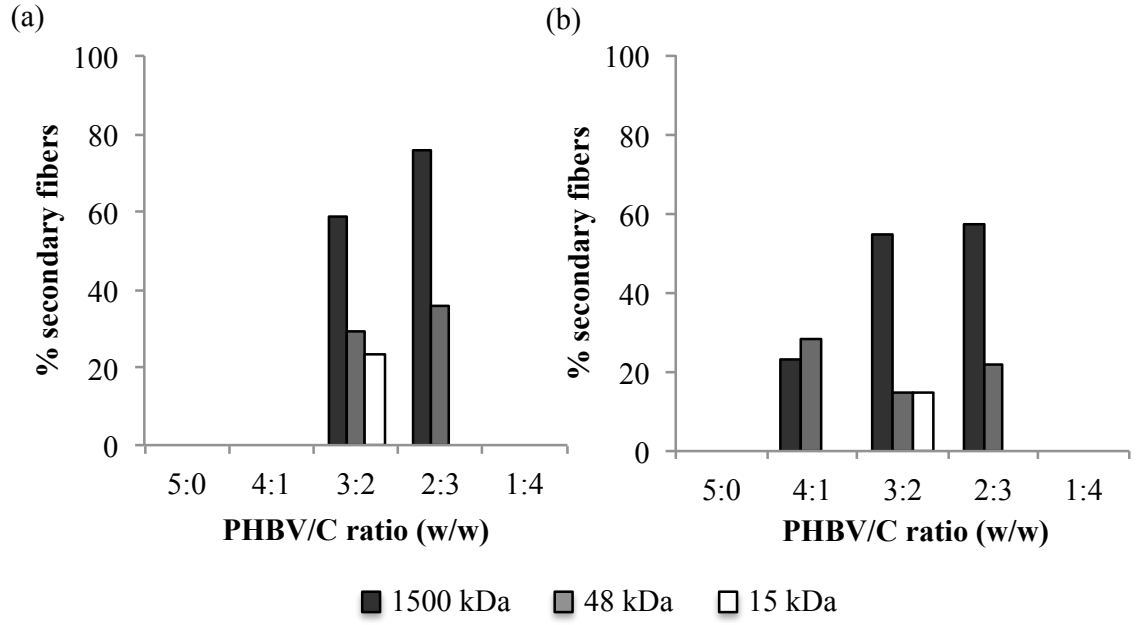

Figure 2.5. Relative frequency of secondary fibers in electrospun PHBV/C mats: (a) TFA/HFIP 3:7 (v/v) (b) TFA/HFIP 1:1 (v/v).

Secondary fibers mostly occurred for intermediate PHBV/C ratios (PHBV/C 3:2 and 2:3 (w/w)) and as chitosan MW increased. The fiber branching process may be related to polymer segregation, as a result of solution instability, during the jet stretching. Polymer blends are, in general, thermodynamically instable and this instability increases with the increase of polymer concentration and MW. During the electrospinning process, as the jet travels from the needle to the collector, solvent evaporates and the polymeric concentration becomes higher, increasing the instability of the system. This instability can reach a limit where separation of phases occurs and two kinds of fibers are formed. Phase separation as a result of solvent evaporation during the electrospinning process has been described and includes formation of core-sheath structures (Lopes-da-Silva *et al.* 2009; Wei *et al.* 2005), hollow (Zhang *et al.* 2009), and porous nanofibers (Han *et al.* 2005). However, no report was found describing a similar behavior of phase separation, *i.e.* branching of fibers.

To study the effect of PHBV/C ratio and chitosan MW on fiber diameters, the average diameter of main and secondary fibers were calculated. **Figure 2.6** displays the average diameter of the main fibers as a function of PHBV/C ratio and chitosan MW.

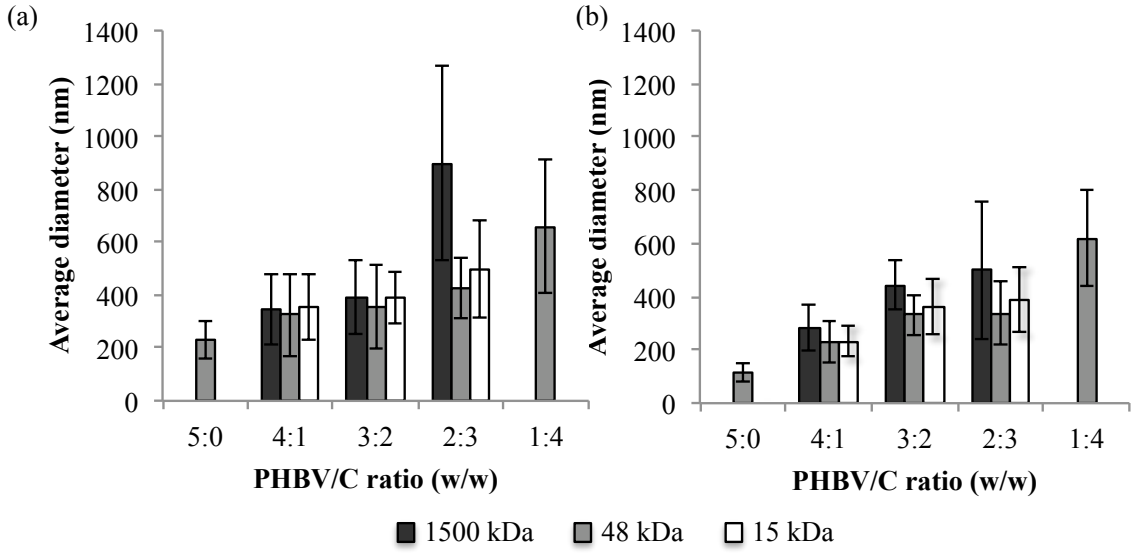

Figure 2.6. Average main fiber diameters of PHBV/C mats: (a) TFA/HFIP 3:7 (v/v) (b) TFA/HFIP 1:1 (v/v).

The average diameters of PHBV/C main fibers were in the range of 115-900 nm, increasing with the increase of chitosan content, irrespective of the chitosan MW or solvent composition. Increasing the amount of chitosan also tended to increase the dispersion of fiber diameters, to change the fiber shapes from tubular-like to more flat ribbon-like morphologies and to increase the connection between fibers.

One could expect that the presence of chitosan would increase the conductivity of the solutions and consequently could lead to higher elongation forces and thinner fibers. However, solution viscosity also increased significantly as the chitosan content increased. For the same electrostatic force, a higher solution viscosity will result in a higher viscoelastic force to be overcome, and thus the polymer fibers will be less stretched, originating thicker fibers.

Chitosan MW had a complex effect on the main fiber diameters. Fibers with chitosan 1500 kDa had larger diameters than the lower MW samples. Chitosan 48 kDa, however, originated fibers with lower diameters than the 15 kDa sample. As the MW decreases, the solution viscosity reduces, and, consequently, diameter of fibers would decrease. However, as PHBV molecules branch off during the jet path, forming secondary fibers, the main fiber diameter decreases. Therefore, despite the higher viscosity of the 48 kDa chitosan

solution compared to the lowest MW sample, the more extensive formation of secondary fibers contributes to the neat reduction in the main fiber diameter.

Unlike main fibers, the secondary fiber diameter decreased with the increase of chitosan content. The average secondary fiber diameters of the electrospun mats are represented in **Figure 2.7**.

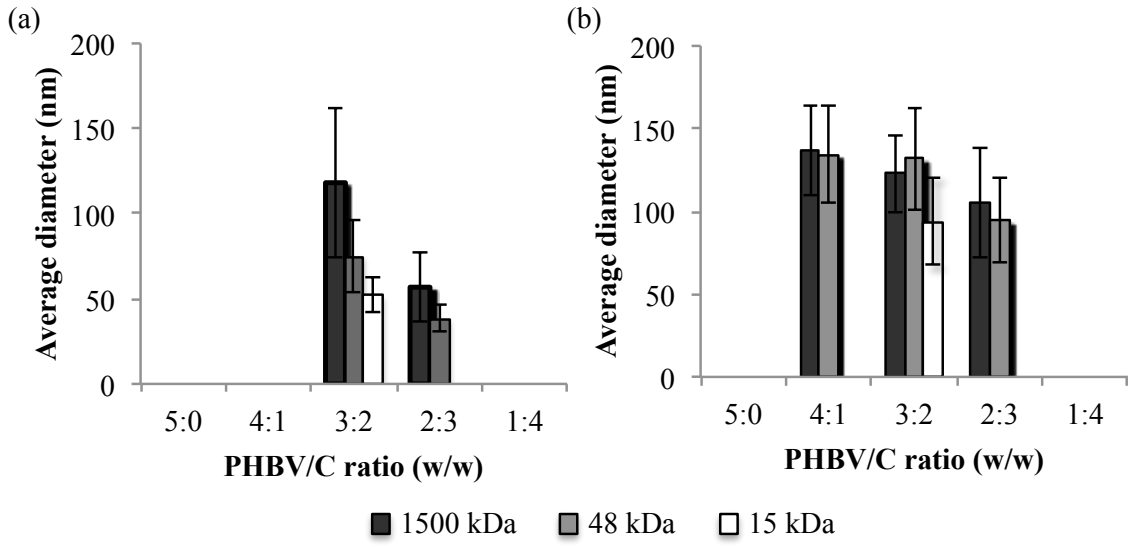

Figure 2.7. Average secondary fiber diameters of PHBV/C mats: (a) TFA/HFIP 3:7 (v/v) (b) TFA/HFIP 1:1 (v/v).

As previously assumed, secondary fibers are formed due to polymer separation during the electrospinning process. Moreover, it is well established that fiber diameter increases with the increase of polymer concentration (Veleirinho *et al.* 2008). Considering that the diameter of secondary fibers reduced as PHBV content decreased one can infer that these fibers were mostly made of PHBV.

Chitosan dissolution, on the contrary, was facilitated by the increase of TFA content. This explains why secondary fibers were formed for PHBV/C 4:1 (w/w) when higher concentration of TFA was used (Figure 2.7b). For higher chitosan contents (PHBV/C 3:2 and 2:3 (w/w)), however, the relative frequency of secondary fibers decreased with the decrease of HFIP in the solvent.

Rupture of fibers was a specific characteristic of the pristine PHBV mat (**Figure 2.8** a). This morphological detail was also frequently observed on secondary fibers of the PHBV/C mats as illustrated in Figure 2.8 b, and is thought to result from the stiffness of PHBV polymer in comparison to chitosan. This result is in accordance with the established hypothesis that secondary fibers were essentially composed by PHBV.

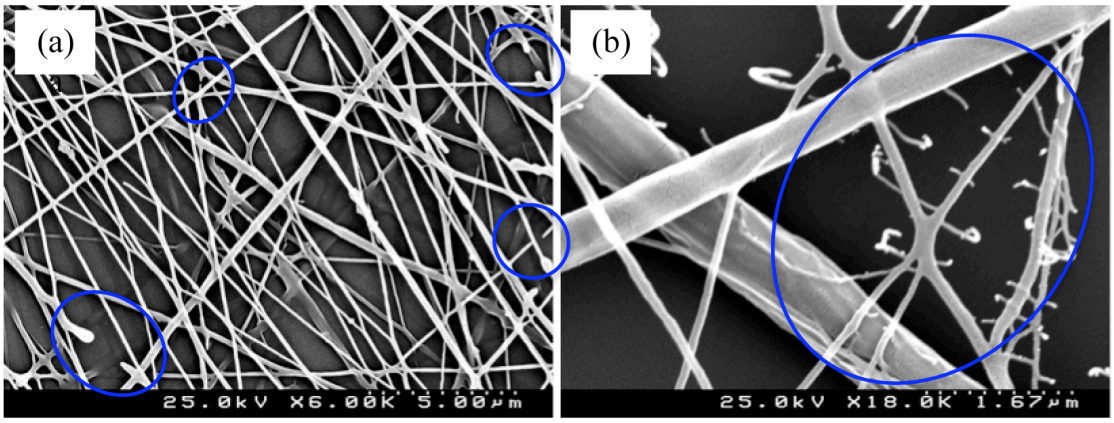

Figure 2.8. SEM micrographs showing broken fibers: (a) PHBV/C 5:0 (w/w) in TFA/HFIP 1:1 (b) PHBV/$C_{1500\ kDa}$ 2:3 (w/w) in TFA/HFIP 1:1 (v/v).

2.3.5. FTIR analysis

Figure 2.9 displays FTIR spectra of PHBV and PHBV/C blends. The FTIR spectra of the nanofibrous membranes electrospun from different PHBV/C ratios showed characteristic peaks of both polymers, confirming the presence of both in the fibers. The typical bands at 3342 and 3280 cm^{-1} (O-H and N-H stretching) were observed in the spectrum of chitosan. As expected, with the increase of PHBV the relative strength of these peaks decreased. Also, the υ_{O-H} band shifts to higher wavenumber with the PHBV content increasing probably due to the occurrence of intermolecular hydrogen bonds between chitosan (O-H) and PHBV (C=O). The bands appearing in the region around 2870-2970 cm^{-1} correspond to the C-H aliphatic stretches.

In the region of the carbonyl stretching and fingerprint region the FTIR spectrum of PHBV electrospun fibers showed a characteristic absorption band at 1718 cm^{-1} which is attributed to the C=O stretching of the ester groups of PHBV. Other characteristics bands are observed at 1098 cm^{-1} (symmetric C-O stretching) and at 1128 cm^{-1} (asymmetric C-O

stretching). The FTIR spectrum of the as-received chitosan showed the characteristic amide bands, *i.e.,* at 1644 cm^{-1} for C=O stretching of amide I and at 1560 cm^{-1} for the N–H deformation in the CONH plane of amide II. The amide band has shifted about 30 cm^{-1} for the hybrid PHBV/C fibers compared to the behavior of the powder as-received chitosan, supporting the possible occurrence of intermolecular hydrogen bonds between both polymers in the hybrid fibers. As expected, with the increase of PHBV, the relative strength of the characteristic amide bands decreased, and the relative strength of peak at 1718 cm^{-1} increased.

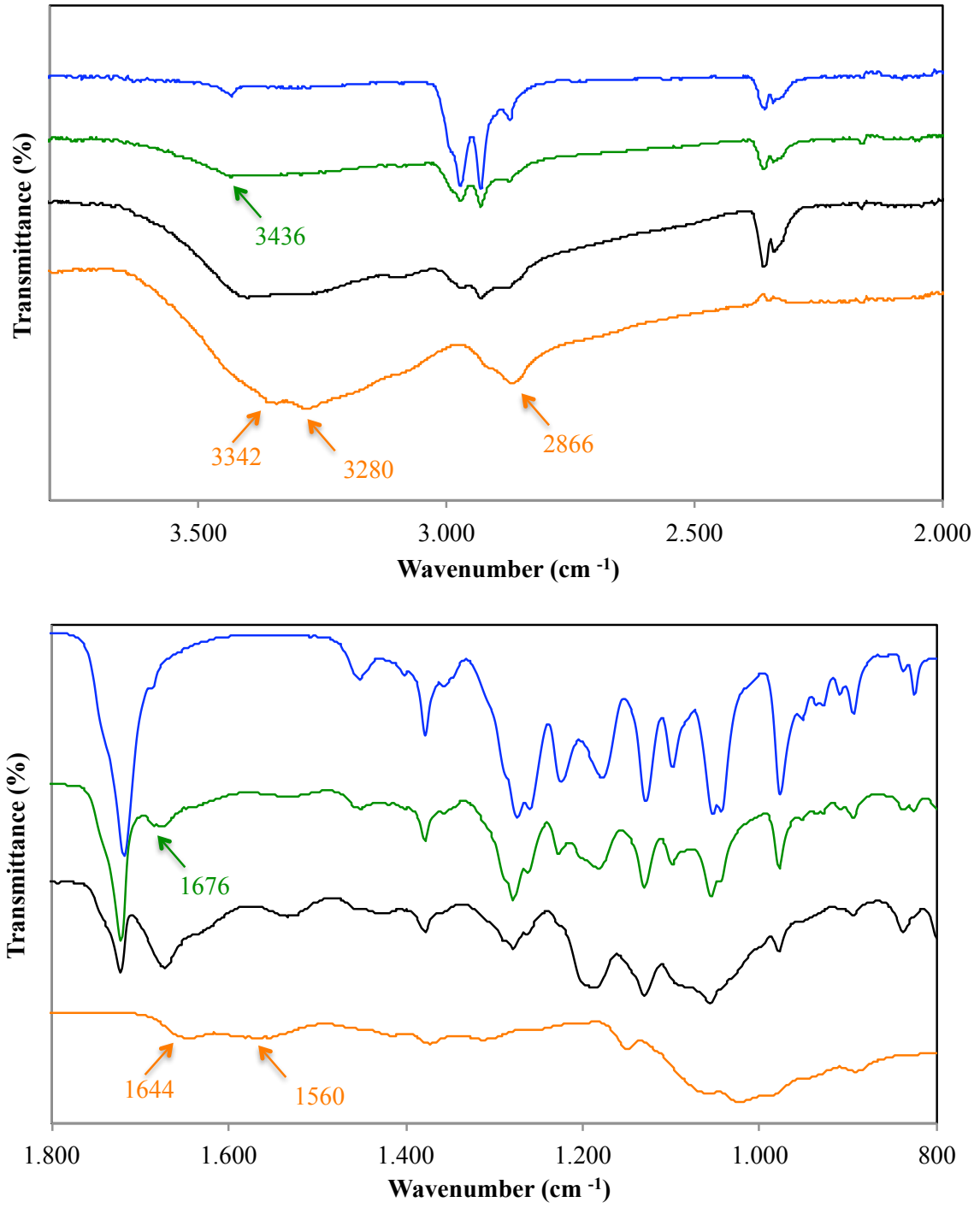

Figure 2.9. FTIR spectra obtained for electrospun fibers of PHBV/C 5:0 (w/w), PHBV/C $_{48\ kDa}$ 4:1 (w/w), PHBV/C $_{48\ kDa}$ 2:3 (w/w) (TFA/HFIP 1:1 (v/v)), and for as-received chitosan.

2.3.6. *In* vitro degradation of the scaffolds

The *in vitro* degradation tests under physiological conditions revealed the very low degradation rate of the PHBV fibrillar mats, with about 95% mass retention after 28 days, and the increasing biodegradability of the hybrid mats as the chitosan content increased (**Figure 2.10**). Changes in morphology and integrity of the electrospun fibers during the biodegradation tests have been analyzed by SEM (**Figure 2.11**). At higher chitosan content water penetration proceeds faster and the lost of fiber integrity occurs very quickly too. In the presence of a lower amount of the more hydrophilic polymer, the water penetration is expected to be slower and at least initially the mass loss is probably confined to the surface layers of the material. After 1 hour treatment fiber integrity is still preserved but extensive morphological changes have already occurred. Chitosan addition turns out to be an effective way to control the degradation rate of the electrospun PHBV scaffolds.

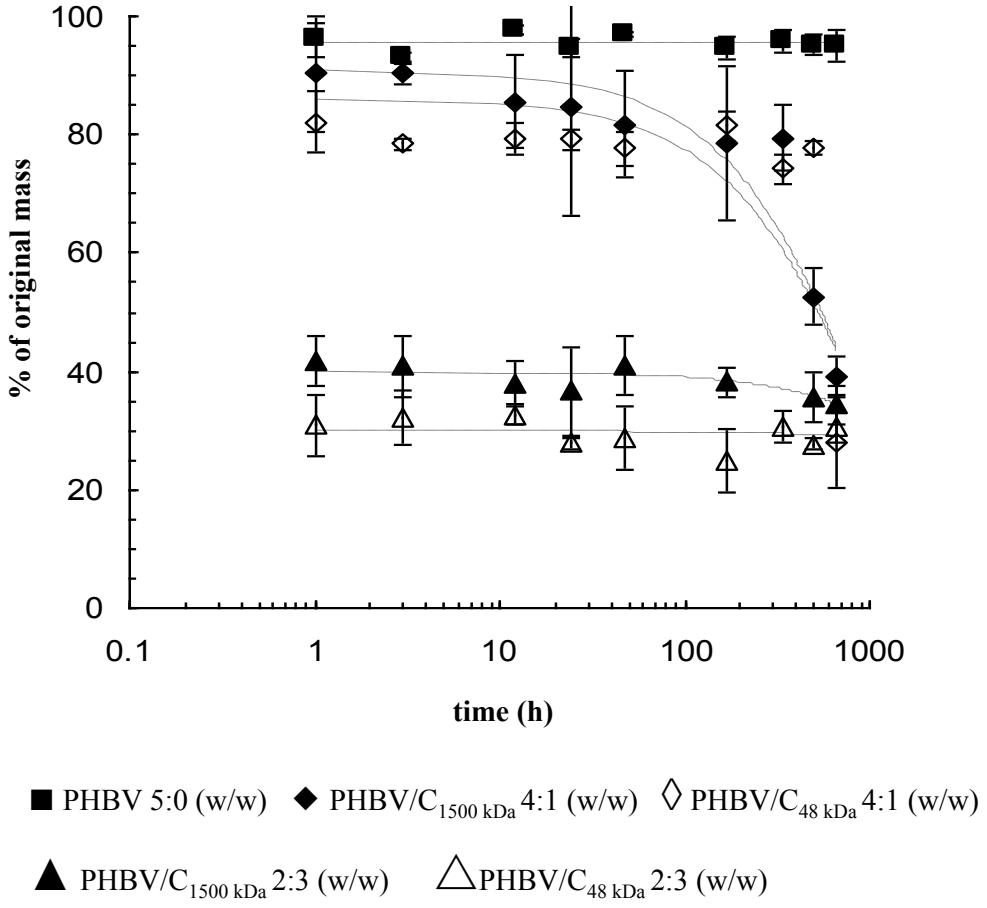

Figure 2.10. *In vitro* degradation of mats containing different PHBV/C ratios and chitosan MW (TFA/HFIP 1:1 v/v used as solvent).

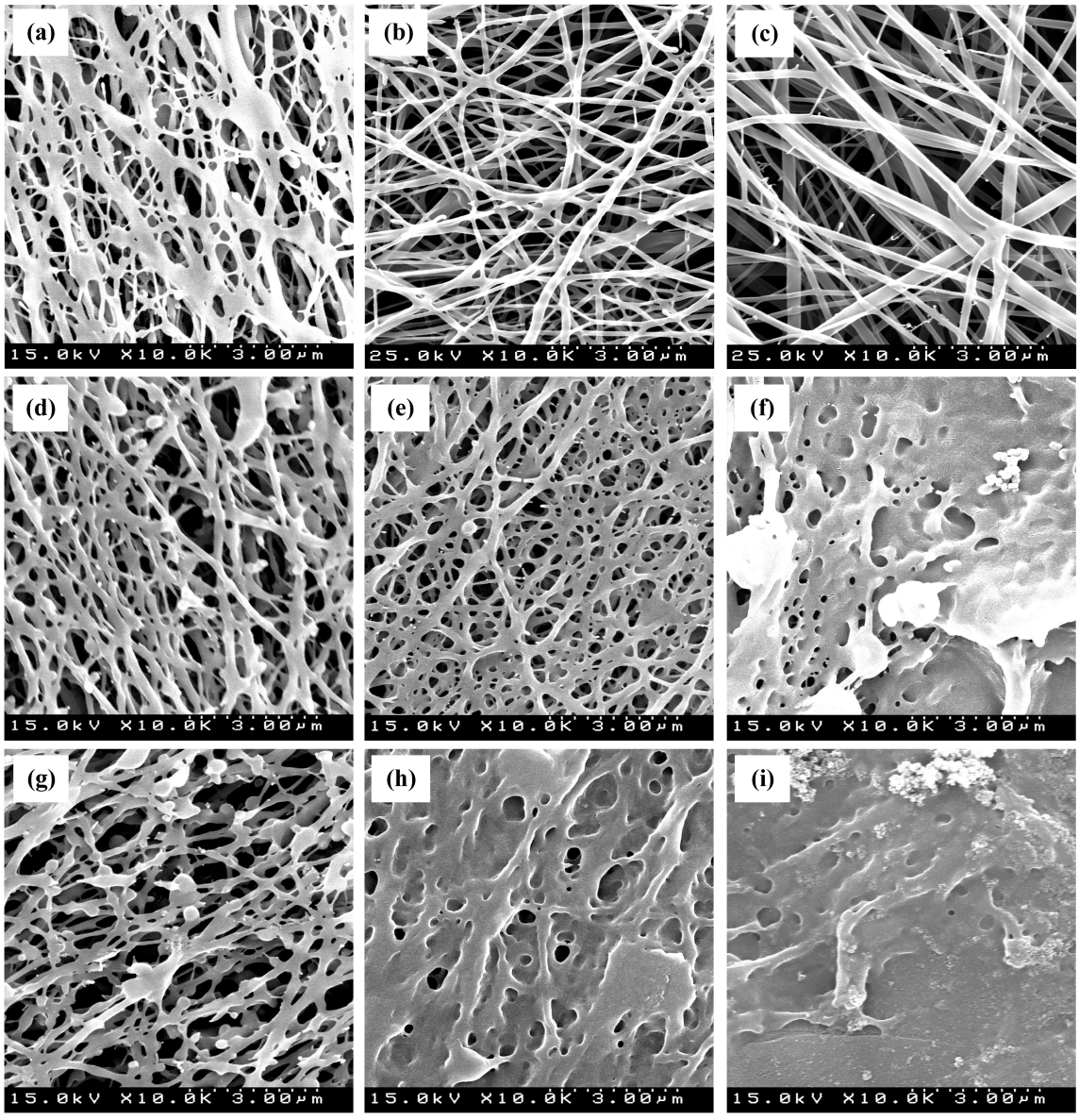

Figure 2.11. SEM images of electrospun fibers degraded in PBS (pH 7.4) at 37 ºC for (a-c) 0, (d-f) 1 hour, and (g- i) 28 days. Left column for a PHBV/C 5:0 (w/w), middle column PHBV/$C_{48\ kDa}$ 4:1 (w/w), and right column for PHBV/$C_{48\ kDa}$ 2:3 (w/w). TFA/HFIP 1:1 v/v used as solvent.

2.3.7. Biological studies

Amongst all blends, PHBV/C_{48kDa} samples exhibited, in general, a better electrospinnability, *i.e.* fiber formation from a wider PHBV/C ratio range, superior jet stability, and, consequently, improved macroscopic homogeneity of the mat. Indeed,

PHBV/$C_{48\ kDa}$ 4:1 (w/w) and PHBV/$C_{48\ kDa}$ 2:3 (w/w) (from now on designated as PHBV/C 4:1 (w/w) and PHBV/C 2:3 (w/w), respectively) electrospun from solutions in TFA/HFIP 1:1 (v/v), were selected to perform the biological assays to evaluate their potential as scaffolds for skin engineering. The difference in polymer composition between these samples resulted in both morphological and degradation changes. **Figure 2.12** summarizes morphological characteristics and degradation information for these scaffolds.

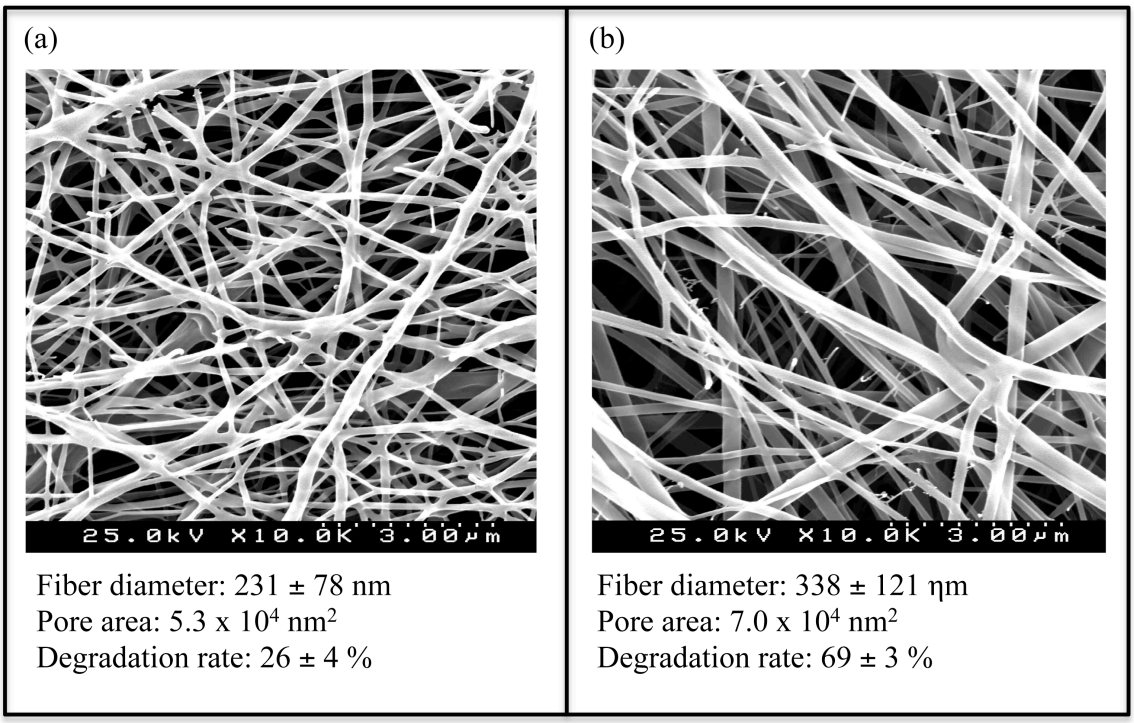

Figure 2.12. SEM images showing the morphology of fibers electrospun from PHBV/C 48 kDa solutions in TFA/HFIP 1:1 (v/v), at two different polymer ratios: (a) 4:1 and (b) 2:3 (w/w). Also shown are the fiber average diameters, pore area, and degradation rates (as % mass loss) obtained after 14 days in a phosphate buffer solution (pH 7.4) at 37 °C.

2.3.7.1. Cell culture studies

Figure 2.13 displays results from the indirect cytotoxicity assay. The indirect cytoxicity assay is used to evaluate the release of cytotoxic compounds from the scaffold to the extraction medium. These compounds can include soluble components from scaffolds *i.e.* chitosan or residues from the fabrication process, such as TFA or HFIP. The MTT assay to

measure the viability of cells revealed that none of the scaffold extraction media was toxic to L929 fibroblasts.

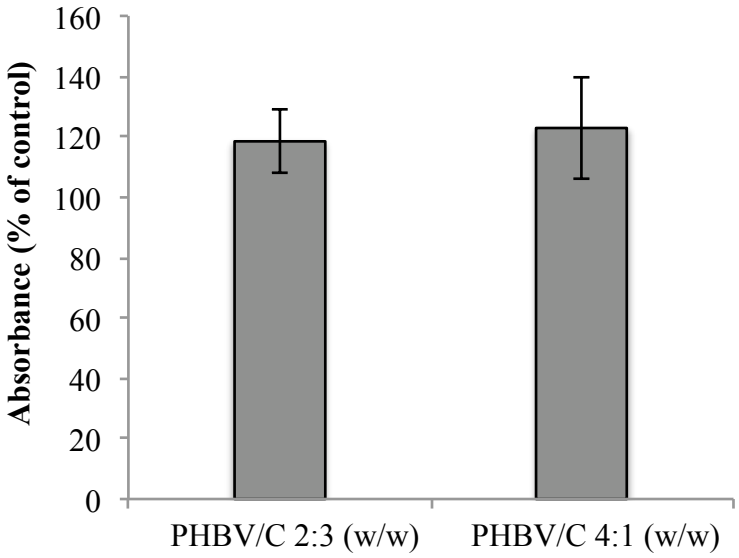

Figure 2.13. Absorbance 540 nm (% of control) obtained in the indirect cytotoxicity assay of L929 cells cultured on PHBV/C 2:3 (w/w) and PHBV/C 4:1 (w/w) scaffolds. No significant differences were detected.

The viability of fibroblasts cultivated on the PHBV/C scaffolds for 2, 7, and 14 days was evaluated by MTS assay. This assay quantifies the soluble formazan resulting from the reduction of the MTS tetrazolium compound in the mitochondria of living cells. The quantity of formazan product is measured spectrophotometrically (absorbance at 490 nm) and is directly proportional to the number of living cells in culture. The MTS assay revealed a similar cell viability profile for both scaffolds, with an increase in the number of living cells promoted by the scaffold-interaction during the first seven days of the experiment (**Figure 2.14**). After the 1st week the PHBV/C 4:1 (w/w) experimental group reached a stationary phase while the cells seeded on PHBV/C 2:3 (w/w) showed a slight decrease in the viability, probably related to the higher degradation rate observed for this scaffold, with an inherent higher loss of sites for cell attachment.

Figure 2.15 displays SEM images of L929 cultured on PHBV/C 2:3 and PHBV/C 4:1 (w/w) for 12 hours and 2 days, while **Figure 2.16** shows the corresponding CLSM images after 12 hours, 2 days, and 7 days seeding. Both microscopic techniques showed

that L929 fibroblasts adhered to the blended fibers after 12 hours seeding, followed by a clear morphological change to well spread cells on the scaffolds, and an intense proliferation activity. Indeed, after 7 days of culture cells were confluent on the surface of both PHBV/C scaffolds under study (Figure 2.16).

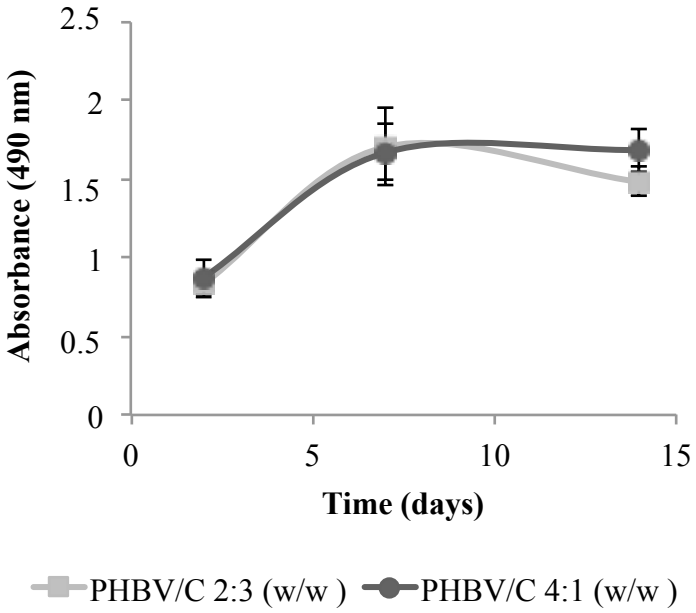

Figure 2.14. Viability of L929 cells cultured on PHBV/C 2:3 and 4:1 (w/w) scaffolds for 2, 7, and 14 days measured via MTS assay. No significant differences were detected.

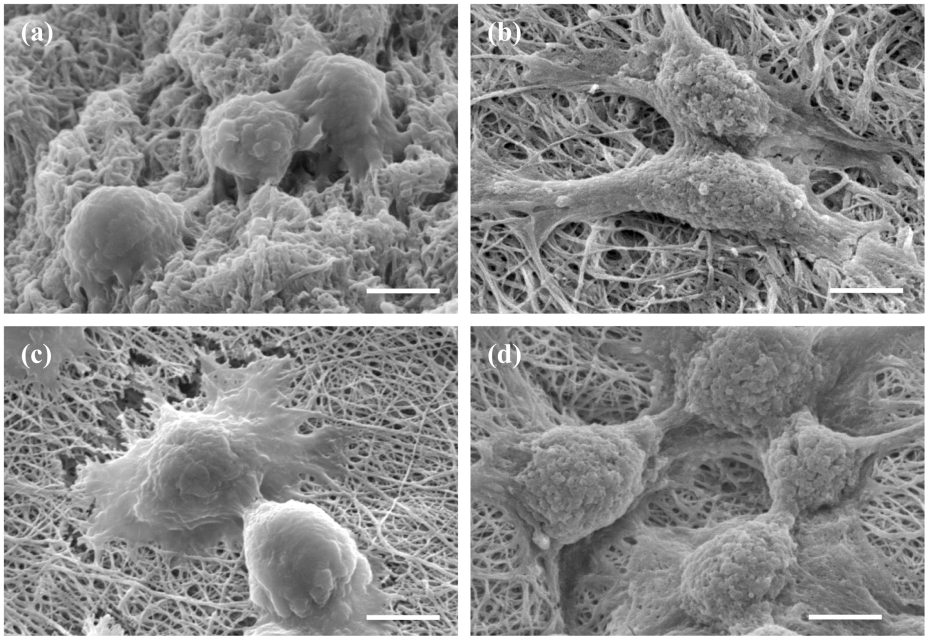

Figure 2.15. SEM images of L929 cells cultured on PHBV/C 2:3 (w/w) (a and b) and 4:1 (w/w) (c and d) scaffolds for 12 hours (a and c) and 2 days (b and d). Bar = 5 μm.

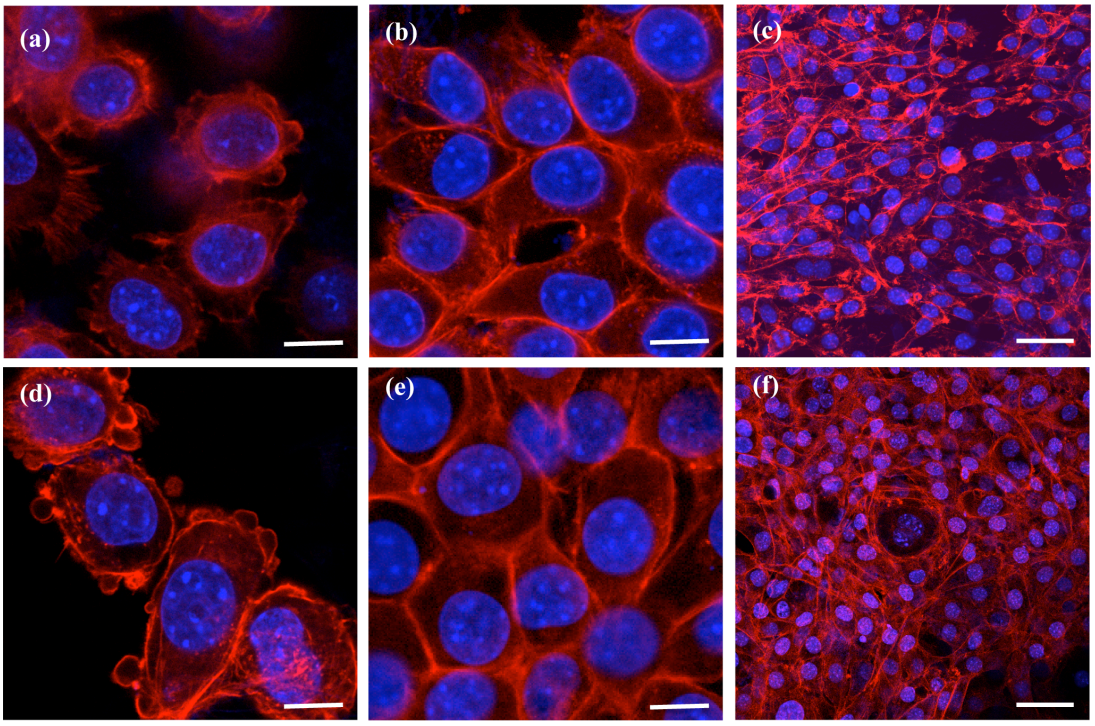

Figure 2.16. CLSM images of L929 fibroblasts cultured on PHBV/C 2:3 (w/w) (a-c) and PHBV/C 4:1 (w/w) (d-f), for 12 hours (a and d), 2 days (b and e), and 7 days (c and f). F-actin (red) and nucleus (blue) stained with Alexafluor 546 conjugated to phalloidin and DAPI, respectively. Scale bar = 10 μm (a, b, d, and e) and = 50 μm (c and f).

Immunolabeling of fibronectin was performed in order to verify the presence of fibronectin from ECM on the surface of the scaffolds. As previously mentioned, in natural environment, adhesion of cells to the ECM occurs via focal adhesion, an integrin mediated process that involves binding of integrin from the plasma membrane to a specific peptide sequences such as the RGD of ECM proteins. These integrin mediated adhesions, *i.e.* focal adhesions, activate multiple signaling pathways, and have a tremendous impact on the survival and proliferation of anchorage dependent cells. On artificial substrata, where the RGD sequence is not present, adhesion can be initially mediated by proteins adsorbed on the surface of the material (*e.g.,* originating from serum). Subsequently, the attached cells would be able to produce and secrete their own ECM, creating a coating layer on the scaffolds surface, which facilitates further cellular activities. Both PHBV/C 2:3 and PHBV/C 4:1 (w/w) scaffolds showed a plenty fibronectin distribution on their surfaces after 2 days of culture (**Figure 2.17**).

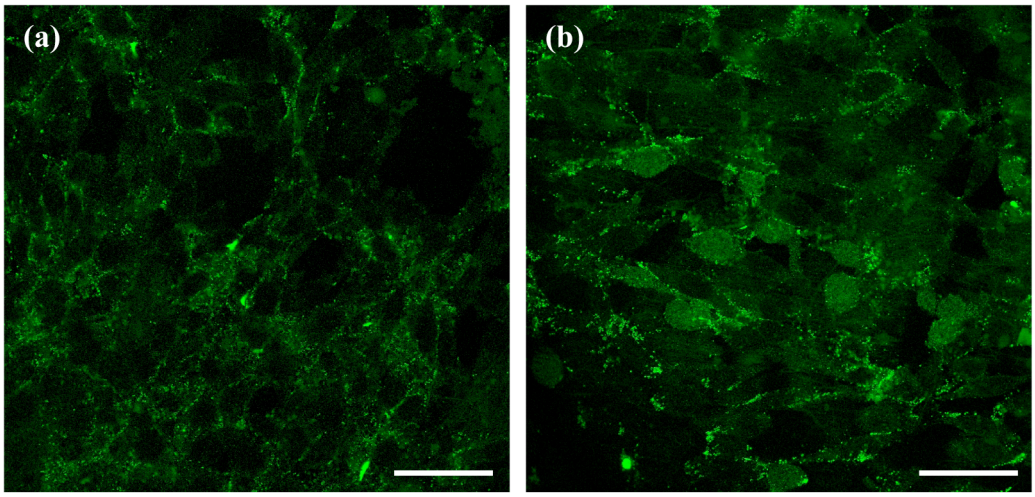

Figure 2.17. Immunolabeling of extracellular fibronectin (green) deposited on the surface of PHBV/C 2:3 (w/w) (a) and PHBV/C 4:1 (w/w) (b) scaffold after 48 days of incubation with L929 cells. Bar = 50 μm.

Figure 2.18 displays the cells' cytoskeleton area, measured with basis on the CLSM pictures, as function of culture time. Changes in fibroblasts morphology were observed 12 hours after seeding, but the increase in cell's area only occurred after the second day of culture. Cells cultured on PHBV/C 4:1 (w/w) scaffold reached higher levels of spreading,

i.e. their cytoskeleton areas were significantly greater than the related to cells cultured on PHBV/C 2:3 (w/w) (day 7).

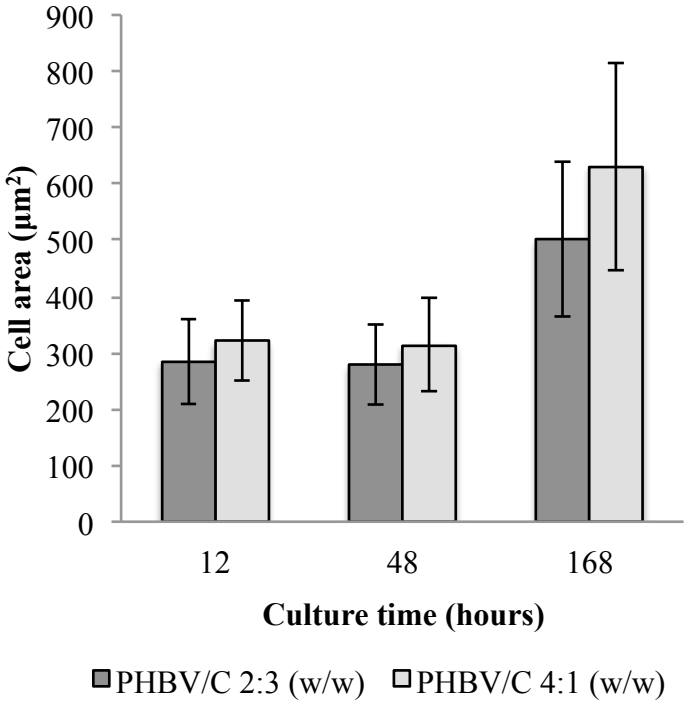

Figure 2.18. Cytoskeleton area of L929 cells cultured on PHBV/C scaffolds as a function of culture time. Different letters indicate significant differences ($p < 0.05$).

Vinculin is an intracellular protein involved in the focal adhesion process and commonly used as a focal adhesion marker. This protein belongs to the adhesion complex and is expressed when a focal adhesion takes place. Due to features described above, the immunolabeling of vinculin was performed to study the adhesion of cells on the hybrid scaffolds. **Figure 2.19** shows the focal adhesion sites evidenced by vinculin immunostaining, obtained for the L929 cells adhered to the surface of PHBV/C scaffolds. Higher levels of vinculin expression were found in cells cultured on PHBV/C 4:1 (w/w) scaffold, indicating the occurrence of important levels of cellular adhesion in this scaffold. An increase of vinculin expression as a function of the incubation time was also observed. Adhesion is a crucial attribute for the survival of anchorage dependent cells and affects several subsequent cellular activities, including spreading, proliferation, and ECM

production (McGrath 2007). Furthermore, in the absence or even with limited sites for adhesion, potentially adherent cells can induce apoptosis (Chen *et al.* 1997). In this context, consistent adhesion levels may improve cell survival and, consequently, are a fundamental condition for provisional skin scaffolds, since they constitute a basis for cell adhesion in the lack of natural ECM. The adhered cells are thus able to assume their role in the tissue regeneration process, affording proliferation, migration, ECM synthesis and tissue organization.

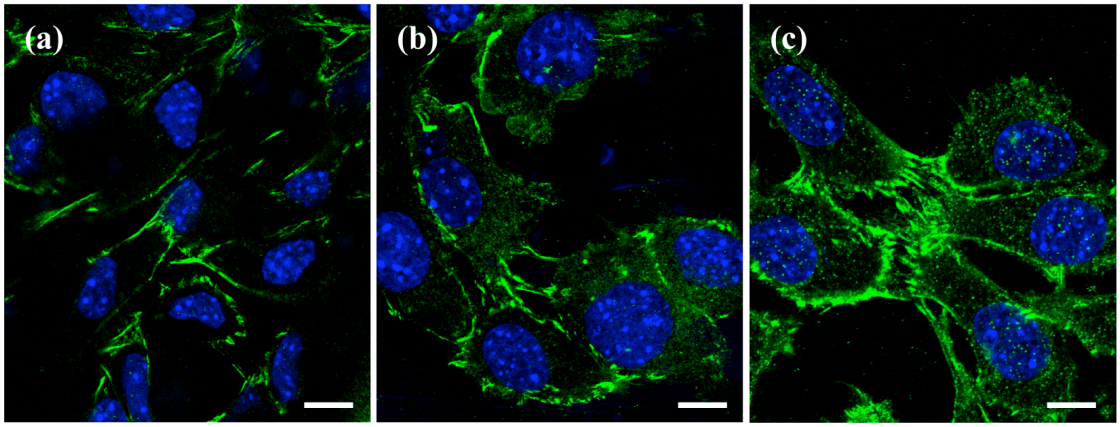

Figure 2.19. CLSM images of L929 fibroblasts cultured on (a) PHBV/C 2:3 (w/w) and (b) and (c) PHBV/C 4:1 (w/w), for 2 days (a and b) and 7 days (c). Vinculin (green) and nucleus (blue) stained with anti-vinculin monoclonal antibody followed by Alexafluor 488 goat anti-mouse and DAPI, respectively. Scale bar =10 μm.

Although cell proliferation can be monitored by microscopic analysis of cell growth, the EdU uptake assay has been used as a specific method to study proliferation. EdU is a nucleoside analogue that binds to DNA during cell division. The percentage of proliferative cells was measured after attachment, *i.e.* 12 hours after seeding, for PHBV/C scaffolds and the control. **Figure 2.20** displays the percentage of proliferating cells cultured on the electrospun scaffolds. PHBV/C 4:1 (w/w) displays a higher tendency to stimulate cell proliferation (53±9 %) as compared to PHBV/C 2:3 (w/w) (32±9 %), supporting the better performance of the PHBV/C 4:1 (w/w) scaffold as a substratum for cell attachment, *i.e.* to promote higher levels of adhesion and spreading.

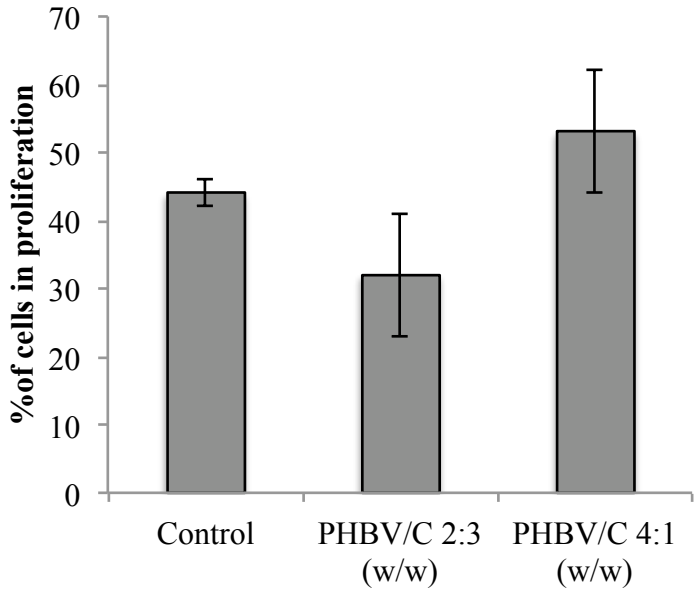

Figure 2.20. Percentage of proliferating cells measured by the EdU assay. Different letters indicate significant differences ($p < 0.05$).

The annexin V/ PI dual staining was used to investigate eventual occurrence of cell death by apoptosis or necrosis in the cultures. Annexin V probe binds to phosphatidylserine exposed on the plasma membrane of apoptotic cells while PI is used to identify membrane damage of necrotic cells. To perform this study, both adhered and detached cells, *i.e.* death cells in the culture medium, were collected. **Figure 2.21** shows that low levels of cell death, either by apoptosis or necrosis were found (97.7 ± 0.6 of viability) for cells cultured on the PHBV/C 4:1 (w/w) scaffold. Furthermore, this scaffold decreased almost six times the necrotic cell death in comparison to control. On the other hand, PHBV/C 2:3 (w/w) exhibited a considerable level of necrotic death (17.7 ± 4.5 %). Necrotic death is related to the loss of membrane integrity and in this case may result from the higher content of the chitosan. It is speculated that the polycationic nature of chitosan in the pH conditions of the culture medium (7.2) may interact electronically with the fibroblasts' plasma membrane, causing a loss of membrane integrity and/or functionality in any extension. In fact, although chitosan has long been considered a safe material, there are several reports showing toxicity of chitosan, particularly in a nano-dimensional scale (Qi *et al.* 2007; Loh *et al.* 2010; Hu *et al.* 2011).

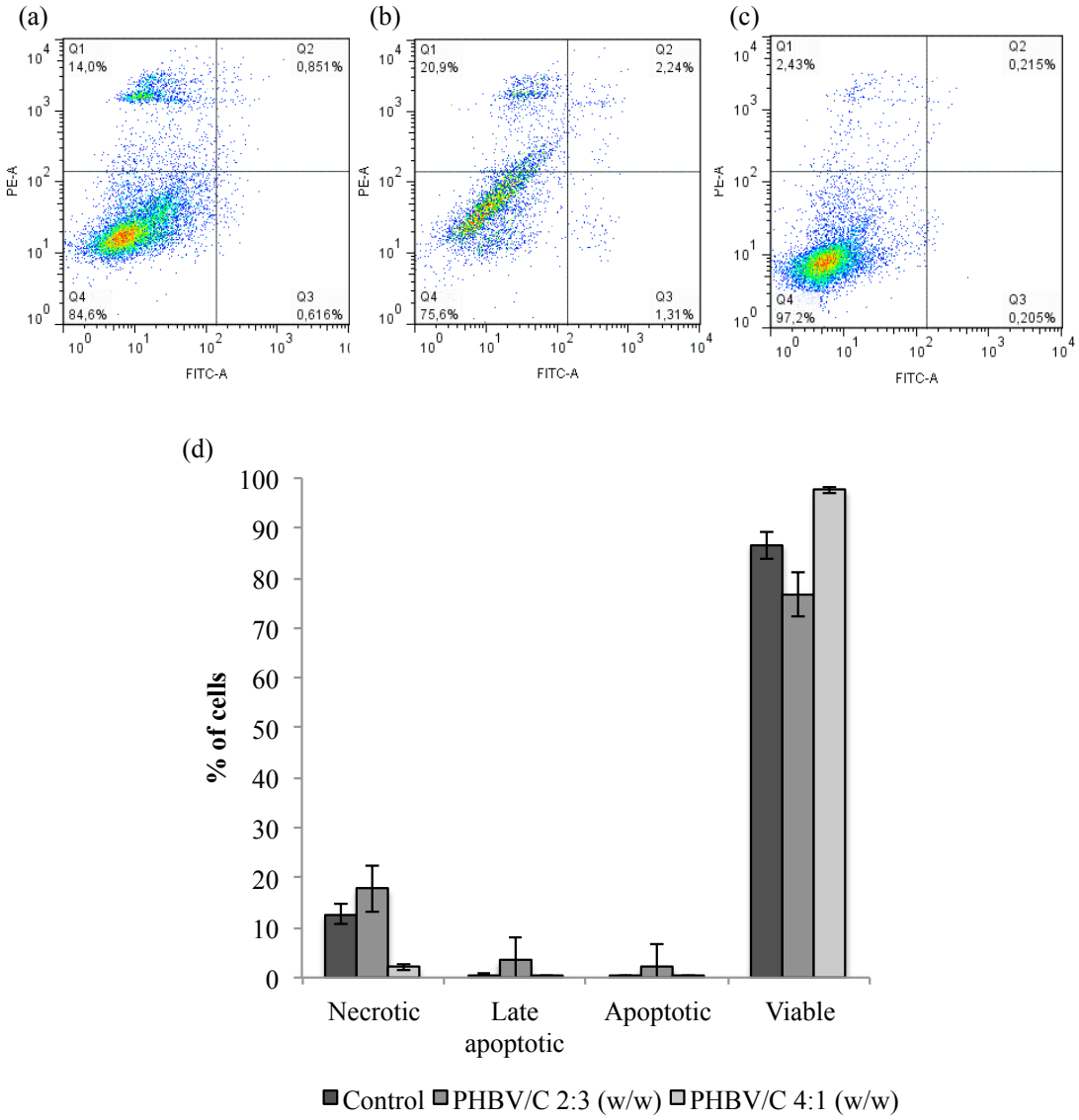

Figure 2.21. Annexin V-FITC/PI flow cytometry analysis of cell death after 48 hours of incubation on (a) control, (b) PHBV/C 2:3 (w/w), and (c) PHBV/C 4:1 (w/w). Viable cells (Annexin V-FITC negative/PI negative) are in the lower left quadrants; apoptotic cells (Annexin V-FITC positive/PI negative) are in the lower right quadrants; late apoptotic cells (Annexin V-FITC positive/PI positive) are in the upper right quadrants; and necrotic cells (Annexin V-FITC negative/PI positive) are in the upper left quadrants. The cytograms are representative of three independent experiments. Mean ± standard deviation of cell stages (d).

2.3.7.2. Wound healing assay

The ability of scaffolds to promote tissue regeneration *in vivo* was evaluated on skin full-thickness wounds implemented on the back of Wistar rats. The scaffold instantly adhered to the wound, absorbing the biofluids and showing itself as an hydrate membrane. The healing process was studied macroscopically and histologically for 21 days.

Wound areas, expressed as percentage of the initial wound area, and plotted in **Figure 2.22** as a function of the treatment time with each scaffold. At the 3rd day after injury, no significant differences were found among treatments in respect to wound closure. However, on the 7th day post-surgery PHBV/C 4:1 (w/w) group showed significant smaller wound areas (26 ± 11 %), compared to control (59 ± 17 %). At the 14th day, 44% of wounds treated with PHBV/C 4:1 (w/w) were totally healed, compared to 25% of PHBV/C 2:3 (w/w) treatment and 13% of control, supporting the important role of the PHBV/C 4:1 (w/w) hybrid scaffold to promote skin healing.

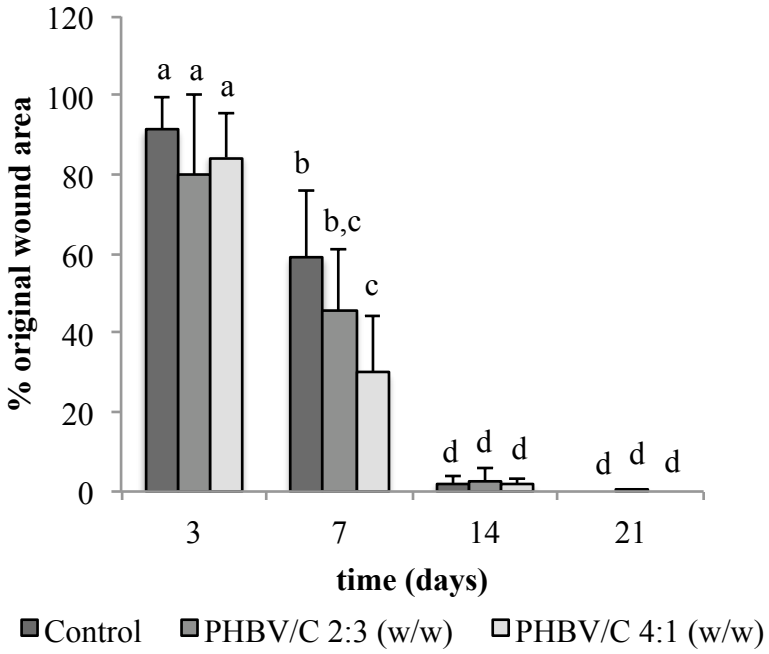

Figure 2.22. Wound area for PHBV/C 2:3 (w/w), PHBV/C 4:1 (w/w), and control groups during the wound-healing assay. Different letters indicate significant differences ($P<0.05$).

Histological classification of wound tissues was performed by microscopy, enabling to identify the distribution of wound phases for each treatment (**Figure 2.23**). The density of PMN and MN cells were also calculated and are shown in **Figure 2.24** as a function of treatment time with each scaffold.

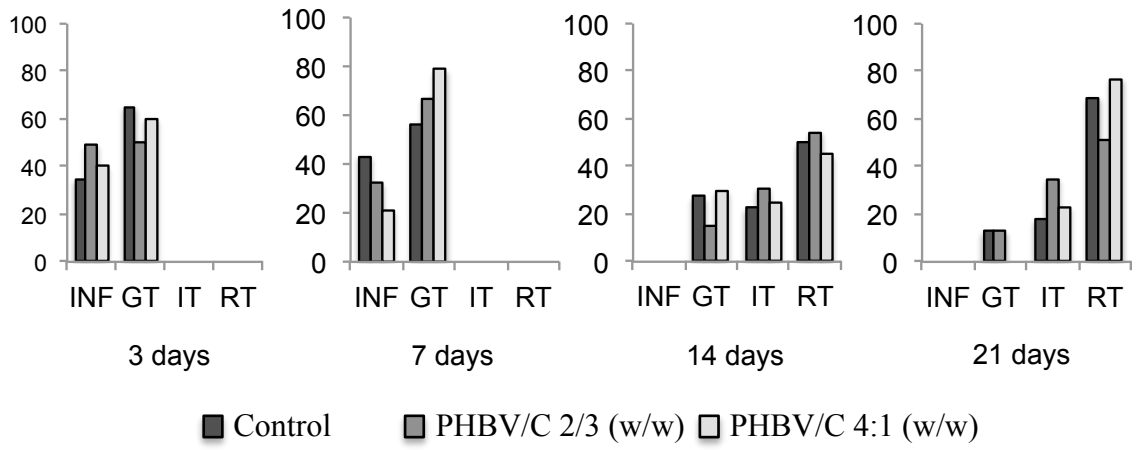

Figure 2.23. Histological classification of wound tissues 3, 7, 14, and 21 days after injury for control and PHBV/C scaffolds: IF (inflammatory infiltrate), GT (granulation tissue), IM (immature regenerated tissue), and RT (remodeled tissue).

As expected for the inflammatory phase, the 3rd day after injury was characterized by high densities of PMN leukocytes for all treatments. PHBV/C 4:1 (w/w) exhibited the higher density of PMN cells in comparison to PHBV/C 2:3 (w/w) and control. The lower levels of PMN on PHBV/C 2:3 (w/w) are probably attributed to the higher concentration of chitosan in this scaffold and its antimicrobial activity (Cai *et al.* 2010; Liu *et al.* 2001), whereas the lower levels of PMN cells found in the control group are probably related to the physical protection against external contaminants. Nevertheless, 7 days after injury, a substantial decrease of PMN cells was found on PHBV/C scaffolds but not on the control, where an increase of PMN cells was observed. At this stage, wound tissues from PHBV/C 4:1 (w/w) group were predominantly formed by granulation tissue while on the control group, considerable areas of inflammatory infiltrate were still found.

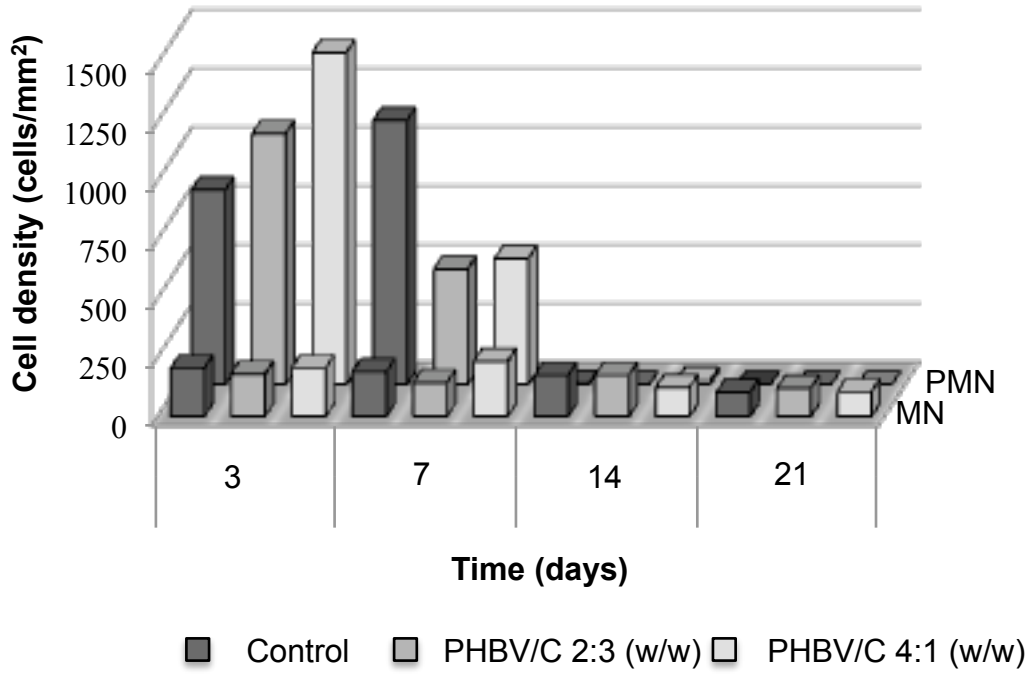

Figure 2.24. PMN and MN leukocyte densities during the wound healing process in rats.

Two weeks after injury, PMN leukocytes were rarely found and the proliferative phase was almost complete in all treatments. In accordance with the wound closure results, the process of re-epithelialization was advanced in PHBV/C 4:1 (w/w). It is especially noteworthy that no traces of PHBV/C scaffolds residues were found on tissues at day 14, demonstrating a biodegradation rate suitable for skin repair. At the 21st day, wounds were completely re-epithelized in all groups, however tissues from PHBV/C 4:1 (w/w) group exhibited a higher level of tissue organization, with hair bulbs and glands distributed in the newly formed tissue, mature blood vessels, and arrangement of collagen fibers resembling normal skin tissue (**Figure 2.25**).

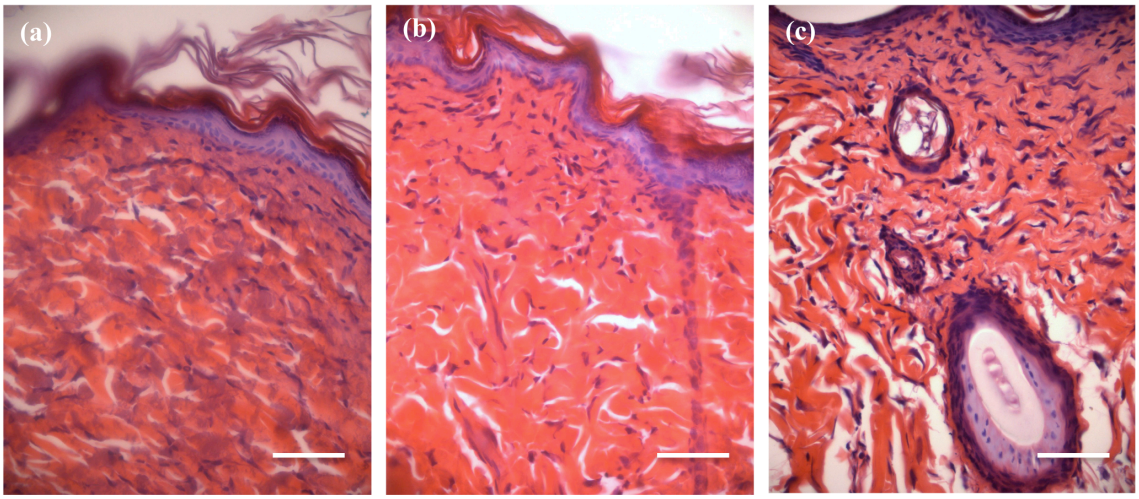

Figure 2.25. Histological sections showing the HE staining 21 days after surgical injury. Control (a), PHBV/C 2:3 (w/w) (b), and PHBV/C 4:1 (w/w) (c). Bar = 50 μm.

MN cells are usually recruited when a more specialized defense is required to neutralize the aggressor, or as a response to a foreign material. For all treatments, relatively low densities of MN cells were found. Decreasing densities of these cells were observed with time, an additional evidence of the biocompatibility features and biodegradability property of PHBV/C biomaterial.

2.4. Conclusion

Hybrid nanofibrous mats of PHBV and chitosan were successfully produced by electrospinning using TFA and HFIP blends as the solvent. Solvent characteristics, polymer ratio and chitosan MW affected the electrospinnability of the solutions and the morphology of the mats. The 48 kDa chitosan was found to have the best electrospinnability, once nanofibers were obtained for all PHBV/C ratios, except for pure chitosan. For the other chitosan samples (15 and 1500 kDa), the maximum chitosan concentration suitable for fiber formation was 6 wt.%.

During electrospinning, the thermodynamical instability of the polymer blends led to separation of phases and, consequently, a phenomenon of fiber ramification occurred. This phenomenon was characterized by ramifications of the main fibrous structure, giving rise

to short interrupted secondary fibers, with smaller diameters. These secondary fibers occurred more often in PHBV/C 3:2 and 2:3 (w/w) and with the increase of chitosan MW.

In general, the average of main fiber diameters increased as chitosan content and MW increased and decreased with the decrease of HFIP concentration in solution. On the other hand, the average diameter of secondary fibers decreased as chitosan content and MW increased and increased with the decrease of HFIP concentration in the solution.

In vitro and *in vivo* pre-clinical studies demonstrated the great potential of PHBV/C electrospun mats as scaffolds for promoting skin regeneration. The two PHBV/C ratios selected to perform the biological studies, 4:1 and 2:3 (w/w), were biocompatible and suitable for supporting cell growth. *In vitro*, PHBV/C [4:1] has shown a superior ability for improving fibroblasts adhesion and growth, compared to PHBV/C [2:3]. The characteristics of PHBV/C [4:1] scaffold, *i.e.* morphology, PHBV/C ratio, and biodegradation rate, confer an additional advantage to better fit the *in vivo* wound healing process. Taking together the properties of PHBV/C scaffolds might be instrumental in providing alternative tools for the dermal wounds therapeutics.

3.Dual-fiber mats as new support support matrices and vehicles for for bioactive compounds

3.1. Introduction

3.1.1. Nanofiber mats as vehicles for bioactive compounds

Besides all the mentioned advantages of the electrospinning process, another interesting ability of this technique is the incorporation of bioactive compounds in the mats through their direct dissolution in the polymeric solution. While solvent evaporates and polymer molecules are stretched to form the nanofibers, the non-polymeric bioactive molecules, *i.e.* synthetic drugs or natural compounds, are expected to be entrapped into the nanofibrous mesh.

Numerous studies are available about the incorporation of different drugs in nanofibrous electrospun mats, including antibiotics (Kenawy *et al.* 2002), analgesics (Taepaiboon *et al.* 2007), anti-inflammatory (Shen *et al.* 2011), and anti-cancer compounds (Chen *et al.* 2010). An interesting approach is the development of systems for controlled release of drugs, such as that developed by Kenawy *et al.* (2002) where a constant release of tetracycline from the electrospun poly(ethylene-*co*-vinylacetate) and PLA blend system was achieved for a period of 5 days.

Despites the enormous advantages and importance of phytotherapeutics, few reports are found in the literature regarding the incorporation of natural compounds in electrospun mats. The complex composition of plant extracts and problems related with solubility, characterization, and standardization, often limit the use of natural compounds in biomaterials. Nevertheless, few examples are found about the incorporation of plant extracts in electrospun materials, such as the cellulose acetate electrospun mats containing curcumin from *Curcuma longa* L., (Suwantong *et al.* 2007a) widely known for its anti-tumor, antioxidant, and anti-inflammatory properties. The chemical integrity of curcumin was maintained after the electrospinning process and the materials revealed good potential as transdermal patches. Likewise, Sikareepaisan *et al.* (2008) and Suwantong *et al.* (2008) have studied, *in vitro,* the incorporation of *Centella asiatica* L. Urban extract in electrospun fibers of gelatin and cellulose acetate, respectively. The herbal extract has demonstrated a positive effect on the treatment of wounds and burns.

Incorporation of bioactive compounds in the electrospun materials could be particularly useful in skin healing or skin engineering applications, as the removal of the wound dressing material for topical administration of medicines, may damage the wound bed, delaying the wound healing process and causing pain. Taking this idea into consideration, Thakur *et al.* (2008) have fabricated PLA electrospun mats containing anesthesic and antibiotic compounds, lidocaine and mupirocin, respectively. A controlled release system with a burst release of the anesthesic, for an initial relief of pain, and a diffusion-mediated mechanism for a prolonged antibiotic release was developed. *In vitro* analysis confirmed that the antibiotic maintain its activity in the electrospun mats. More recently, Suganya *et al.* (2011) reported the development of PCL/PVP electrospun mats as release systems for *Tecomella undulate* extract, a medicinal plant widely known for its traditional application in the wound healing process.

In this chapter we explore the incorporation of bioactive natural compounds into the PHBV/C scaffolds developed in chapter 2. For the present study, we have selected two bioactive extracts from natural origin and with potential effect on the skin healing process: the leaf storage parenchyma of *Aloe barbadensis* Miller, *i.e.* aloe vera gel, and the aqueous extract of *Ilex paraguariensis* leaf. The first one, aloe gel, has a well-known influence on the wound healing process while the aqueous extract of *I. paraguariensis* has recently demonstrated a positive effect on the blood vessel formation, which is also useful in the regeneration process. A brief review of the composition and properties of these two biological extracts is given below.

3.1.2. *Aloe barbadensis* Miller

Aloe barbadensis Miller is a member of the Liliaceae family. The leaf storage parenchyma of *A. barbadensis*, usually referred as aloe vera gel, contains 99% of water and the remaining dry matter contains mostly carbohydrates (72%), proteins (15%), and mineral elements (Femenia *et al.* 1999). Minor compounds also found in aloe gel include vitamins, enzymes, steroids, and salicylic acid, among many others (Choi and Chung 2003). Several pharmacological activities have been attributed to the rich matrix of aloe vera components, including, immunomodulatory, anti-inflammatory, anti-oxidant, anti-cancer, and anti-allergenic properties, among many others. An excellent review on the relationship between

Aloe vera components and their biological effects was provided by Choi and Chung (2003). Among all the biological effects of aloe gel, the most traditional is probably the wound and burn healing effects. In fact, aloe vera gel has been used to treat wounds and burns at least since roman time and, nowadays, aloe gel and its components have been incorporated in numerous cosmetics and therapeutic products (Reynolds and Dweck 1999). The wound healing effect of aloe gel has been attributed to several different components such as the manose-6-phosphate (Davis *et al.* 1994), acemannan (Jettanacheawchankit *et al.* 2009), and also to a glycoproteic fraction (Choi *et al.* 2001). The remarkable features of aloe matrix, however, lie also in the synergetic action among their components.

The mechanisms through which aloe gel acts in wound healing process are complexes. For instance, Chithra *et al.* (1998) have shown that aloe gel enhanced the synthesis of ECM components during the wound healing process. On the other hand, Jettanacheawchankit *et al.* (2009) have demonstrated that the acemannan component of aloe gel promoted the oral wound healing via the induction of fibroblast proliferation and stimulation of keratinocyte growth factor-1, VEGF, and type I collagen expressions. More recently, the oral administration of aloe gel in rats was shown to enhance the inflammatory cell infiltration, angiogenesis, ECM deposition, and epithelialization, as well as the levels of TGF-β and VEGF growth factors (Atiba *et al.* 2011). Also the antioxidant, bactericidal and fungicidal effects of aloe vera gel may also have a positive role in the wound healing process (Ranjani *et al.* 2010; Rosca-Casian *et al.* 2007).

Due to all mentioned positive effects of the aloe vera gel, we have selected this phytochemical product to incorporate into the electrospun scaffolds for skin repair, aiming a positive effect in the wound healing process.

3.1.3. *Ilex paraguariensis*

Ilex paraguariensis St. Hill is an aboreous Aquifoliaceae plant native from South America countries. Its leaves and twigs are marketed as a fresh product, sold to yerba mate processing companies that dry, grind, and pack it. This processed product of *I. paraguariensis* has been used by local populations to prepare, by means of infusion, a beverage named *mate* (Spanish-speaking) or *chimarrão* (Portuguese-speaking populations) (Lunceford and Gugliucci 2005).

Interesting biological effects of *I. paraguariensis* aqueous extract have been reported, such as diuretic (Bastos *et al.* 2006), choleretic (Gorzalczany *et al.* 2001), antioxidant (Gugliucci 1996), neural stimulant, hypocholesterolemic, hepatoprotective, vasorelaxant, and atherosclerosis inhibition (Arbiser *et al.* 2005). More recently the effect of *I. paraguariensis* on the blood vessel formation by vasculogenesis and angiogenesis has been reported. Indeed, in an *in vivo* yolk-sac membrane assay, *I. paraguariensis* aqueous extract increased the number of blood vessels in more than 90% (Strassmann *et al.* 2008).

It is well accepted that angiogenesis plays a critical role in the wound healing process. During the wound healing process, the damaged blood vessels are replaced from intact capillaries, and the newly formed blood vessels are one of the most important components of granulation tissue, being responsible for providing nutrition and oxygen to the regenerating tissue. Inadequate angiogenesis is many times in the origin of impaired wound healing. Indeed, it has been demonstrated that inhibition of angiogenesis with administration of TNP-470, a potent anti-angiogenic compound, significantly decreased wound healing in a dose-dependent manner (Klein *et al.* 1999). Similarly, Kurosaka *et al.* (2009) have demonstrated that reduced angiogenesis causes a delayed wound healing and have also elucidated the role of the angiogenic factor, angiotensin II. In a complementary approach, Galiano *et al.* (2004) have demonstrated that topical VEGF accelerates diabetic wound healing through increased angiogenesis. In this context, we hypothesized that the *I. paraguariensis* aqueous extract may have a positive effect in the wound healing process due to its pro-angiogenic activity. For that reason, we have selected this plant extract for incorporation in the electrospun scaffolds for application in skin engineering.

3.1.4. Electrospinning solvents and the incorporation of biocompounds

Although the incorporation of bioactive molecules in the electrospun biomaterials through direct dissolution in the electrospinning solution is simple in theory, most of the polymeric systems require organic solvents that can degrade the bioactive molecules or impair their biological activity. Particularly, the PHBV/chitosan system described is chapter 2, uses a blend of a strong acid (TFA) and fluorinated alcohol (HFIP) for the nanofiber production and the processing time for the electrospinning of a 20 mL solution is approximately 42 hours. These conditions make unfeasible the direct addition of the bioactive plant extracts

to the spun solution, as bioactivity would probably be lost due to degradation of compounds. To allow the addition of the bioactive molecules in the PHBV/C mats, we have developed a dual syringe electrospinning system in which an aqueous polymer solution is used as vehicle for the incorporation of plant extracts.

3.1.5. Electrospinning in aqueous solution

Although most of the electrospun nanofibers are produced from organic solutions, there are also some polymers that could be electrospun into fibers in aqueous conditions, *e.g.* PVA, PEO, and silk (Zhu *et al.* 2008; Liu *et al.* 2007; Koski *et al.* 2004). PVA is a semi-crystalline polymer that shows an excellent electrospinnability in aqueous solution (Koski *et al.* 2004). Furthermore, PVA has been used as co-polymer to enhance electrospinnability and mechanical properties of biopolymers such as chitosan (Lin *et al.* 2006). The biocompatibility of PVA allows its application in biomaterials for tissue engineering of bone and skin (Gupta *et al.* 2009; Aramwit *et al.* 2010; You *et al.* 2004; Gao *et al.* 2012). Here, we used an aqueous solution of PVA and chitosan as vehicle for the incorporation of bioactive compounds of *A. barbadensis* and *I. paraguariensis*. PVA/chitosan fibers were combined with the PHBV/C ones, using a dual syringe electrospinning system, in order to create dual-polymer composite fibrous mats. The PHBV/C 4:1 (w/w) was selected for the dual-fiber system since it exhibited the best performance as scaffold for skin regeneration, as previously discussed in chapter 2. Morphological characterization, as well as bioactive compounds distribution in the mats, were performed and the potential of dual-fiber mats for skin engineering was analyzed *in vitro* and *in vivo*.

3.2. Experimental

3.2.1. Materials

All chemicals were of analytical grade and obtained from Sigma-Aldrich (Sigma-Aldrich Chemical Company, St. Louis, MO). All biological supplies were purchased from Invitrogen (Invitrogen Grand Island, NY, USA) unless otherwise noted. Aloe vera leaves (*Aloe barbadensis* Miller) were kindly supplied by "Naturama Sucos Integrais do Brasil

Ltda". *Ilex paraguariensis* leaves were gently donated by "Matevel-Erva Mate Verdinha, Ltda".

3.2.2. Preparation of aloe gel

Fresh *A. barbadensis* leaves (~ 2 years age) from several plants were collected and washed with tap water. The basal (~1 cm) and apical (~10 cm) extremities, as well as the rind, were removed with a sharp blade. The clear pulp was homogenized with a multimixer (Walita, Billy RI 1340) and filtered under vacuum using a polyester mesh, in order to obtain the fresh aloe gel.

3.2.3. *Ilex paraguariensis*

3.2.3.1. Preparation of aqueous extract

I. paraguariensis leaves were collected from adult mate plants (about 5-year-old) in Catanduvas (South Catarina, Brazil). The leaves were dried at 45 °C, powdered, and stored at -20ºC.

The aqueous extract of *I. paraguariensis* was prepared according to Strassmann *et al.* (2008) with some modifications. Briefly, 2 g of leaves (dry weight) were added to 50 mL of ultrapure water, followed by boiling (20 min.) under reflux in a Soxhlet apparatus. The aqueous extract was recovered by filtration on a cellulose support, lyophilized, and stored at -20ºC.

3.2.3.2. Effect of aqueous extract on vasculogenesis and angiogenesis

The experiment was approved by Animal Ethics Committee of UFSC (PP00069/2006).

The effect of *I. paraguariensis* aqueous extract on the blood vessel formation by vasculogenesis and angiogenesis was evaluated by the yolk-sac membrane *in vivo* assay, following described.

Chicken fertilized eggs (*Gallus domesticus*) supplied by "Tyson, S.A." were incubated at 37 °C and 30% relative humidity.

The treatments (n=8) were administered by implanting sterile disk-shaped PET pieces (2 mm diameter and ~ 0.5 mm thickness; one disk per embryo) impregnated with aqueous extracts of *I. paraguarensis* (10 μL), at five concentrations: 0.015; 0.045; 0.15; 0.45 and 1.5 mg of lyophilized extract/mL of water. PET disks (water ultrafiltered as vehicle; pH 7.2) were used as negative control.

For vasculogenesis study, after a preliminary period of 48 hours of incubation, a 10 mm diameter window was opened in the eggshell (adjacent to the embryo). For each treatment, the disk was implanted in the outer one-third surface of the yolk-sac membrane, near the embryo, where blood islands were present. The shell window was subsequently closed with black binding cellophane tape, and the egg returned to the incubator. Two days after implantation the zone around the disk was examined under a stereoscopic microscope (Olympus, Tokyo, Japan equipped with a digital camera Moticam 1000), as illustrated in **Figure 3.1**. The effects in vessel formation were determined by the increase or decrease in vessel number intercepting the PET disk as compared to the control.

For angiogenesis study, after a preliminary period of 48 hours of incubation, a 10 mm diameter window was opened in the eggshell in order to prevent embryo adhesion, and immediately closed with black binding cellophane tape. After another 48 hours of incubation, the tape was removed and the treatment disks were implanted on the blood vessels of the outer one-third surface of the yolk-sac membrane. The window was closed and the eggs were re-incubated for another 24 hours. Afterward, the vessels around the disk were observed using a stereoscopic, as described for the vasculogenesis procedure.

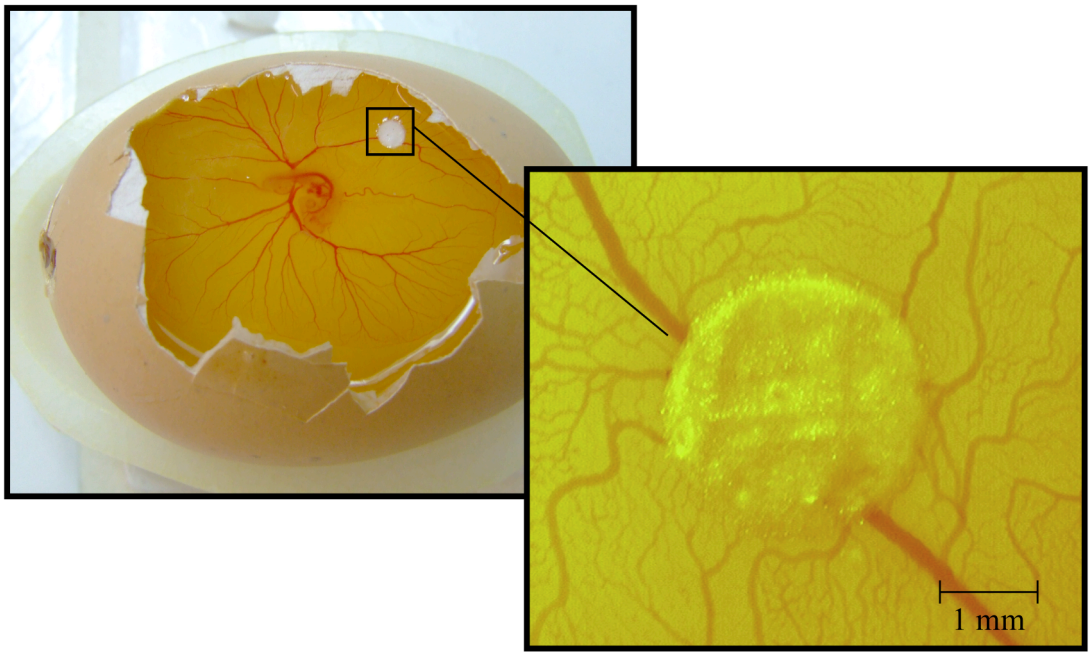

Figure 3.1. Illustrative representation of the blood vessel analysis in the yolk-sac membrane assay.

3.2.4. Scaffolds fabrication by electrospinning

A dual syringe electrospinning apparatus was used to fabricate the dual-fiber mats of PHBV/chitosan (PHBV/C) and PVA/chitosan (PVA/C) (**Figure 3.2**). One of the syringes was loaded with 10 wt.% of PHBV/C 4:1 (w/w) in TFA/HFIP 1:1 (v/v) (one of the spun solutions described in chapter 2). The second syringe was loaded with 10 wt.% of PVA/$C_{1500\ kDa}$ 9:1 (w/w) in 0.2 mol/L acetic acid. The bioactive extracts, *A. barbadensis* and *I. paraguariensis* were directly added to the PVA/chitosan solution (final concentration of 1 wt.% and 0.01 wt.%, respectively). The solutions were maintained under stirring during the electrospinning process. The electrospinning process was conducted at 22 kV of applied voltage, with a flow rate of 8 μL/min and a needle tip-to-collector distance of 14 cm. Fibers were collected as a nonwoven fibrous mat on the rotating drum (900 rpm), in air and at room conditions (20 ± 2 ºC, 45–50% RH). The scaffolds were dried at 35ºC for 24 hours. **Table 3.1**. summarizes the chemical composition of the electrospinning solutions and final electrospun mats.

Table 3.1. Solution and electrospun mat composition.

	Solution composition[a]	**Dry mat composition**[b]
Dual-fiber	**Syringe 1**: PHBV/C_{48kDa} 4:1 (w/w) (10 wt.%) in TFA/HFIP 1:1 (v/v) **Syringe 2**: PVA/$C_{1500\ kDa}$ 9:1 (w/w) (10 wt.%) in 0.2 mol/L acetic acid	45.0% PVA 40.0% PHBV 10.0% Chitosan 48 kDa 5.0% Chitosan 1500 kDa
Aloe_dual-fiber	**Syringe 1**: PHBV/C_{48kDa} 4:1 (w/w) (10 wt.%) in TFA/HFIP 1:1 (v/v) **Syringe 2**: PVA/$C_{1500\ kDa}$ 9:1 (w/w) (10 wt.%) + *A. barbadensis* (1 wt.%) in 0.2 mol/L acetic acid	42.9% PVA 38.1% PHBV 9.5% Chitosan 48 kDa 4.8% Chitosan 1500 kDa 4.8% *A. barbadensis*
Ilex_dual-fiber	**Syringe 1**: PHBV/C_{48kDa} 4:1 (w/w) (10 wt.%) in TFA/HFIP 1:1 (v/v) **Syringe 2**: PVA/$C_{1500\ kDa}$ 9:1 (w/w) (10 wt.%) + *I. paraguariensis* aqueous extract (0.01 wt.%) in 0.2 mol/L acetic acid	45.0% PVA 40.0% PHBV 10.0% Chitosan 48 kDa 5.0% Chitosan 1500 kDa 0.05% *I. paraguariensis*
Bioactive dual-fiber	**Syringe 1**: PHBV/C_{48kDa} 4:1 (w/w) (10 wt.%) in TFA/HFIP 1:1 (v/v) **Syringe 2**: PVA/$C_{1500\ kDa}$ 9:1 (w/w) (10 wt.%) + *A. barbadensis* gel (1 wt.%) + *I. paraguariensis* aqueous extract (0.01 wt.%) in 0.2 mol/L acetic acid	42.9% PVA 38.1% PHBV 9.5% Chitosan 48 kDa 4.8% Chitosan 1500 kDa 4.8% *A. barbadensis* 0.05% *I. paraguariensis*

[a] Initial composition of the spun solutions;

[b] Final composition of the electrospun fibrous mats, assuming that all solvents have been removed during the electrospinning process.

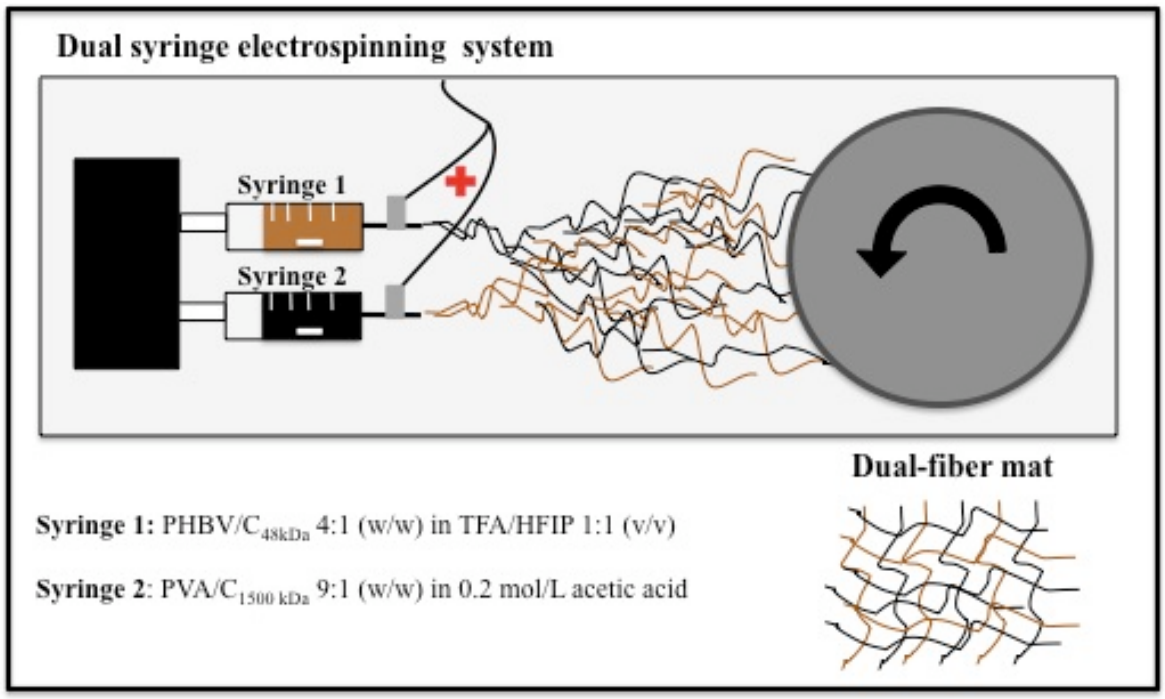

Figure 3.2. Schematic representation of the dual syringe electrospinning system.

3.2.5. Scaffolds characterization

Electrospun mats were analyzed by SEM (Hitachi S4100) at an accelerating voltage of 25 kV and by ATR-FTIR, using a Golden-gate single reflection ATR in a Bruker IFS-spectrometer at a resolution of 8 cm^{-1} and 256 co-added scans.

3.2.6. Biological studies

In vitro cell culture studies were conducted using mouse fibroblast cells (L929). The detailed description of cell culture conditions, as well as the experimental procedures of the indirect cytotoxicity and MTS assays, SEM and CLSM analysis of cells cultured on the scaffolds are described in chapter 2 (§ 2.2.5.4).

For the live/dead assay (Molecular probes, Invitrogen) cells were cultured on sterile scaffold pieces (24-well plates, 1 x 10^5 cells/well) for 2, 7, and 14 days, at 37 °C in a wet atmosphere containing 5% CO_2. Cell culture medium was replaced every 3 days. Afterwards, the culture medium was removed and 100 μl of PBS solution containing of 4 μM of ethidium homodimer-1 and 2 μM of calcein AM (live/dead kit components) were

added. Cells were re-incubated for 45 minutes, mounted and observed on a fluorescence microscope (Olympus BX41).

The wound healing model used to evaluate the scaffolds in the skin healing process is described in chapter 2 (§ 2.2.6).

3.2.7. Statistics

Statistical analysis was carried out using Instat 3.0. Results were expressed as the mean ± standard deviation and compared through one-way ANOVA and Tukey-Kramer multiple comparisons test. $P < 0.05$ was considered statistically significant.

3.3. Results and discussion

In this chapter we describe the development of a dual-polymer composite fibrous mat prepared by a dual electrospinning system in which one syringe was loaded with PHBV/C in the organic solvents and the other with PVA/C in aqueous solution, in order to obtain dual-fiber electrospun mats. Plant extracts from *A. barbadensis* and *I. paraguariensis* with bioactivity in the wound healing process were added to the aqueous solution. We have selected *A. barbadensis* gel for its well-recognized effects on the wound healing process and the aqueous extract of *I. paraguariensis* for its positive effect on the blood vessel formation. A detailed description of the dual-fiber mats morphological characterization, as well as the fiber and plant extracts distribution in the mats, is given below.

3.3.1. Morphological analysis of PVA/chitosan nanofibers

SEM analysis revealed that the PVA/chitosan solution produced a typical nonwoven mesh of cylindrical nanofibers (**Figure 3.3** a). The addition of *A. barbadensis* (Figure 3.3 b), *I. paraguariensis* (Figure 3.3 c), or both extracts (Figure 3.3 d) did not promote considerable modifications on the fibrous morphology, *i.e.* beads or clusters formation, suggesting that the plant extracts solubilized well in the electrospinning solutions and were successfully incorporated into the PVA/chitosan fibers.

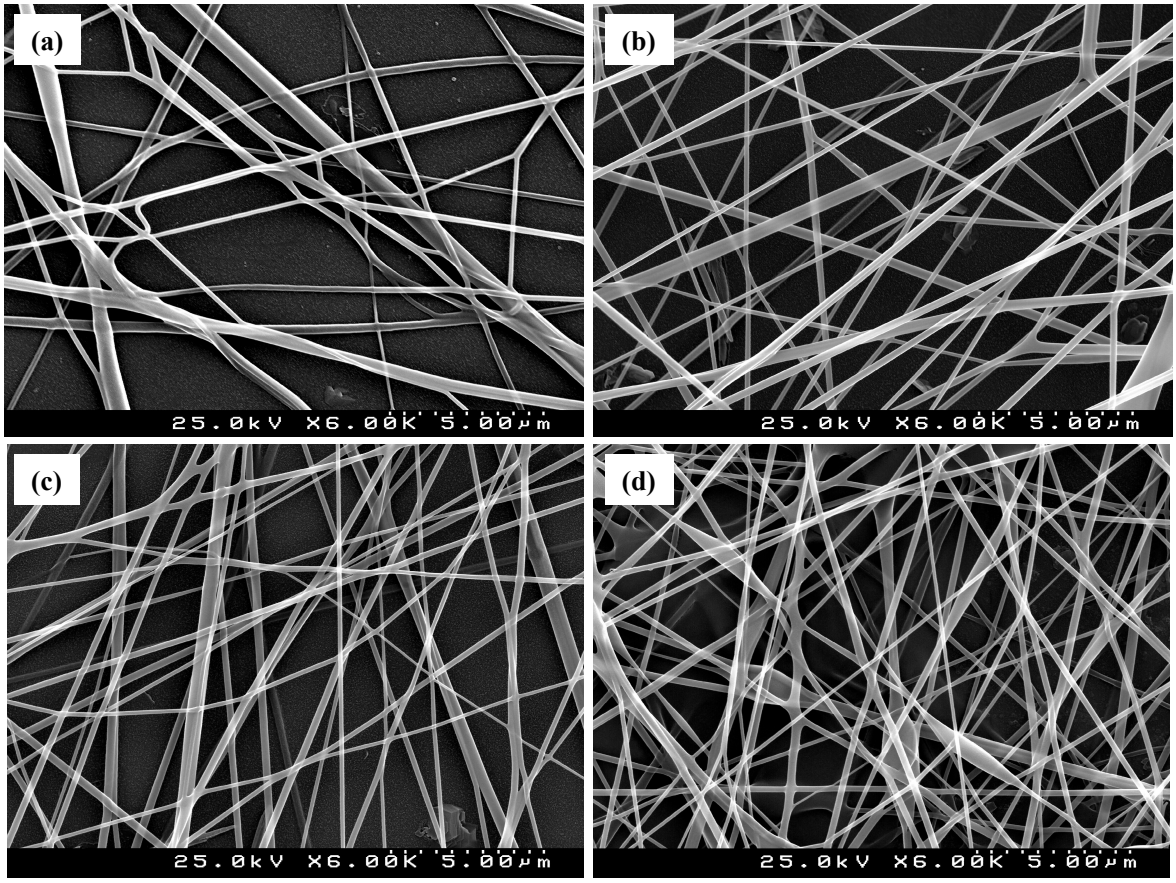

Figure 3.3. Representative SEM images of fibers obtained from electrospinning solutions of (a) PVA/chitosan 9:1 (w/w) (10 wt.%) in acetic acid 0.2 M (spun S_2), (b) S_2 + 1 wt.% of *A. barbadensis*, (c) S_2 + 0.01 wt.% of *I. paraguariensis* aqueous extract, and (d) S_2 + 1wt.% of *A. barbadensis* + 0.01 wt.% of *I. paraguariensis* aqueous extract.

3.3.2. Distribution of PHBV/chitosan and PVA/chitosan fibers in the dual-fiber mat

As previously mentioned, the dual-fiber mats were obtained by simultaneously electrospinning two different polymer solutions, one of PHBV and chitosan and the other of PVA and chitosan. In the electrospinning apparatus that has been used, the two syringes were displayed in parallel, in a top-bottom position, and pointing to the center of the rotating collector (Figure 3.2). The system was designed in order to homogeneously combine the two kinds of fibers during the trajectory of the jet to the collector. The distribution of the fibers in the mat was analyzed by SEM and FTIR. As illustrated in **Figure 3.4,** the dual-fiber mat evidenced morphological characteristics from both fibers (PHBV/C and PVA/C). Typical morphological details from the PHBV/C mat such as the smaller fiber diameter or the presence of ramifications and ruptures in the fibers (Figure

3.4 a), as well as from the PVA/chitosan mat such as the long cylindrical fiber shape, with higher diameters and no ramifications (Figure 3.4 b), were found all over the dual-fiber mat (Figure 3.4 c).

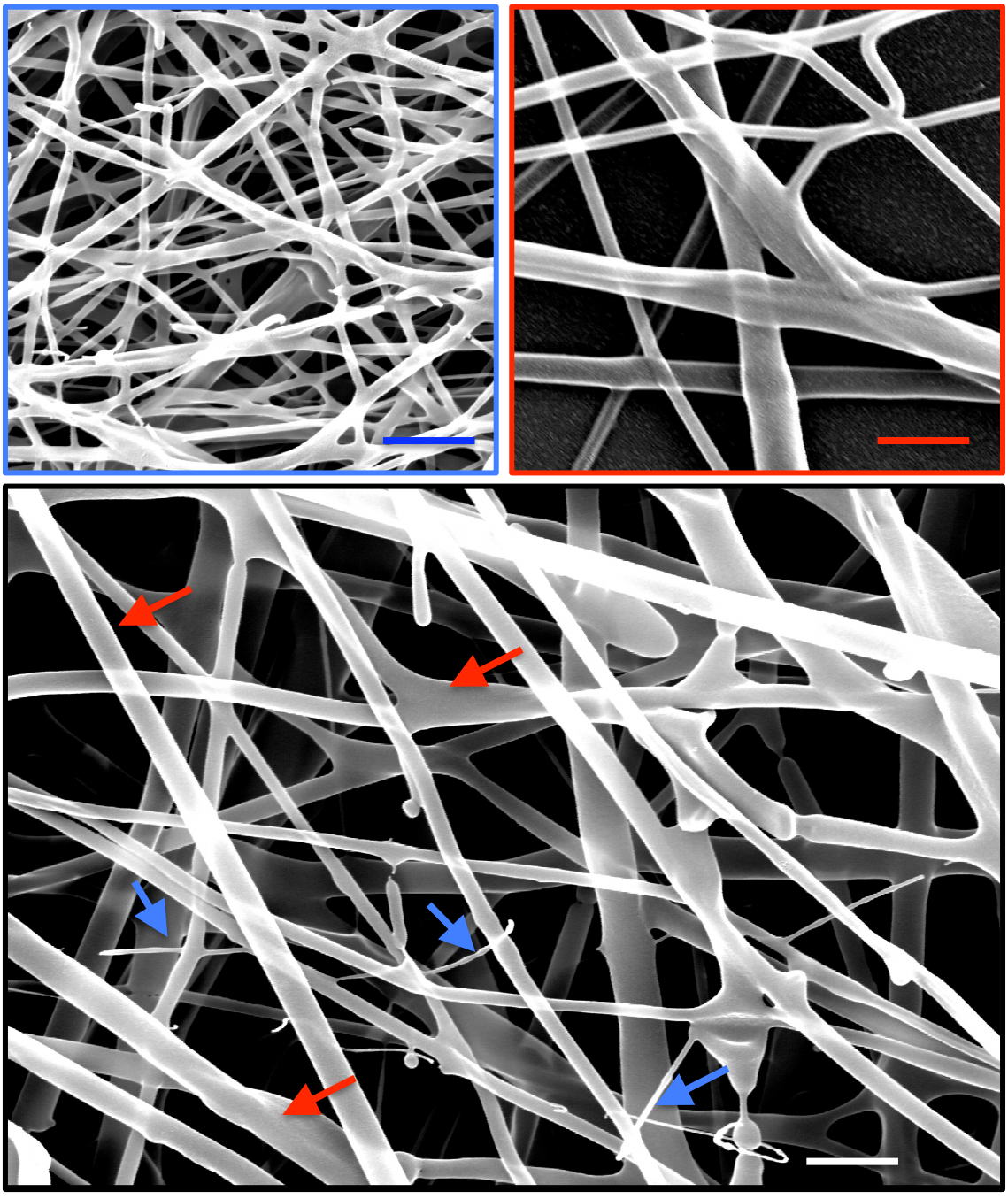

Figure 3.4. SEM images of (a) PHBV/C mat, (b) PVA/C mat, and (c) dual-fiber mat. Blue arrows evidence details from the PHBV/C fibers and red arrows from the PVA/C ones. Bar = 1μm.

Figure 3.5 displays the FTIR spectra of PHBV/C and dual-fiber mat. The addition of the PVA/C component caused subtle modifications on the FTIR spectrum profile. In fact, the major differences in the FTIR bands are derived from the differences in the relative concentration of chitosan between the two mats (the relative amount of chitosan in PHBV/C 4:1 (w/w) is 20% while in dual-fiber mat is 15%). Therefore, the dual-fiber FTIR spectrum exhibited a decreased intensity of absorption of the chitosan bands, including the broad band observed from 3650 to 3050 cm^{-1} (O-H stretching), the peak at 1680 cm^{-1} (C=O, amide I), and the N-H deformation of amide II at 1560 cm^{-1}. Similar spectra profiles were found for different regions of the dual-fiber mat, confirming the homogeneous distribution of the PHBV/C and PVA/chitosan fibers within the final fibrous mats.

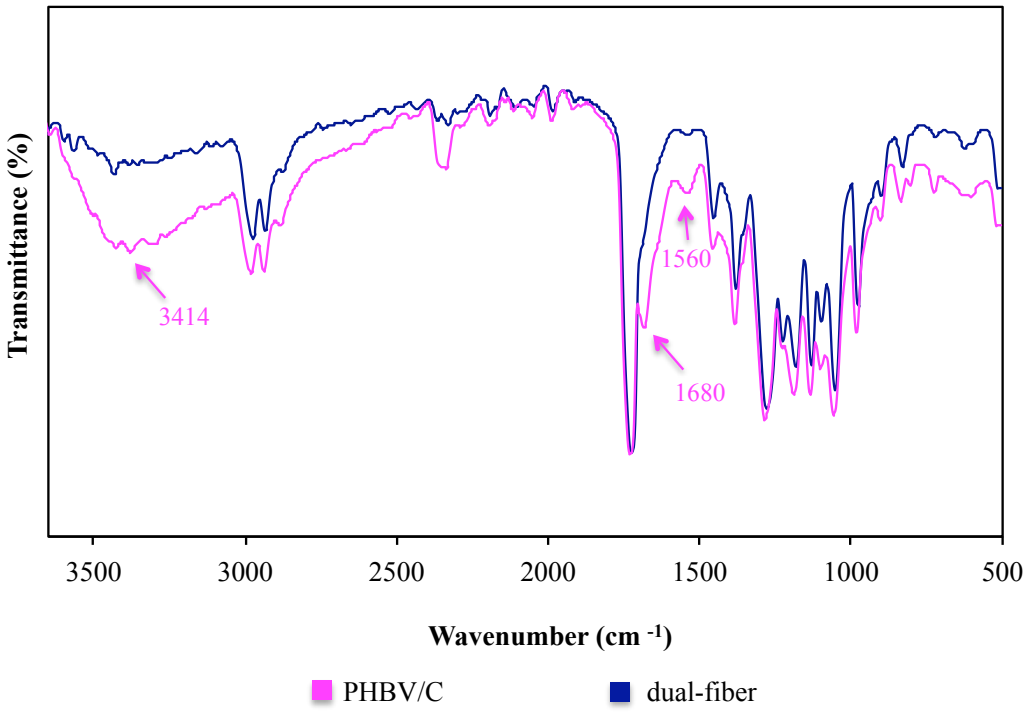

Figure 3.5. FTIR spectra obtained for electrospun fibers of PHBV/C 4:1 (w/w) and dual-fiber mat.

3.3.3. Distribution of bioactive extracts in the dual-fiber mats

Figure 3.6 displays representative SEM images of dual-fiber and bioactive dual-fiber mats. No important evidences of beads or clusters were found in the bioactive dual-fiber mat. This result also suggests a good incorporation and distribution of the bioactive extracts inside the fibers. An apparent effect of fiber diameter reduction was detected with the addition of the bioactive extracts. This reduction may be attributed to the presence of

salts and other components from the plant extracts that increase the solution conductivity and, consequently, the fiber stretching during electrospinning, resulting in the decrease of fiber diameter.

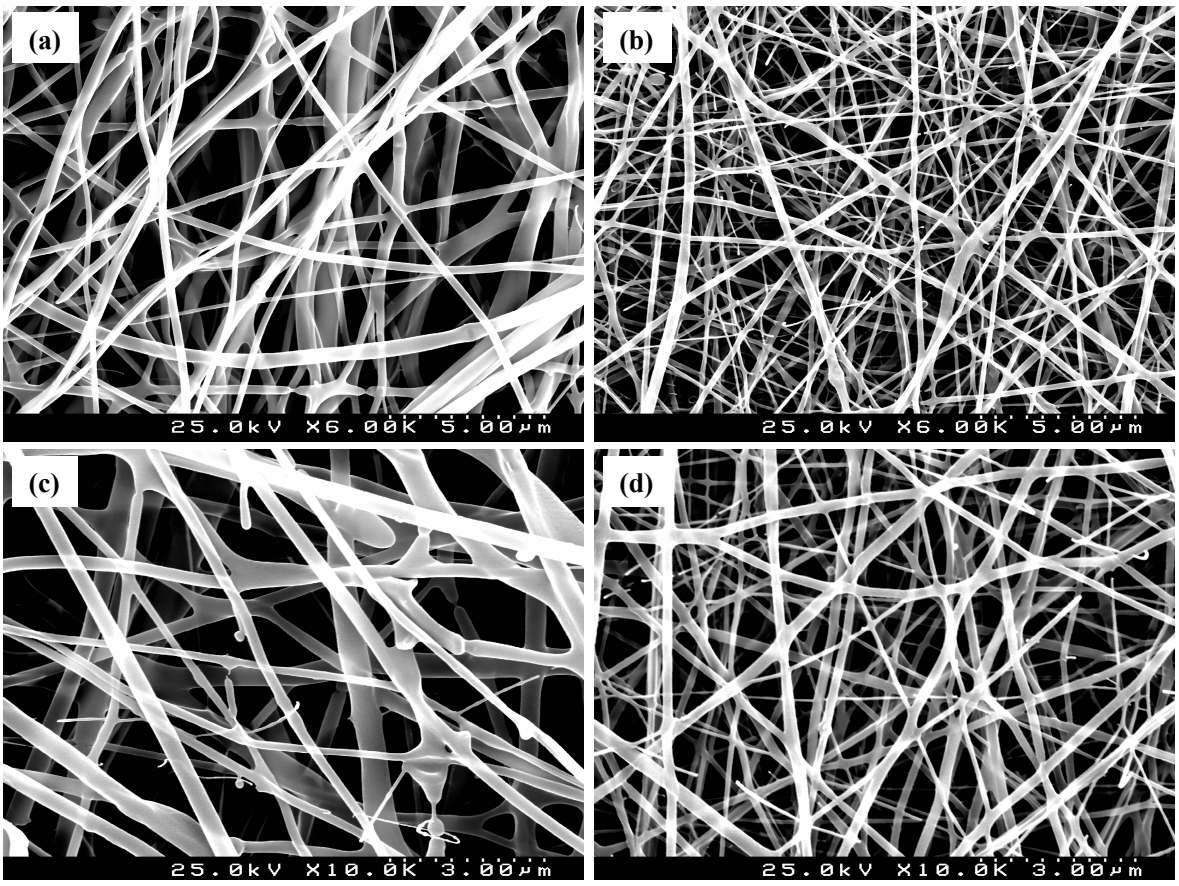

Figure 3.6. SEM pictures of (a and c) dual-fiber mat and (b and d) bioactive dual-fiber mat at 6000x (a and b) and 10000x magnification (c and d).

The distribution of the *A. barbadensis* gel and *I. paraguariensis* aqueous extract in aloe_dual-fiber and ilex_dual-fiber mats was also analyzed by FTIR (**Figure 3.7** and **Figure 3.8**, respectively).

The addition of the *A. barbadensis* extract (final concentration of 4.8%, dry weight) promoted considerable changes in the FTIR spectrum of the dual-fiber mat. Among these changes are the enormous increase in the intensity of the band ranging from 3700-3035 cm^{-1} (O-H stretching) and in the peak at 2950 cm^{-1} (C-H stretching), the occurrence of a new peak at 1680 cm^{-1} (C=O stretching of amide I), and the increase in the absorption

intensity of bands between 1150-980 cm^{-1} (C-O stretching) and 600-890 cm^{-1} (C-N-H and C=C-N-H deformation). These changes in the infrared absorption profile of the aloe_dual-fiber mat are attributed to several different functional groups of compounds found in the complex matrix of aloe gel (FTIR spectrum in red, Figure 3.7), including proteins, sugars, alcohols, organic acids, and esters, among many others.

Modifications on the FTIR spectrum of the dual-fiber mat due to the addition of *I. paraguariensis* extract include an increase in the broad band at 3700-3050 cm^{-1} (O-H stretching), in the 2940 cm^{-1} peak (C-H stretching), and in the 1540 cm^{-1} band (N-H deformation of amide II) (Figure 3.8). The occurrence of a new peak at 1680 cm^{-1} (C=O, amide I) and the increase in the intensity of bands at 600-890 cm^{-1} (C-N-H and C=C-N-H deformation region) found in the FTIR spectrum of ilex_dual-fiber mat also result from the inclusion of the compounds present in the *I. paraguariensis* extract. These changes are mainly attributed to the xanthines *e.g.* caffeine and theobromine, as well as polyphenols from the *I. paraguariensis* extract.

FTIR analysis of the bioactive dual-fiber mat (**Figure 3.9**) showed the increase in the strength of peaks associated to both *A. barbadensis* gel and *I. paraguariensis* extract (many times coincident), including the increase in the intensity of the band ranging from 3700-3035 cm^{-1} (O-H stretching), in the peaks at 2950 cm^{-1} (C-H stretching) and at 1540 cm^{-1} (N-H deformation of amide II), the occurrence of a new peak at 1680 cm^{-1} (C=O stretching of amide I), and the increase in the absorption intensity of bands between 1150-980 cm^{-1} (C-O stretching) and 600-890 cm^{-1} (C-N-H and C=C-N-H deformation).

Additionally, FTIR analysis confirmed a good distribution of the bioactive extracts in the dual-fiber mats as no important changes were found in the spectra obtained from different regions of the electrospun mats.

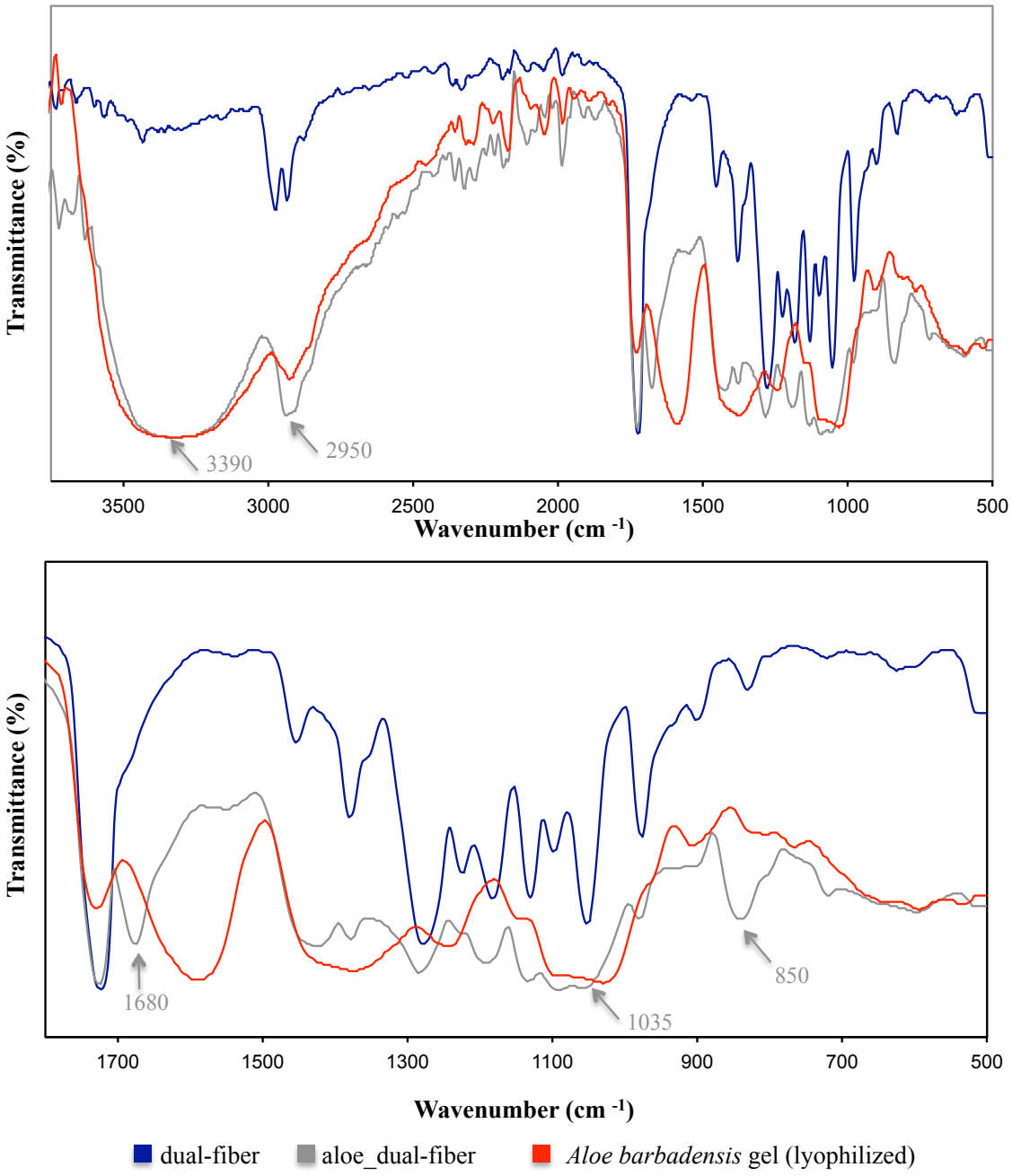

Figure 3.7. FTIR spectra obtained for electrospun fibers of dual-fiber, aloe_dual-fiber, and lyophilized aloe vera gel. Whole spectra (top) and fingerprint region (bottom).

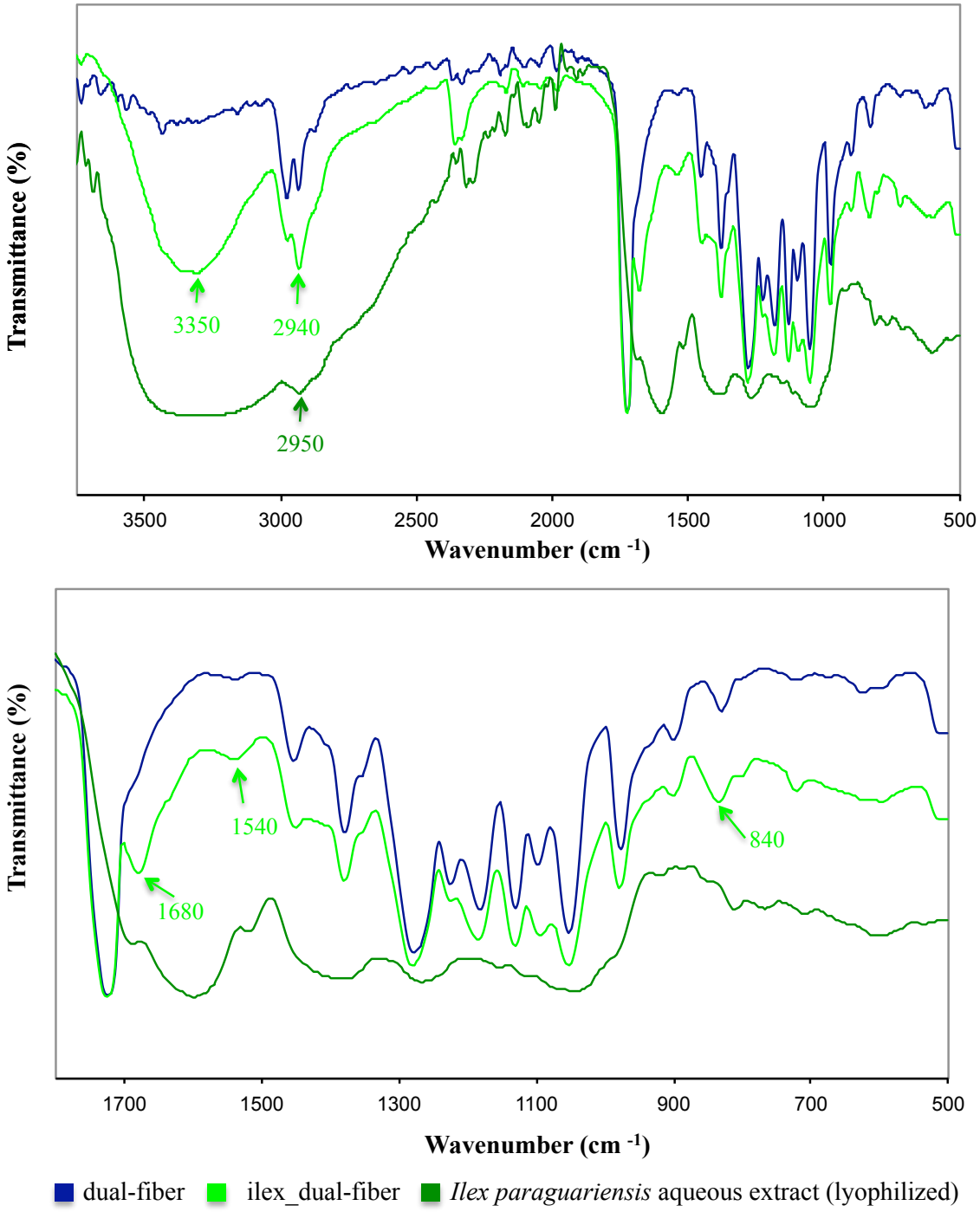

Figure 3.8. FTIR spectra obtained for electrospun fibers of dual-fiber, ilex_dual-fiber, and lyophilized *I. paraguariensis* aqueous extract. Whole spectra (top) and fingerprint region (bottom).

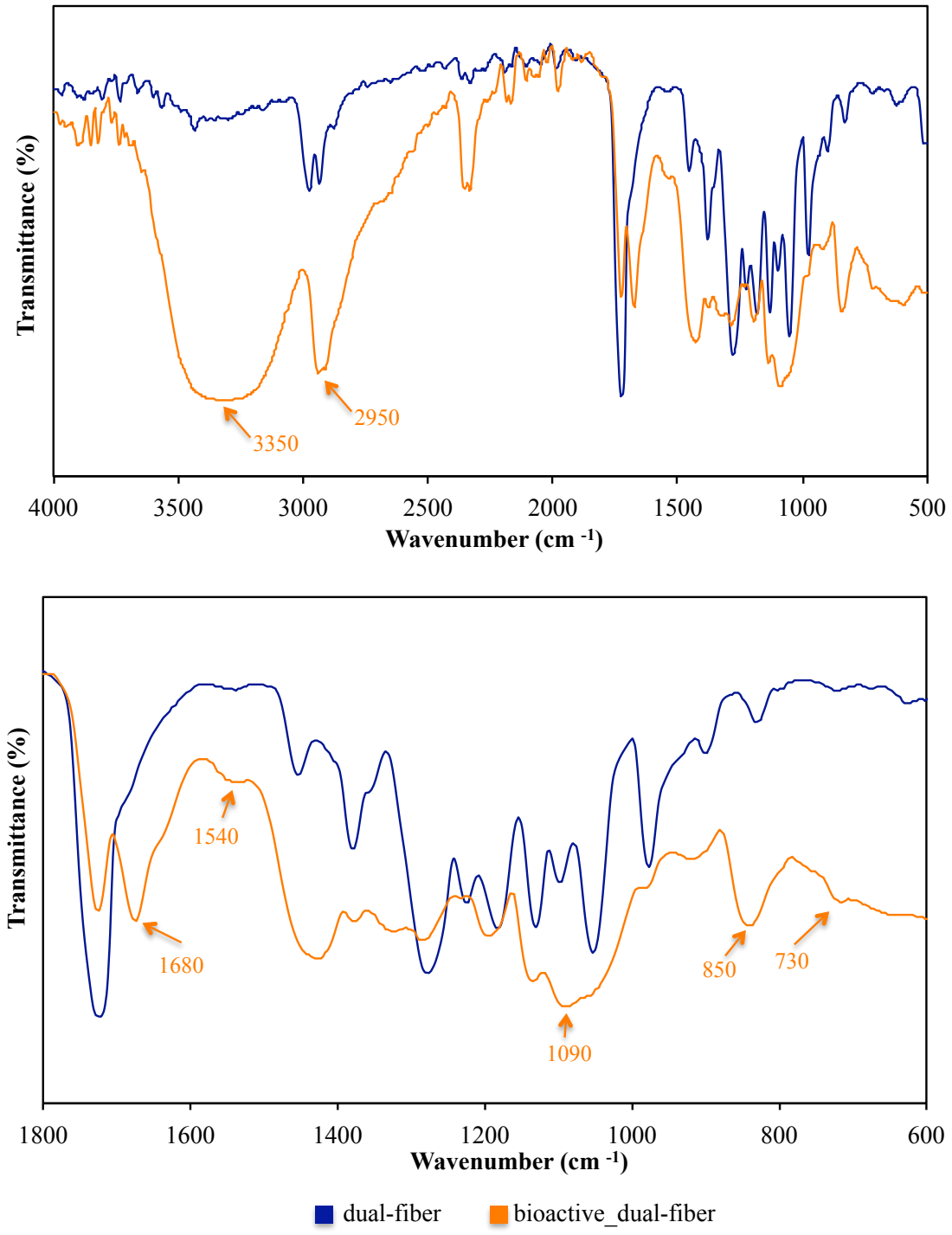

Figure 3.9. FTIR spectra obtained for electrospun fibers of dual-fiber and bioactive dual-fiber mats. Whole spectra (top) and fingerprint region (bottom).

3.3.4. Biological studies

Following a similar approach already described in chapter 2, the potential of the dual-fiber electrospun mats as scaffolds for skin engineering, with or without addiction of plant

bioactive extracts, was analyzed by combining *in vitro* cell culture studies with an *in vivo* wound healing assay. In this chapter, however, we focused on comparing the dual-fiber with the single-fiber PHBV/C mat (PHBV/C 4:1 (w/w)) and also on the effects of the bioactive extracts addition. These results will be discussed in the following subsections, but firstly, the results obtained for the effect of the *I. paraguariensis* aqueous extract on the blood vessel formation will be analyzed.

3.3.4.1. Pro-vasculogenic and pro-angiogenic effects of the aqueous extract of *I. paraguariensis*

In a recent study, Strassmann *et al.* (2008) have shown the positive effect of *I. paraguariensis* aqueous extract in blood vessel formation. Considering that angiogenesis is a key phenomenon in the tissue regeneration process, as the newly formed tissues depend on the reestablishment of the new vasculature for nutrition and oxygen, the addition of pro-angiogenic agents may have a positive effect on the wound healing process. There are two main mechanisms of blood vessel formation: vasculogenesis and angiogenesis. The first one is limited to the early embryonic period, where the development of blood vessels occurs from *in situ* differentiation of mesodermal progenitor endothelial cells to endothelial cells. These precursor cells are recruited from mesoderm areas adjacent to the embryo and/or originated by local cell division, organizing blood islands and establishing a primordial vascular plexus (DeRuiter *et al.* 1993). Later, a subsequent remodeling of these preexisting vessels (angiogenesis) gives rise to a more refined microvasculature that accompanies the growth and shaping of the body (Folkman 1971). In the yolk-sac membrane assay, processes of vasculogenesis and angiogenesis coexist. Nevertheless, in the first 4 days the primordial vessels are essentially formed from the blood islands by vasculogenesis, and afterwards angiogenesis predominates. We used the yolk-sac membrane assay to confirm the positive effect of the aqueous extract of *I. paraguariensis* reported by Strassmann *et al.* (2008). However, the effects of the extract on both vaculogenesis and angiogenesis were tested. **Figure 3.10**. displays the results obtained in the yolk-sac membrane assay.

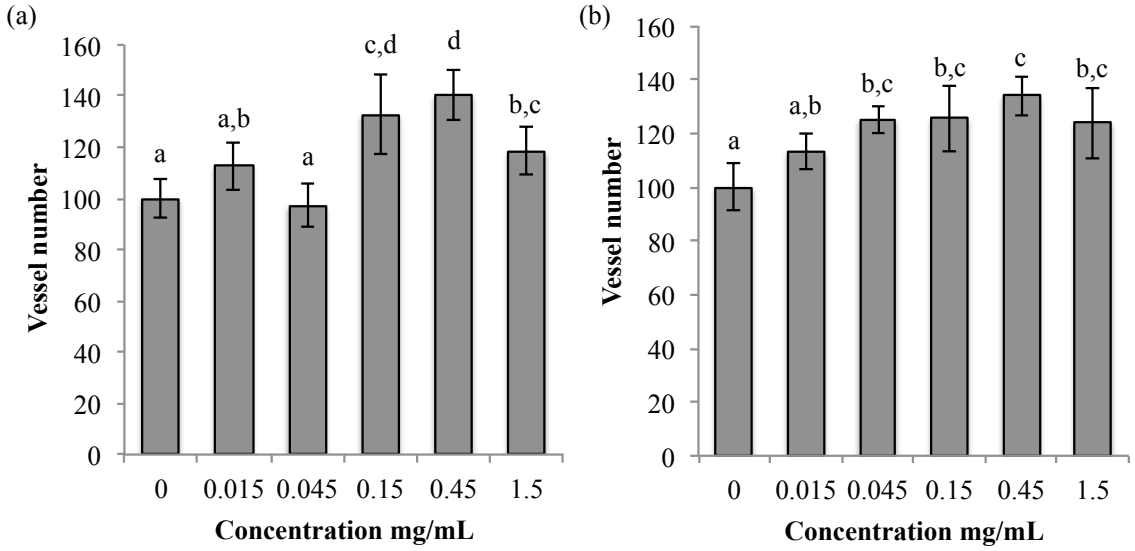

Figure 3.10. Effects of *I. paraguariensis* aqueous extract on the formation of blood vessels by (a) vasculogenesis and (b) angiogenesis. Different letters indicate significant differences at $P<0.05$.

Regarding to vasculogenesis, the aqueous extract of *I. paraguariensis* significantly increased the formation of new blood vessels for concentrations higher than 0.15 mg/mL (recall that 10 μL of the aqueous extract was added into a 2 x 0.5 mm PET disk). The highest effect was for the concentration of 0.45 mg/mL, where the percentage of blood vessels around the disk was 40 ± 10 % higher than the control. The extract also increased significantly the formation of blood vessels by angiogenesis for concentrations higher than 0.045 mg/mL. The highest pro-angiogenic effect was also observed for 0.45 mg/mL, where an increase of 34 ± 7 % of control was observed. Illustrative examples of the effect of *I. paraguariensis* aqueous extract on the blood vessel formation are displayed in **Figure 3.11**.

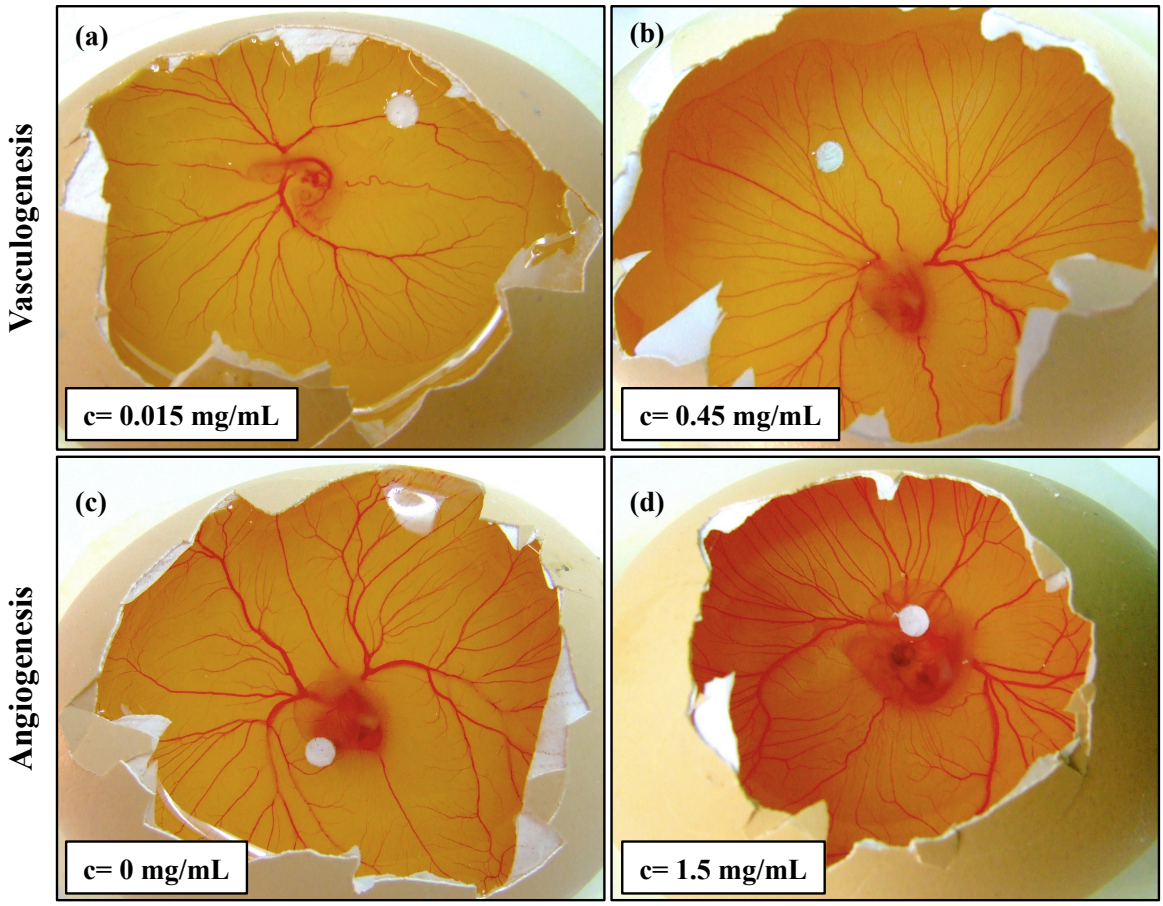

Figure 3.11. Representative examples illustrating the effects of *I. paraguariensis* aqueous extract on vasculogenesis and angiogenesis.

3.3.4.2. Cell viability and growth

As previously mentioned, the main purpose of this study is the development of a new dual-fiber electrospinning system suitable for the incorporation of bioactive plant extracts into the polymeric electrospun fibers. Several details were analyzed, including the configuration of the electrospinning system, the characteristic of the vehicle fibers (PVA/chitosan fibers), the distribution of fibers and extracts within the mats, among others. Other important aspects could also have been explored, for example the concentration of the bioactive extracts in the electrospun mats, but we were compiled to limit the number of variables in this initial phase of investigation, giving its exploratory nature.

With respect to the indirect cytotoxicity assay, no significant differences were found among PHBV/C, dual-fiber, and bioactive dual-fiber scaffolds (**Figure 3.12**). This result

indicates that, for the period analyzed, there was no evidence of cytotoxic compounds released from the scaffolds.

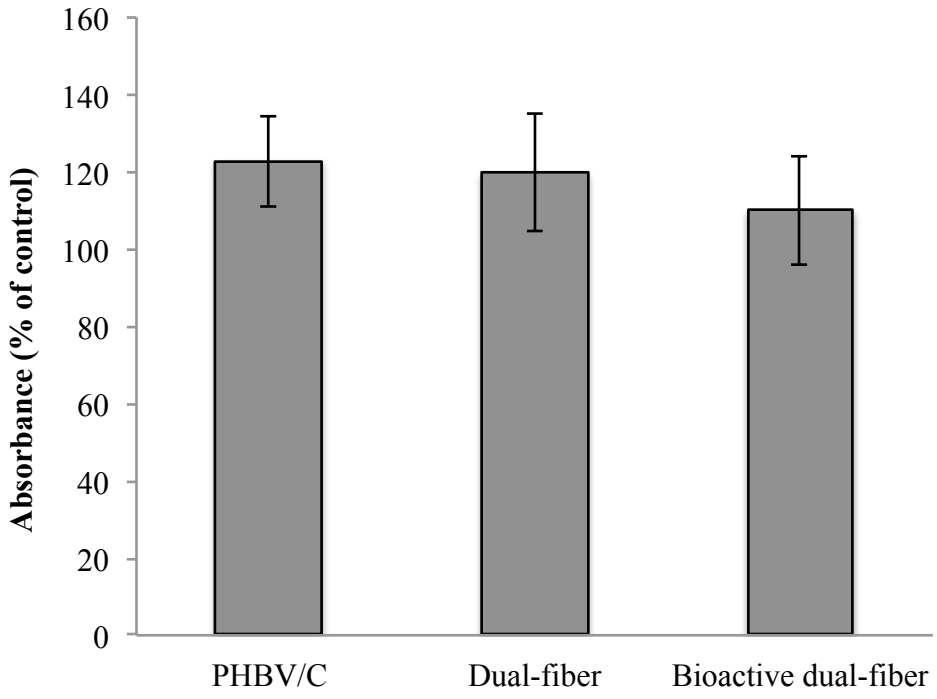

Figure 3.12. Absorbance 540 nm (% of control, *i.e*. TCP) of L929 cells cultivated on the PHBV/C 4:1 (w/w), dual-fiber, and bioactive dual-fiber scaffolds extraction media. No significant differences were observed (P>0.05).

L929 cells were cultivated on PHBV/C, dual-fiber, and bioactive dual-fiber scaffolds for different intervals. Viability, adhesion, and growth of cells were analyzed combining MTS colorimetric assay, with SEM, and different fluorescence cell staining procedures such as the live/dead, actin, and vinculin staining assays.

Live /dead assay is a fluorescence cell viability assay, where live and dead cells are simultaneously stained with calcein AM and ethidium homodimer-1, respectively. Non-fluorescent calcein AM is transported through the membranes of living cells and further enzymatically converted by intracellular estereases into calcein, producing a green fluorescence. On the other hand, the ethidium homodimer-1 only permeates membrane damaged cells, where it binds to cell nucleus, producing a red fluorescence. Therefore, this assay is used to evaluate cytotoxic and is particularly interesting for analysis of cells cultivated on biomaterials. As a fluorescence labeling technique, this assay gives a rapid illustration of how viable and dying cells are distributed on the scaffolds.

Results from MTS assay are plotted in **Figure 3.13**. During the first 7 days of culture, an increase in the absorbance was observed for all scaffolds, which is indicative of the increase of cells metabolic activity. After 7 days of culture, all scaffolds already exhibited a confluent layer of cells, as evidenced in pictures from the live/dead assay (**Figure 3.14**) and thereby, the cell growth stabilized on the subsequent days of culture, as illustrated by the MTS assay (absorbance stabilizes).

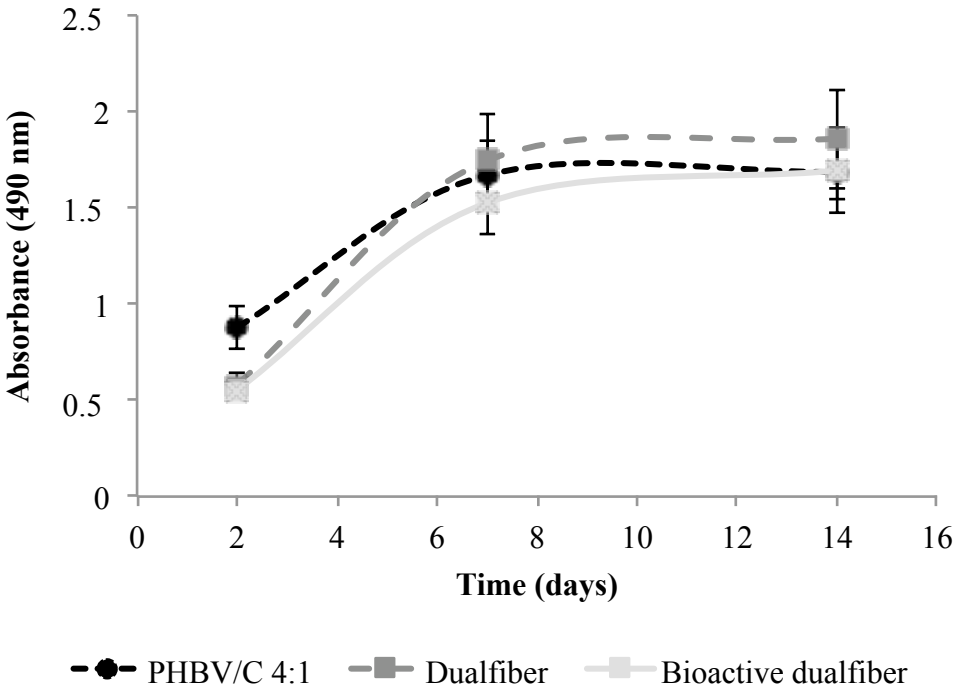

Figure 3.13. MTS assay for cells cultured on the PHBV/C 4:1 (w/w), dual-fiber, and bioactive dual-fiber scaffolds for 2, 7, and 14 days.
No significant differences were observed among treatments (P>0.05).

Although cells reached confluence on all scaffolds, live/dead assay indicated a slight increase in the number of dead cells for PHBV/C 4:1 (w/w), comparing to the dual-fiber scaffolds, at the 14th day of culture (Figure 3.14).

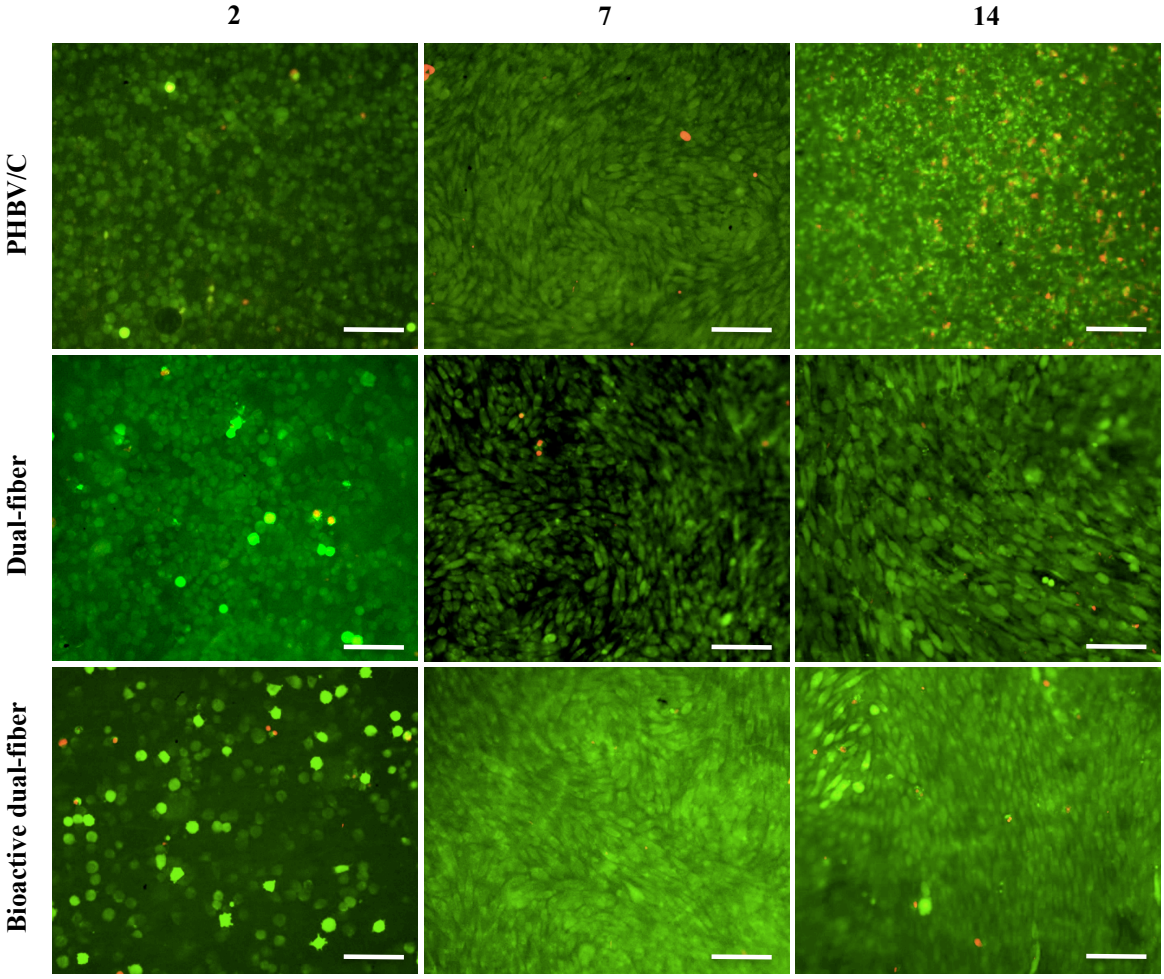

Figure 3.14. Live/dead assay of cells cultured on the PHBV/C 4:1 (w/w), dual-fiber, and bioactive dual-fiber scaffolds for 2, 7, and 14 days. Live cells appear in green and dead cells in red. Bar=100 μm.

Figures 3.15 and **Figure 3.16** display representative examples of SEM pictures obtained from L929 cells cultured on PHBV/C 4:1, dual-fiber, and bioactive dual-fiber, for different growing times. SEM pictures revealed that cells attached to multiple fibers of the scaffolds, showing a spherical morphology after 12 hours of culture that successively changed to a well-spread morphology, during the subsequent days of culture. At the 7th day after seeding, a confluent layer of cells and its extracellular secreted products, *i.e.* ECM, covered almost all the surface of scaffolds. SEM analysis of the bioactive dual-fiber scaffold also revealed that after hydrating, the mat surface became very irregular (shrinkage) and cells tended to form clusters, mainly during the first 2 days of culture. This

phenomenon is probably attributed to the high water absorption capacity of aloe gel present in this mat.

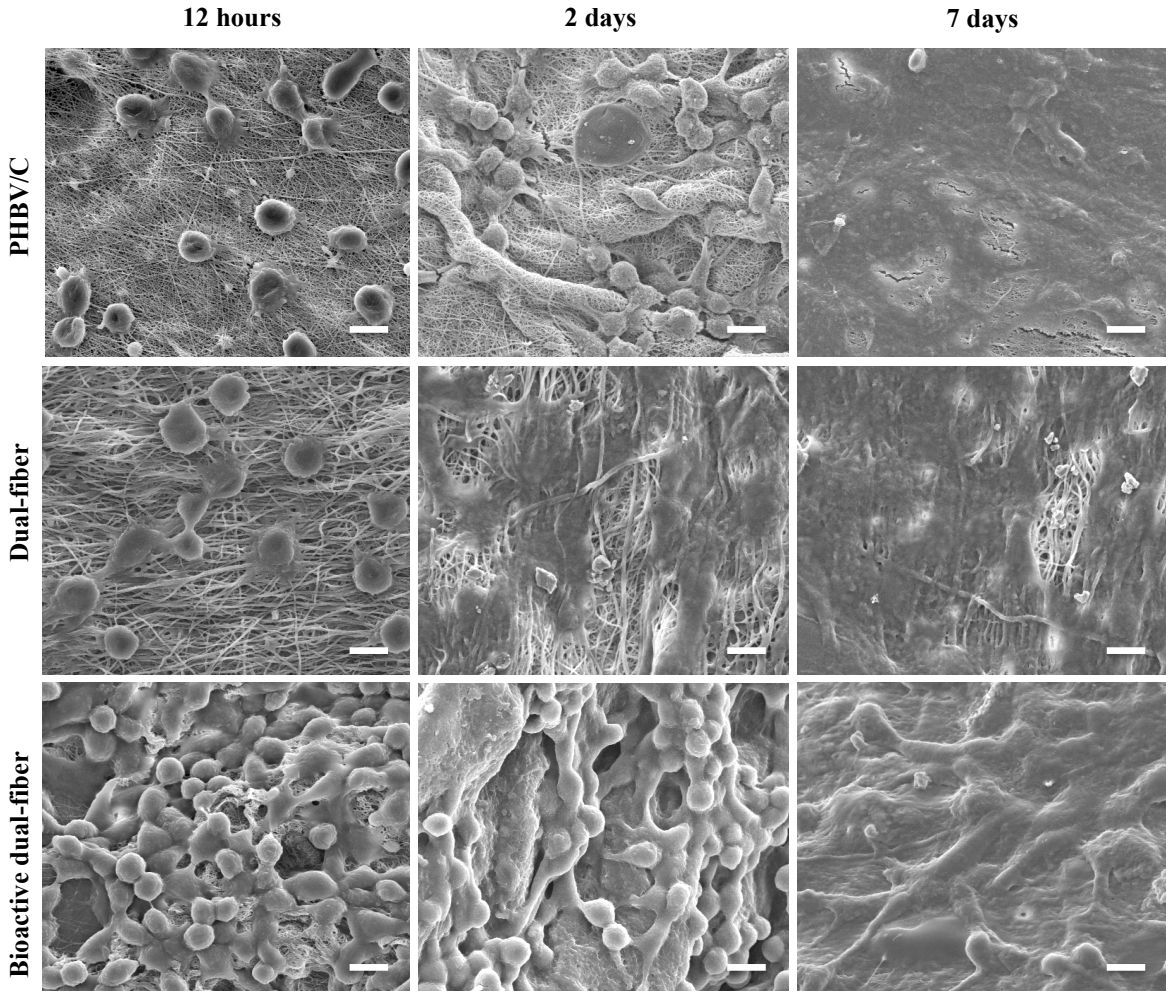

Figure 3.15. SEM analysis of cells cultured on PHBV/C 4:1 (w/w), dual-fiber, and bioactive dual-fiber scaffolds for 12 hours, 2 days, and 7 days after seeding. Bar= 10μm.

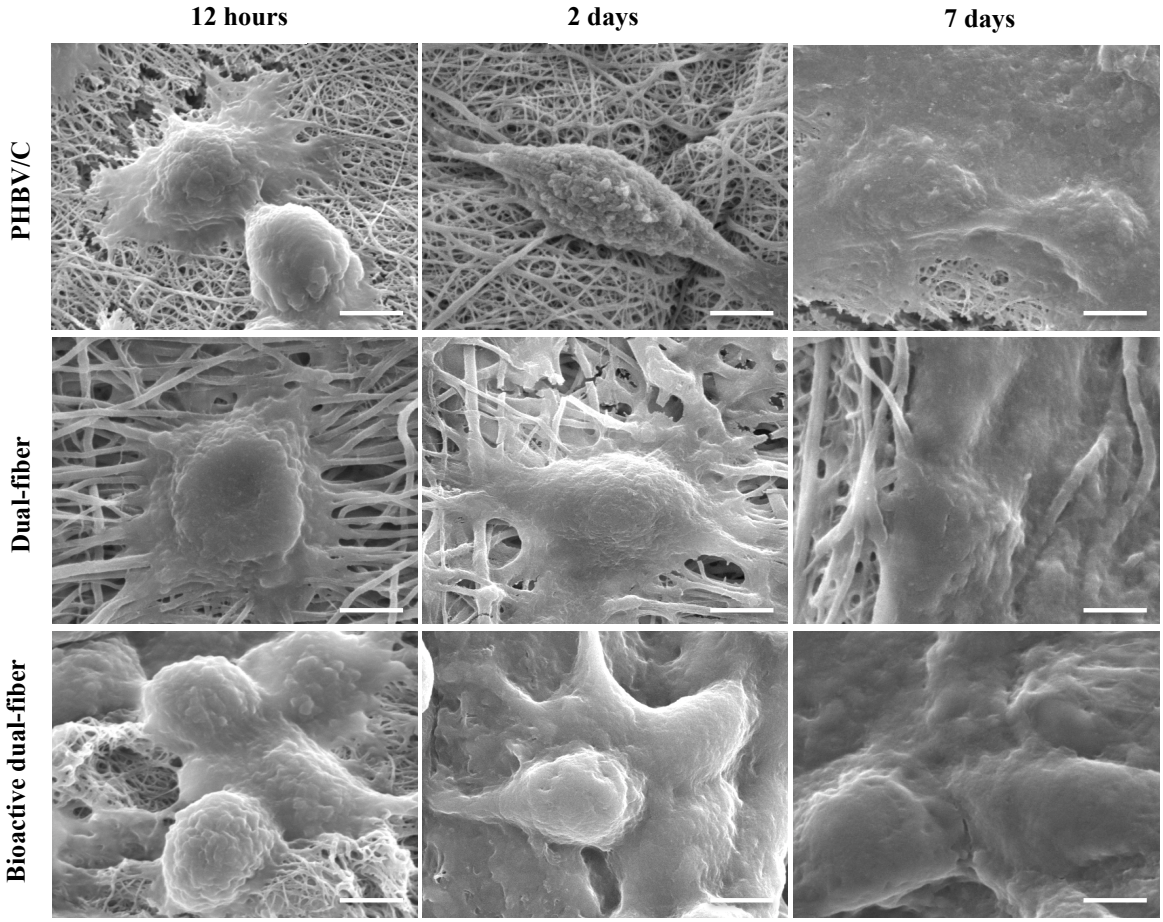

Figure 3.16. SEM analysis (high magnification) of cells cultured on PHBV/C 4:1 (w/w), dual-fiber, and bioactive dual-fiber scaffolds for 12 hours, 2 days and 7 days after seeding. Bar = 5 μm.

CLSM of actin and nucleus showed similar cell behavior found by SEM analysis, *i.e.* initial lower level of spreading and cell cluster for cells cultured on bioactive dual-fiber scaffolds, in comparison to those cultured on PHBV/C and dual-fiber scaffolds (**Figure 3.17)**. At the 7th day of culture a confluent layer of L929 cells covering the scaffold surfaces, with similar levels of cell spreading, was observed in the three scaffolds, as illustrated in **Figure 3.18**.

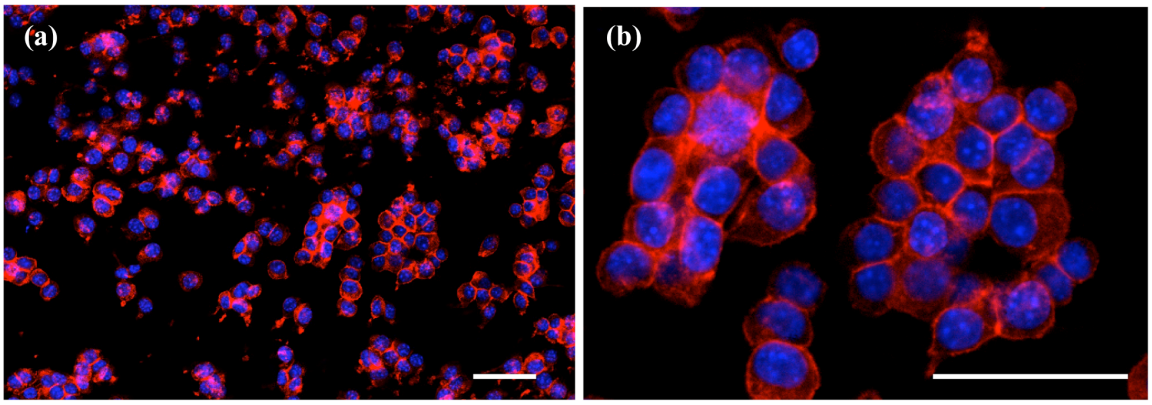

Figure 3.17. CLSM images (a) low magnification and (b) high magnification of L929 fibroblasts cultured on bioactive dual-fiber scaffolds for 12 hours. F-actin (red) and nucleus (blue) stained with Alexafluor 546 conjugated to phalloidin and DAPI, respectively. Scale bar = 50 μm.

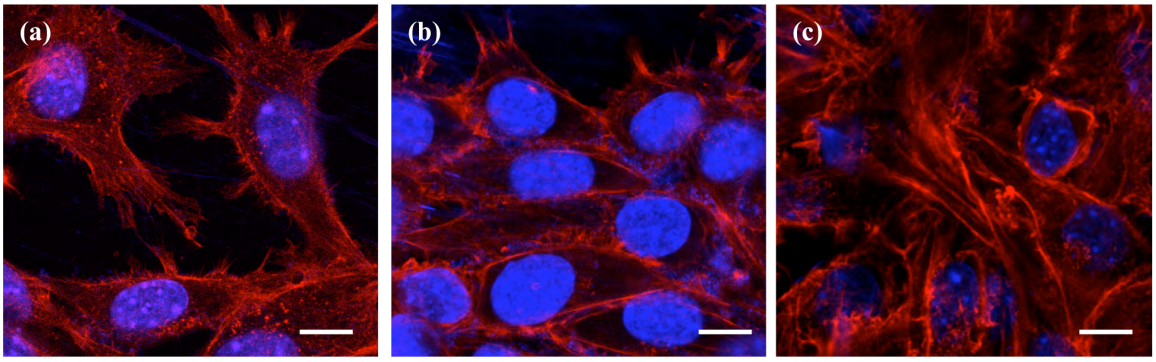

Figure 3.18. CLSM images of L929 fibroblasts cultured on (a) PHBV/C 4:1 (w/w), (b) dual-fiber, and (c) bioactive dual-fiber scaffolds for 7 days. F-actin (red) and nucleus (blue) stained with Alexafluor 546 conjugated to phalloidin and DAPI, respectively. Scale bar = 10 μm**.**

Representative examples of the vinculin immunolabeling of L929 cells cultivated on the PHBV/C and bioactive dual-fiber scaffolds for 2 days are displayed in **Figure 3.19**. The focal adhesion analysis, *i.e.* vinculin immunolabeling, suggests a slight increase in the number of focal adhesion points in the bioactive dual-fiber scaffold, compared to the dual-fiber scaffold, mainly at the 2nd day of culture. Proteins from aloe gel present in the bioactive dual-fiber scaffold may contain RGD sequences or enhance the adhesion of serum proteins (by changing the biomaterial surface properties), which may facilitate focal adhesion contacts.

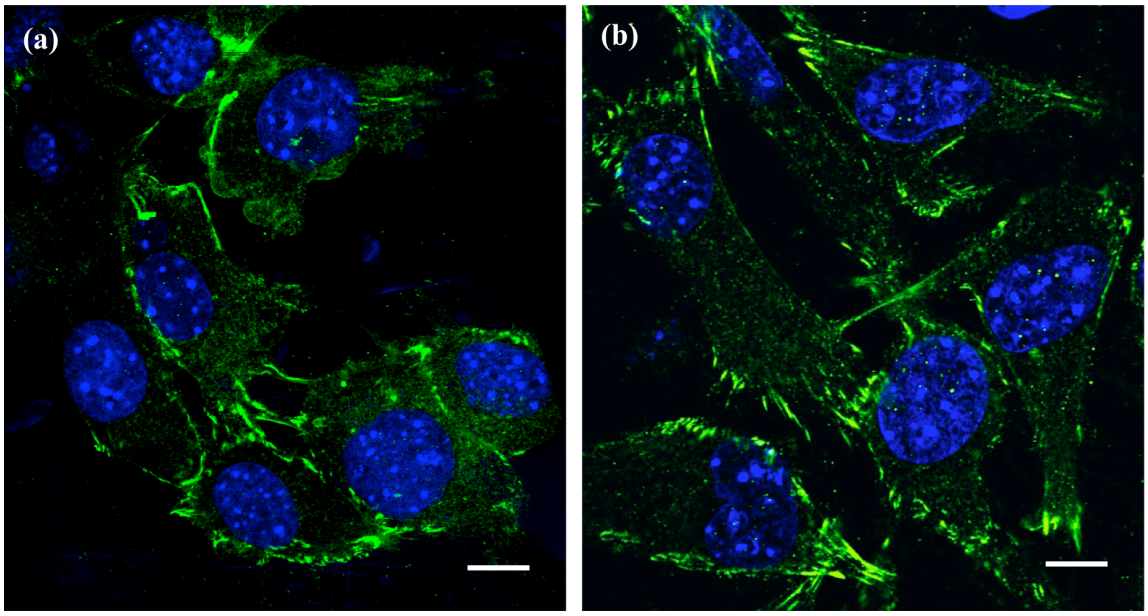

Figure 3.19. CLSM images of L929 fibroblasts cultured on (a) PHBV/C 4:1 (w/w) and (b) bioactive dual-fiber scaffolds for 2 days. Vinculin (green) and nucleus (blue) stained with anti-vinculin monoclonal antibody followed by Alexafluor 488 goat anti-mouse and DAPI, respectively. Scale bar =10 μm.

3.3.5. Wound healing assay

The potential of the dual-fiber and bioactive dual-fiber electrospun mats as scaffolds for skin regeneration was tested in the full-thickness wound healing model, previously used to evaluate the PHBV/C single fiber scaffolds. **Figure 3.20** shows the wound area reduction for the different treatments.

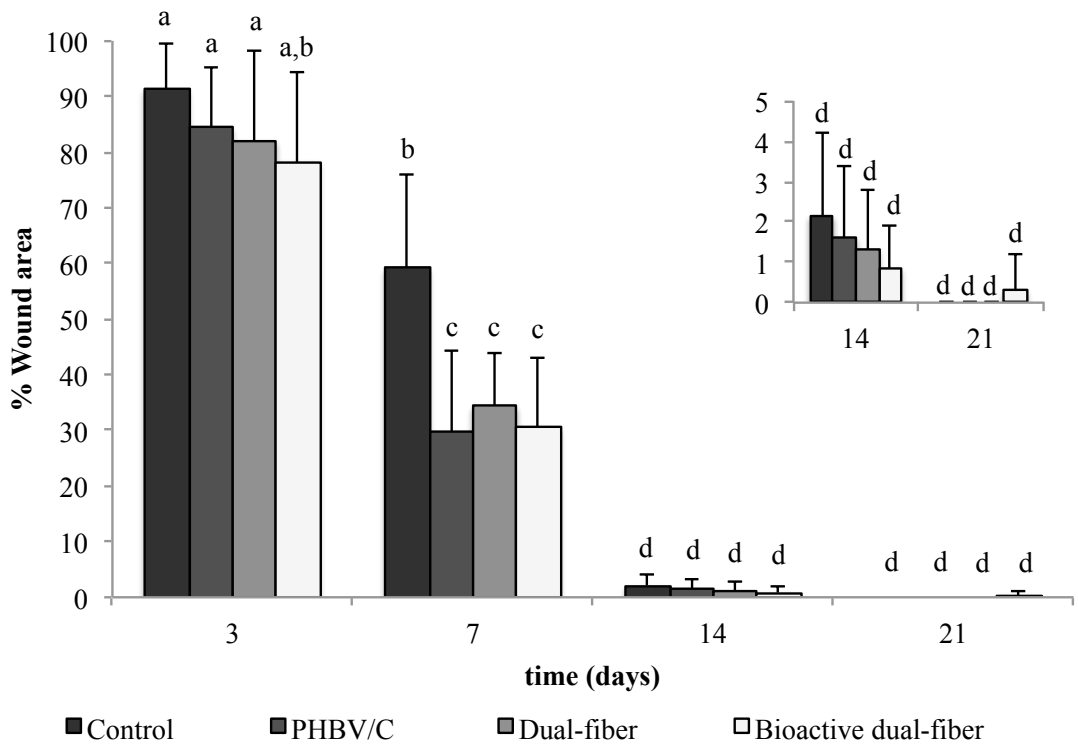

Figure 3.20. Wound area (% of initial wound area) as a function of time for different treatments tested. Different letters indicate significant difference ($P<0.05$).

The three electrospun scaffolds showed a significant reduction of wound area at the 7th day post injury compared to control (Tegaderm ®), but no significant differences were found among them during the experimental time.

The densities of PMN and MN cells are plotted **Figure 3.21.** The electrospun scaffolds (PHBV/C, dual-fiber, and bioactive dual-fiber) showed shorter inflammatory phases in comparison to control, since the peak of PMN leucocytes occurred on the 3rd day after injury for those scaffolds and on the 7th day after injury for control. In respect to MN leukocyte densities, similar levels were found on day 3 and 7 after injury, however, on day 14 and 21, an increased density of these cells was found for bioactive dual-fiber scaffold. In fact, addition of the bioactive extracts increased the MN cell density approximately 2 times at day 14 and 3 times at day 21. This result may suggest a tendency for chronic inflammation caused by compounds from the bioactive dual-fiber scaffolds.

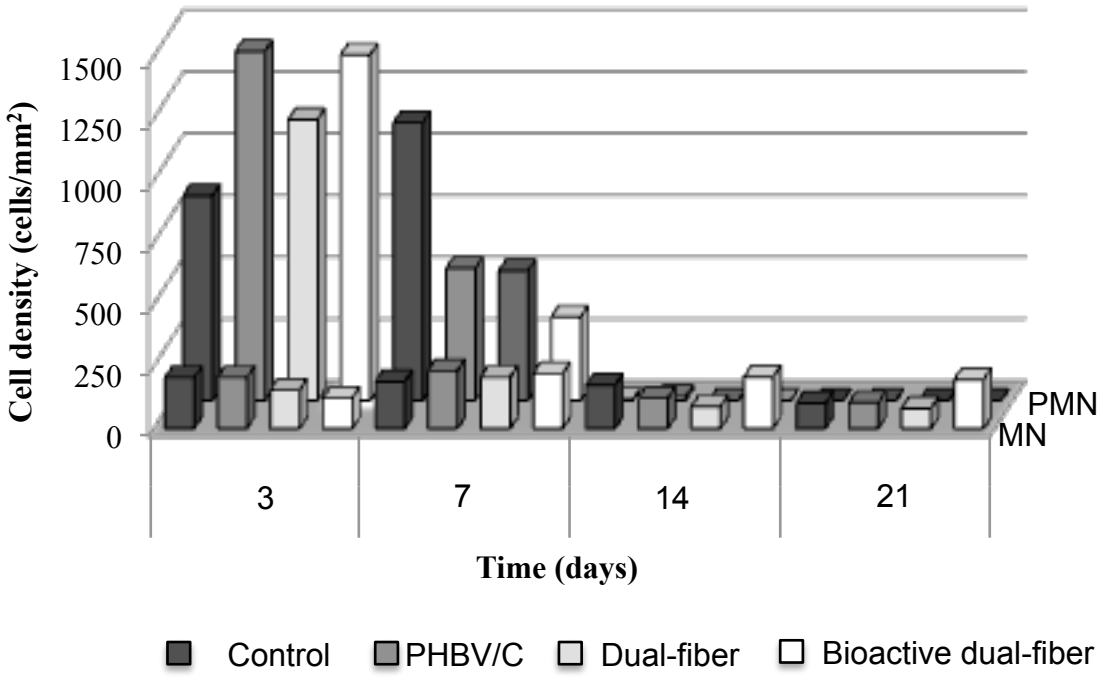

Figure 3.21. PMN and MN cell densities during the wound healing process.

3.4. Conclusions and further studies

In this chapter we report the development of new dual-fiber electrospun mats made of PHBV/chitosan and PVA/chitosan. The configuration of the electrospinning dual syringe system allowed an homogeneous distribution of the two kinds of fibers. PVA/chitosan fibers were used as vehicle for bioactive plant extracts. Combining SEM and FTIR analysis, we verified that the bioactive extracts were successfully incorporated and homogeneously distributed within the fibrous mats, without formation of beads or clusters. The dual-fiber mats, alone or enriched with the bioactive extracts, showed a good potential as scaffolds for L929 fibroblasts growth. Few differences were found as a result of the bioactive extracts addition in the dual-fiber scaffolds, which include the formation of L929 cell clusters in the first 2 days of culture and the enhanced focal adhesion, *i.e.* vinculin expression. After 7 days of culture, however, similar level cell spreading and confluence (~100% of confluence) were observed on both dual-fiber scaffolds, with or without the bioactive compounds. Also, *in vivo*, those scaffolds showed a similar performance as

scaffolds for wound regeneration, although a slight increase of MN leucocyte density was observed for the bioactive dual-fiber treatment.

In summary, this study constituted an initial investigation of the potential of dual-fiber PHBV/PVA/chitosan based mats as scaffolds for skin regeneration and vehicles for incorporation of bioactive compounds. Other important aspects remain to be explored, including:

- Processing conditions that may have influence on the bioactivity of the compounds, such as the high voltage applied and the molecular interactions established between bioactive compounds and fibers components. Therefore, further studies are needed to elucidate if the bioactive compounds maintain their bioactivity in the electrospun mats;
- Examination of the ideal concentration of the bioactive extracts incorporated into the mats and their release profile *in vitro* and *in vivo*.

The dual-fiber system here presented may be used as a vehicle for incorporation not only of *A. barbadensis* and *I. paraguariensis* extracts, but also of other herbal or synthetic compounds.

4. Electrospun PET mat as a non-non-absorbable wound dressing

dressing

4.1. Introduction

In chapters 2 and 3 we reported the use of biodegradable electrospun mats as scaffolds for skin repair. Besides absorbable biomaterials, non-degradable materials are also used in wound care as removable wound dressing materials. Non-adherent films such as Tegaderm® and Bioclusive®, for example, are widely used products in the wound healing treatment, either as a primary or a secondary dressing. In fact, the British Pharmacopoeia have divided dressing materials in two subcategories, passive products, which protect and cover the wounds, and interactive products, which contain substances that actively participate in the wound healing process. Several examples of passive products are available commercially such as gauzes of cotton, viscose and polyesters, non-adherent films, and tulles. Bioactive wound dressings include films, foams, hydrocolloids, hydrogels, and scaffolds with variable compositions.

In general, an ideal wound dressing should protect against external contaminants, maintain a moist environment, remove the excess of exudate, allow gas exchange, provide thermal insulation, cause no trauma on removing or toxicity to the wound tissues (Abdelrahman and Newton 2011). Notwithstanding, each wound has particular characteristics and, therefore, a specific treatment must be provided. Indeed, a broad spectrum of wound dressing products with distinct characteristics is available in the market. A meticulous analysis of the wound bed and a careful selection of the wound care product are determinant for the treatment success. For instance, polyurethane semi-occlusive films such as Tegaderm® and Bioclusive® are indicated for dry superficial wounds, surgical wounds or for use as a secondary dressing. Hydrogels such as Tegagel®, Nu-gel®, and Biodress®, foams (*e.g.* Hidrosorb and Softfoam) and hydrocolloids (e.g. Duoderm®) are used in low to moderately exuding wound or necrotic wounds. Sponges (*e.g.* Tielle®) and alginate based dressings such as Calcicare®, Sãf-gel® and Seasorb® are the materials of choice for moderate or heavy exuding and bleeding wounds, due to their high liquid uptake capacity. Non-adherent dressings, *e.g.* Telfa Ouchless®, Melolin®, and Mepore® cause no trauma on removal but have a minimal absorptive capacity and therefore are indicated for light exuding and superficial wounds (Abdelrahman and Newton 2011; Stashak *et al.* 2004; Fonder *et al.* 2008).

Nonwoven materials possess several features that make them attractive as wound dressing materials such as the high area to volume ratio, the high absorbent capacity, the improved conformability and flexibility, and the great versatility of manufacturing technology and design. Indeed, nonwoven materials have been increasingly incorporated into wound care products and several nonwoven materials are found in the market including nonwoven calcium alginate fibers (Algisite M®), sodium carboximethylcellulose fibers (Aquacel®), and nonwoven polyethylene (Alicoat®), among many others (Mao and Russell 2004). An important emerging class of nonwoven materials regards the electrospun nonwoven mats. Because of their inherent properties several electrospun materials have been proposed as wound dressing materials, as already discussed in previous chapters. Nevertheless, the absolute majority of electrospun materials proposed for treating wounds concerns to biodegradable biomaterials that act as absorbable scaffolds during the tissue regeneration process. Notwithstanding, electrospun mats of non-degradable polymers such as PET could also be used as removable wound dressing materials. Nanofibrous mats of PET have already been produced by electrospinning and possess several characteristics that match the ideal criteria of a removable wound dressing material, in particular:

(1) The microporosity of PET mats may function as a microbiological barrier. In fact, PET membranes are made of successive layers of small pores impermeable to several microorganisms and other contaminants, thus protecting against infection;
(2) Due to their hydrophobic nature, PET mats may be non-adhesive to the wound, thus avoiding trauma on removing;
(3) The mechanical proprieties of PET electrospun mats such as a high tensile strength (2.7 ± 0.2 MPa) and relatively high elongation (35 ± 8 %) are important for mechanical protection (Veleirinho *et al.* 2008);
(4) Due to their high porosity and high hydrophobicity, PET electrospun materials are non permeable to liquid water but allow the excess fluid to be loss by vapor transmission, preventing dehydration and providing a moist semi-occlusive environment adequate for the wound healing process (Hong and Kang 2006);
(5) The low density of the electrospun PET mats (~ 0.091 g/cm^{-3}), as well as their softness, may be ideal for promoting comfort and alleviating pain (Veleirinho *et al.* 2008).

In this chapter we explore the potential of an electrospun PET mat as a removable wound dressing material. For that, a full-thickness wound healing experiment was conducted with Wistar rats and the effects of PET wound dressing on the inflammatory and proliferative phases of the wound healing process were analyzed.

4.2. Experimental

4.2.1. Materials

PET pellets were kindly supplied by Flexitex (Portugal). All chemicals were of analytical grade and obtained from Sigma-Aldrich Chemical Company.

4.2.2. Fabrication of PET mat by electrospinning

A 30% (w/v) PET solution was prepared in a blend of TFA and dichloromethane (DCM) (8:2) v/v by moderate stirring for 2 hours at room temperature. These PET concentration and solvent have been shown to allow for good polymer solubility and electrospinnability (Veleirinho *et al.* 2008). Electrospinning was performed using the experimental set up previously described in chapter 2 (§2.2.4). The process was conducted at 26 kV of applied voltage, with a flow rate of 0.080 mL/min and a needle tip-to-collector distance of 12 cm. A total solution volume of 20 mL was electrospun and fibers were collected as a nonwoven fibrous mat on the rotating drum (900 rpm), in air and at room conditions (20 ± 2 ºC, 45–50% relative humidity). The mat was dried at 35 ºC for 24 hours.

4.2.3. Morphological analysis

Morphology of the fibrous mat was investigated by SEM. Small sections of the scaffolds were sputter-coated with gold and analyzed using a scanning electron microscope (Hitachi S4100) at an accelerating voltage of 25 kV.

Image processing was performed using the ImageJ - 1.37c software. Five random images (1000X magnification) were obtained for each sample. Fiber diameters were calculated from at least 100 measurements of the sample fibers. SEM images were thresholded and

pore areas were automatically calculated using the "analyze particle" tool of ImageJ (n>200).

4.2.4. Wound healing assay

The full-thickness wound healing experiments were in compliance with all the criteria, technical standards and international animal research rights recommended by the Brazilian College on Animal Experimentation. The Ethical Committee on Research of the Santa Catarina South University (UNISUL) has approved this study. The animals were kept throughout the experiment in the Operative Technique and Experimental Surgery Laboratory at UNISUL in ambient temperature, continuous air flow, free of noise and stress and obeying natural day and night cycles. They remained in individual cages on shelves in the same distance from the light source with feed and water *ad libitum*.

Male Wistar rats (*Rattus norvegicus albinus*), aged 3 months and weighing 300± 50 g were obtained from the UNISUL Central Biotery. Animals were divided in two groups (n=9/group), the control group corresponding to untreated/uncovered wounds and the PET treated group.

Rats were anesthetized with a single intramuscular injection of ketamine (90 mg/kg) and xylazine (15 mg/kg). After manual depilation and antisepsis with polyvinylpyrrolidone, a full thickness wound with a surface area of 1.5 cm x 2.5 cm was made on the dorsum of the rat using a sterile surgical scalpel blade. The wound was covered with an equal size of PET mat (PET group) and left uncovered in the control group. The edges of PET mat were fixed to the wound with interrupted suture. After surgery, animals were housed individually and observed daily.

Animals were sacrificed on the 3rd, 7th, and 14th postoperative days in a carbon dioxide chamber. Wound tissues were dissected and fixed in buffered formaldehyde solution (10%, pH 7.2) for 48h.

4.2.4.1. Histopathological analysis

For histopathological analysis, tissues were dehydrated, embedded in paraffin according to standard procedures and cut into 5 μm sections. For each animal 25 sections were taken

(5x5 sections, separated by 25μm of distance). Sections were stained with HE and the slides were observed and photographed with an optical microscope (Leica DMRBE). The density of PMN and MN leukocytes, fibroblasts and fibrocytes were calculated for 5 areas (0.004 mm^2) per section. A total of 125 areas were analyzed for each animal.

4.2.5. Statistics

Statistical analysis was conducted using Instat 3.0. Results were expressed as the mean ± standard deviation and compared through one-way ANOVA, Tukey-Kramer multiple comparisons test (for parametric data) and Mann–Whitney U test (for non-parametric data). $P < 0.05$ was considered statistically significant.

4.3. Results and discussion

4.3.1. Morphological analysis

SEM analysis of PET mat revealed a typical nonwoven fibrous structure with high porosity and a random fibrous arrangement (**Figure 4.1**).

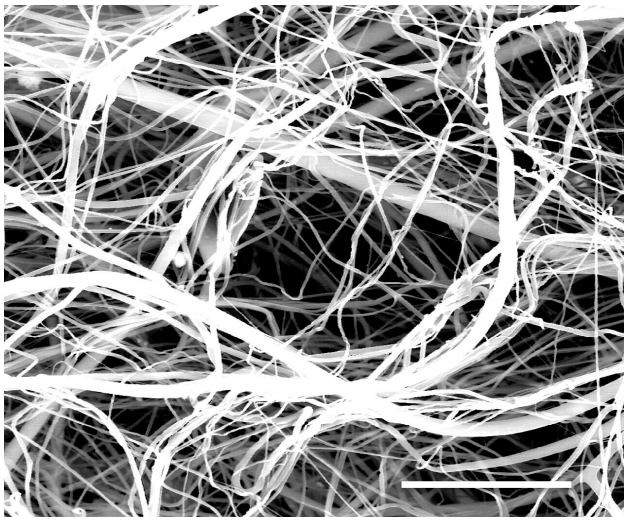

Figure 4.1. SEM image of PET mat.

The average fiber diameter was 0.71 ± 0.28 μm and the average pore area was 9.4 μm^2. In electrospun materials, pores are formed through the random layer-by-layer deposition of the nanofibers and, as expected, relative wide ranges of pore areas are obtained. The pore area distribution of PET mat is displayed in **Figure 4.2**. The electrospun PET mat showed pores ranging from 1.0 to 64.2 μm^2, however more than 50% of pores were smaller than 5 μm^2.

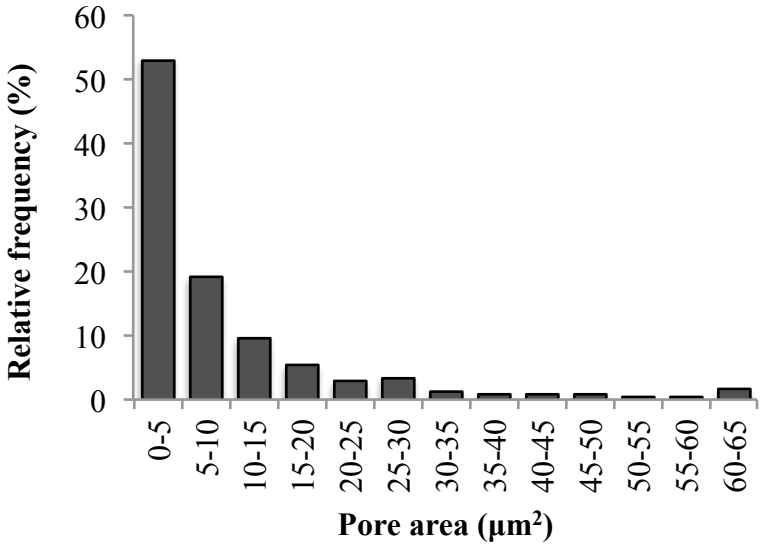

Figure 4.2. Pore area distribution of PET mat.

An ideal wound dressing material should maintain a moist clean environment that prevents mechanical trauma, reduces edema and stimulates repair. The electrospun non-degradable mat of PET possesses several characteristics attractive for this application, including the microporosity, the low density, the high hydrophobicity, and the adequate mechanical properties. Furthermore, PET is a biocompatible low-cost polymer and the versatility of the electrospinning technology allows the development of several distinct material designs. In this context, we hypothesize that when used as a wound dressing, PET mat may have a positive effect on the wound healing process of low exudate, non-infected wounds. To test this hypothesis, a full thickness wound was created on the back of Wistar rats and the electrospun PET mat was placed on the top of the wound as a wound dressing material. Details of macroscopic and histological results will be discussed in the following subsections.

4.3.2. Macroscopic observations of the wound healing process

As previously referred, the PET membrane was developed to act as a non-adherent removable wound dressing material. On the contrary to PHBV mats, as previously discussed in chapter 2 and 3, PET mat did not adhere well to the wound bed and fixation had to be provided in order to keep the dressing on the wound site during the experimental period, due to the natural behavior of the testing animals. Adhesive tape, *i.e.* micropore surgical tape®, was not effective in fixing the dressing to the back of the animals. Hence, although this procedure does not simulate the real application of the wound dressing in the human being, fixation of the four edges of the mat with interrupted suture was the only feasible solution. An adequate design for use in human being must be further explored.

During the postoperative period, although the PET wound dressing did not immediately adhere to the fresh wound, it was observed that the electrospun mat strongly adhered to the wound bed, after hemostasis has been initiated and the fibrin clot formed. Later, as re-epithelialization occurred it was observed that the new epidermis and dermis were growing over the dressing material, incorporating the mat in the subcutaneous tissue. Because PET is a non-degradable material, this is an extremely disadvantageous outcome. Further details of this finding will be provided at subsection 4.3.3.3. **Figure 4.3** shows illustrative pictures of the wounds in the control and PET treated groups on the 3rd, 7th, and 14th day after injury.

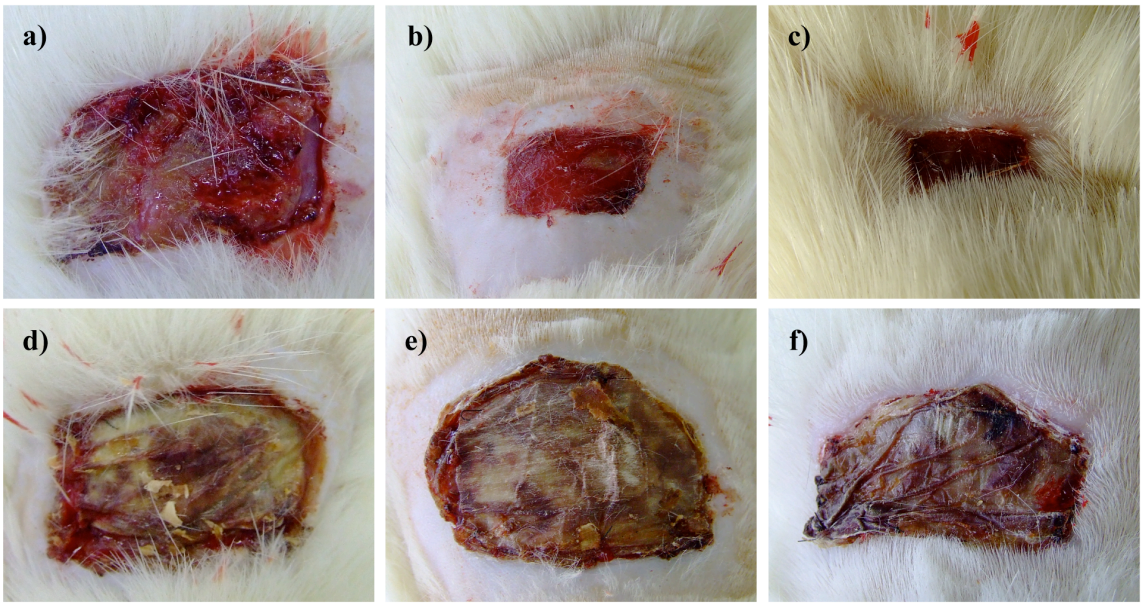

Figure 4.3. Macroscopic observation of the wound bed on control (a-c) and PET group (d-f) on the 3rd (a and d), 7th (b and e), and 14th (c and f) postoperative day.

4.3.3. Histopathological analysis

Wound tissues were collected at different intervals, 3, 7, and 14 days, and subjected to histopathological analysis. Illustrative examples of histological sections obtained from control and PET groups during the experimental period are displayed in **Figure 4.4** (low magnification) and in **Figure 4.5** (high magnification). At the 3rd day after injury, inflammatory cells were found in both experimental groups, however in lower densities for PET group. At day 7, wounds were mostly composed by granulation tissue with high densities of fibroblast, whereas on day 14 a regenerated tissue with an increased density of fibrocytes and collagen fibers were observed.

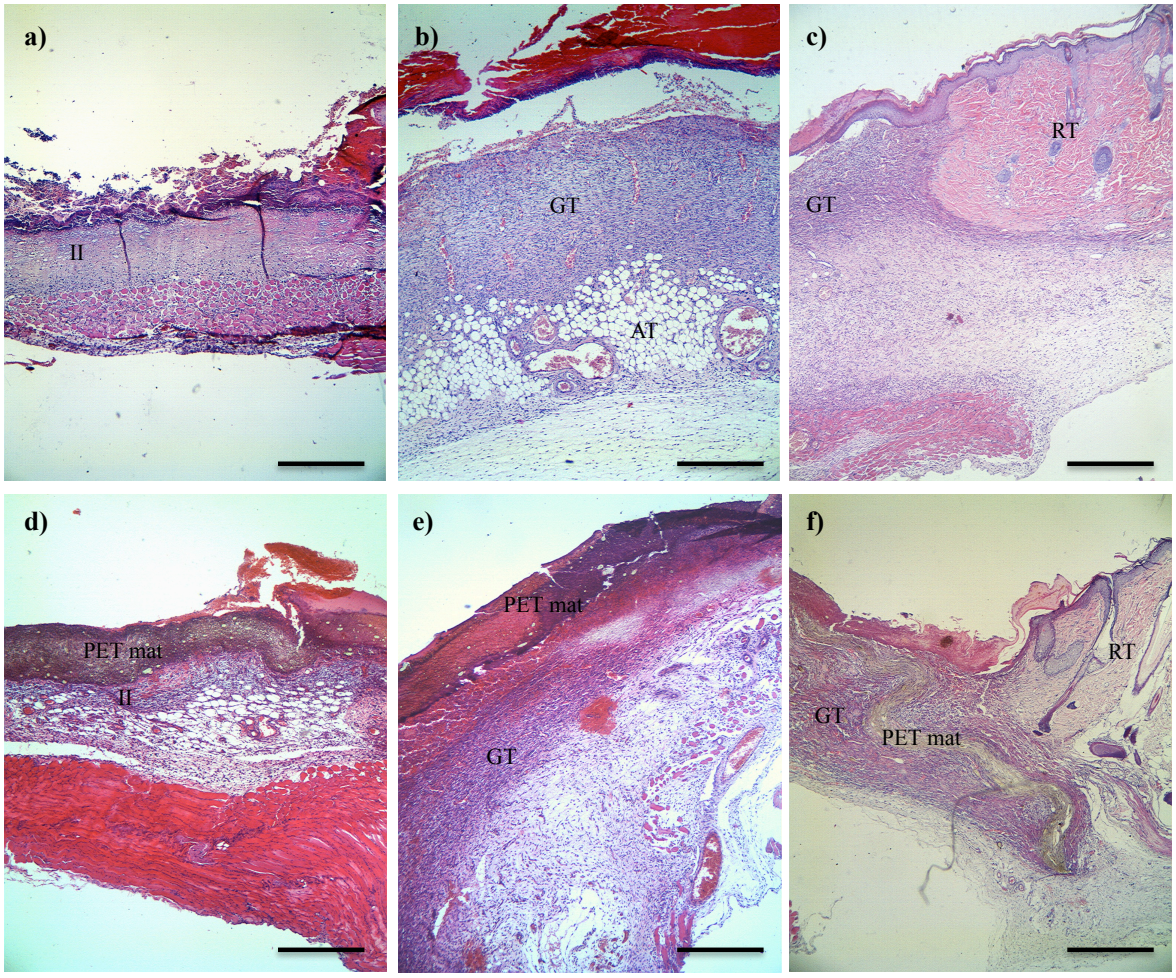

Figure 4.4. HE staining of histological sections (magnification = 40x) representative of control (a-c) and PET (d-f) wounds on the 3rd (a and d), 7th (b and e), and 14th (c and f) postoperative day. (II) Inflammatory infiltrate, (GT) granulation tissue, (AT) adipose tissue, (RT) regenerated tissue. Bar = 500 μm.

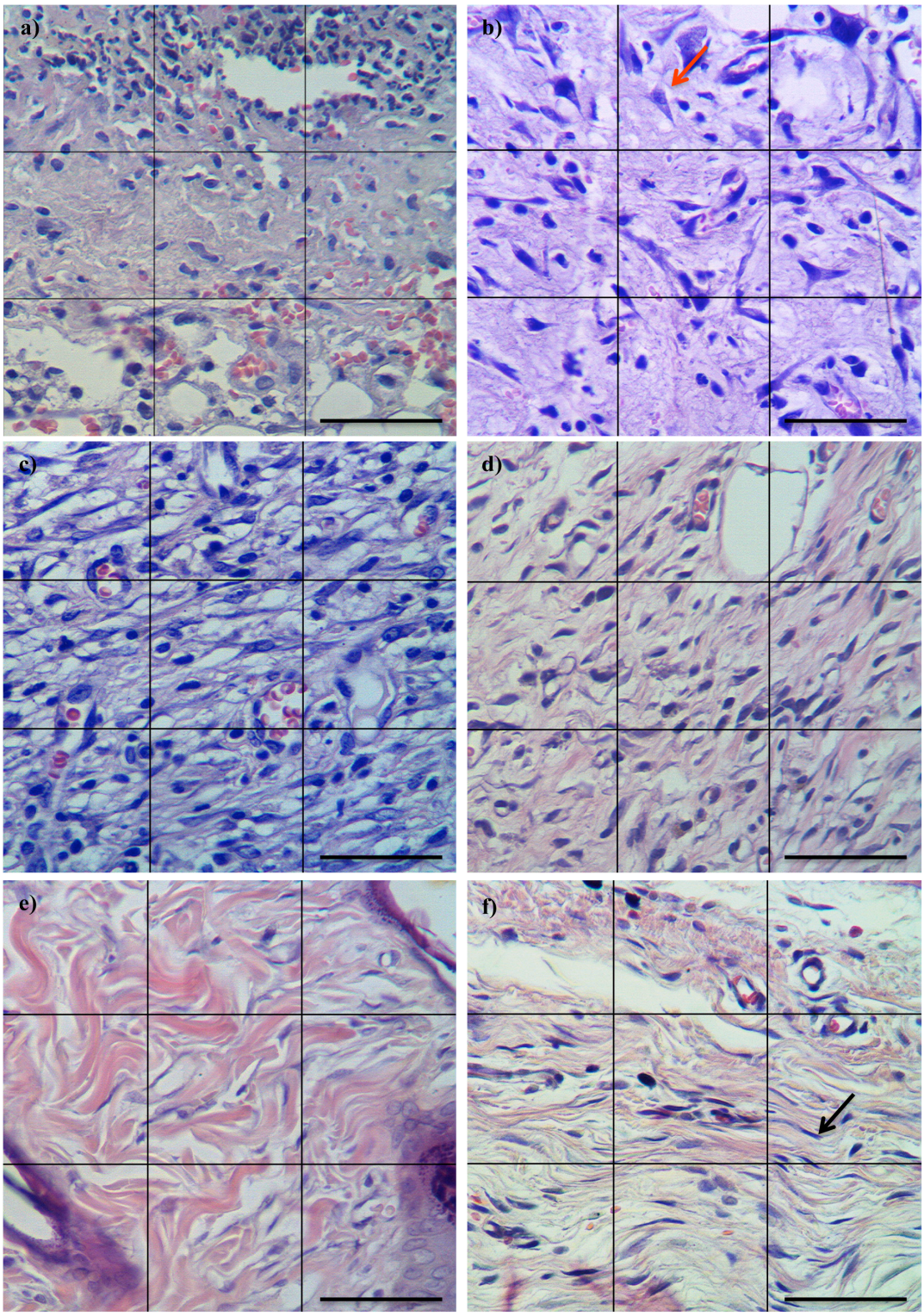

Figure 4.5. HE staining of histological sections (magnification = 400x) of control (a, c, and e) and PET treated (b, d, and f) wounds on the 3rd (a and b), 7th (c and d), and 14th (e and f) postoperative day. Red arrow points to a fibroblast and black arrow points to a fibrocyte typical morphology. Bar = 50 μm.

4.3.3.1. Effect of PET wound dressing on the inflammatory phase of the wound healing process

When an injury destroys the protection conferred by the skin, allowing microorganisms and other contaminants to invade the inner tissues, an important inflammatory response is triggered out in order to prevent infection or major tissue damages. Since a rapid response is needed, PMN cells rapidly achieve the local of injury and start to act against contaminants. Although PMN inflammatory cells are rapid and efficient, these leucocytes are also very destructive and an inherent damage to the surrounding tissues is usually associated with their action. As a consequence, several symptoms are associated with the acute inflammatory phase, including swelling, redness, heat, pain and loss of function. To study the effect of PET wound dressing on the inflammatory phase of the wound healing, PMN and MN densities were calculated and plotted (**Figure 4.6)**. Significant lower PMN densities were found in animals treated with the electrospun PET mat, at the 3rd and 7th postoperative days, compared to control ($P<0.05$). This result indicates a less pronounced acute inflammatory phase, which is probably attributed to the physical protection conferred by the electrospun mat. In fact, PET electrospun mat possesses a dense microporous structure that acts as a filter, protecting the wound bed against microorganisms and other contaminants.

MN leucocytes, which include monocytes, macrophages and lymphocytes arrive later at the wound site (approximately 48h after injury), although being more specific and less destructive to the surrounding tissues in comparison to PMN cells. Both PMN and MN levels tend to decrease as the inflammation progresses. It is generally accepted that persistent high levels of MN cells for several days are indicative of chronic inflammation. Here, decreasing densities of MN leucocytes with time were found for control and PET groups. In fact, animals treated with PET mat exhibited a significant lower density of MN cells at day 3, which is probably attributed again to the physical protection conferred by the mat. At the 7th and 14th postoperative days, although lower MN density levels were also found for PET group, the differences were not statistically significant.

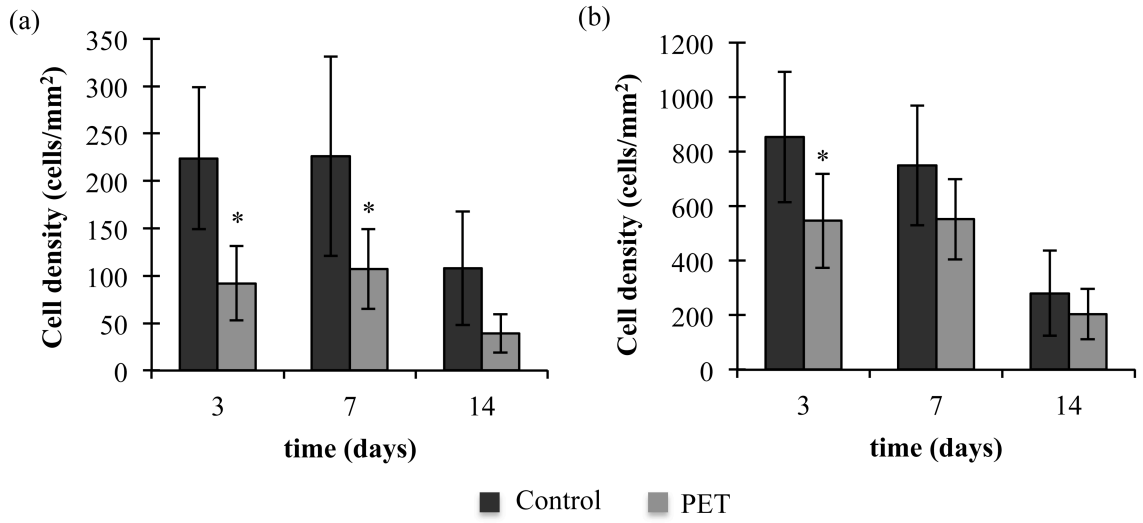

Figure 4.6. (a) PMN and (a) MN leucocyte densities for control and PET treated groups at 3, 7, and 14 days after injury. (*) Indicates significant differences between control and PET groups ($P<0.05$).

These results are very encouraging since the inflammatory phase is a determinant step of the wound healing process. In fact, several complications that result from an inadequate inflammatory phase including infection, necrosis, or chronic inflammation may result in impaired wound healing. Additionally, reduced inflammation results in fewer inflammatory symptoms and less pain.

Following, the effects of the PET wound dressing on the proliferative phase of the wound healing will be discussed.

4.3.3.2. Proliferative phase

Once inflammation is controlled the proliferative phase initiates in order to regenerate the damaged tissue. Fibroblasts are the key component of the proliferative phase as they are responsible for synthesis and secretion of collagen and other ECM components as well as cytokines and growth factors essential to the wound healing process. Fibroblast usually refers to an active stage of the cell while the term fibrocyte corresponds to a less active state of the same cell. Active fibroblasts are large cells with big nuclei and spread cytoplasms, whereas inactive fibroblast or fibrocytes are smaller with less prominent, heterochromatic nuclei (Junqueira and Carneiro 2005), as illustrated in Figure 4.5.

Fibroblasts have a peak of activity in the proliferative phase as they become activated to synthetize ECM components. In homeostasis, on the other hand, the less active fibrocyte stage is usually predominant. Both fibroblast and fibrocyte densities for PET and control groups were calculated and are plotted in **Figure 4.7**. The peak activity of fibroblasts occurred on the 3rd day after injury for PET group and on the 7th postoperative day for control. This difference is evidenced in figure 4.5 (a and b) as fibroblasts are largely found on PET group, while the wound tissues for the control group were still predominantly characterized by high density of leucocytes. This result indicates that the proliferative phase initiated earlier in the PET group, which probably results from the less pronounced inflammatory phase found in this group. Nevertheless, as wound healing proceeded, no significant differences were found in respect to fibroblast or fibrocyte densities. Instead, the control group showed a higher degree of tissue maturation at day 14, with a fibrillar arrangement of collagen and the presence of skin appendages (figure 4.5 e and f).

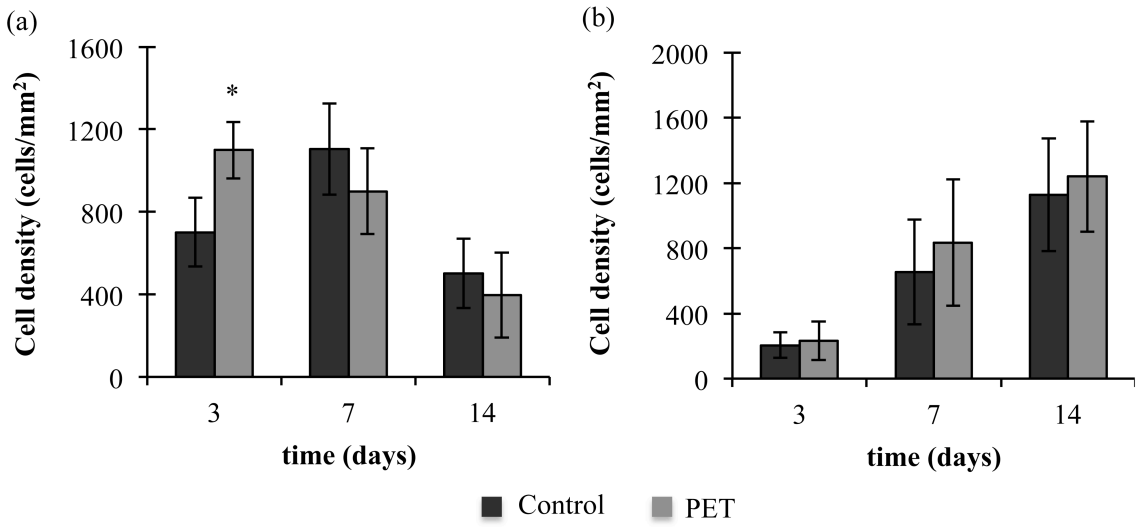

Figure 4.7. (a) Fibroblast and (b) fibrocyte densities for control and PET groups 3, 7, and 14 days after injury. (*) Indicates significant differences between control and PET groups ($P<0.05$).

4.3.3.3. Re-epithelialization

Despites the positive effect of PET wound dressing in the inflammatory phase of the wound healing, a considerable delay on re-epithelialization was detected for the wounds treated with the PET mat. The average wound area of control and PET groups on the 3rd, 7th, and 14th postoperative days is plotted in **Figure 4.8.** In fact, the average wound area

observed for the animals treated with the PET mats at day 7 (5.5 ± 0.6 cm^2) was approximately 2 times higher than control (2.3 ± 0.3 cm^2). At the 14th postoperative day this difference was even bigger, as PET group exhibited an average wound area more than four times greater than control (4.0 ± 0.6 cm^2 and 0.7 ± 0.1 cm^2, respectively).

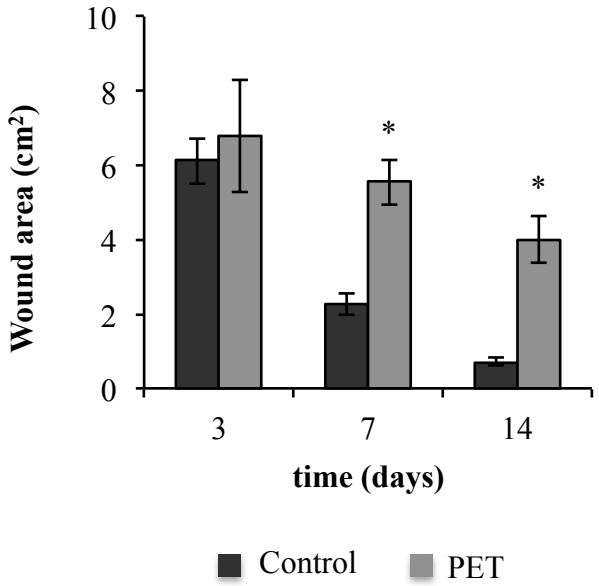

Figure 4.8. Average wound area of control and PET groups on the 3rd, 7th, and 14th day after injury. (*) Indicates significant differences between control and PET groups (P<0.05).

The explanation for the delayed re-epithelialization observed on PET group lies on the fact that instead of acting as a removable dressing material, PET mat was incorporated on the subcutaneous region of animals as re-epithelialization occurred above the material. **Figure 4.9** shows the regenerated epidermis and dermis beyond the dressing material. As a microporous membrane, PET mat hampers the blood vessel access to the epithelial cells growing on the upper surface of the mat, thus delaying re-epithelialization.

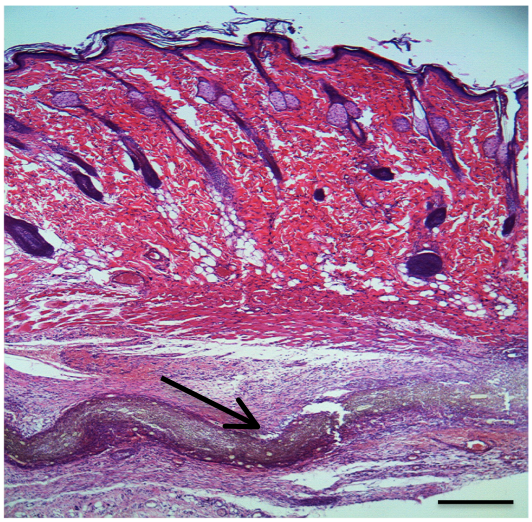

Figure 4.9. HE staining of a histological section of PET group at the 7th day after injury illustrating the incorporation of PET mat in the subcutaneous region of the newly formed tissue. The arrow points to PET wound dressing lying beyond the dermal tissue. Bar=500 μm.

4.4. Conclusions

The main purpose of this chapter was to test the potential of a non-degradable electrospun PET mat as a removable wound dressing material. The *in vivo* wound healing model used revealed that although PET electrospun mat had a positive effect on the inflammatory and early proliferative phase, a delay in the re-epithelialization was detected for this experimental group. In fact, the regeneration of epidermis and dermis occurred above the PET mat, resulting in the incorporation of the dressing material in the subcutaneous tissue. Since PET is a non-degradable polymer this result constraints the application of PET mat as a wound dressing material. Notwithstanding, results from this study also opened other possibilities of application for PET electrospun mat, as positive aspects were also observed. For instance, an important evidence was that no signs of foreign body reaction was found in animals treated with the PET electrospun mat. Hence, in the following chapter the application of PET mat as a non-degradable scaffold for tissue engineering will be explored.

5.PET/chitosan non-degradable scaffolds for tissue engineering

engineering

5.1. Introduction

In the previous chapter we reported the use of an electrospun mat of PET as a removable dressing material. Results from the *in vivo* wound healing model showed that instead of acting as a removable dressing, the regenerated dermis and epidermis grow above the mat, incorporating the material in the subcutaneous region of the rats. Although undesirable for that specific purpose, the good mat integration into the tissues with no important inflammatory response associated opens a new range of possible applications for PET electrospun mats. Indeed, in the present chapter we explore the potential of PET electrospun mats as non-degradable scaffolds for tissue engineering applications. In despite of PET advantageous characteristics, the high hydrophobicity of this synthetic polymer restricts certain applications in the biomedical field. Combination with hydrophilic biopolymers can be an effective way to overcome this limitation.

In fact, surface properties of the nanofibers have relevant importance for cell adhesion and biocompatibility. Hydrophilic surfaces have long been recognized to promote cellular growth and improved biocompatibility. Many attempts have been pursuit to achieve this goal. The preparation of hybrid electrospun nanofibrous scaffolds (Zhang *et al.* 2010; Casper *et al.* 2005), the use of post-electrospinning protein surface-coating approaches (Shi *et al.* 2010; Li *et al.* 2008), surface modification by covalent attachment of biomolecules onto the surface of hydrophobic polymeric nanofibers (Mattanavee *et al.* 2009), or specific bioactivation by covalent attachment of cell-adhesion-mediating peptides (Grafahrend *et al.* 2008) are among the strategies successfully explored to improve the cytocompatibility of these materials.

As previously described in chapter one, architecture is also determinant for cell-scaffold interactions. Fiber size and orientation, porosity, distribution and pore size of biomaterials affect cell behavior, *i.e.* morphology, attachment, differentiation, and function, and are important factors to optimize the scaffold potential as substratum for cells. Hence, manipulation of the scaffold architecture constitutes an important tool to control scaffold-cell interactions and, eventually, to obtain scaffolds with tunable properties and optimized designs for a certain application.

The possibility of tuning the physical/chemical properties, morphology and three-dimensional (3D) structure of fibrous scaffolds, and thus scaffold-cell interactions, may allow the tailoring and control of cell adhesion, growth and proliferation and thus the materials' final ability to act as a tissue engineering scaffold.

Chitosan has shown ideal properties for biomedical applications such as biocompatibility, wound healing effect, anti-inflammatory and antimicrobial activity, as already mentioned. When used as a co-polymer in hybrid biomaterials, chitosan can not only improve hydrophilicity but also enhance architecture and biological properties, including several advantageous characteristics in electrospun nanofibrous scaffolds (Ignatova *et al.* 2009; Duan *et al.* 2007; Lopes-da-Silva *et al.* 2009).

The preparation of PET and PET/chitosan mats by electrospinning was already demonstrated (Veleirinho *et al.* 2008; Lopes-da-Silva *et al.* 2009; Jung *et al.* 2007). PET mats showed a 3D fibrous structure with high porosity and good mechanical properties. Addition of chitosan promoted considerable changes in morphological and mechanical properties of the mats (Lopes-da-Silva *et al.* 2009), and also better cell adhesion (Jung *et al.* 2007). At the present chapter, our aim was to use this previous knowledge as a tool to manipulate the architecture and composition of non-degradable scaffolds and to study their effect on cell behavior. Scaffold architectures were controlled by varying PET/C ratio, chitosan MW and by post-electrospinning cross-linking with glutaraldehyde. The final effects on cell adhesion, morphology, and proliferation were studied *in vitro* using L929 fibroblasts as model.

5.2. Experimental

5.2.1. Materials

PET pellets were kindly supplied by Flexitex (Portugal). A commercial chitosan sample with medium MW (85% deacetylated) was purchased from Sigma-Aldrich Chemical Company. Chitosan samples with different MW were obtained by controlled oxidative fragmentation as previously described in chapter 2 (section 2.2.2). All chemicals were of

analytical grade and obtained from Sigma-Aldrich Chemical Company. All biological supplies were purchased from Invitrogen unless otherwise noted.

5.2.2. Scaffolds fabrication by electrospinning

A 30 wt.% PET solution was prepared in a blend TFA and DCM 8:2 (v/v) by moderate stirring for 2 hours at room temperature. PET/C blends were prepared by adding chitosan (2, 4 and 6 wt. %) to the 30% PET solution and stirring for 3 hours at room conditions. Chitosan samples with variable MW (15, 22, and 48 kDa) were tested.

The electrospinning process was conducted at 26 kV of applied voltage, with a flow rate of 80 μL/min (V=20 mL) and a needle tip-to-collector distance of 12 cm. Fibers were collected as a nonwoven fibrous mat on the rotating drum (900 rpm), in air and at room conditions (20 ± 2 ºC, 45–50% RH). The scaffolds were dried at 35 ºC for 24 hours. Selected scaffolds were cross-linked with glutaraldehyde vapor in a glass chamber (20 ± 2 ºC) for 12 hours. After treatment, scaffolds were dried at 35 ºC for 24 hours to remove residual glutaraldehyde.

5.2.3. Morphological analysis

Morphology of the fibrous scaffolds was investigated by SEM and images were processing using ImageJ - 1.37c software, as described in chapter 4 (section 4.2.3).

5.2.4. FTIR

The nanofibrous mats were characterized by ATR-FTIR, using a Golden-gate single reflection ATR in a Bruker IFS-spectrometer at a resolution of 8 cm^{-1} and 256 co-added scans.

5.2.5. Water contact angle (WCA) measurements

The wettability of scaffolds was assessed by the sessile drop method using a contact angle system OCA-20 (DataPhysics Instruments). A drop of distilled water (1 μL) was automatically dispensed on the scaffold surface and the WCA and drop life times were

calculated using the software SCA 20. At least 10 measurements were taken for each sample.

5.2.6. Cell culture

In vitro cell culture studies were conducted using mouse fibroblast cells (L929). The detailed description of the cell culture conditions, as well as the experimental procedures of the indirect cytotoxicity and MTS assays, SEM and CLSM analysis, and the annexin V and PI staining of cells cultured on the scaffolds are described in chapter 2 (subsection 2.2.5.4).

3D projections of L929 cells cultured on PET/C scaffolds were constructed to evaluate the internal cell colonization. For that, chitosan was stained with FITC, previously to electrospinning process, according to the method described by Ma *et al.* (2003).

5.2.7. Statistics

Statistical analysis was carried out using Instat 3.0. Results were expressed as the mean ± standard deviation, and compared through one-way ANOVA and Tukey-Kramer multiple comparisons test. $P < 0.05$ was considered statistically significant.

5.3. Results and discussion

Solutions of PET and PET/C were successfully electrospun into nano and microfibers, which were collected as nonwoven mats with a 3D architecture. Typical electrospun structures with random fiber orientation and high porosity were obtained for all polymer solutions tested.

As already broadly described, manipulation of electrospinning parameters can be an effective way to control the morphology of electrospun mats (Theron *et al.* 2004; Tan *et al.* 2005). Among these parameters, solution properties have the greatest impact on the final characteristics of these mats (Veleirinho *et al.* 2008). Substantial changes on the architecture and properties of the fibrous scaffolds, *e.g.* fiber diameter, pore sizes, surface roughness, and wettability, were achieved by varying the composition of electrospinning

solution, *i.e.* chitosan concentration (2, 4 or 6 wt.%) and MW (15, 22 or 48 kDa) and by post-electrospinning cross-linking.

5.3.1. Effect of chitosan concentration and MW on fiber diameter

Table 5.1 displays the average fiber diameter as a function of chitosan concentration and MW. Average fiber diameters of the electrospun scaffolds varied from 0.71 μm (PET) to 3.01 μm (PC_{15}5:1), depending on the concentration and MW of chitosan. Fiber diameters increased with the increase of chitosan content for all MW tested. The increase of solution viscosity caused by the presence of chitosan resulted in higher resistance against the increase of surface area during the formation of the electrospinning jets and, consequently, fibers with higher diameters were obtained, in accordance with previous findings (McKee *et al.* 2004). Addition of chitosan also leaded to wider fiber diameter ranges, what may be related to the inherent high chemical variability of chitosan samples, *e.g.* MW distribution and acetylation degree (**Figure 5.1**).

Additionally, it was also observed a tendency for the fiber diameter to increase as the chitosan MW decreases. This behavior may be attributed to the higher mobility of the smaller chitosan molecules that migrate to the outer layer of the nanofibers, increasing diameter (Lopes-da-Silva *et al.* 2009). Based on the fiber diameter differences, five mats (PET, PC_{48}15:1, PC_{48}5:1, PC_{15}15:1 and PC_{15}5:1) were selected to perform further studies.

Table 5.1. Fiber diameters (mean ± standard deviation) obtained for scaffolds prepared from PET and PET/C solutions, at different chitosan concentrations (2, 4, and 6 wt.%, corresponding to PET/C ratios of 15:1, 7.5:1, and 5:1, respectively) and MW, and for selected cross-linked fibers (CL). Abbreviated designations for each scaffold are also shown and will be used throughout the text. Different superscript letters within a column indicate significant differences ($P < 0.05$).

PET/C ratio (w/w)	Chitosan MW (kDa)	Fiber diameters (μm)
1:0	--	0.71 ± 0.28 (PET) [a]
		0.64 ± 0.27 (PETCL) [a]
15:1	15	0.88 ± 0.44 (PC_{15}15:1) [a]
		0.65 ± 0.33 (PC_{15}15:1CL) [a]
	22	0.83 ± 0.33 (PC_{22}15:1) [a]
	48	0.89 ± 0.28 (PC_{48}15:1) [a]
		0.84 ± 0.40 (PC_{48}15:1CL) [a]
7.5:1	15	1.85 ± 0.47 (PC_{15}7.5:1) [b]
	22	1.74 ± 0.69 (PC_{22}7.5:1) [b]
	48	1.61 ± 0.65 (PC_{48}7.5:1) [b]
5:1	15	3.01 ± 0.72 (PC_{15}5:1) [c]
		2.24 ± 0.85 (PC_{15}5:1CL) [d]
	22	2.32 ± 0.98 (PC_{22}5:1) [d]
	48	2.30 ± 0.78 (PC_{48}5:1) [d]
		2.22 ± 0.75 (PC_{48}5:1CL) [d]

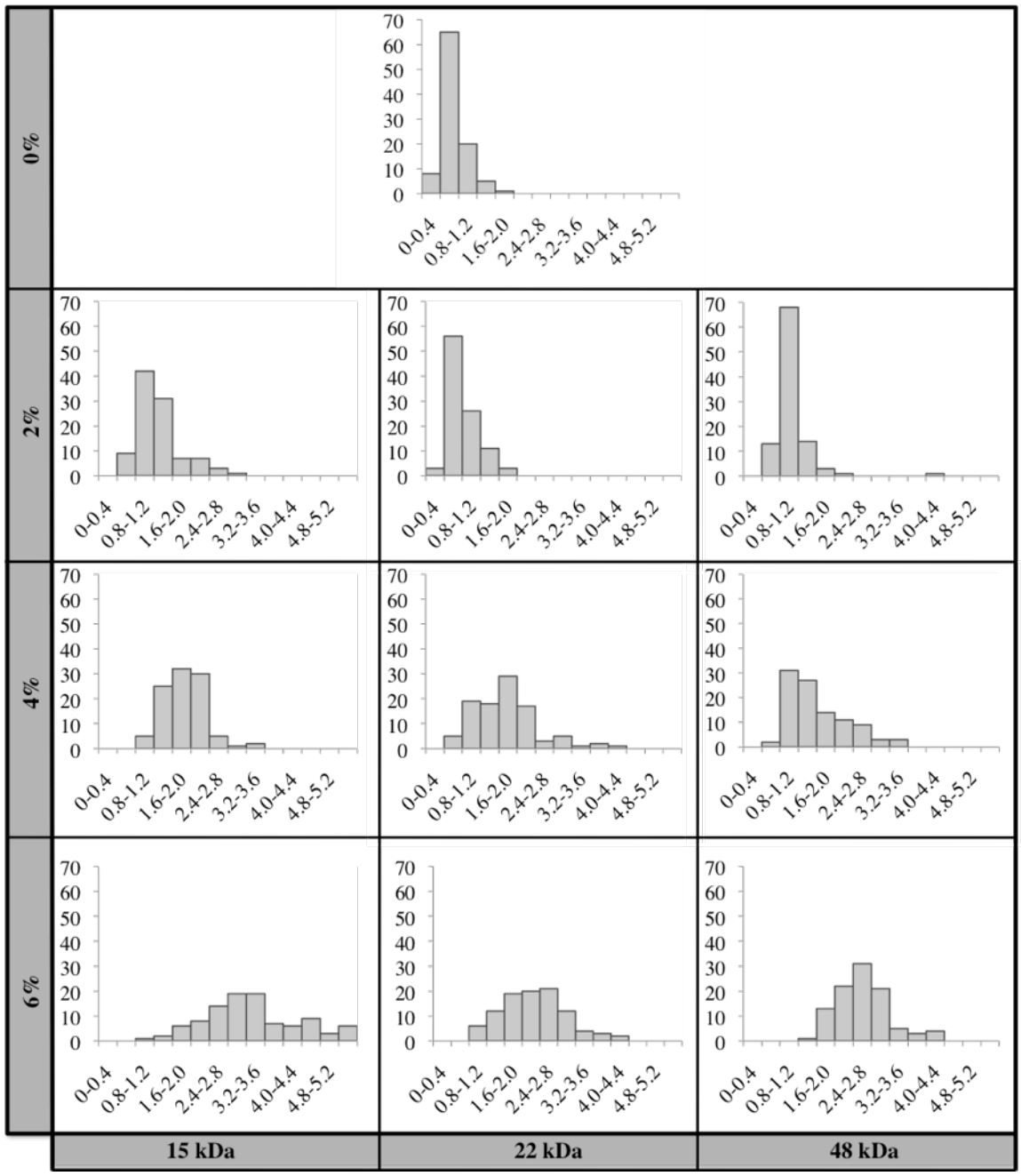

Figure 5.1. Fiber diameter histograms of PET and PET/C scaffolds, obtained by changing chitosan concentration (0, 2, 4, and 6 wt.%) and MW (15, 22, and 48 kDa).

5.3.2. Pore area characterization

Pore area and pore area distribution define whether cells can populate the scaffold three-dimensionally or not. **Figure 5.2** represents the pore area distributions of PET and PET/C scaffolds. Electrospun mats were characterized by a wide pore size distribution given that pores are formed by a random fiber deposition during the electrospinning process. Larger pores and wider pore area ranges were observed as chitosan content increases and chitosan MW decreases.

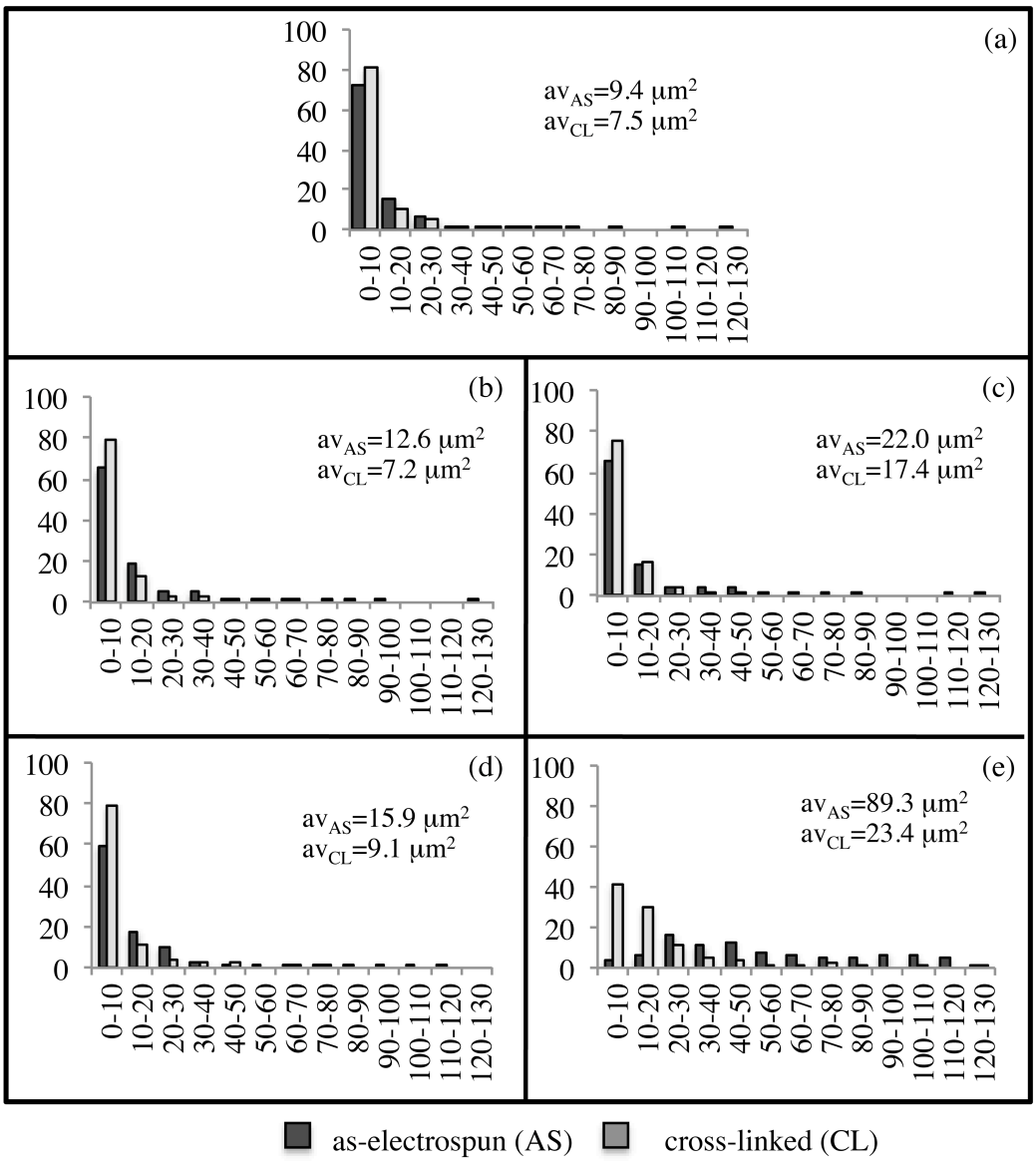

Figure 5.2. Pore area distributions of as-electrospun (AS) and CL scaffolds a) PET, b) PC_{48}15:1, c) PC_{48}5:1, d) PC_{15}15:1 and e) PC_{15}5:1. Inserts show the average values. x-Axis represents pore areas (μm^2) and y-axis the relative frequency (%).

5.3.3. Post-electrospinning cross-linking

Cross-linking was carried out by treating the scaffolds with glutaraldehyde vapor for 12 hours. **Figure 5.3** shows the SEM images of PET, PC_{48}5:1, and PC_{15}5:1 AS and CL scaffolds as examples. The morphology of the PET scaffold was not altered with cross-linking. However, several modifications on the microscopic structure of PET/C scaffolds were observed, especially for scaffolds with higher chitosan content (PC_{48}5:1 and PC_{15}5:1). Among them, changes on fiber morphology, from a straight to a curly shape, the increase of fiber surface roughness, and the increased proximity among fibers were the most evident ones.

Average fiber diameters of selected cross-linked PET and PET/C scaffolds are also shown in Table 5.1. The decrease of fiber diameter with cross-linking treatment was significant ($P<0.05$) for the scaffolds with the lowest MW chitosan (PC_{15}15:1 and PC_{15}5:1). Among these scaffolds the highest decrease was observed for the scaffold with higher chitosan content where the average fiber diameter decreased from 3.01 ± 0.72 μm to 2.24 ± 0.85 μm.

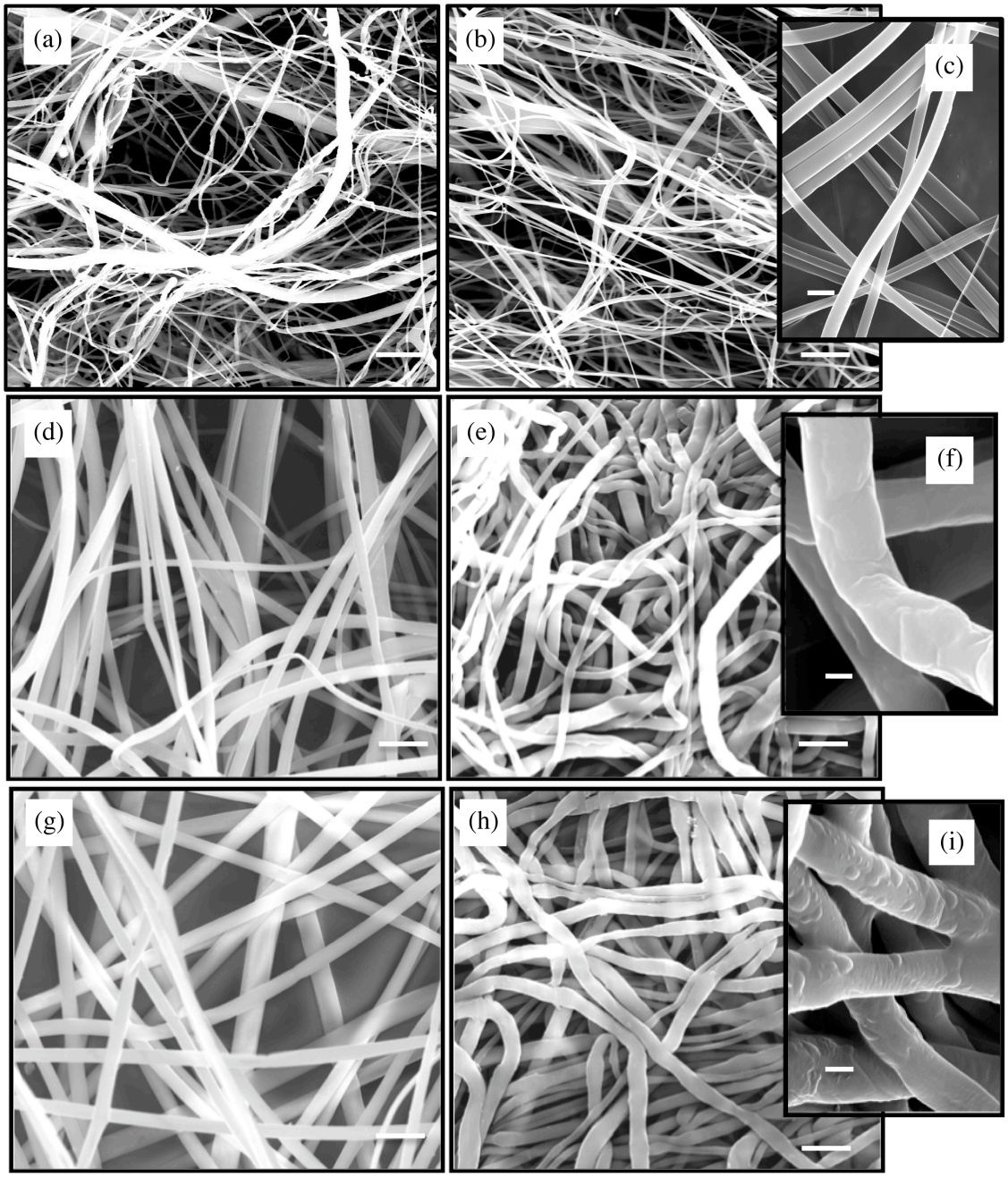

Figure 5.3. SEM micrographs of scaffolds a) PET, b) PETCL, c) PETCL high magnification, d) $PC_{48}5{:}1$, e) $PC_{48}5{:}1CL$, f) $PC_{48}5{:}1CL$ high magnification, g) $PC_{15}5{:}1$, h) $PC_{15}5{:}1CL$ and i) $PC_{15}5{:}1CL$ high magnification. Bar = 10 μm (a, b, d, e, g, and h) or = 1 μm (c, f, and i).

A decrease in pore areas with cross-linking (Figure 5.2 and 5.3) was observed for all scaffolds and this decrease was more pronounced as the chitosan content increased and MW decreased.

Cross-linking of chitosan with glutaraldehyde occurs through a Schiff's base reaction between the aldehyde ends of the cross-linking agent and the amine groups of chitosan to form imine functions. ATR-FTIR spectra were obtained for the AS and CL mats (**Figure 5.4**). FTIR analysis confirmed the cross-linking of chitosan molecules through the formation of imine functions. Indeed, an increase in the intensity of 1680 cm^{-1} peak (C=N imine bond) was observed with cross-linking of the fibrous mats while the intensity of the 1540 cm^{-1} peak decreased due to the decrease of the free amine groups. The formation of bindings within a single fiber led to a decreased in fiber diameter and an increase of surface roughness. Similar morphological changes were previously observed as a result of chitosan cross-linking with glutaraldehyde (Monteiro and Airoldi 1999; Gupta and Jabrail 2007). In addition, new bindings between adjacent fibers caused fiber approaching each other and, consequently, a reduction of pore areas. Therefore, the cross-linking process may be used as a strategy not only to decrease the solubility of the more hydrophilic polymer in aqueous media but also to manipulate the morphology of PET/C fibrous scaffolds.

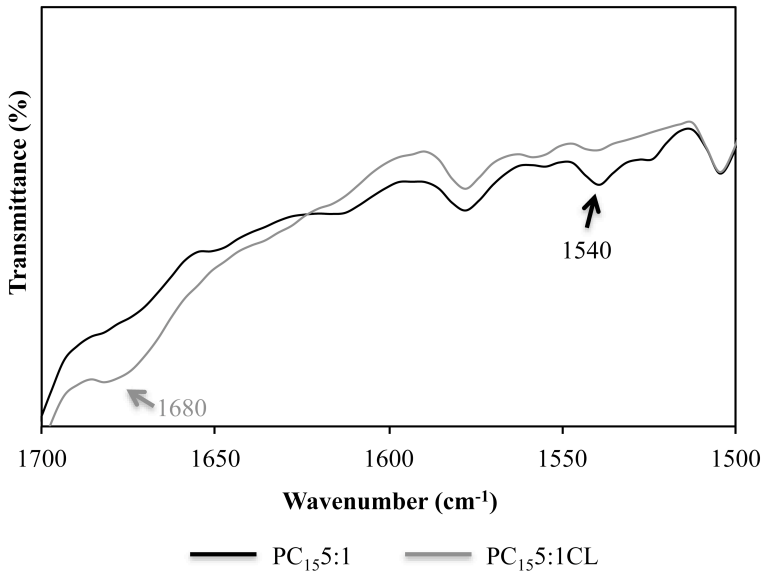

Figure 5.4. FTIR spectra (1700 – 1500 cm^{-1} region) of PC_{15}5:1 and PC_{15}5:1CL scaffolds.

5.3.4. Surface properties

WCAs and drop lives were measured in order to evaluate the wettability of AS and CL scaffolds (results are displayed in **Table 5.2**). As expected, the PET scaffold exhibited a

high hydrophobicity. The WCA measurements showed no significant differences among PET, $PC_{48}15:1$, and $PC_{15}15:1$. For these scaffolds, drops showed long life times (>600 s), with little decrease of WCA with time. However, a significant decrease of WCA was observed for scaffolds $PC_{48}5:1$ and $PC_{15}5:1$ ($P<0.05$), which clearly indicates an improvement on scaffolds hydrophilicity with the increase of chitosan content. In addition, water drops on these scaffolds were rapidly absorbed due to their high water uptake capacity and high pore sizes.

Cross-linking treatment increased the hydrophobicity of $PC_{48}5:1$ and $PC_{15}5:1$ scaffolds ($P<0.05$), an expected effect since this treatment results in diminishing the number of chitosan's free amine groups. This increase of surface hydrophobicity also reflected in the drop life, which rose from 6 s to more than 600 s.

Table 5.2. WCA (mean ± standard deviation) and drop life time for PET and PET/C scaffolds. Different superscript letters within a column indicate significant differences. ($P < 0.05$).

	WCA (º)	**Drop life (s)**
PET	133.2 ± 2.9^{a}	$> 600^{a}$
$PC_{48}15:1$	137.3 ± 1.7^{a}	$> 600^{a}$
$PC_{48}5:1$	119.9 ± 7.3^{b}	6^{b}
$PC_{15}15:1$	138.8 ± 1.8^{a}	$> 600^{a}$
$PC_{15}5:1$	125.2 ± 4.6^{b}	6^{b}
$PC_{48}15:1CL$	132.6 ± 3.9^{a}	$> 600^{a}$
$PC_{48}5:1CL$	127.4 ± 6.5^{c}	$> 600^{a}$
$PC_{15}15:1CL$	132.3 ± 3.2^{a}	$> 600^{a}$
$PC_{15}5:1CL$	135.0 ± 4.7^{a}	$> 600^{a}$

5.3.5. Cell studies

Differences in architecture and composition of the scaffolds are expected to define the cellular environment and consequently to have a remarkable influence in cell activity. Therefore, after the initial screening of the scaffold characteristics, three samples (PET, PC_{15}5:1 and PC_{15}5:1CL) were picked to study L929 cell behavior *in vitro* since the major differences in architecture were found among them.

Figure 5.5. displays the results from the indirect cytotoxicity assay. No significant differences were found in respect to viability of cells cultured in the scaffolds extraction media (measured via MTT assay) in comparison to control, *i.e.* fresh medium. This result indicates that, for the time analyzed, no cytotoxic compounds were released from the scaffolds ($P<0.05$).

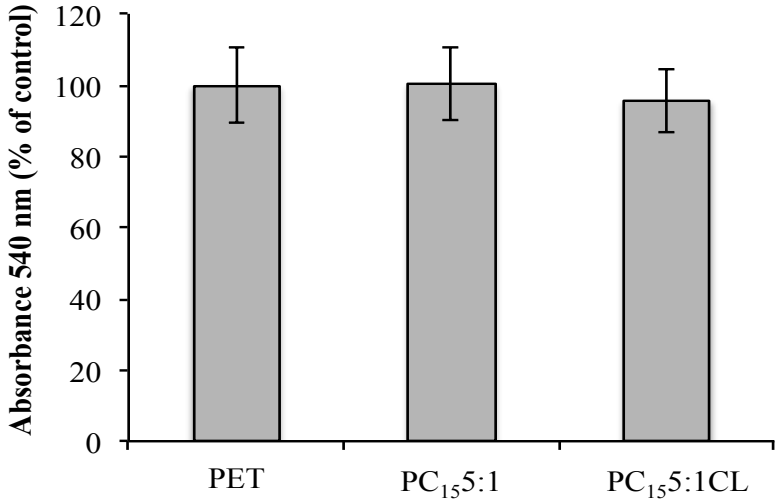

Figure 5.5. Indirect cytotoxicity evaluation of nanofibrous scaffolds based on the viability of fibroblasts (L929) cultured in the extraction media. The viability of cells cultured in fresh media was used as control. No significant differences were found.

The viability of fibroblasts cultivated on PET and PET/C scaffolds for 2, 7, and 14 days was evaluated by MTS assay (**Figure 5.6)**. All samples showed a rapid cell growth during the first 7 days of culture, followed by a stationary phase. PET scaffold exhibited higher levels of cell viability when compared to PET/C scaffolds.

The viability of anchorage dependent cells, such as fibroblasts, is greatly influenced by the cell adhesion processes. Cell-substrate contact area can determine whether or not a cell

proliferates, becomes quiescent or dies (McGrath 2007). Here, viability, adhesion, morphology, and proliferation of cells in the scaffolds were evaluated combining SEM, CLSM, and immunochemical techniques.

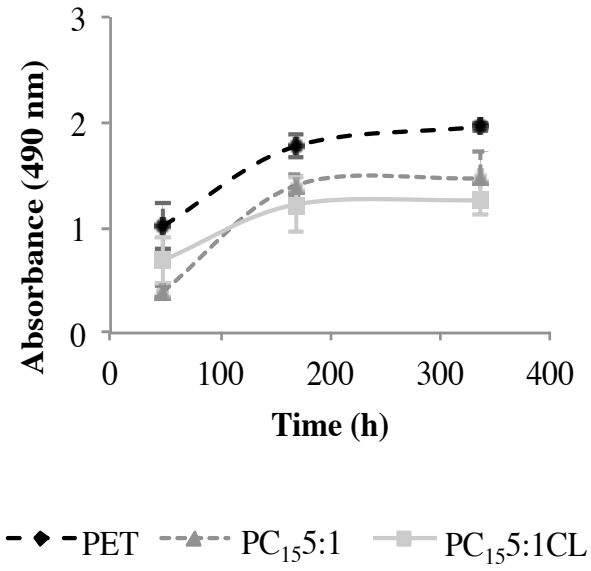

Figure 5.6. Viability of L929 cells cultured on PET, PC_{48}5:1, and PC_{48}5:1CL scaffolds for 2, 7, and 14 days measured via MTS assay. No significant differences were found.

Figure 5.7 displays SEM and CLSM micrographs illustrating the evolution of adhesion and spreading of L929 cells in PET scaffold, as an example. Twelve hours after seeded on PET and PET/C scaffolds, fibroblasts showed a circular morphology, typical of the early stages of adhesion. Following, cell proliferation and spreading took place and fibroblasts shape changed to a well-spread morphology with multiple cellular extensions adhering to the substratum. During the subsequent days of culture, cells exhibited intensive growth and abundant secretion of ECM that partially covered the scaffold surfaces.

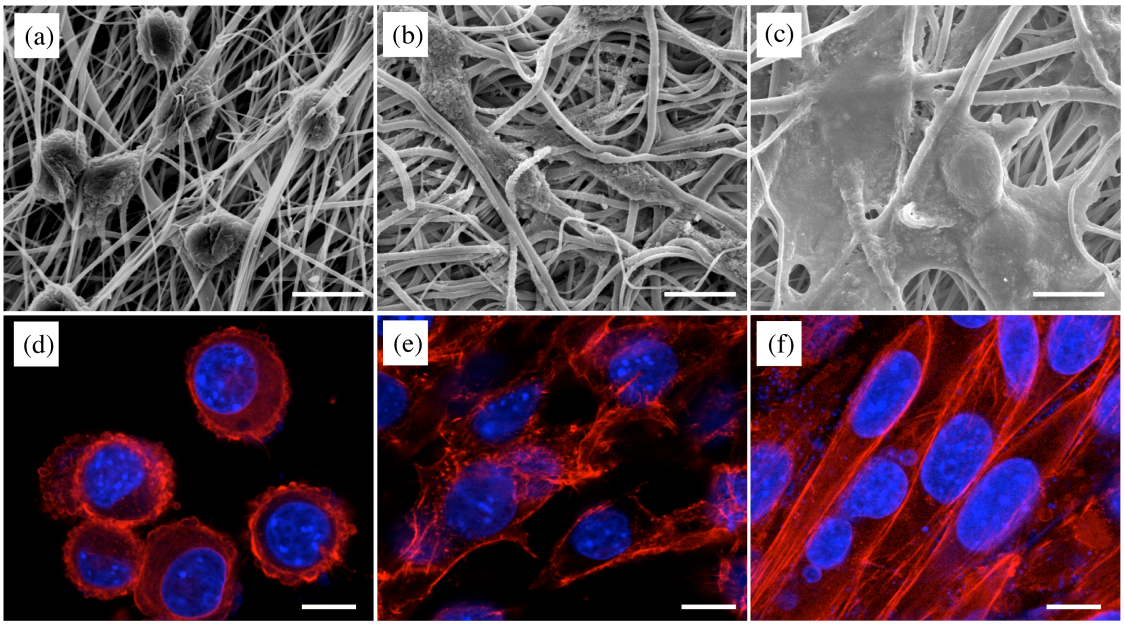

Figure 5.7. SEM images (a- c) and CLSM images (d-f) of L929 fibroblasts cultured on PET scaffold for 12 hours (a and d), 48 hours (b and e), and 7 days (c and f). F-actin (red) and nucleus (blue) stained with Alexafluor 546 conjugated to phalloidin and DAPI, respectively. Bar = 10 μm.

Cell adhesion and spreading was clearly influenced by the fiber size and porosity of the scaffold. High magnification SEM images of L929 fibroblasts adhered to PET, PC_{15}5:1 and PC_{15}5:1 CL fibers are displayed in **Figure 5.8**. On PET scaffold, cells tended to adhere to bundles of fibers spreading over them due to the small fiber diameter (0.71 ± 0.28 µm). On the other hand, on PC_{15}5:1 and PC_{15}5:1 CL, fibroblasts generally adhered to single fibers, as a result of the higher fiber diameters (3.01 ± 0.72 µm and 2.24 ± 0,85 µm, respectively) and larger pore sizes.

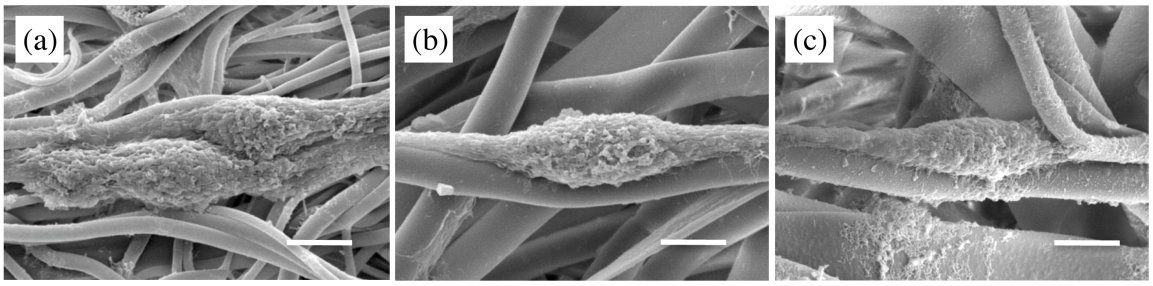

Figure 5.8. SEM micrographs of L929 fibroblasts cultured on a) PET, b) PC_{15}5:1, and c) PC_{15}5:1 CL scaffolds after 48 hours incubation. Scale bar = 5 μm.

Labeling of actin filaments, vinculin, and nucleus was carried out in order to study adhesion of L929 fibroblasts cultured on the electrospun scaffolds. **Figure 5.9** shows representative CLSM images for PET and PC_{15}5:1 scaffolds and **Figure 5.10** displays the cytoskeleton area and density of cells cultured on the scaffolds for 12 hours, 48 hours, and 7 days. An increase of cell density over the incubation time was observed for all the scaffolds, and higher density levels were obtained for PET scaffold. Cytoskeleton area of cells cultured on the scaffolds increased after 48 hours, and the highest mean cytoskeleton area was achieved for PET scaffold.

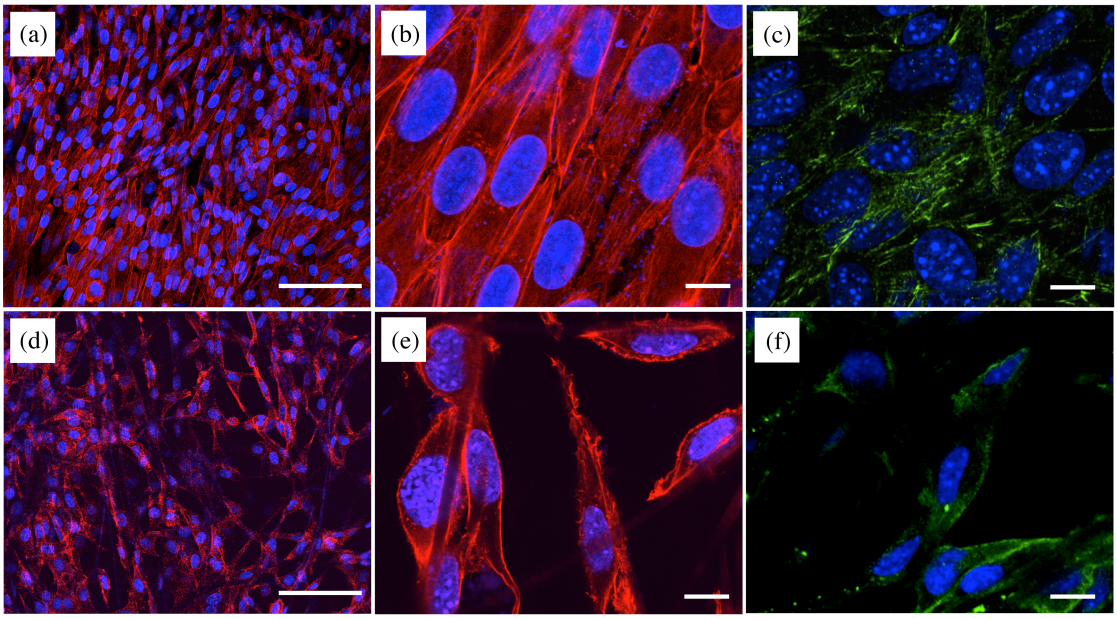

Figure 5.9. CLSM images of L929 fibroblasts after 7 days of incubation on PET (a-c) and PC_{15}5:1 (d-f) scaffolds. F-actin (red), vinculin (green) and nucleus (blue) stained with phalloidin Alexafluor 546 conjugated, anti-vinculin monoclonal antibody followed by Alexafluor 488 goat anti-mouse, and DAPI, respectively. Scale bar = 100 μm (a and d) or =10 μm (b, c, e, and f).

Fiber diameter and architecture influenced the cell spreading process. Higher levels of spreading, *i.e.* cytoskeleton area and vinculin expression, were achieved for cells cultured on PET scaffolds. The mean cytoskeleton area of cells cultured on PET scaffold was 565 ± 149 µm at day 7, significantly greater than cells cultivated on PC_{15}5:1 (473± 119 µm) and PC_{15}5:1 CL (350± 74 µm). The lower pore areas of PET scaffold (9.4 μm^2) allow cells to spread across pores and establish several adhesion points on neighbor fibers. On the other hand, on PC_{15}5:1 and PC_{15}5:1 CL cells were not able to cover the pores due to their higher

areas (89.3 μm^2 and 23.4 μm^2, respectively) and the spreading process was limited to the diameter of the fiber.

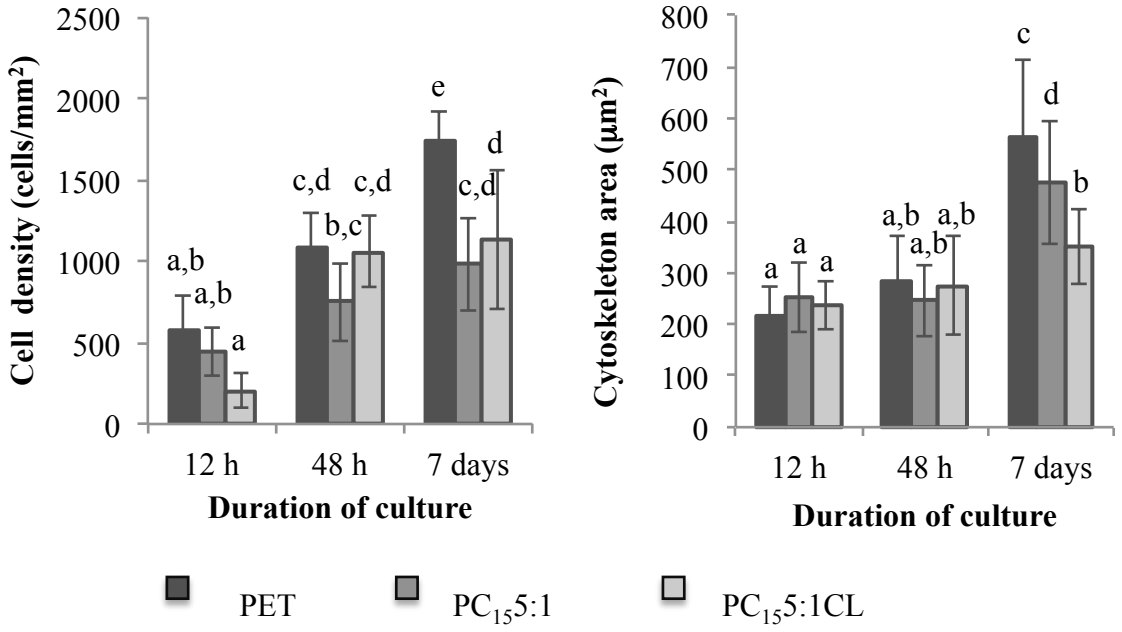

Figure 5.10. Cell density (a) and cytoskeleton area (b) of L929 cells as a function of culture time, obtained for PET, PC_{15}5:1, and PC_{15}5:1CL scaffolds. Different letters indicate significant differences ($p < 0.05$).

Since RGD motives are absent in PET or PET/C scaffolds, focal adhesion of L929 cells may initially occur via proteins adsorbed from serum containing medium. Cells would be able to secrete ECM components after attached to the scaffolds, improving cell spreading and adhesion. Immunolabeling of ECM fibronectin was performed after 2 and 7 days of culture. Results showed considerable amounts of extracellular fibronectin in the superficial and internal structure of the scaffolds, 2 days after seeding (**Figure 5.11**). The presence of ECM components in the scaffolds creates an environment even more similar to natural tissues, enhancing scaffolds' ability to support cell growth.

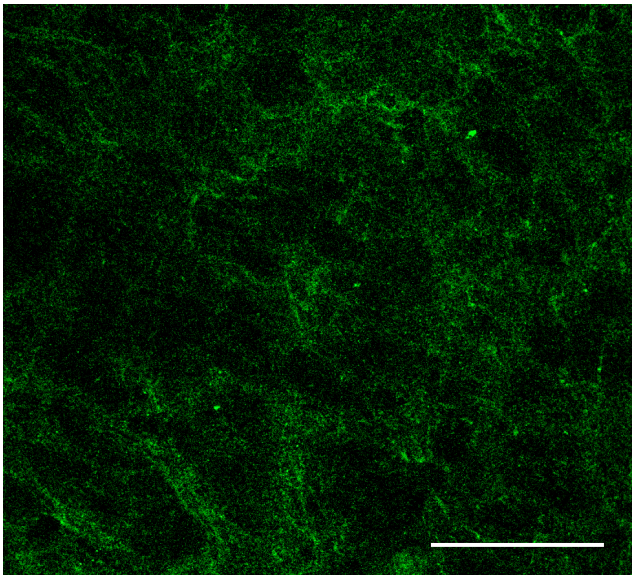

Figure 5.11. Immunolabeling of extracellular fibronectin (green) deposited on the surface of PET scaffold after 7 days of incubation with L929 cells. Bar= 50 μm.

Several studies have demonstrated the antiapoptotic effect of focal adhesion on anchorage dependent cells (Sonoda *et al.* 2000). Chen *et al.* (1997) have shown that cells underwent programmed cell death when spreading was limited to islands of 20 μm of diameter. However, if the spaces among multiple islands were lower than 10 μm, cells were able to spread across the spaces and establish focal adhesion points on the neighbor adhesion islands, switching off apoptosis. Double staining of fibroblasts with annexin V and PI was carried out in order to test whether the limited area for cell adhesion of PET/C fibers was related to the lower densities of cells cultivated on these scaffolds via apoptosis induction. Cytograms of annexin V vs. PI uptake in the L929 cells cultured on the electrospun scaffolds are shown in **Figure 5.12**. In accordance with the MTS results and microscopical analysis previously described, the percentage of viable cells was significantly higher in PET scaffold (92.4 ± 0.8%) compared to PC_{15}5:1 and PC_{15}5:1CL (81.7± 8.3% and 75.7± 2.8, respectively). Higher percentage of early apoptotic cells were found in cell populations cultured on PC_{15}5:1 and PC_{15}5:1CL (4.1±1.0 and 4.9±1.6) than in PET scaffold (1.6±1.0). Apoptosis induction may be related to the limited area available for the cell adhesion and spreading on PET/C scaffolds. Additionally, higher indices of necrosis were also found in the population of cells cultured on PC_{15}5:1 and PC_{15}5:1CL scaffolds (16.2±0.4 and 12.5±1.4) compared to PET scaffold (4.2±0.9). Since the indirect cytotoxicity assay showed no evidence of toxic compounds released to the medium, results

suggest that chitosan molecules exposed on the fiber surface may induce necrotic cell death. Indeed, the polycationic nature of chitosan may interact and damage the plasma membrane of cells, as already observed for PHBV/C blends (reported in chapter 2, subsection 2.3.7.1).

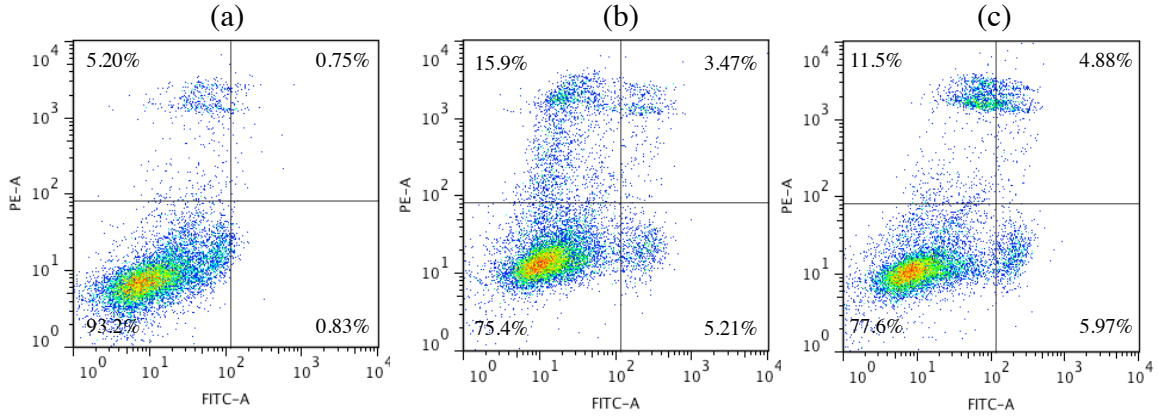

Figure 5.12. Annexin V-FITC/PI flow cytometry analysis of cell death after 48 hours of incubation in a) PET, b) PC_{15}5:1, and c) PC_{15}5:1 CL. Viable cells (Annexin V-FITC negative/PI negative) are in the lower left quadrants; Apoptotic cells (Annexin V-FITC positive/PI negative) are in the lower right quadrants; late apoptotic cells (Annexin V-FITC positive/PI positive) are in the upper right quadrants; necrotic cells (Annexin V-FITC negative/PI positive) are in the upper left quadrants. The cytograms are representative of three independent experiments.

EdU proliferation assay was used to measure the ability of cells to proliferate when attached to the nanofibrous scaffolds. **Figure 5.13** displays the percentage of proliferating cells cultured on the electrospun scaffolds (% of control). Higher level of proliferation was observed for cells cultivated on PET scaffolds compared to PET/C scaffolds. Again, the higher proliferative activity is probably correlated with the improved adhesion and spreading of fibroblasts on this scaffold.

Cross-linking of the PET/C scaffold had a negative effect on the viability and adhesion of fibroblasts. A decrease in cell spreading and density was observed when comparing the AS and CL scaffolds. A possible explanation is related to the decrease of fiber diameter and, consequently, the available area for cell adhesion. Additionally, although cross-linking decreased the pore size, a single fiber attachment was also predominantly found on PC_{15}5:1CL scaffold, which demonstrates that this decrease was not enough for cell spreading through pores.

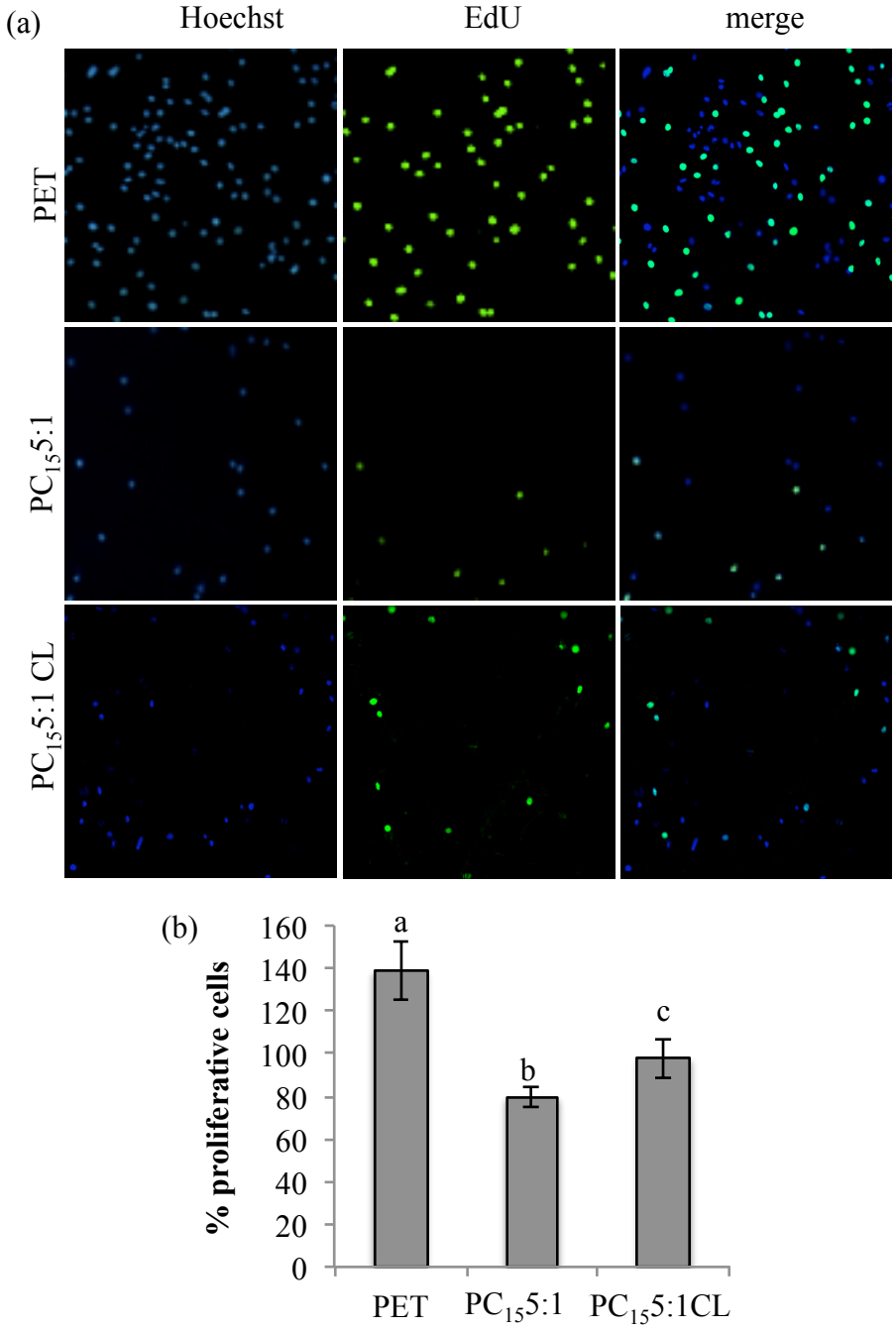

Figure 5.13. EdU incorporation assay of L929 cultured on PET, PC_{15}5:1, and PC_{15}5:1 CL. (a) Fluorescence micrographs of proliferative cells (green) stained with EdU Alexafuor 488 and nuclei (blue) counterstained with DAPI (100x magnification). (b) Quantitation of proliferative cells mean ± S.D measured from 10 fields from 3 independent experiments. Results are expressed as % of control, *i.e.* TCP. Different letters indicate significant differences ($P < 0.05$).

Even though there are many studies showing that chitosan improves the biological performance of biomaterials, higher levels of viability, adhesion, and proliferation were obtained for cells cultivated on PET scaffold. The architecture of the scaffold seems to play a more important role on cell viability and growth than any chemical surface changes introduced by the presence of the hydrophilic biopolymer. In this context, the lower fiber diameters and lower pore sizes of PET scaffolds proved to be more suitable for fibroblasts growth. On the other hand, the higher pores of PET/C scaffolds allowed L929 cells to cross those pores and penetrate through the fibers (as illustrated in **Figure 5.14**).

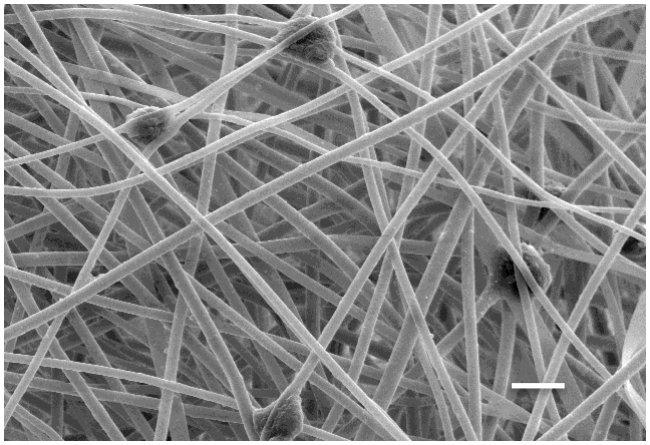

Figure 5.14. SEM image evidencing the relative size of L929 fibroblasts (12 hours after seeding) and PC_{15}5:1 scaffold pore size. Bar= 10 μm.

3D CLSM (through z-axis) were performed to confirm that cells were able to cross pores and colonize the inside of these scaffolds. After 48h, cells were found within the section of the PET/C scaffolds, in a 3D culture while on PET scaffold a superficial cell growth was predominant (**Figure 5.15**). Depending on the application requirements, both 2D (monolayer) and 3D culture may be suitable.

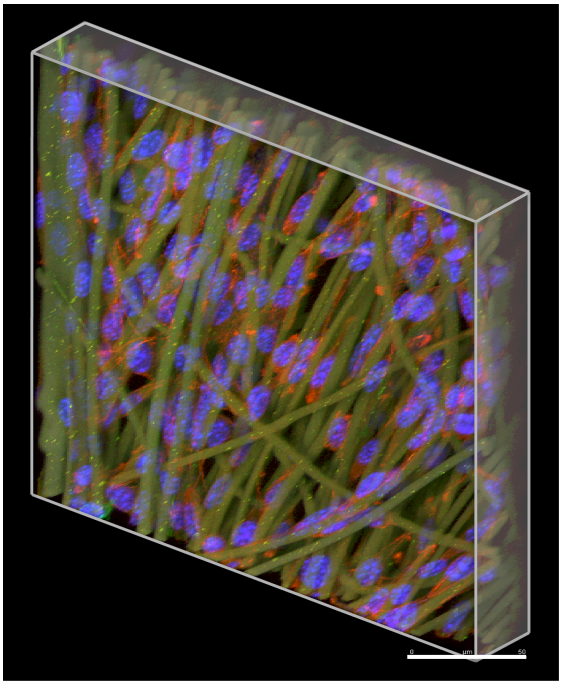

Figure 5.15. CLSM 3D projection of L929 cells cultivated on PC_{15}5:1 scaffold for 48h. Fibers (green), F-actin (red) and nucleus (blue) stained with FITC, Alexafluor 546 conjugated to phalloidin and DAPI, respectively. Scale bar = 50 μm.

5.4. Conclusions

This chapter reports the preparation of PET and PET/C electrospun scaffolds followed by the analysis of their architecture and physicochemical properties. Secondly, the effects of the scaffolds were assayed on the cell growth. Properties of the scaffolds, *e.g.* morphology and wettability, were manipulated through the variation of the electrospinning solution composition and post-electrospinning cross-linking. *In vitro* experiments with L929 fibroblasts revealed how these changes can modulate cell behavior and cell-scaffold interactions, including viability, adhesion, spreading, and proliferation. Although the fiber composition and scaffold architecture were not varied independently, the scaffold with smaller fiber diameters and pore areas has demonstrated to allow higher levels of fibroblasts adhesion, spreading, and proliferation, while a 3D cell colonization was achieved for scaffolds with higher fiber diameters. These results provide important information not only for this specific polymeric system (PET/C), but also for outlining strategies to enhance the design of other biomaterials towards a better biological performance.

6.PET and PET/chitosan electrospun hybrid mats as as abdominal meshes for hernia repair

6.1. Introduction

6.1.1. Incisional hernias: occurrence and treatment

Incisional hernia is a frequent complication of laparotomy due to the decrease of abdominal strength in the injured tissue. In fact, 10-15% of all patients eventually develop an incisional hernia after an abdominal surgery. Hysterectomy, cesarean section, and emergency laparotomies for generalized peritonitis are particularly likely to herniation. Medical conditions such as obesity, respiratory and circulatory diseases, and chronic constipation often contribute to hernia formation, recurrence and development of related complications (Anthony *et al.* 2000; Gecim *et al.* 1996).

Traditionally, hernia repair have been performed by primary closure. This procedure, however, has been associated to unacceptable high reoccurrence rates (46 -54 %) (Luijendijk *et al.* 2000; Anthony *et al.* 2000; Gecim *et al.* 1996). Implementation of a tension-free repair, by using a prosthetic biomaterial, *i.e.* abdominal mesh, to substitute or reinforce abdominal strength at the damaged area has decreased the recurrence rates to 23-29 % (Luijendijk *et al.* 2000; Anthony *et al.* 2000). All over the world, prosthetic mesh repair have been replacing the primary closure of abdominal defects, in particular for defects larger than 3 cm. In USA more than 90% of incisional hernias are already being repaired with prosthetic meshes (Kingsnorth and LeBlanc 2003). Numerous materials are commercially available, the most common are macroporous meshes made of PET (*e.g.* Mersilene® and Parietex®), polypropylene (Marlex®, Prolene®, and Surgipro®), and polytetrafluorethylene (Gore-Tex®).

6.1.2. Complications of prosthetic mesh use

Although the recurrence of hernias has decreased with the use of abdominal meshes, serious complications have been associated with this procedure, including infection, visceral adhesions to the mesh, seroma, mechanical failure of the mesh, and foreign body reaction (Carbajo *et al.* 1999; Robinson *et al.* 2005). For instance, Robinson *et al.* (2005) studied 252 cases of complications associated to the use of abdominal meshes and detected

that infection was the most frequent problem, representing 42% of the total cases. Another important conclusion of this study was that specific complications were related to specific materials, for example, polypropylene mesh (Sepra ®) undergone higher mechanical failure, while biomaterial meshes (Surgisis Gold® and Alloderm ®) had more host reactions, and PTFE meshes caused more intestinal adhesions. More recently, studying 32 cases of infection associated to different meshes, Tolino *et al.* (2009) verified that 69% of the patients had to be operated again for mesh removal, which required 51 operations for more than 3 years.

Besides infection, host reaction and intestinal adhesions to the abdominal mesh are complications of major concern after the prosthetic material implantation. Further details covering this subject will be reviewed in the subsequent subsections.

6.1.2.1. Intestinal adhesions

Adhesion of organs to the implanted material is a serious complication related to the use of abdominal meshes. Bowel adhesion is particularly problematic as it causes severe complications including bowel obstruction, enterocutaneous fistula, and chronic pain. In a prospective analysis, Menzies and Ellis (1990) used laparoscopy to assess the formation of adhesions and verified that 93% of patients who had undergone laparotomy developed intra-abdominal adhesions. This study also showed that the adhesiolysis procedure represented 0.9% of total surgeries and 3.3% of all laparotomies carried out at the "Academic Surgical Unit of Westminster Hospital".

It is well established that the intra-abdominal adhesion is related to an inflammatory response to injuries, foreign bodies or infection. As a typical inflammatory process, adhesiogenesis initiates very early after the placement of the prosthetic mesh. In fact, in laboratory experiments, Baptista *et al.* (2000) have demonstrated that adhesions were already formed at the first postoperative day and did not progress after day 7. Indeed, the adhesion formation follows a very similar pathway to the wound healing process, which includes recruitment of inflammatory cells to the injured area, fibrin matrix formation, collagens deposition and maturation (Milligan and Raftery 1974). Several methods have been investigated to prevent adhesion including the use of fibrinolytic agents, antibiotics or anti-inflammatory drugs (Chu *et al.* 2011; Suckow *et al.* 2010; Bothin *et al.* 2003). Also,

the use of non-adhesive layers or coatings has been tried although with limited success (van't Riet *et al.* 2003; Bellon *et al.* 1996). Notwithstanding, the development of new materials that prevent adhesiogenesis is still an issue of enormous importance.

6.1.2.2. Foreign body reaction

Once a biomaterial is implanted in the body, a normal wound healing response initiates as a result from injury. As described in chapter 1, the wound healing process begins with homeostasis and a subsequent acute inflammatory phase, characterized by a dense PMN infiltration. With implanted non-degradable biomaterials, however, inflammation usually progresses to a chronic state as a result of body inability to eliminate the foreign body. Hence, macrophages are recruited and adhere to the surface of the biomaterial in an attempt to phagocytize and degrade the foreign body. The size and the chemical composition of the non-degradable biomaterials, however, usually lead to a frustrated phagocytosis. As a consequence, macrophages fuse together in order to form multinucleated cells, *i.e.* foreign body giant cells (FBGC), as a strategy to isolate the foreign material. Apart from FBGC and macrophages, fibroblasts are also active elements of non-immunogenic foreign body granulomas, being responsible for synthesizing a dense layer of collagen that isolates the granuloma from the surrounding tissue (granuloma capsule). The extent and the duration of the foreign body reaction depend both on the properties of the biomaterial and on the characteristics of the tissue were the material is implanted. Many times, the foreign body reaction persists for the lifetime of the biomaterial without committing the normal function of the tissue. Excellent reviews are available for in depth information on foreign body reaction to biomedical devices (Babensee *et al.* 1998; Anderson *et al.* 2008).

6.1.3. Electrospun materials as meshes for abdominal hernia repair

Apart from preventing adhesion, it is generally accepted that the ideal abdominal mesh should be chemically inert and stable for long periods, cause no immune or inflammatory response, and fulfill the required mechanical needs for the application. In this context, electrospun mats of non-degradable polymers emerge as potential alternative meshes for abdominal defect repair.

As previously described in chapter 4, PET can be electrospun into nanofibrous nonwoven mats, with an average fiber diameter of 0.71 ± 0.28 μm and with a microporous structure (94.9% of porosity and an average pore area of 9.4 μm^2). These morphological characteristics, together with the high hydrophobicity of this material (WCA ≈ 133 º) are thought to be ideal for prevention of visceral adhesion to the mesh. According to Matthews *et al.* (2003) biomaterials with pores lower than 75 μm reduce the occurrence of bowel adhesions. Besides, PET is a highly biocompatible, biostable, and non-degradable polymer and possesses the mechanical features required for this application. Even more, the low density of the electrospun PET mats (~ 0.091 g/cm^{-3}) and the high malleability of these materials (Veleirinho *et al.* 2008) may promote an enhanced adaptation and comfort to the patient.

On the one hand the mesh must prevent adhesions to the visceral tissues, but on the other hand the parietal side should also promote a good integration to the adjacent conjunctive tissue. Indeed, McGinty *et al.* (2005) have demonstrated that a better incorporation of the mesh in the parietal side reduces the number and the severity of adhesion formation on the visceral side. Composite meshes, with a visceral side that minimizes adhesions and a parietal side that maximizes tissue ingrowth have been designed. A well-known example is Dualmesh®, a PTFE mesh with a microporous layer that is turned to the visceral side and a macroporous layer designed to promote tissue ingrowth on the parietal side. Another example is Parietex®, a PET mesh with one of the sides (parietal side) covered with collagen to promote tissue integration.

In this chapter we describe the application of three electrospun non-absorbable fibrous mats, composed by PET fibers, PET/chitosan (PET/C) hybrid fibers, and double-layer (DL) PET/chitosan mesh, respectively, in the repair of abdominal defects. An *in vivo* study with Wistar rats was performed to evaluate the clinical and histological aspects of the use of these electrospun mats as meshes for abdominal hernia repair.

The PET mesh is expected to restrict the parietal tissue integration due to its small pores and hydrophobic characteristics. Hence, with the aim of enhancing the interaction of the mesh with the parietal conjunctive tissue, PET/C and double layer (DL) meshes were designed. Compared to PET, PET/C mats show higher fiber diameters, larger pores, lower

hydrophobicity and enhanced mechanical strength (Chapter 5) (Lopes-da-Silva *et al.* 2009).

Moreover several reports on the anti-inflammatory and wound healing effects of chitosan are found in literature, which may be useful to inhibit adhesiogenesis and to attenuate the typical symptoms of the post-surgery period (Zheng and Zhu 2003; Ueno *et al.* 2001; VandeVord *et al.* 2002; Ueno *et al.* 1999).

The dual layer mesh (DL), containing one layer of PET and one layer of PET/C, was used with the PET side turned to the visceral side while the PET/C layer was in contact with the parietal side.

6.2. Experimental

6.2.1. Material

Samples of PET and chitosan (15 kDa) were the same used in chapters 4 and 5. All chemicals were of analytical grade and obtained from Sigma-Aldrich (Sigma-Aldrich Chemical Company). Marlex® (Intracorp) was purchase from *Cirurgica Passos Lda*.

6.2.2. Meshes fabrication

Preparation and characterization of PET and PET/C (PC_{15}5:1) mats are described in chapter 5. DL meshes were fabricated by electrospinning of 10 mL PET solution 30 wt.% followed by 10 mL of PET/C solution (30 wt.% PET, 6 wt.% chitosan 15 kDa). Fibers were collected as a nonwoven fibrous mat on the rotating drum (900 rpm), in air and at room conditions (20 ± 2 ºC, 45–50% RH) and the mat was dried at 35 ºC for 24 hours.

Morphology of DL meshes was also analyzed by SEM in a scanning electron microscope (Hitachi S4100) at an accelerating voltage of 25 kV. Pictures of transversal and longitudinal sections of both layers of the mat were obtained.

Previously to biological assays, all meshes were sterilized under UV light for 1 hour (both faces), immersed in ethanol 70% (v/v) for 10 minutes and washed with physiological solution.

6.2.3. Animal model

Animal experiments were approved by Animal Ethics Committee of UFSC (PP0406/2009). Male Wistar rats 3 months age and weighting 250-300 g were obtained from the Central Biotery of UFSC. Animals were randomly distributed among the 7 treatments, according to **Table 6.1** (n=8).

Table 6.1. Experimental groups of incisional hernia repair.

Group	Chemical composition	Duration of experiment (days)	Fiber diameter (μm)	Pore area (μm^2)	Mesh thickness (mm)
Marlex30	Polypropylene	30	177 ± 24	31400	0.22 ± 0.07
Marlex90		90			
PET30	PET	30	0.71 ± 0.28	9.4	0.31 ± 0.02
PET90		90			
PET/C	PET/C 5:1 (w/w)	30	3.01 ± 0.72	89.3	0.49 ± 0.09
DL	PET + PET/C 5:1 (w/w)	30	N.A.	N.A.	0.52 ± 0.05
WovenPET	PET	30	342 ± 68*	N.A.	0.46 ± 0.11

* Average diameter of the multifilament yarn;

N.A. not applicable.

A graphical illustration of the surgical procedure is provided in **Figure 6.1**. After an intramuscular injection of a mixture of ketamine (90 mg/kg) and xylazine (15 mg/kg) and abdominal shaving, a 5 cm skin paramedian incision was made at the left size, using a sterile scalpel blade (Figure 6.1 (a) and (b)). Skin was dissected to expose the underlying abdominal fascia (Figure 6.1 (c)) and a 1.5 x 1.5 cm defect of anterior abdominal wall was created by the complete resection of abdominal layers (Figure 6.1 (d) and (e)). The edges of the meshes (2.0 x 2.0 cm) were sutured to the remaining muscle of the abdominal wall with interrupted suture (Figure 6.1 (f)) and also with simple running suture all over the borders (Figure 6.1 (g) and (h)), using 5-0 polypropylene. The skin was closed with intradermal suture with nylon 4-0 monofilament (Figure 6.1 (i)). Animals were allowed to recover from anesthesia, housed in individual cages, and observed daily for evidence of wound complications (such as inflammation, infection, seroma, abscess, hematoma or skin dehiscence).

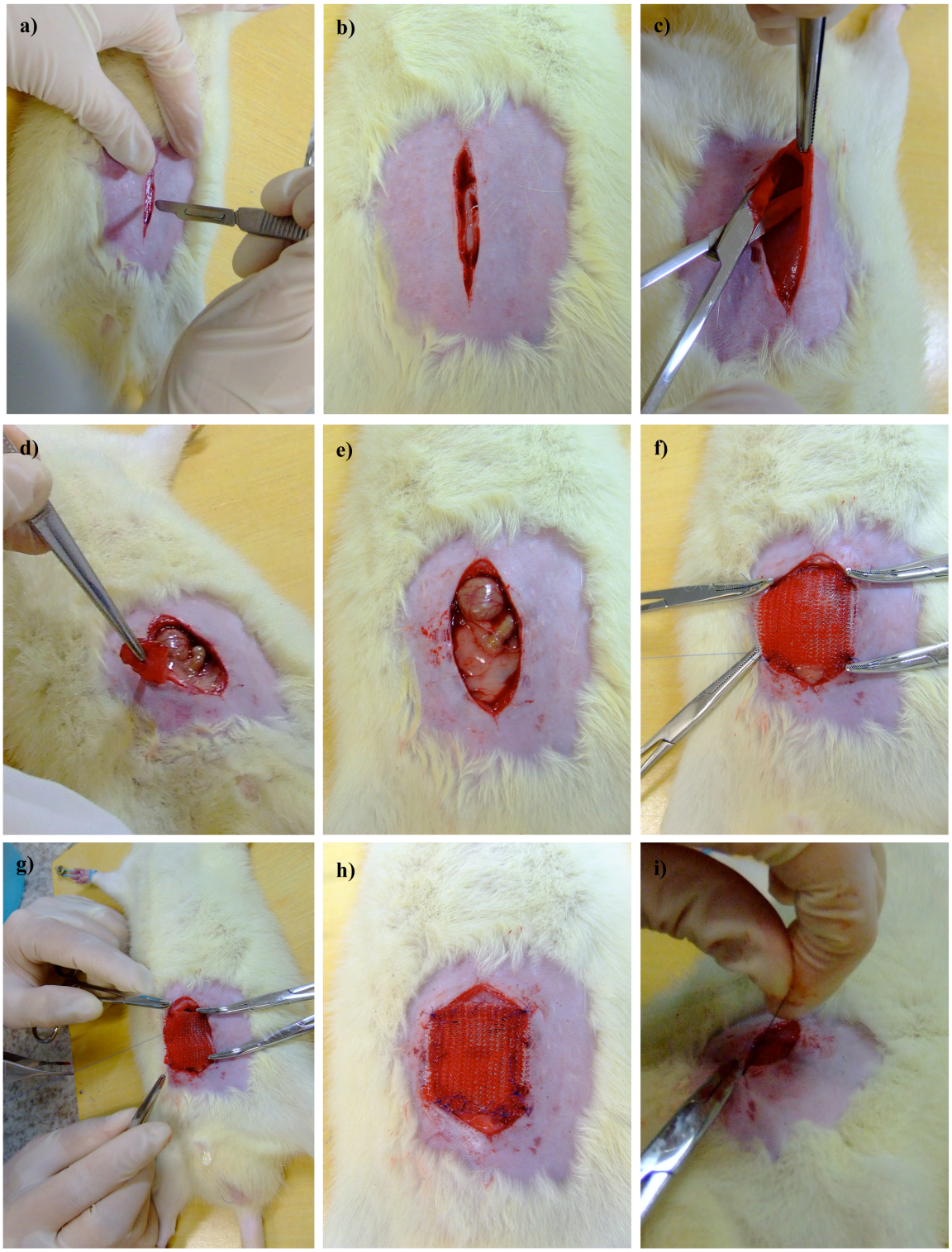

Figure 6.1. Graphic illustration of the incisional hernia model.

On day 30 and 90 post-surgery, animals were sacrificed in a carbon dioxide chamber, and the presence of inflammation, seroma, abscess, hematoma, skin dehiscence or infection was analyzed. The abdominal wall was carefully excised well away from the mesh (as illustrated in **Figure 6.2 (a)**), to preserve any adherence to the bowel or omentum (after adhesion analysis, tissue was completely excised and collected for histopathological analysis). Tissues were fixed in buffered formaldehyde solution (10%, pH 7.2), divided in 2 parts, embedded in paraffin, and sectioned at 4 μm thickness, according to **Figure 6.2 (b)**. Giemsa and HE staining were performed and samples were analyzed under an optical microscope. The thickness of the foreign body granuloma was measured and the total number of FBGC surrounding the mesh was determined.

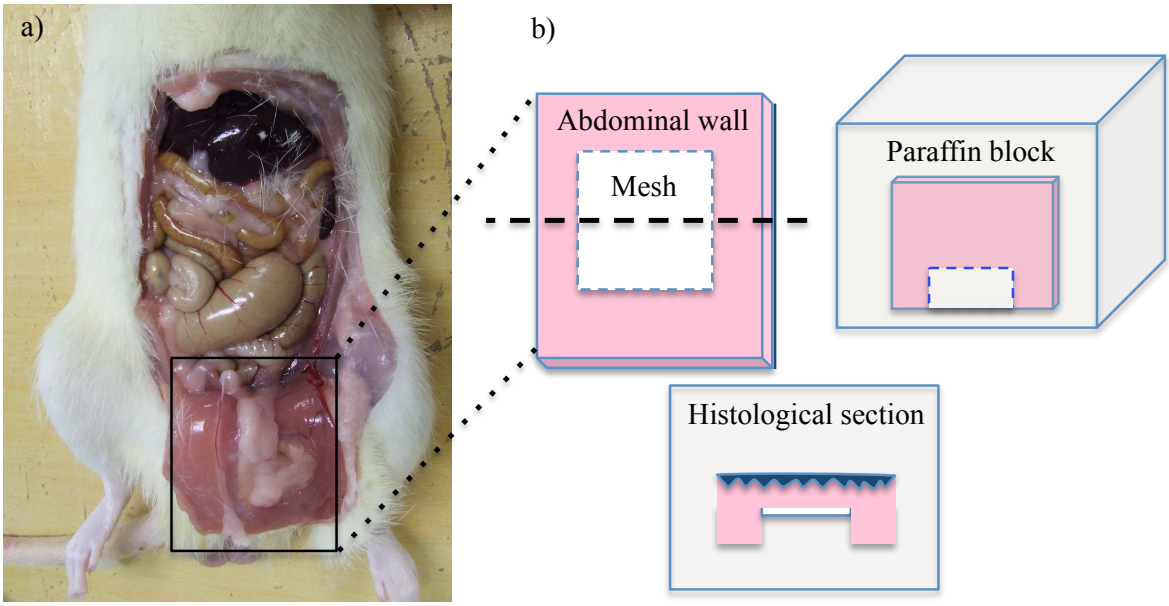

Figure 6.2. Illustrative representation of (a) excision of abdominal mesh and surrounding tissues and (b) preparation of histological sections.

6.2.4. Statistics

Statistical analysis was carried out using Instat 3.0. Results were expressed as the mean ± standard deviation and compared through one-way ANOVA, Tukey-Kramer multiple comparisons test (for parametric data) and Mann–Whitney U test (for non-parametric data). $P < 0.05$ was considered statistically significant.

6.3. Results and discussion

Several biomaterials have been used as prosthetic meshes for abdominal wall repair, e.g incisional hernia repair. Among them, non-absorbable polymers with recognized biocompatibility such as polypropylene, PET or PTFE are the most common. Although a considerable improvement in the recurrence rate was already achieved with these materials, in comparison to the traditional suture technique, several problems are still associated with this procedure. Among them, the formation of adhesions between the mesh and the bowel is one of major concern since it results in several complications such as chronic pain, bowel obstruction or enterocutaneous fistula.

As previously mentioned, during the electrospinning process a polymeric solution is transformed in a nonwoven nanofibrous mesh with unique properties. Some of these properties such as low density, microporosity and hydrophobicity are thought to be advantageous for application in hernia repair. Following, clinical and histopathological results of the application of non-degradable PET and PET/C mats in the repair of incisional hernia are discussed.

6.3.1. Characterization of meshes

The morphology and properties of PET and PET/C meshes are described in chapter 4 and 5. DL mat is a composite mesh with one layer of PET and one layer of PET/C nanofibers. PET layer was thought to prevent formation of bowel adhesions while PET/C layer was designed to stimulate the integration of the mesh in the subcutaneous tissue, thus reinforcing the mechanical strength of the prosthetic wall. **Figure 6.3** displays a SEM picture of the transversal section of the DL mesh, evidencing PET (bottom) and PET/C (top) layers. The PET layer presents a more compact fiber organization when compared to the PET/C layer, confirming the lower porosity already discussed in chapter 5.

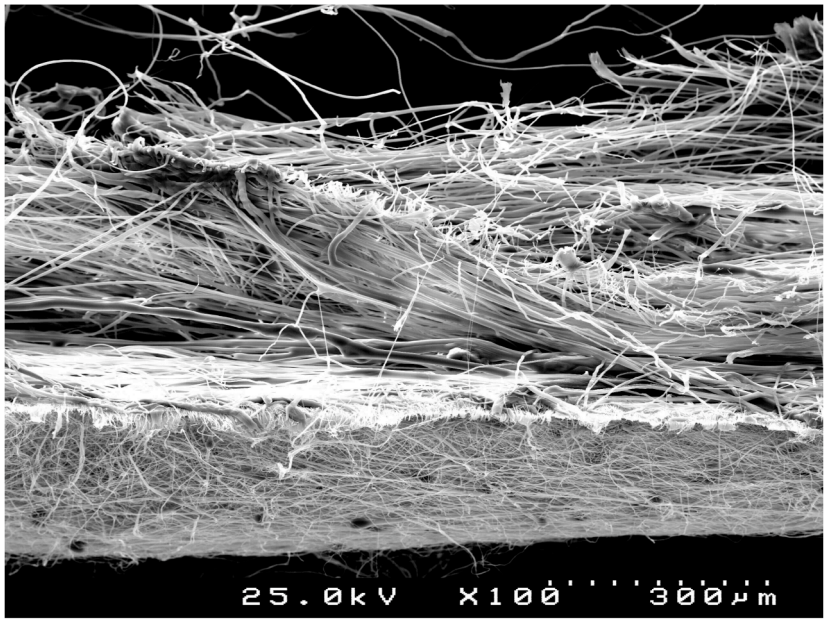

Figure 6.3. SEM image of a transversal section of DL mesh.

6.3.2. Surgical procedure and postoperative period

A pilot study was conducted in order to assess the feasibility of the experimental methodology. Originally, the defect was placed at the *alba linea* and the skin was closed by interrupted suture. High levels of skin closure failure from animal over-grooming were found (more than 50%, independently of the group). These problems were solved by dislocating the defect to the paramedian plane and performing an intradermal suture. This strategy was subsequently implemented on the final methodology.

Following the creation of the abdominal defect by resection of 1.5 x1.5 cm of the Wistar rats' abdominal muscle, the prosthetic meshes were implanted and fixed through the borders to the remaining muscle. The suture of the electrospun meshes was easily performed with no breakage occurrences. In fact, electrospun meshes were more suitable and more resistant to suture than the Marlex mesh used as the control, where an extra margin of around 5 mm was used to avoid breaking of filaments. Additionally, the stiffness of Marlex mesh may constantly damage the surrounding tissues, causing discomfort and pain to the patient. In fact, Marlex mesh is even perceived through the skin by touching. Electrospun meshes on the other hand, were much more soft, malleable, and adaptable. In

spite of it, these meshes performed well their role of containing visceral components and no cases of mesh rupture were found during the experimental period.

During the postoperative period some complications such as local inflammation, abscess, or skin dehiscence were registered. **Table 6.2** displays macroscopic complications found through the postoperative period. Local inflammation, characterized by redness or swelling, was the most common complication found, with higher incidence rates observed for PET/C and DL groups, occurring in 50% and 75% of the animals, respectively. Inflammation tended to decrease and many times to disappear with time, while abscess and skin dehiscence persisted until the end of the experimental period.

Table 6.2. Occurrence rate (%) of complications during postoperative period (PO)* and euthanize day (E).

	Marlex30		PET30		PET/C		DL		Woven PET	
	PO	**E**	**PO**	**E**	**PO**	**E**	**PO**	**E**	**PO**	**E**
Inflammation	37.5	12.5	37.5	25	50	0	75	37.5	0	0
Dehiscence	12.5	12.5	0	0	0	0	12.5	12.5	0	0
Serome or abscess	12.5	12.5	12.5	12.5	0	0	12.5	12.5	0	0
Adhesion	N.A.	omentum	N.A.	omentum	N.A.	omentum	N.A.	omentum	N.A.	omentum

* Complications were observed for at least 1 day of the PO;

N.A. Not available.

Unexpectedly, no visceral adhesions were found on the experimental groups. Omentum adhesions, on the other hand, were present in all animals. In contrast to bowel adhesions that can lead to serious complications, omentum adhesions are clinically irrelevant (Karabulut *et al.* 2006). In fact, some authors have even suggested the interposition of omentum between the prosthetic mesh and the viscera, which was shown to be effective in restricting bowel adhesions, both in pre-clinical and clinical studies (Karabulut *et al.* 2006; Bingener *et al.* 2004).

Figure 6.4 displays illustrative examples of skin dehiscence found on an animal of the Marlex group and an omentum adhesion to a PET mesh.

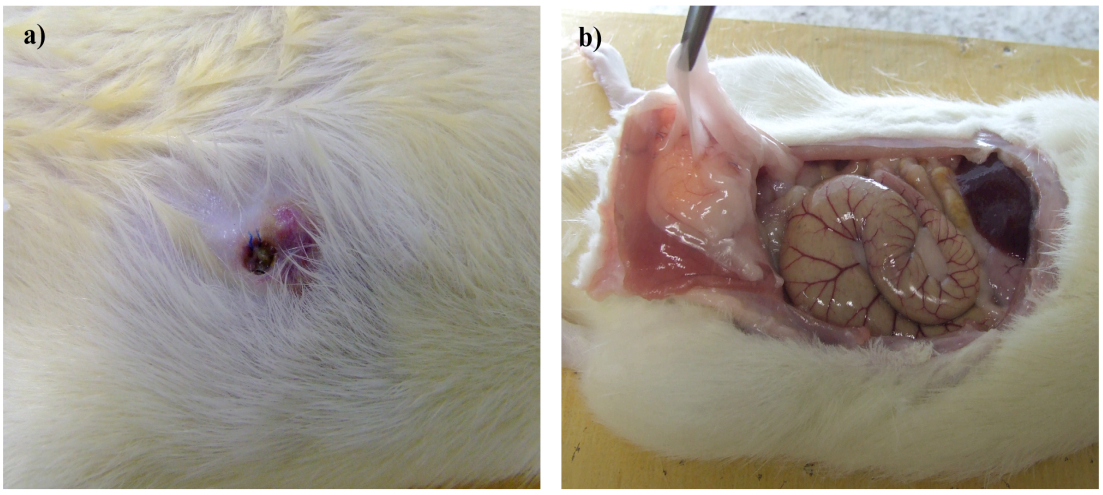

Figure 6.4. Examples of (a) skin dehiscence and (b) omentum adhesion to a PET mesh.

If, on the one hand, these results suggest the good potential of the electrospun mats in preventing intestinal adhesions, on the other hand they also lead us to question the feasibility of the experimental model. In the literature significant rates of intestinal adhesion to Marlex meshes are often reported (van't Riet *et al.* 2003; Menzies and Ellis 1990), either on animal or human, but in the present study no evidence of bowel adhesion was found. In fact, although rodent models are usually the first approach for testing abdominal meshes, several limitations are associated with this model, namely the huge difference on the size and abdominal tension between human and rats. Notwithstanding, rodent models are certainly an essential step of the pre-clinical trial of a biomaterial, providing significant information about the mechanisms underlying the success of hernia repair (DuBay *et al.* 2005; Ayubi *et al.* 2008; Macleod *et al.* 2005). The foreign body reaction to the prosthetic mesh, which will be discussed in the following subsection, is an important subject that can be extensively explored with this model.

6.3.3. Histopathological analysis

Tissues were collected and subjected to histological analysis to evaluate the inflammatory

response to the prosthetic biomaterials. All animals showed a typical non-immunogenic granuloma surrounding the mesh structure as illustrated in **Figure 6.5**. The mean thickness of the granuloma and the average number of FBGC are plotted in **Figure 6.6**.

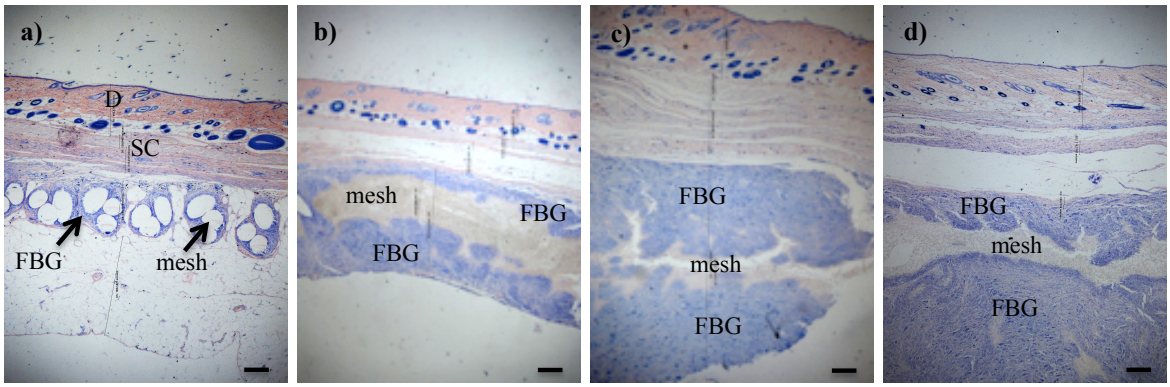

Figure 6.5. Histological sections evidencing the foreign body granuloma (Giemsa staining) of (a) Marlex30, (b) PET30, (c) PET/C, and (d) DL groups. (D) dermis, (SC) subcutaneous tissue, and (FBG) foreign body granuloma. Bar=220 μm.

Surprisingly large granulomas were found in animals treated with the electrospun meshes, compared to control, *i.e.* Marlex. In fact, the average size of PET granuloma was 4.2 times greater than control. This is an unexpected result since the chemical composition of the mesh is 100% PET, a high biocompatible polymer, as already mentioned. Moreover, the *in vitro* cytotoxicity assay and the *in vivo* wound healing assay demonstrated the high biocompatibility of the electrospun PET mat (see chapters 4 and 5).

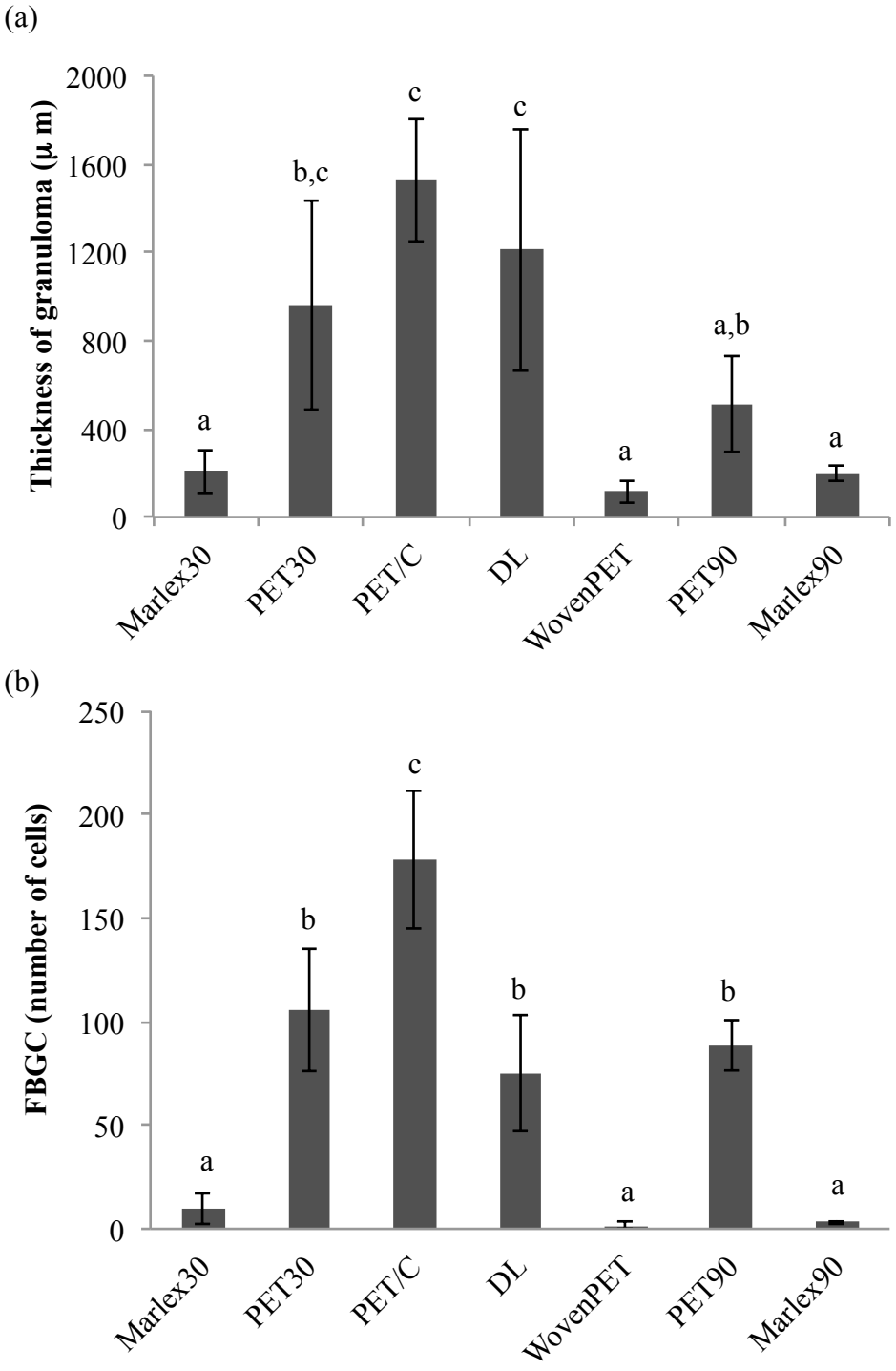

Figure 6.6. (a) Granuloma thickness and (b) number of FBGC surrounding the abdominal meshes. Different letters indicate significant differences (P<0.05).

Chitosan containing meshes, PET/C and DL, showed even larger granulomas (7.4 and 5.9 times greater than control, respectively). Despites the numerous reports of the anti-inflammatory and wound healing effects of chitosan, in this specific application chitosan had a negative impact and led to an increased inflammatory response. The foreign body granulomas were mostly composed of macrophages, FBGC, and fibroblasts. Huge amounts of FBGC were found in tissues surrounding the electrospun meshes, evidencing a typical foreign body reaction. For instance, PET and PET/C meshes showed, respectively, 11.5 and 19.3 times more FBGC than the control. Several illustrative examples of those multinucleated cells in tissues treated with different meshes are displayed in **Figure 6.7**. Interestingly, most of the times the FBGC were enclosing one or more nanofibers in an attempt to isolate the foreign material. Considering the high biocompatibility of PET in its bulk form, we hypothesize that, in some way, the nanodimension of the material elicited the huge foreign body reaction found in animals where the electrospun meshes had been implanted.

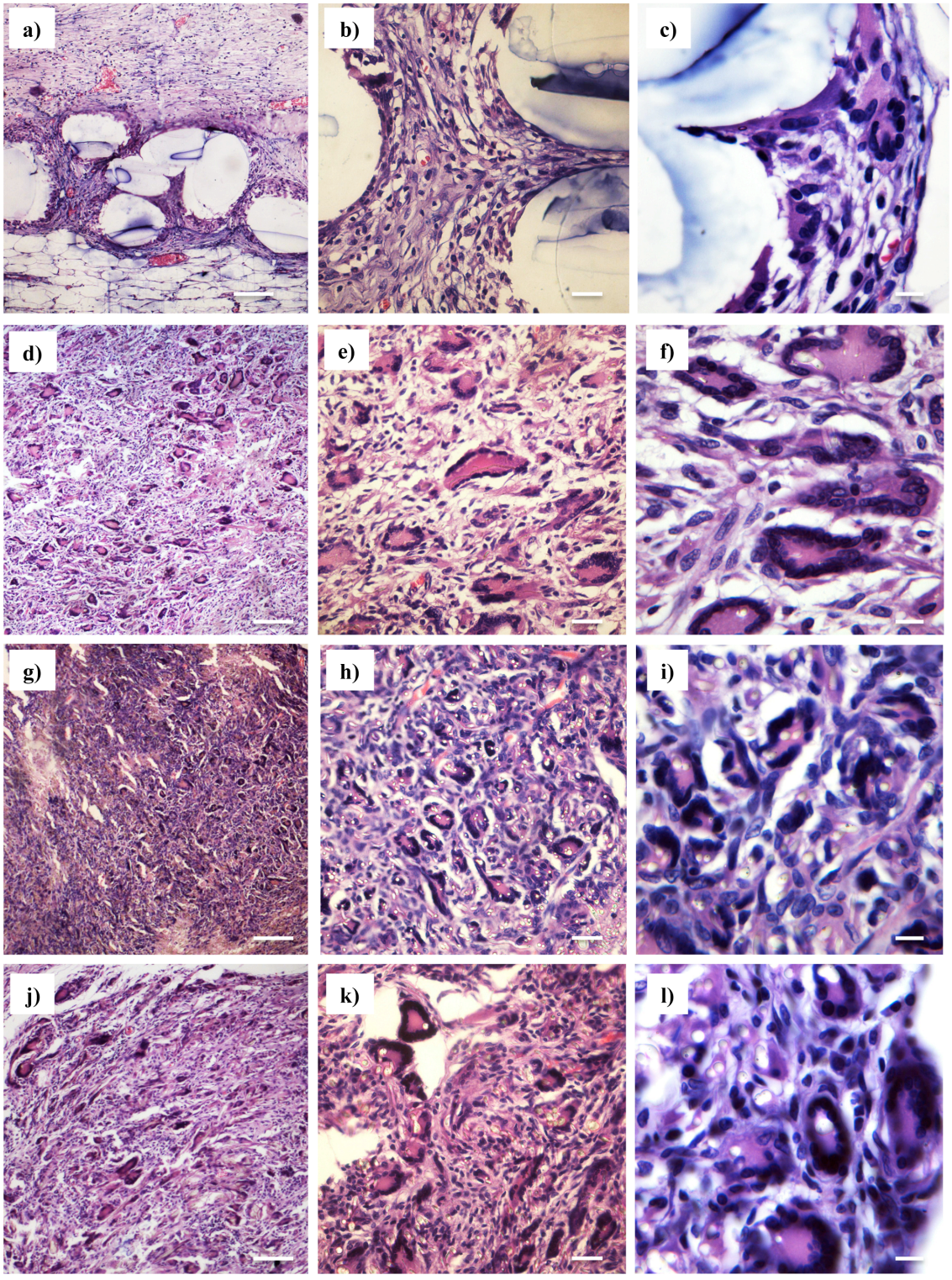

Figure 6.7. Representative examples of the foreign body reaction (HE staining) of (a- c) Marlex30, (d-f) PET30, (g- i) PET/C, and (j- l) DL groups. Bar = 100 μm (a, d, g, and j) = 25 μm (b, e, h, and k), and = 10 μm (c, f, i, and l).

Two main questions arose from this scenario: How does the foreign body reaction progress with time? Would the increase of filaments' diameter of PET mesh decrease the magnitude of the foreign body reaction? To answer the first question, PET and Marlex group were selected to perform an experiment with 90 days of duration (PET90 and Marlex90 groups). **Figure 6.8** displays illustrative examples of histological sections (HE staining) of Marlex90 and PET90 groups. The average granuloma thickness of PET group decreased from 959 ± 473 μm to 513 ± 217 μm and the number of FBGC decreased from 106 ± 30 to 89 ±12 (Figure 6.6). Although these differences were not statistically significant ($p>0.05$), the results obtained indicate some tendency for a decrease of the foreign body reaction with the time, probably due to a progress of the chronic inflammation, even thought there is still a large foreign body reaction persisting 90 days after the mesh implantation.

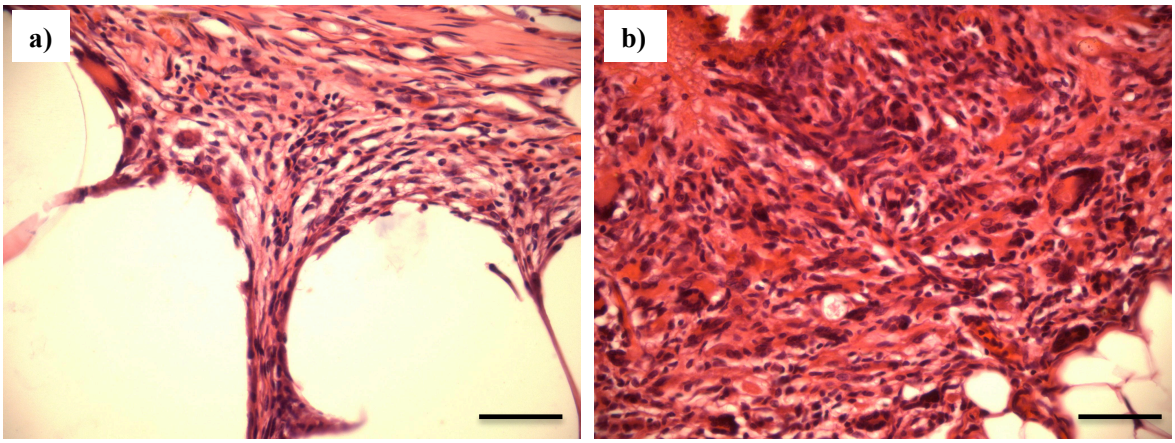

Figure 6.8. Representative examples of the foreign body reaction (HE staining) of (a) Marlex90 and (b) PET90. Bar = 50 μm.

Although, most of times, the foreign body reaction has few clinical implications and is limited to the close periphery of the implanted material, it is always a disadvantageous condition. Indeed, chronic inflammation has been assumed to underlie most of chronic diseases, including cancer, cardiovascular diseases, and diabetes, for example (Bartsch and Nair 2006; Manabe 2011).

In order to confirm the hypothesis that the large foreign body responses observed in the animals implanted with the electrospun meshes were related to the nanostructure of those materials, a new group implanted with a woven mesh of PET microfibers was included in the experiment (wovenPET group).

A minimum granulomatous reaction was observed in animals implanted with wovenPET mesh. In fact, this group exhibited an average granuloma thickness less than half of control and FBGC were rarely found (**Figure 6.9**). Furthermore, no complications were found during the postoperative period even though omentum adhesions were also observed Table 6.2).

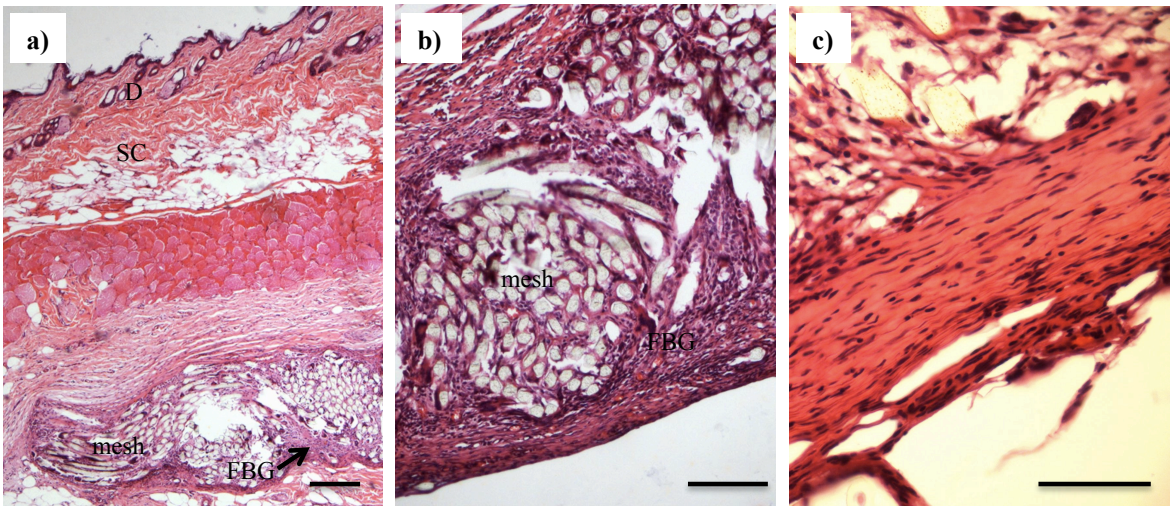

Figure 6.9. Representative examples at different magnification of the foreign body reaction observed on wovenPET group (HE staining). (D) dermis, (SC) subcutaneous tissue, and (FBG) foreign body granuloma. Bar = 200 μm (a), 100 μm (b), and 25 μm (c).

These results are consistent with our hypothesis that the huge foreign body reaction found is probably related to the nanostructure of the electrospun meshes. Considering this evidence, we point out three main factors that may have contributed to the exacerbated foreign body reaction found in animals implanted with electrospun mats:

(1) The high surface area to volume ratio of the electrospun materials;

(2) The extension of the trauma and the location of the lesion;

(3) The dimension of the nanofibers, which approximate the size of some microorganisms, *e.g.* bacteria.

It is well established that the properties of biomaterials such as size, chemical composition, surface properties, and architecture, as well as the specific characteristics of the tissue where the biomaterial is implanted, influence the foreign body response (Kamath *et al.*

2008; Hu *et al.* 2001). Among surface properties, the material ability to adsorb proteins plays a key role, as those proteins and not the material composition by itself constitute the major contributors for the foreign body reaction (Hu *et al.* 2001). Several authors have demonstrated that the increase of the biomaterial surface area promotes higher levels of protein adsorption. For instance, Shalumon *et al.* (2011) have demonstrated the increase of protein adsorption with the increase of surface area per volume ratio of PCL electrospun mats. In fact, decreasing the fiber diameter from a micrometric (10 μm) to a nanometric range (250 nm) doubled the amount of protein adsorbed on the material surface. A correlation between the material's surface area and the amount of protein adsorbed was also demonstrated for PLA nanofibrous scaffolds (Leong *et al.* 2009).

In addition, higher foreign body reactions are often found for biomaterials with greater surface areas (Voskerician *et al.* 2006; Sanchez *et al.* 2011). Specifically related to abdominal defect repairs, Conze *et al.* (2004) have verified a large foreign body reaction for a multifilament small diameter mesh of polypropylene. In fact, the diameter of the foreign body granuloma 90 days after the mesh placement, decreased from 106.5 μm to 70.9 μm by increasing the filament diameter from 0.6 mm to 2.5 mm.

Controversially, there are also reports showing a decrease of inflammatory response with the decrease of fiber diameter. For example, Saino *et al.* (2011) showed that the decrease of fiber diameter of electrospun PLA fibrous mats reduced the *in vitro* macrophage activation and the secretion of pro-inflammatory molecules. Likewise, a decrease of the granuloma thickness associated to subcutaneous PCL implants, from ~ 38 μm for a PCL film to ~ 8 μm or ~ 4 μm, for aligned or nonwoven electrospun nanofibers, respectively, was also reported (Cao *et al.* 2010).

The second aspect that may have influenced the large foreign body reaction found is related to the extension of the lesion caused and the specific characteristics of the tissues where the materials had been implanted. As described in chapter 4, the same PET electrospun mat was implanted on the skin of Wistar rats with a minimum foreign body reaction. The surgical procedure of the abdominal mesh implantation, however, involves the creation of a 1.5 x 1.5 cm defect by complete resection of the abdominal wall. This is a severe trauma if we consider the relative size of the animal and, consequently, a large inflammatory response may be induced. Furthermore, specific characteristics of the

implantation local such as cell composition and function, vascularization, ECM composition, and contact with ascitic fluid, for example, have also an important effect on the foreign body reaction.

The third point regards the mechanisms involved in the interaction between cells and nanostructures. Materials are becoming smaller than the basic body unity, *i.e.* the cell. How does that influence the cell-material interaction? Despite enormous progress of nanotechnology over the past decades, the risks involved in the use of nanostructure materials as biomaterials are still poorly understood (Soto *et al.* 2007; Stern and McNeil 2008). Indeed, few studies are found in the literature that evaluate the inflammatory and the immune response to nanofibrous materials. For instance, 5301 matches are obtained on the search for topics of "electrospinning or electrospun" and "bio*" in the scientific research platform (Thomson Reuters Web of Knowledge). Adding the field "foreign body reaction" only 5 matches are obtained. This evidence illustrates that further studies regarding this issue are required.

6.4. Concluding remarks and future work

Despites PET and PET/C electrospun meshes have demonstrated a good performance during the implantation surgery, adequate mechanical attributes, and no evidences of intestinal adhesion, a large foreign body reaction was also found. This was an unexpected and undesirable result, however several conclusions arose from the present study, including:

- The reduced dimension of nanofibers and the high surface area to volume ratio of electrospun nonwoven materials may induce a high foreign body reaction, depending on the extension and location of the lesion;
- Chitosan had a negative effect on the inflammation process resultant from the abdominal mesh implantation, as postoperative complications and foreign body reaction were increased in animals treated with chitosan containing meshes;
- There is a wide open field to investigate the mechanisms that govern the interaction between cells and nanomaterials and to comprehend the risks of nanostructured biomaterials implantation;

Although not a primary objective of this study, an interesting result was the potential use of woven PET meshes for incisional hernia repair. PET woven, a cost-effective material, showed a better performance as abdominal mesh than control, *i.e.* Marlex, and emerges as a new possibility for the incisional hernia treatment. Further studies to evaluate the potential of this material are required.

7.Concluding remarks and recommendations for future work

work

This thesis focuses on the development of new electrospun materials with application in tissue engineering. Two distinct polymer systems were explored: a biodegradable one based on poly(3-hydroxybutyrate-*co*-3-hydroxyvalerate and chitosan blends with application in skin engineering and a non-degradable with poly(ethylene terephthalate) as the structural polymer. Two distinct applications were explored for PET non-degradable materials: removable wound dressing membranes and prosthetic meshes for abdominal defect repair. During the course of this exploratory investigation several interesting results were achieved, but also, as expected, some difficulties were found.

The development of novel electrospun blends of PHBV and chitosan was the first important achievement. Several strategies to manipulate the morphology of these electrospun mats such as by varying the PHBV/C ratio, chitosan MW, or solvent composition were studied. These findings constitute an important tool to design a biomaterial with the required characteristics. In order to investigate cell-scaffold interactions, fibroblasts were selected as the cell model and viability, adhesion, spreading, proliferation, ECM secretion, and dead of these cells when cultured on the scaffolds were studied. The PHBV/C hybrid mats demonstrated ability to support fibroblast growth. In fact, fibroblasts adhered, spread over several nanofibers and secreted ECM components, forming a 2D confluent layer on the scaffolds. The PHBV/C ratio of 4:1 (w/w) showed a superior performance for fibroblasts growth, as higher levels of viability, adhesion, and spreading were found, in comparison to the ratio of 2:3 PHBV/C (w/w). In this scaffold with higher chitosan content, an increase in cell death by necrosis was found. *In vivo*, the PHBV/C 4:1 (w/w) hybrid scaffold has also demonstrated the best potential for promoting skin regeneration, decreasing the duration and extension of the inflammatory phase of the wound healing, with a consequent advance on the proliferative phase, and a higher level of tissue regeneration 21 days after injury.

A novel dual-fiber mat was successfully developed with the purpose of incorporating bioactive compounds into the hybrid PHBV/C electrospun mats, using an additional aqueous polymer solution of PVA/chitosan. Although only a slight modification on the biological performance of the scaffolds resulted from the plant extracts addition, the developed electrospinning configuration allowed an homogeneous distribution of the two kind of fibers within the mat and the successful incorporation of plant extracts from *Aloe*

barbadensis and *Ilex paraguariensis*, what can open new routes to prepare bioactive and functional polymer nanofibers. Notwithstanding, further studies are required to verify if the biological activities are preserved in the fibrous mats and to control the release profile of the bioactive compounds.

The second polymer system under studied was based on the synthetic non-degradable polyester, PET. Initial efforts have been carried out to develop a removable wound dressing material, based on known properties of electrospun PET mats (*e.g.* microporosity, hydrophobicity, and biocompatibility), potentially attractive for a wound dressing material. When tested *in vivo*, however, a strong affinity between the wound tissues and the PET mat was found, which seriously undermines the intended application. Although undesirable considering that specific application, results from this study opened new ways of application for PET electrospun mats, for example as a non-degradable scaffold for tissue engineering.

The development of PET based non-degradable scaffolds was the subsequent target and chitosan was added to the system in order to enhance biological properties and also as a tool to control scaffolds' morphology. Similarly to the PHBV/C hybrid system, we have studied the effect of PET/C ratio and chitosan MW on the final characteristics of the electrospun mats and also on their performance as scaffolds for tissue engineering. PET based scaffolds showed to be suitable for supporting cell growth and substantial differences were found as a result of scaffold morphological changes. Higher levels of adhesion, spreading, and superficial proliferation were achieved for PET scaffold due to its smaller fiber and pore sizes. Addition of chitosan allowed cell penetration and internal colonization (3D culture) through the increase of fiber diameter and pore area.

The study and application of PET and PET/C non-degradable scaffolds as prosthetic meshes for abdominal repair was another goal of this work. These electrospun materials have demonstrated a good performance during surgery, an adequate mechanical strength, and no evidences of intestinal adhesion throughout the postoperative period. However, these materials also elicited a significant inflammatory response when used in this specific application. In fact, PET nanofibers caused an enormous foreign body reaction that was not found for PET microfibers, pointing out for the need of further studies in order to investigate and comprehend the risks of the use of nanostructured biomaterials.

Recommendations for future work:

- ✓ Other biomedical applications for the PHBV/C scaffolds can be explored, for example: as support for grow and differentiation of stem cells, treatment of diabetic foot ulcers or other chronic wounds, scaffolds for the treatment of spinal cord lesions, among many others.
- ✓ The study regarding the dual-fiber system developed must be deepen in order to comprehend several aspects that have not been elucidated such as bioavailability and the bioactivity of the entrapped compounds, as well as their release profile *in vitro* and *in vivo*. This dual-fiber system can be used as a vehicle for incorporation not only of *A. barbadensis* and *I. paraguariensis* extracts, but also of other herbal or synthetic compounds.
- ✓ Despite the advantageous results obtained for the PET/C electrospun mats in cell culture experiments, *in vivo* studies to evaluate their biocompatibility are indispensable, especially considering the foreign body reaction observed for abdominal implantation.
- ✓ Deeper studies are needed in order to elucidate the mechanisms involved in the huge foreign body reaction observed with the abdominal implantation of the electrospun PET and PET/C mats. In fact, these results demonstrate that there is a wide open field to investigate the interactions between cells and non-degradable nanostructured biomaterials and comprehend the risks of their implantation.

References

Abdelrahman, T., and H. Newton. 2011. Wound dressings: principles and practice. 29 (10):491-495.

Alipour, S. M., M. Nouri, J. Mokhtari, and S. H. Bahrami. 2009. Electrospinning of poly(vinyl alcohol)-water-soluble quaternized chitosan derivative blend. *Carbohydrate Research* 344 (18):2496-2501.

Amiraliyan, N., M. Nouri, and M. H. Kish. 2009. Effects of Some Electrospinning Parameters on Morphology of Natural Silk-Based Nanofibers. *Journal of Applied Polymer Science* 113 (1):226-234.

Anderson, J. M., A. Rodriguez, and D. T. Chang. 2008. Foreign body reaction to biomaterials. *Seminars in Immunology* 20 (2):86-100.

Anthony, T., P. C. Bergen, L. T. Kim, M. Henderson, T. Fahey, R. V. Rege, and R. H. Turnage. 2000. Factors affecting recurrence following incisional herniorrhaphy. *World Journal of Surgery* 24 (1):95-101.

Aramwit, P., T. Siritientong, S. Kanokpanont, and T. Srichana. 2010. Formulation and characterization of silk sericin-PVA scaffold crosslinked with genipin. *International Journal of Biological Macromolecules* 47 (5):668-675.

Arbiser, J. L., X. C. Li, C. F. Hossain, D. G. Nagle, D. M. Smith, P. Miller, B. Govindarajan, J. DiCarlo, K. R. Landis-Piwowar, and Q. P. Dou. 2005. Naturally occurring proteasome inhibitors from mate tea (*Ilex paraguayensis*) serve as models for topical proteasome inhibitors. *Journal of Investigative Dermatology* 125 (2):207-212.

Atiba, A., H. Ueno, and Y. Uzuka. 2011. The effect of aloe vera oral administration on cutaneous wound healing in type 2 diabetic rats. *Journal of Veterinary Medical Science* 73 (5):583-589.

Avella, M., E. Martuscelli, and M. Raimo. 2000. Review - Properties of blends and composites based on poly(3-hydroxy)butyrate (PHB) and poly(3-hydroxybutyrate-hydroxyvalerate) (PHBV) copolymers. *Journal of Materials Science* 35 (3):523-545.

Ayubi, F. S., P. J. Armstrong, M. S. Mattia, and D. M. Parker. 2008. Abdominal wall hernia repair: a comparison of Permacol (R) and Surgisis (R) grafts in a rat hernia model. *Hernia* 12 (4):373-378.

Babensee, J. E., J. M. Anderson, L. V. McIntire, and A. G. Mikos. 1998. Host response to tissue engineered devices. *Advanced Drug Delivery Reviews* 33 (1-2):111-139.

Badami, A. S., M. R. Kreke, M. S. Thompson, J. S. Riffle, and A. S. Goldstein. 2006. Effect of fiber diameter on spreading, proliferation, and differentiation of osteoblastic cells on electrospun poly(lactic acid) substrates. *Biomaterials* 27 (4):596-606.

Baptista, M. L., M. E. Bonsack, I. Felemovicius, and J. P. Delaney. 2000. Abdominal adhesions to prosthetic mesh evaluated by laparoscopy and electron microscopy. *Journal of the American College of Surgeons* 190 (3):271-280.

Barnes, C. P., S. A. Sell, E. D. Boland, D. G. Simpson, and G. L. Bowlin. 2007. Nanofiber technology: Designing the next generation of tissue engineering scaffolds. *Advanced Drug Delivery Reviews* 59 (14):1413-1433.

Bartsch, H., and J. Nair. 2006. Chronic inflammation and oxidative stress in the genesis and perpetuation of cancer: role of lipid peroxidation, DNA damage, and repair. *Langenbecks Archives of Surgery* 391 (5):499-510.

Bashur, C. A., L. A. Dahlgren, and A. S. Goldstein. 2006. Effect of fiber diameter and orientation on fibroblast morphology and proliferation on electrospun poly(d,l-lactic-co-glycolic acid) meshes. *Biomaterials* 27 (33):5681-5688.

Bastos, D. H. M., A. C. Fornari, Y. S. Queiroz, and E. A. F. S. Torres. 2006. Bioactive compounds content of chimarrão infusions related to the moisture of yerba maté (*Ilex paraguariensis*) leaves. *Brazilian Archives of Biology and Technology* 49 (3):399-404.

Bellon, J. M., L. A. Contreras, J. Bujan, and A. C. S. Martin. 1996. Experimental assay of a Dual Mesh(R) polytetrafluoroethylene prosthesis (non-porous on one side) in the repair of abdominal wall defects. *Biomaterials* 17 (24):2367-2372.

Bingener, J., G. B. Kazantsev, S. Chopra, and W. H. Schwesinger. 2004. Adhesion formation after laparoscopic ventral incisional hernia repair with polypropylene mesh: a study using abdominal ultrasound. *JSLS : Journal of the Society of Laparoendoscopic Surgeons / Society of Laparoendoscopic Surgeons* 8 (2):127-131.

Blackwood, K. A., R. McKean, I. Canton, C. O. Freeman, K. L. Franklin, D. Cole, I. Brook, P. Farthing, S. Rimmer, J. W. Haycock, A. J. Ryan, and S. MacNeil. 2008. Development of biodegradable electrospun scaffolds for dermal replacement. *Biomaterials* 29 (21):3091-3104.

Blanchemain, N., S. Haulon, B. Martel, M. Traisnel, M. Morcellet, and H. F. Hildebrand. 2005. Vascular PET prostheses surface modification with cyclodextrin coating: development of a new drug delivery system. *European Journal of Vascular and Endovascular Surgery* 29 (6):628-632.

Boretos, J. W., and M. Eden. 1984. *Contemporary biomaterials: material and host response, clinical applications, new technology, and legal aspects*: Noyes Publications.

Bothin, C., T. Midtvedt, and L. Perbeck. 2003. Orally delivered antibiotics which lower bacterial numbers decrease experimental intra-abdominal adhesions. *Langenbecks Archives of Surgery* 388 (2):112-115.

Boudreau, N., and M. J. Bissell. 1998. Extracellular matrix signaling: integration of form and function in normal and malignant cells. *Current Opinion in Cell Biology* 10 (5):640-646.

Bowers, S. L. K., I. Banerjee, and T. A. Baudino. 2010. The extracellular matrix: At the center of it all. *Journal of Molecular and Cellular Cardiology* 48 (3):474-482.

Brown, N. H. 2000. Cell-cell adhesion via the ECM: integrin genetics in fly and worm. *Matrix Biology* 19 (3):191-201.

Cai, Z. X., X.-M. Mo, K.-H. Zhang, L.-P. Fan, A.-L. Yin, C.-L. He, and H.-S. Wang. 2010. Fabrication of chitosan/silk fibroin composite nanofibers for wound-dressing applications. *International Journal of Molecular Science* 11: 3529-3539.

Cao, H., K. McHugh, S. Y. Chew, and J. M. Anderson. 2010. The topographical effect of electrospun nanofibrous scaffolds on the *in vivo* and *in vitro* foreign body reaction. *Journal of Biomedical Materials Research Part A* 93A (3):1151-1159.

Carbajo, M. A., J. C. M. del Olmo, J. I. Blanco, C. de la Cuesta, M. Toledano, F. Martin, C. Vaquero, and L. Inglada. 1999. Laparoscopic treatment vs open surgery in the solution of major incisional and abdominal wall hernias with mesh. *Surgical Endoscopy-Ultrasound and Interventional Techniques* 13 (3):250-252.

Casper, C. L., J. S. Stephens, N. G. Tassi, D. B. Chase, and J. F. Rabolt. 2004. Controlling surface morphology of electrospun polystyrene fibers: Effect of humidity and molecular weight in the electrospinning process. *Macromolecules* 37 (2):573-578.

Casper, C. L., N. Yamaguchi, K. L. Kiick, and J. F. Rabolt. 2005. Functionalizing electrospun fibers with biologically relevant macromolecules. *Biomacromolecules* 6 (4):1998-2007.

Chan, C. H., C. Kummerlowe, and H. W. Kammer. 2004. Crystallization and melting behavior of poly (3-hydroxybutyrate)-based blends. *Macromolecular Chemistry and Physics* 205 (5):664-675.

Chen, C. S., M. Mrksich, S. Huang, G. M. Whitesides, and D. E. Ingber. 1997. Geometric control of cell life and death. *Science* 276 (5317):1425-1428.

Chen, G. Q., and Q. Wu. 2005. The application of polyhydroxyalkanoates as tissue engineering materials. *Biomaterials* 26 (33):6565-6578.

Chen, J.-P., G.-Y. Chang, and J.-K. Chen. 2008. Electrospun collagen/chitosan nanofibrous membrane as wound dressing. *Colloids and Surfaces a-Physicochemical and Engineering Aspects* 313:183-188.

Chen, J. P., G. Y. Chang, and J. K. Chen. 2006. Electrospun collagen/chitosan nanofibrous membrane as wound dressing. Paper read at Asian Conference on Nanoscience and Nanotechnology (AsiaNANO 2006), Nov 01-04, at Busan, South Korea.

Chen, P., Q.-S. Wu, Y.-P. Ding, M. Chu, Z.-M. Huang, and W. Hue. 2010. A controlled release system of titanocene dichloride by electrospun fiber and its antitumor activity *in vitro*. *European Journal of Pharmaceutics and Biopharmaceutics* 76 (3):413-420.

Chen, Y., G. Yang, and Q. Chen. 2002. Solid-state NMR study on the structure and mobility of the noncrystalline region of poly(3-hydroxybutyrate) and poly(3-hydroxybutyrate-co-3-hydroxyvalerate). *Polymer* 43 (7):2095-2099.

Chithra, P., G. B. Sajithlal, and G. Chandrakasan. 1998. Influence of Aloe vera on the glycosaminoglycans in the matrix of healing dermal wounds in rats. *Journal of Ethnopharmacology* 59 (3):179-186.

Choi, J. S., K. W. Leong, and H. S. Yoo. 2008. *In vivo* wound healing of diabetic ulcers using electrospun nanofibers immobilized with human epidermal growth factor (EGF). *Biomaterials* 29 (5):587-596.

Choi, S., and M. H. Chung. 2003. A review on the relationship between aloe vera components and their biologic effects. *Seminars in Integrative Medicine* 1 (1):53-62.

Choi, S. W., B. W. Son, Y. S. Son, Y. I. Park, S. K. Lee, and M. H. Chung. 2001. The wound-healing effect of a glycoprotein fraction isolated from aloe vera. *British Journal of Dermatology* 145 (4):535-545.

Chong, E. J., T. T. Phan, I. J. Lim, Y. Z. Zhang, B. H. Bay, S. Ramakrishna, and C. T. Lim. 2007. Evaluation of electrospun PCL/gelatin nanofibrous scaffold for wound healing and layered dermal reconstitution. *Acta Biomaterialia* 3 (3):321-330.

Chu, D. I., R. Lim, S. Heydrick, M. L. Gainsbury, R. Abdou, L. D'Addese, K. L. Reed, A. F. Stucchi, and J. M. Becker. 2011. N-acetyl-L-cysteine decreases intra-abdominal adhesion formation through the upregulation of peritoneal fibrinolytic activity and antioxidant defenses. *Surgery* 149 (6):801-812.

Chuangchote, S., T. Sagawa, and S. Yoshikawa. 2009. Electrospinning of poly(vinyl pyrrolidone): Effects of solvents on electrospinnability for the fabrication of poly(p-phenylene vinylene) and TiO(2) nanofibers. *Journal of Applied Polymer Science* 114 (5):2777-2791.

Conze, J., R. Rosch, U. Klinge, C. Weiss, M. Anurov, S. Titkowa, A. Oettinger, and V. Schumpelick. 2004. Polypropylene in the intra-abdominal position: influence of pore size and surface area. *Hernia : the journal of hernias and abdominal wall surgery* 8 (4):365-372.

Davis, R. H., J. J. Donato, G. M. Hartman, and R. C. Haas. 1994. Anti-inflammatory and wound healing activity of a growth substance in Aloe vera. *Journal of the American Podiatric Medical Association* 84 (2):77-81.

DeRuiter, M. C., R. E. Poelmann, M. M. T. Mentink, L. Vaniperen, and A. C. Gittenberger-De Groot. 1993. Early formation of the vascular system in quail embryos. *Anatomical Record* 235 (2):261-274.

Duan, B., C. H. Dong, X. Y. Yuan, and K. D. Yao. 2004. Electrospinning of chitosan solutions in acetic acid with poly(ethylene oxide). *Journal of Biomaterials Science-Polymer Edition* 15 (6):797-811.

Duan, B., L. Wu, X. Li, X. Yuan, X. Li, Y. Zhang, and K. Yao. 2007. Degradation of electrospun PLGA-chitosan/PVA membranes and their cytocompatibility *in vitro*. *Journal of Biomaterials Science-Polymer Edition* 18 (1):95-115.

DuBay, D. A., X. Wang, B. Adamson, W. M. Kuzon, R. G. Dennis, and M. G. Franz. 2005. Progressive fascial wound failure impairs subsequent abdominal wall repairs: A new animal model of incisional hernia formation. *Surgery* 137 (4):463-471.

Femenia, A., E. S. Sanchez, S. Simal, and C. Rossello. 1999. Compositional features of polysaccharides from Aloe vera (Aloe barbadensis Miller) plant tissues. *Carbohydrate Polymers* 39 (2):109-117.

Folkman, J. 1971. Tumor angiogenesis: therapeutic implications. *New England Journal of Medicine* 285 (21):1182-1186.

Fonder, M. A., G. S. Lazarus, D. A. Cowan, B. Aronson-Cook, A. R. Kohli, and A. J. Mamelak. 2008. Treating the chronic wound: A practical approach to the care of nonhealing wounds and wound care dressings. *Journal of the American Academy of Dermatology* 58 (2):185-206.

Formhals, A. 1934. Process and apparatus for preparing artificial threads, edited by U. S. P. a. T. Office.

Galiano, R. D., O. M. Tepper, C. R. Pelo, K. A. Bhatt, M. Callaghan, N. Bastidas, S. Bunting, H. G. Steinmetz, and G. C. Gurtner. 2004. Topical vascular endothelial growth factor accelerates diabetic wound healing through increased angiogenesis and by mobilizing and recruiting bone marrow-derived cells. *American Journal of Pathology* 164 (6):1935-1947.

Gao, C., Q. Gao, Y. Li, M. N. Rahaman, A. Teramoto, and K. Abe. 2012. Preparation and *in vitro* characterization of electrospun PVA scaffolds coated with bioactive glass for bone regeneration. *Journal of biomedical materials research. Part A* 100 (5):1324-1334.

Gecim, I. E., S. Kocak, S. Ersoz, C. Bumin, and D. Aribal. 1996. Recurrence after incisional hernia repair: Results and risk factors. *Surgery Today-the Japanese Journal of Surgery* 26 (8):607-609.

Geng, X. Y., O. H. Kwon, and J. H. Jang. 2005. Electrospinning of chitosan dissolved in concentrated acetic acid solution. *Biomaterials* 26 (27):5427-5432.

Gentsch, R., F. Pippig, S. Schmidt, P. Cernoch, J. Polleux, and H. G. Boerner. 2011. Single-step electrospinning to bioactive polymer nanofibers. *Macromolecules* 44 (3):453-461.

Gopal, R., S. Kaur, Z. W. Ma, C. Chan, S. Ramakrishna, and T. Matsuura. 2006. Electrospun nanofibrous filtration membrane. *Journal of Membrane Science* 281 (1-2):581-586.

Gorzalczany, S., R. Filip, M. D. R. Alonso, J. Miño, G. E. Ferraro, and C. Acevedo. 2001. Choleretic effect and intestinal propulsion of 'mate' (*Ilex paraguariensis*) and its substitutes or adulterants. *Journal of Ethnopharmacology* 75 (2-3):291-294.

Grafahrend, D., J. L. Calvet, K. Klinkhammer, J. Salber, P. D. Dalton, M. Moeller, and D. Klee. 2008. Control of protein adsorption on functionalized electrospun fibers. *Biotechnology and Bioengineering* 101 (3):609-621.

Gugliucci, A. 1996. Antioxidant effects of Ilex paraguariensis: Induction of decreased oxidability of human LDL *in vivo*. *Biochemical and Biophysical Research Communications* 224 (2):338-344.

Gupta, A., R. Kumar, N. K. Upadhyay, P. Surekha, and P. K. Roy. 2009. Synthesis, Characterization and efficacy of chemically crosslinked PVA hydrogels for dermal wound healing in experimental animals. *Journal of Applied Polymer Science* 111 (3):1400-1408.

Gupta, K. C., and F. H. Jabrail. 2007. Glutaraldehyde cross-linked chitosan microspheres for controlled release of centchroman. *Carbohydrate Research* 342 (15):2244-2252.

Han, I., K. J. Shim, J. Y. Kim, S. U. Im, Y. K. Sung, M. Kim, I.-K. Kang, and J. C. Kim. 2007. Effect of poly(3-hydroxybutyrate-co-3-hydroxyvalerate) nanofiber matrices cocultured with hair follicular epithelial and dermal cells for biological wound dressing. *Artificial Organs* 31 (11):801-808.

Han, S. O., W. K. Son, J. H. Youk, T. S. Lee, and W. H. Park. 2005. Ultrafine porous fibers electrospun from cellulose triacetate. *Materials Letters* 59 (24-25):2998-3001.

Hong, K. H. 2007. Preparation and properties of electrospun poly (vinyl alcohol)/silver fiber web as wound dressings. *Polymer Engineering and Science* 47 (1):43-49.

Hong, K. H., and T. J. Kang. 2006. Hydraulic permeabilities of PET and nylon 6 electrospun fiber webs. *Journal of Applied Polymer Science* 100 (1):167-177.

Hsu, C. M., and S. Shivkumar. 2004. Nano-sized beads and porous fiber constructs of poly(epsilon-caprolactone) produced by electrospinning. *Journal of Materials Science* 39 (9):3003-3013.

Hu, S. G., C. H. Jou, and M. C. Yang. 2003a. Antibacterial and biodegradable properties of polyhydroxyalkanoates grafted with chitosan and chitooligosaccharides via ozone treatment. *Journal of Applied Polymer Science* 88 (12):2797-2803.

Hu, S. G., C. H. Jou, and M. C. Yang. 2003b. Protein adsorption, fibroblast activity and antibacterial properties of poly(3-hydroxybutyric acid-co-3-hydroxyvaleric acid) grafted with chitosan and chitooligosaccharide after immobilized with hyaluronic acid. *Biomaterials* 24 (16):2685-2693.

Hu, W. J., J. W. Eaton, and L. P. Tang. 2001. Molecular basis of biomaterial-mediated foreign body reactions. *Blood* 98 (4):1231-1238.

Hu, Y.-L., W. Qi, F. Han, J.-Z. Shao, and J.-Q. Gao. 2011. Toxicity evaluation of biodegradable chitosan nanoparticles using a zebrafish embryo model. *International Journal of Nanomedicine* 6:3351-3359.

Huss, F. R. M., E. Nyman, J. S. C. Bolin, and G. Kratz. 2010. Use of macroporous gelatine spheres as a biodegradable scaffold for guided tissue regeneration of healthy dermis in humans: An *in vivo* study. *Journal of Plastic, Reconstructive & Aesthetic Surgery* 63 (5):848-857.

Iannace, S., G. Sabatini, L. Ambrosio, and L. Nicolais. 1995. Mechanical behaviour of composite artificial tendons and ligaments. *Biomaterials* 16 (9):675-680.

Ignatova, M., N. Manolova, N. Markova, and I. Rashkov. 2009. Electrospun non-woven nanofibrous hybrid mats based on chitosan and pla for wound-dressing applications. *Macromolecular Bioscience* 9 (1):102-111.

Jansen, E. J. P., R. E. J. Sladek, H. Bahar, A. Yaffe, M. J. Gijbels, R. Kuijer, S. K. Bulstra, N. A. Guldemond, I. Binderman, and L. H. Koole. 2005. Hydrophobicity as a design criterion for polymer scaffolds in bone tissue engineering. *Biomaterials* 26 (21):4423-4431.

Jettanacheawchankit, S., S. Sasithanasate, P. Sangvanich, W. Banlunara, and P. Thunyakitpisal. 2009. Acemannan stimulates gingival fibroblast proliferation; expressions of keratinocyte growth factor-1, vascular endothelial growth factor, and type I collagen; and wound healing. *Journal of Pharmacological Sciences* 109 (4):525-531.

Jin, H. J., S. V. Fridrikh, G. C. Rutledge, and D. L. Kaplan. 2002. Electrospinning *Bombyx mori* silk with poly(ethylene oxide). *Biomacromolecules* 3 (6):1233-1239.

Jung, K.-H., M.-W. Huh, W. Meng, J. Yuan, S. H. Hyun, J.-S. Bae, S. M. Hudson, and I.-K. Kang. 2007. Preparation and antibacterial activity of PET/chitosan nanofibrous mats using an electrospinning technique. *Journal of Applied Polymer Science* 105 (5):2816-2823.

Junqueira, L. C., and J. Carneiro. 2005. *Basic Histology: Text & Atlas*: McGraw-Hill.

Kamath, S., D. Bhattacharyya, C. Padukudru, R. B. Timmons, and L. Tang. 2008. Surface chemistry influences implant-mediated host tissue responses. *Journal of Biomedical Materials Research Part A* 86A (3):617-626.

Karabulut, B., K. Sonmez, Z. Turkyilmaz, B. Demirogullari, R. Karabulut, C. Sezer, N. Sultan, A. C. Basaklar, and N. Kale. 2006. Omentum prevents intestinal adhesions to mesh graft in abdominal infections and serosal defects. *Surgical Endoscopy and Other Interventional Techniques* 20 (6):978-982.

Karim, M. R., and M. S. Islam. 2011. Thermal behavior with mechanical property of fluorinated silane functionalized superhydrophobic pullulan/poly(vinyl alcohol) blends by electrospinning method. *Journal of Nanomaterials*.

Kasaai, M. R., J. Arul, and C. Charlet. 2000. Intrinsic viscosity-molecular weight relationship for chitosan. *Journal of Polymer Science Part B-Polymer Physics* 38 (19):2591-2598.

Kasten, P., I. Beyen, P. Niemeyer, R. Luginb¸hl, M. Bohner, and W. Richter. 2008. Porosity and pore size of [beta]-tricalcium phosphate scaffold can influence protein production and osteogenic differentiation of human mesenchymal stem cells: An *in vitro* and *in vivo* study. *Acta Biomaterialia* 4 (6):1904-1915.

Katti, D. S., K. W. Robinson, F. K. Ko, and C. T. Laurencin. 2004. Bioresorbable nanofiber-based systems for wound healing and drug delivery: Optimization of fabrication parameters. *Journal of Biomedical Materials Research Part B-Applied Biomaterials* 70B (2):286-296.

Kenawy, E. R., G. L. Bowlin, K. Mansfield, J. Layman, D. G. Simpson, E. H. Sanders, and G. E. Wnek. 2002. Release of tetracycline hydrochloride from electrospun poly(ethylene-co-vinylacetate), poly(lactic acid), and a blend. *Journal of Controlled Release* 81 (1-2):57-64.

Khil, M. S., S. R. Bhattarai, H. Y. Kim, S. Z. Kim, and K. H. Lee. 2005. Novel fabricated matrix via electrospinning for tissue engineering. *Journal of Biomedical Materials Research Part B-Applied Biomaterials* 72B (1):117-124.

Khil, M. S., D. I. Cha, H. Y. Kim, I. S. Kim, and N. Bhattarai. 2003. Electrospun nanofibrous polyurethane membrane as wound dressing. *Journal of Biomedical Materials Research Part B-Applied Biomaterials* 67B (2):675-679.

Kim, S.-S., M. Sun Park, O. Jeon, C. Yong Choi, and B.-S. Kim. 2006. Poly(lactide-co-glycolide)/hydroxyapatite composite scaffolds for bone tissue engineering. *Biomaterials* 27 (8):1399-1409.

Kim, T. G., and T. G. Park. 2006. Biomimicking extracellular matrix: Cell adhesive RGD peptide modified electrospun poly(D,L-lactic-Co-glycolic acid) nanofiber mesh. *Tissue Engineering* 12 (2):221-233.

Kingsnorth, A., and K. LeBlanc. 2003. Hernias: inguinal and incisional. *Lancet* 362 (9395):1561-1571.

Klein, S. A., S. J. Bond, S. C. Gupta, O. A. Yacoub, and G. L. Anderson. 1999. Angiogenesis inhibitor TNP-470 inhibits murine cutaneous wound healing. *Journal of Surgical Research* 82 (2):268-274.

Klosterhalfen, B., U. Klinge, and V. Schumpelick. 1998. Functional and morphological evaluation of different polypropylene-mesh modifications for abdominal wall repair. *Biomaterials* 19 (24):2235-2246.

Koski, A., K. Yim, and S. Shivkumar. 2004. Effect of molecular weight on fibrous PVA produced by electrospinning. *Materials Letters* 58 (3-4):493-497.

Kumbar, S. G., R. James, S. P. Nukavarapu, and C. T. Laurencin. 2008. Electrospun nanofiber scaffolds: engineering soft tissues. *Biomedical Materials* 3 (3).

Kuppan, P., K. S. Vasanthan, D. Sundaramurthi, U. M. Krishnan, and S. Sethuraman. 2011. Development of poly(3-hydroxybutyrate-co-3-hydroxyvalerate) fibers for skin tissue engineering: effects of topography, mechanical, and chemical stimuli. *Biomacromolecules* 12 (9):3156-3165.

Kurosaka, M., T. Suzuki, K. Hosono, Y. Kamata, A. Fukamizu, H. Kitasato, Y. Fujita, and M. Majima. 2009. Reduced angiogenesis and delay in wound healing in angiotensin II type 1a receptor-deficient mice. *Biomedicine & Pharmacotherapy* 63 (9):627-634.

Lee, I. S., O. H. Kwon, W. Meng, and I. K. Kang. 2004. Nanofabrication of microbial polyester by electrospinning promotes cell attachment. *Macromolecular Research* 12 (4):374-378.

Lee, J. J., S.-G. Lee, J. C. Park, Y. I. Yang, and J. K. Kim. 2007. Investigation on biodegradable PLGA scaffold with various pore size structure for skin tissue engineering. *Current Applied Physics* 7 (Supplement 1):e37-e40.

Leong, M. F., K. S. Chian, P. S. Mhaisalkar, W. F. Ong, and B. D. Ratner. 2009. Effect of electrospun poly(D,L-lactide) fibrous scaffold with nanoporous surface on attachment of porcine esophageal epithelial cells and protein adsorption. *Journal of Biomedical Materials Research Part A* 89A (4):1040-1048.

Li, D., Y. L. Wang, and Y. N. Xia. 2003. Electrospinning of polymeric and ceramic nanofibers as uniaxially aligned arrays. *Nano Letters* 3 (8):1167-1171.

Li, D., and Y. N. Xia. 2004. Direct fabrication of composite and ceramic hollow nanofibers by electrospinning. *Nano Letters* 4 (5):933-938.

Li, L., and Y. L. Hsieh. 2006. Chitosan bicomponent nanofibers and nanoporous fibers. *Carbohydrate Research* 341 (3):374-381.

Li, X., K. L. Liu, M. Wang, S. Y. Wong, W. C. Tjiu, C. Bin He, S. H. Goh, and J. Li. 2009. Improving hydrophilicity, mechanical properties and biocompatibility of poly (R)-3-hydroxybutyrate-co-(R)-3-hydroxyvalerate through blending with poly (R)-3-hydroxybutyrate -alt-poly(ethylene oxide). *Acta Biomaterialia* 5 (6):2002-2012.

Li, X., J. Xie, X. Yuan, and Y. Xia. 2008. Coating Electrospun Poly(epsilon-caprolactone) Fibers with Gelatin and Calcium Phosphate and Their Use as Biomimetic Scaffolds for Bone Tissue Engineering. *Langmuir* 24 (24):14145-14150.

Lin, T., J. Fang, H. Wang, T. Cheng, and X. Wang. 2006a. Using chitosan as a thickener for electrospinning dilute PVA solutions to improve fibre uniformity. *Nanotechnology* 17 (15):3718-3723.

Liu, X. F., Y. L. Guan, D. Z. Yang, Z. Li, and K. Yao. 2001. Antibacterial action of chitosan and carboxymethylated chitosan, Journal of Applied Polymer Science 79:1324-1335.

Liu, X., L. Ma, Z. Mao, and C. Gao. 2011. Chitosan-based biomaterials for tissue repair and regeneration. In *Chitosan for Biomaterials Ii*, edited by R. P. M. M. R. A. A. Jayakumar, 81-127.

Liu, Y., J. Chen, V. Misoska, and G. G. Wallace. 2007. Preparation of novel ultrafine fibers based on DNA and poly(ethylene oxide) by electrospinning from aqueous solutions. *Reactive and Functional Polymers* 67 (5):461-467.

Loh, J. W., G. Yeoh, M. Saunders, and L.-Y. Lim. 2010. Uptake and cytotoxicity of chitosan nanoparticles in human liver cells. *Toxicology and Applied Pharmacology* 249 (2):148-157.

Lopes-da-Silva, J. A., B. Veleirinho, and I. Delgadillo. 2009. Preparation and characterization of electrospun mats made of pet/chitosan hybrid nanofibers. *Journal of Nanoscience and Nanotechnology* 9 (6):3798-3804.

Lowery, J. L., N. Datta, and G. C. Rutledge. 2010. Effect of fiber diameter, pore size and seeding method on growth of human dermal fibroblasts in electrospun poly(epsilon-caprolactone) fibrous mats. *Biomaterials* 31 (3):491-504.

Lu, Q. J., A. Simionescu, and N. Vyavahare. 2005. Novel capillary channel fiber scaffolds for guided tissue engineering. *Acta Biomaterialia* 1 (6):607-614.

Lubiatowski, P., J. Kruczynski, A. Gradys, T. Trzeciak, and J. Jaroszewski. 2006. Articular Cartilage Repair by Means of Biodegradable Scaffolds. *Transplantation Proceedings* 38 (1):320-322.

Luijendijk, R. W., W. C. J. Hop, P. van den Tol, D. C. D. de Lange, M. M. J. Braaksma, J. N. M. Ijzermans, R. U. Boelhouwer, B. C. de Vries, M. K. M. Salu, J. C. J. Wereldsma, C. M. A. Bruijninckx, and J. Jeekel. 2000. A comparison of suture repair with mesh repair for incisional hernia. *New England Journal of Medicine* 343 (6):392-398.

Lukashev, M. E., and Z. Werb. 1998. ECM signalling: orchestrating cell behaviour and misbehaviour. *Trends in Cell Biology* 8 (11):437-441.

Lunceford, N., and A. Gugliucci. 2005. Ilex paraguariensis extracts inhibit AGE formation more efficiently than green tea. *Fitoterapia* 76 (5):419-427.

Ma, L., C. Y. Gao, Z. W. Mao, J. Zhou, J. C. Shen, X. Q. Hu, and C. M. Han. 2003. Collagen/chitosan porous scaffolds with improved biostability for skin tissue engineering. *Biomaterials* 24 (26):4833-4841.

Ma, Z., M. Kotaki, T. Yong, W. He, and S. Ramakrishna. 2005a. Surface engineering of electrospun polyethylene terephthalate (PET) nanofibers towards development of a new material for blood vessel engineering. *Biomaterials* 26 (15):2527-2536.

Macleod, T. M., G. Williams, R. Sanders, and C. J. Green. 2005. Histological evaluation of Permacol (TM) as a subcutaneous implant over a 20-week period in the rat model. *British Journal of Plastic Surgery* 58 (4):518-532.

Manabe, I. 2011. Chronic Inflammation Links Cardiovascular, Metabolic and Renal Diseases. *Circulation Journal* 75 (12):2739-2748.

Mao, N., and S. J. Russell. 2004. Nonwoven wound dressings. *Textile Progress* 36 (4):1-57.

Mattanavee, W., O. Suwantong, S. Puthong, T. Bunaprasert, V. P. Hoven, and P. Supaphol. 2009. Immobilization of Biomolecules on the Surface of Electrospun Polycaprolactone Fibrous Scaffolds for Tissue Engineering. *Acs Applied Materials & Interfaces* 1 (5):1076-1085.

Matthews, B. D., B. L. Pratt, H. S. Pollinger, C. L. Backus, K. W. Kercher, R. F. Sing, and B. T. Heniford. 2003. Assessment of adhesion formation to intra-abdominal polypropylene mesh and polytetrafluoroethylene mesh. *Journal of Surgical Research* 114 (2):126-132.

McGinty, J. J., N. J. Hogle, H. McCarthy, and D. L. Fowler. 2005. A comparative study of adhesion formation and abdominal wall ingrowth after laparoscopic ventral hernia repair in a porcine model using multiple types of mesh. *Surgical Endoscopy and Other Interventional Techniques* 19 (6):786-790.

McGrath, J. L. 2007. Cell spreading: The power to simplify. *Current Biology* 17 (10):R357-R358.

McKee, M. G., G. L. Wilkes, R. H. Colby, and T. E. Long. 2004. Correlations of solution rheology with electrospun fiber formation of linear and branched polyesters. *Macromolecules* 37 (5):1760-1767.

Meng, W., S. Y. Kim, J. Yuan, J. C. Kim, O. H. Kwon, N. Kawazoe, G. P. Chen, Y. Ito, and I. K. Kang. 2007. Electrospun PHBV/collagen composite nanofibrous scaffolds for tissue engineering. *Journal of Biomaterials Science-Polymer Edition* 18 (1):81-94.

Meng, W., Z. C. Xing, K. H. Jung, S. Y. Kim, J. Yuan, I. K. Kang, S. C. Yoon, and H. I. Shin. 2008. Synthesis of gelatin-containing PHBV nanofiber mats for biomedical application. *Journal of Materials Science-Materials in Medicine* 19 (8):2799-2807.

Menzies, D., and H. Ellis. 1990. Intestinal-obstruction from adhesions - how big is the problem. *Annals of the Royal College of Surgeons of England* 72 (1):60-63.

Milligan, D. W., and A. T. Raftery. 1974. Observations on pathogenesis of peritoneal adhesions - light and electron microscopical study. *British Journal of Surgery* 61 (4):274-280.

Min, B.-M., G. Lee, S. H. Kim, Y. S. Nam, T. S. Lee, and W. H. Park. 2004. Electrospinning of silk fibroin nanofibers and its effect on the adhesion and spreading of normal human keratinocytes and fibroblasts *in vitro*. *Biomaterials* 25 (7-8):1289-1297.

Monteiro, O. A. C., and C. Airoldi. 1999. Some studies of crosslinking chitosan-glutaraldehyde interaction in a homogeneous system. *International Journal of Biological Macromolecules* 26 (2-3):119-128.

Moreno, M. J., A. Ajji, D. Mohebbi-Kalhori, M. Rukhlova, A. Hadjizadeh, and M. N. Bureau. 2011. Development of a compliant and cytocompatible micro-fibrous polyethylene terephthalate vascular scaffold. *Journal of Biomedical Materials Research Part B-Applied Biomaterials* 97B (2):201-214.

Moroni, L., R. Licht, J. de Boer, J. R. de Wijn, and C. A. van Blitterswijk. 2006. Fiber diameter and texture of electrospun PEOT/PBT scaffolds influence human mesenchymal stem cell proliferation and morphology, and the release of incorporated compounds. *Biomaterials* 27 (28):4911-4922.

Moukwa, M. 1997. The development of polymer-based biomaterials since the 1920s. *JOM Journal of the Minerals, Metals and Materials Society* 49 (2):46-50.

Neves, A. A., N. Medcalf, and K. M. Brindle. 2005. Influence of stirring-induced mixing on cell proliferation and extracellular matrix deposition in meniscal cartilage constructs based on polyethylene terephthalate scaffolds. *Biomaterials* 26 (23):4828-4836.

Ng, R., X. Zhang, N. Liu, and S.-T. Yang. 2009. Modifications of nonwoven polyethylene terephthalate fibrous matrices via NaOH hydrolysis: Effects on pore size, fiber diameter, cell seeding and proliferation. *Process Biochemistry* 44 (9):992-998.

Ohkawa, K., D. I. Cha, H. Kim, A. Nishida, and H. Yamamoto. 2004. Electrospinning of chitosan. *Macromolecular Rapid Communications* 25 (18):1600-1605.

Papenburg, B. J., S. Sch¸ller-Ravoo, L. A. M. Bolhuis-Versteeg, L. Hartsuiker, D. W. Grijpma, J. Feijen, M. Wessling, and D. Stamatialis. 2009. Designing porosity and topography of poly(1,3-trimethylene carbonate) scaffolds. *Acta Biomaterialia* 5 (9):3281-3294.

Peesan, M., R. Rujiravanit, and P. Supaphol. 2006. Electrospinning of hexanoyl chitosan/polylactide blends. *Journal of Biomaterials Science-Polymer Edition* 17 (5):547-565.

Pitzer, G. B., and K. G. Patel. 2011. Proper care of early wounds to optimize healing and prevent complications. *Facial plastic surgery clinics of North America* 19 (3):491-504.

Powell, H. M., and S. T. Boyce. 2008. Fiber density of electrospun gelatin scaffolds regulates morphogenesis of dermal-epidermal skin substitutes. *Journal of Biomedical Materials Research Part A* 84A (4):1078-1086.

Qi, L., Z. Xu, and M. Chen. 2007. *In vitro* and *in vivo* suppression of hepatocellular carcinoma growth by chitosan nanoparticles. *European Journal of Cancer* 43 (1):184-193.

Ranjani, M., S. Rajan, and P. Brindha. 2010. Antioxidant and Antibacterial Potentials of Aloe vera Juice Extract against Wound Isolates. *Journal of Pure and Applied Microbiology* 4 (2):733-739.

Reynolds, T., and A. C. Dweck. 1999. Aloe vera leaf gel: A review update. *Journal of Ethnopharmacology* 68 (1-3):3-37.

Rho, K. S., L. Jeong, G. Lee, B. M. Seo, Y. J. Park, S. D. Hong, S. Roh, J. J. Cho, W. H. Park, and B. M. Min. 2006. Electrospinning of collagen nanofibers: Effects on the behavior of normal human keratinocytes and early-stage wound healing. *Biomaterials* 27 (8):1452-1461.

Robinson, T. N., J. H. Clarke, J. Schoen, and M. D. Walsh. 2005. Major mesh-related complications following hernia repair - Events reported to the Food and Drug Administration. *Surgical Endoscopy and Other Interventional Techniques* 19 (12):1556-1560.

Rosca-Casian, O., M. Parvu, L. Vlase, and M. Tamas. 2007. Antifungal activity of Aloe vera leaves. *Fitoterapia* 78 (3):219-222.

Saino, E., M. L. Focarete, C. Gualandi, E. Emanuele, A. I. Cornaglia, M. Imbriani, and L. Visai. 2011. Effect of electrospun fiber diameter and alignment on macrophage activation and secretion of proinflammatory cytokines and chemokines. *Biomacromolecules* 12 (5):1900-1911.

Sanchez, V. C., P. Weston, A. Yan, R. H. Hurt, and A. B. Kane. 2011. A 3-dimensional *in vitro* model of epithelioid granulomas induced by high aspect ratio nanomaterials. *Particle and Fibre Toxicology* 8.

Santos, C., P. Seabra, B. Veleirinho, I. Delgadillo, and J. A. L. da Silva. 2006. Acetylation and molecular mass effects on barrier and mechanical properties of shortfin squid chitosan membranes. *European Polymer Journal* 42 (12):3277-3285.

Schreuder-Gibson, H., P. Gibson, K. Senecal, M. Sennett, J. Walker, W. Yeomans, D. Ziegler, and P. P. Tsai. 2002. Protective textile materials based on electrospun nanofibers. *Journal of Advanced Materials* 34 (3):44-55.

Seitz, H., S. Marlovits, I. Schwendenwein, E. M¸ller, and V. VÈcsei. 1998. Biocompatibility of polyethylene terephthalate (TreviraÆ hochfest) augmentation device in repair of the anterior cruciate ligament. *Biomaterials* 19 (1-3):189-196.

Shalumon, K. T., N. S. Binulal, M. Deepthy, R. Jayakumar, K. Manzoor, and S. V. Nair. 2011. Preparation, characterization and cell attachment studies of electrospun multi-scale poly(caprolactone) fibrous scaffolds for tissue engineering. *Journal of Macromolecular Science Part a-Pure and Applied Chemistry* 48 (1):21-30.

Shen, X., D. Yu, L. Zhu, C. Branford-White, K. White, and N. P. Chatterton. 2011. Electrospun diclofenac sodium loaded Eudragit (R) L 100-55 nanofibers for colon-targeted drug delivery. *International Journal of Pharmaceutics* 408 (1-2):200-207.

Shi, J., L. Wang, F. Zhang, H. Li, L. Lei, L. Liu, and Y. Chen. 2010. Incorporating Protein Gradient into Electrospun Nanofibers As Scaffolds for Tissue Engineering. *Acs Applied Materials & Interfaces* 2 (4):1025-1030.

Shin, C., G. G. Chase, and D. H. Reneker. 2005. Recycled expanded polystyrene nanofibers applied in filter media. *Colloids and Surfaces a-Physicochemical and Engineering Aspects* 262 (1-3):211-215.

Sikareepaisan, P., A. Suksamrarn, and P. Supaphol. 2008. Electrospun gelatin fiber mats containing a herbal-Centella asiatica-extract and release characteristic of asiaticoside. *Nanotechnology* 19 (1).

Sombatmankhong, K., N. Sanchavanakit, P. Pavasant, and P. Supaphol. 2007. Bone scaffolds from electrospun fiber mats of poly (3-hydroxybutyrate), poly(3-hydroxybutyrate-co-3-hydroxyvalerate) and their blend. *Polymer* 48 (5):1419-1427.

Sonoda, Y., Y. Matsumoto, M. Funakoshi, D. Yamamoto, S. K. Hanks, and T. Kasahara. 2000. Anti-apoptotic role of focal adhesion kinase (FAK) - Induction of inhibitor-of-apoptosis proteins and apoptosis suppression by the overexpression of FAK in a human leukemic cell line, HL-60. *Journal of Biological Chemistry* 275 (21):16309-16315.

Soto, K., K. M. Garza, and L. E. Murr. 2007. Cytotoxic effects of aggregated nanomaterials. *Acta Biomaterialia* 3 (3):351-358.

Spasova, M., N. Manolova, D. Paneva, and I. Rashkov. 2004. Preparation of chitosan-containing nanofibres by electrospinning of chitosan/poly(ethylene oxide) blend solutions. *E-Polymers*.

Stashak, T. S., E. Farstvedt, and A. Othic. 2004. Update on wound dressings: Indications and best use. *Clinical Techniques in Equine Practice* 3 (2 SPEC. ISS.):148-163.

Stern, S. T., and S. E. McNeil. 2008. Nanotechnology safety concerns revisited. *Toxicological Sciences* 101 (1):4-21.

Strassmann, B. B., A. R. Vieira, E. L. Pedrotti, H. N. F. Morais, P. F. Dias, and M. Maraschin. 2008. Quantitation of methylxanthinic alkaloids and phenolic compounds in mate (Ilex paraguariensis) and their effects on blood vessel formation in chick embryos. *Journal of Agricultural and Food Chemistry* 56 (18):8348-8353.

Subramanian, A., D. Vu, G. F. Larsen, and H. Y. Lin. 2005. Preparation and evaluation of the electrospun chitosan/PEO fibers for potential applications in cartilage tissue engineering. *Journal of Biomaterials Science-Polymer Edition* 16 (7):861-873.

Suckow, M. A., J. P. Hodde, W. R. Wolter, K. V. Wood, M. C. Hiles, and A. D. Janis. 2010. Addition of nimesulide to small intestinal submucosa biomaterial inhibits postsurgical adhesiogenesis in rats. *Journal of Biomedical Materials Research Part B-Applied Biomaterials* 93B (1):18-23.

Suganya, S., T. S. Ram, B. S. Lakshmi, and V. R. Giridev. 2011. Herbal drug incorporated antibacterial nanofibrous mat fabricated by electrospinning: an excellent matrix for wound dressings. *Journal of Applied Polymer Science* 121 (5):2893-2899.

Sun, Z. C., E. Zussman, A. L. Yarin, J. H. Wendorff, and A. Greiner. 2003. Compound core-shell polymer nanofibers by co-electrospinning. *Advanced Materials* 15 (22):1929.

Suwantong, O., P. Opanasopit, U. Ruktanonchal, and P. Supaphol. 2007a. Electrospun cellulose acetate fiber mats containing curcumin and release characteristic of the herbal substance. *Polymer* 48 (26):7546-7557.

Suwantong, O., U. Ruktanonchai, and P. Supaphol. 2008. Electrospun cellulose acetate fiber mats containing asiaticoside or Centella asiatica crude extract and the release characteristics of asiaticoside. *Polymer* 49 (19):4239-4247.

Suwantong, O., S. Waleetorncheepsawat, N. Sanchavanakit, P. Pavasant, P. Cheepsunthorn, T. Bunaprasert, and P. Supaphol. 2007b. *In vitro* biocompatibility of electrospun poly (3-hydroxybutyrate) and poly (3-hydroxybutyrate-co-3-hydroxyvalerate) fiber mats. *International Journal of Biological Macromolecules* 40 (3):217-223.

Taepaiboon, P., U. Rungsardthong, and P. Supaphol. 2007. Effect of cross-linking on properties and release characteristics of sodium salicylate-loaded electrospun poly(vinyl alcohol) fibre mats. *Nanotechnology* 18 (17).

Tan, S. H., R. Inai, M. Kotaki, and S. Ramakrishna. 2005. Systematic parameter study for ultra-fine fiber fabrication via electrospinning process. *Polymer* 46 (16):6128-6134.

Tchemtchoua, V. T., G. Atanasova, A. Aqil, P. Filee, N. Garbacki, O. Vanhooteghem, C. Deroanne, A. Noel, C. Jerome, B. Nusgens, Y. Poumay, and A. Colige. 2011. Development of a chitosan nanofibrillar scaffold for skin repair and regeneration. *Biomacromolecules* 12 (9):3194-3204.

Thakur, R. A., C. A. Florek, J. Kohn, and B. B. Michniak. 2008. Electrospun nanofibrous polymeric scaffold with targeted drug release profiles for potential application as wound dressing. *International Journal of Pharmaceutics* 364 (1):87-93.

Theron, S. A., E. Zussman, and A. L. Yarin. 2004. Experimental investigation of the governing parameters in the electrospinning of polymer solutions. *Polymer* 45 (6):2017-2030.

Tolino, M. J., D. E. Tripoloni, R. Ratto, and M. I. Garcia. 2009. Infections associated with prosthetic repairs of abdominal wall hernias: pathology, management and results. *Hernia* 13 (6):631-637.

Tommeraas, K., Varum, K. M., Christensen, B. E., Smidsrod, O. 2001. Preparation and characterisation of oligosaccharides produced by nitrous acid depolymerisation of chitosan. *Carbohydrate Research* 333:137–144.

Ueno, H., T. Mori, and T. Fujinaga. 2001. Topical formulations and wound healing applications of chitosan. *Advanced Drug Delivery Reviews* 52 (2):105-115.

Ueno, H., H. Yamada, I. Tanaka, N. Kaba, M. Matsuura, M. Okumura, T. Kadosawa, and T. Fujinaga. 1999. Accelerating effects of chitosan for healing at early phase of experimental open wound in dogs. *Biomaterials* 20 (15):1407-1414.

Uyar, T., and F. Besenbacher. 2008. Electrospinning of uniform polystyrene fibers: The effect of solvent conductivity. *Polymer* 49 (24):5336-5343.

van't Riet, M., P. J. D. van Steenwijk, F. Bonthuis, R. L. Marquet, E. W. Steyerberg, J. Jeekel, and H. J. Bonjer. 2003. Prevention of adhesion to prosthetic mesh - Comparison of different barriers using an incisional hernia model. *Annals of Surgery* 237 (1):123-128.

VandeVord, P. J., H. W. T. Matthew, S. P. DeSilva, L. Mayton, B. Wu, and P. H. Wooley. 2002. Evaluation of the biocompatibility of a chitosan scaffold in mice. *Journal of Biomedical Materials Research* 59 (3):585-590.

Veleirinho, B., M. F. Rei, and J. A. Lopes-da-Silva. 2008. Solvent and concentration effects on the properties of electrospun poly(ethylene terephthalate) nanofiber mats. *Journal of Polymer Science Part B-Polymer Physics* 46 (5):460-471.

Vo, N. lcker, D. Klee, Ho, H. cker, and S. Langefeld. 2001. Functionalization of silicone rubber for the covalent immobilization of fibronectin. *Journal of Materials Science: Materials in Medicine* 12:111-119.

Voskerician, G., P. H. Gingras, and J. M. Anderson. 2006. Macroporous condensed poly(tetrafluoroethylene). I. *In vivo* inflammatory response and healing characteristics. *Journal of Biomedical Materials Research Part A* 76A (2):234-242.

Wang, X., D. E. Heath, and S. L. Cooper. 2012. Endothelial cell adhesion and proliferation to PEGylated polymers with covalently linked RGD peptides. *Journal of Biomedical Materials Research Part A* 100A (3):794-801.

Wei, M., J. Lee, B. W. Kang, and J. Mead. 2005. Preparation of core-sheath nanofibers from conducting polymer blends. *Macromolecular Rapid Communications* 26 (14):1127-1132.

Xu, F., F.-Z. Cui, Y.-P. Jiao, Q.-Y. Meng, X.-P. Wang, and X.-Y. Cui. 2009. Improvement of cytocompatibility of electrospinning PLLA microfibers by blending PVP. *Journal of Materials Science-Materials in Medicine* 20 (6):1331-1338.

Yang, F., R. Murugan, S. Wang, and S. Ramakrishna. 2005. Electrospinning of nano/micro scale poly(L-lactic acid) aligned fibers and their potential in neural tissue engineering. *Biomaterials* 26 (15):2603-2610.

Yang, Y., T. Xia, F. Chen, W. Wei, C. Liu, S. He, and X. Li. 2012. Electrospun Fibers with Plasmid bFGF Polyplex Loadings Promote Skin Wound Healing in Diabetic Rats. *Molecular Pharmaceutics* 9 (1):48-58.

Yoshimoto, H., Y. M. Shin, H. Terai, and J. P. Vacanti. 2003. A biodegradable nanofiber scaffold by electrospinning and its potential for bone tissue engineering. *Biomaterials* 24 (12):2077-2082.

You, Y., W. H. Park, B. M. Ko, and B. M. Min. 2004. Effects of PVA sponge containing chitooligosaccharide in the early stage of wound healing. *Journal of Materials Science-Materials in Medicine* 15 (3):297-301.

Yuan, J., Z.-C. Xing, S.-W. Park, J. Geng, I.-K. Kang, J. Yuan, J. Shen, W. Meng, K.-J. Shim, I.-S. Han, and J.-C. Kim. 2009. Fabrication of PHBV/Keratin Composite Nanofibrous Mats for Biomedical Applications. *Macromolecular Research* 17 (11):850-855.

Zhang, K., H. Wang, C. Huang, Y. Su, X. Mo, and Y. Ikada. 2010. Fabrication of silk fibroin blended P(LLA-CL) nanofibrous scaffolds for tissue engineering. *Journal of Biomedical Materials Research Part A* 93A (3):984-993.

Zhang, K., X. F. Wang, D. Z. Jing, Y. Yang, and M. F. Zhu. 2009. Bionic electrospun ultrafine fibrous poly(L-lactic acid) scaffolds with a multi-scale structure. *Biomedical Materials* 4 (3).

Zheng, L.-Y., and J.-F. Zhu. 2003. Study on antimicrobial activity of chitosan with different molecular weights. *Carbohydrate Polymers* 54 (4):527-530.

Zhou, Y., D. Yang, X. Chen, Q. Xu, F. Lu, and J. Nie. 2008. Electrospun water-soluble carboxyethyl chitosan/poly(vinyl alcohol) nanofibrous membrane as potential wound dressing for skin regeneration. *Biomacromolecules* 9 (1):349-354.

Zhu, J., Y. Zhang, H. Shao, and X. Hu. 2008. Electrospinning and rheology of regenerated *Bombyx mori* silk fibroin aqueous solutions: The effects of pH and concentration. *Polymer* 49 (12):2880-2885.

Zuo, W. W., M. F. Zhu, W. Yang, H. Yu, Y. M. Chen, and Y. Zhang. 2005. Experimental study on relationship between jet instability and formation of beaded fibers during electrospinning. *Polymer Engineering and Science* 45 (5):704-709.